POLITECNICO DI MILANO

SCHOOL OF CIVIL, ENVIRONMENTAL AND LAND PLANNING ENGINEERING

MASTER OF SCIENCE IN
ENVIRONMENTAL AND LAND PLANNING ENGINEERING

DATA COLLECTION AND DYNAMIC MODELLING OF AN ANAEROBIC CO-DIGESTION PILOT PLANT

Supervisor:

Prof. Elena Ficara

Co-Supervisor:

Eng. Arianna Catenacci, PhD

Master Thesis of:

Iacopo Del Vecchio

Academic Year 2021-2022

TABLE OF CONTENTS

LIST OF FIGURES

LIST OF TABLES

ABSTRACT

The current thesis work presents the results of an experimentation conducted on a pilot anaerobic digestion plant. The experiment lasted from March 21, 2022 to June 27, 2022. The experimental activity started with a mono-digestion phase using sludge sampled at the Peschiera Borromeo WWTP, and then progressed to a co-digestion phase. Expired yogurt of well-known commercial brands was used as co-feedstock during co-digestion. The reactor operated according to Continuous Stirred Tank Reactor (CSTR) model and an operating volume of 60 L at a temperature of 37 ± 0.5 °C. The pilot plant was fed semi-continuously with an average HRT of 17.1 d. During mono-digestion, when only sludge was fed, the reactor operated with an average OLR of 1.36 $kgVS/m^3/d$. In the co-digestion phase, the OLR was gradually increased by 15%, 20%, 40%, and finally 60%. This phase was characterised by an average OLR of 1.67 $kgVS/m^3/d$. The primary goal of this work was to refine and calibrate a co-digestion model based on ADM1 using the OpenModelica programming platform. The model calibration was performed iteratively using the analytical data from the pilot plant and the results obtained from the BMP and biomass activity tests. The iteration procedure for the model calibration and the introduction of inhibition kinetics proved to be very effective in modelling the batch tests. The statistical indicators Theil's Inequality Coefficient (TIC) and Mean Absolute Relative Error (MARE) were used in order to assess the model performance. For both criteria, the closer the value to zero, the better the model performance. Among the various results, propionate and sludge simulations showed the lowest values of TIC and MARE. However, the model was inefficient in predicting the pilot plant behaviour. Specifically, ammoniacal nitrogen (NH_4^+) and alkalinity output concentrations diverged significantly from the experimental values. Potential causes were identified and recommendations were proposed for future developments.

SOMMARIO

Il presente lavoro di tesi illustra i risultati di una sperimentazione condotta su un impianto pilota di digestione anaerobica. La sperimentazione è durata dal 21 marzo 2022 al 27 giugno 2022. L'attività sperimentale è iniziata con una fase di mono-digestione, utilizzando fanghi campionati presso l'impianto di depurazione di Peschiera Borromeo, per poi passare a una fase di co-digestione. Lo yogurt scaduto di note marche commerciali è stato utilizzato come co-substrato durante la fase co-digestione. Il reattore ha operato secondo un modello CSTR (Continuous Stirred Tank Reactor), con un volume operativo di 60 L a una temperatura di $37 \pm 0,5$ °C. L'impianto pilota è stato alimentato in modalità semi-continua con un tempo di residenza idraulico (HRT) medio di 17.1 d. Durante la fase di mono-digestione, quando è stato alimentato solo il fango, il reattore ha operato con un OLR medio di 1.36 $kgVS/m^3/d$. Nella fase di co-digestione, l'OLR è stato gradualmente aumentato del 15%, 20%, 40% ed infine 60%. Questa fase è stata caratterizzata da un OLR medio di 1.67 $kgVS/m^3/d$. L'obiettivo principale di questo lavoro è stato quello di affinare e calibrare un modello di co-digestione su base ADM1 attraverso la piattaforma di programmazione OpenModelica. La calibrazione del modello è stata eseguita attraverso una procedura iterativa di validazione, utilizzando i dati analitici dell'impianto pilota e i risultati ottenuti dalle prove di BMP e dalle prove di attività della biomassa. Il procedimento iterativo e l'apporto di modifiche al modello, quali l'introduzione di cinetiche di inibizione, si sono rivelati particolarmente efficaci nella rappresentazione dei test in batch. Gli indici statistici TIC (Theil's Inequality Coefficient) e MARE (Mean Absolute Relative Error) sono stati utilizzati per valutare la bontà della simulazione. Per entrambi i criteri, quanto più il valore è vicino allo zero, tanto migliori sono le prestazioni del modello. Tra i vari risultati ottenuti, le prove di attività con il propionato e i test di BMP del fango hanno mostrato i valori più bassi di TIC e MARE. Tuttavia, il modello non si è rivelato altrettanto efficiente nel prevedere il comportamento dell'impianto pilota; in particolare, i risultati relativi alle concentrazioni dell'azoto ammoniacale (NH_4^+) e dell'alcalinità del digestato hanno mostrato un notevole scostamento dai valori sperimentali. Sono state individuate delle possibili cause e forniti suggerimenti per successivi sviluppi.

LIST OF ABBREVIATIONS

AcoD   Anaerobic co-digestion

AD   Anaerobic digestion

ADM1   Anaerobic digestion model No. 1

BMP   Biochemical methane potential

BSA   Bovine serum albumin

COD   Chemical oxygen demand

CSTR   Continuous stirred tank reactor

FAN   Free ammonia nitrogen

HRT   Hydraulic retention time

IWA   International Water Association

LCFA   Long chain fatty acids

OFMSW   Organic fraction of municipal solid waste

OLR   Organic loading rate

PLC   Programmable Logic Controller

SHW   Slaughterhouse wastes

SRT   Solid retention time

TKN   Total Kjeldahl nitrogen

TAN   Total Ammonia nitrogen

TS   Total solids

VFA   Volatile fatty acids

VS   Volatile solids

WS   Waste sludge

WWTP   Wastewater treatment plant

Chapter 1:   INTRODUCTION

1.1 Background

A global challenge of our day is to ensure affordable and clean energy from sustainable sources. Addressing this challenge has resulted in a paradigm shift in many aspects of the economy, including organic waste management. The conventional view of waste as a disposable material is no longer suitable. In a circular economy, organic waste is a resource for energy and nutrient recovery (Nguyen et al., 2021).

A globally emerging practice is to valorise urban organic waste via anaerobic co-digestion (AcoD) using the spare capacity at wastewater treatment plants (WWTPs) (Nghiem et al. 2017, Xie et al. 2018). AcoD at WWTPs refers to the digestion of sewage sludge with one or more co-substrates with high organic content. The theoretical principle of AcoD is the complementarity between nutrient-rich sewage sludge and carbon-rich organic wastes to boost the anaerobic digestion (AD).

Recent success in full-scale AcoD implementation demonstrates the potential role of WWTPs as energy producers. Anaerobic digestion facilities at WWTPs are used to treat sewage sludge with low organic content. Thus, their capacity is governed by hydraulic rather than organic loading. To exploit the spare digestion capacity, organic waste can be co-digested with sewage sludge to increase biogas production. AcoD increases biogas production by 2.5 to 4 times compared to the digestion of only sewage sludge (Shen et al. 2015). Several WWTPs have become net energy producers (Nghiem et al. 2017).

Mathematical modelling helps to minimise the possibility of imbalance and instability in the digestion process at the laboratory scale and in full-scale plants. Indeed, models describing the AcoD process can forecast the impacts of the mixing proportion of two or more co-substrates, organic loadings, and the choosing technique of wastewaters, and can minimise energy usage and time of the procedure (Poggio et al., 2016). Thus, basic kinetic models, AD model No. 1, and other algorithmic methods have been developed (Siddique et al., 2018).

1.2 Goals

The main objective of this dissertation was to calibrate an ADM1 co-digestion model previously developed and employed in Nunziata and Soderino's work (Insights in anaerobic co-digestion via experimental and dynamic modelling tools, 2021), and to refine it on the basis of the limitations that emerged in the earlier investigation. The model was calibrated through an iterative process using data acquired from the monitoring of an anaerobic digestion pilot plant and batch tests performed in the lab. The Monod-type kinetics were replaced in the model with the Haldane inhibition kinetics for the uptake of propionate and acetate.

The experiment was carried out in the San Giuliano Milanese Ovest wastewater treatment facility (GruppoCAP, Amiacque), using waste sludge from the Peschiera Borromeo wastewater treatment plant (GruppoCAP, Amiacque) and expired yogurt previously provided by GruppoCAP. The pilot plant was started up in March, and the monitoring continued until the reactor was shut down on June 27.

1.3 Thesis outline

This thesis has five main chapters that are preceded by an abstract, which is available in both Italian and English.

A general overview of the subject and a brief description of the goals of the current dissertation are offered in the first chapter, which also emphasises the growing focus on co-digestion and the relevance of modelling.

The second chapter provides a literature review about anaerobic digestion, batch tests and mathematical modelling.

The materials and methods employed are thoroughly described in the third chapter. All aspects of the experimentation, including the configuration of the pilot plant, its operating modes, monitoring plan, and analytical methods, are covered in the first part. The model's implementation, the determination of the input state variables, and the calibration process are all addressed in the second part.

The fourth chapter reports and discusses all of the experimental procedures and modelling results.

The main achievements and future developments are finally reported in the fifth and last chapter.

Chapter 2: LITERATURE REVIEW

2.1. *Fundamentals of Anaerobic Digestion*

Anaerobic digestion (AD) is the most common and oldest technology adopted for sludge stabilization and energy recovery. It is a biological treatment, consisting in the degradation of organic matter under anaerobic conditions (i.e. in the absence of oxygen in its molecular form, or bound to other elements, as in the case of nitrate, NO^{3-}). In AD, various microorganisms interact mutually and syntrophically, breaking down complex organic molecules into soluble monomers like amino acids, fatty acids, simple sugars, and glycerols (Anukam et al., 2019). The process finally results in the formation of various products, the most abundant of which are two gases: methane (CH_4) and carbon dioxide (CO_2) (Cecchi et al., 2005). The anaerobic digestion process is a well-understood chain of biochemical reactions that takes place in four steps: hydrolysis, acidogenesis, acetogenesis, and methanogenesis.

2.1.1. *Stages of Anaerobic Digestion*

The conversion of complex organic substrates to methane occurs, as mentioned, through an anaerobic trophic chain. Distinct metabolic groups of microorganisms are involved in it, which differ in terms of both substrates and products of their metabolism. Their anaerobic metabolism results in a sequence of oxidation-reduction reactions that are significantly affected by pH, temperature, type and concentration of the substrates involved.

Hydrolysis

In the first step, organic polymer chains (e.g. lipids, polysaccharides, proteins, and nucleic acids) are depolymerised into simpler molecules (e.g. fatty acids, sugars and amino acids) by enzymes that break down complex organic molecules through extracellular enzymatic reactions and convert them into soluble compounds that are more easily usable in the following stages. It is a relatively slow step that can limit the rate of the overall digestion process, especially when solid waste substrates are used (Anukam et al., 2019).

Acidogenesis

In the second stage, the soluble compounds produced through hydrolysis are converted mainly into volatile fatty acids (VFA), hydrogen, carbon dioxide, ethanol, ammonia (NH_3) and some sulfur compounds. Acidogenic microorganisms generally oxidize simple organic substrates to pyruvate, which is then transformed into volatile fatty acids, alcohols and ketones, which are the starting substrates for the acetogenic phase (Cecchi et al., 2005). The acids produced in this stage are acetic acid (CH_3COOH), propionic acid (CH_3CH_2COOH), butyric acid ($CH_3CH_2CH_2COOH$) and valeric acid ($CH_3CH_2CH_2CH_2COOH$) (Deepanraj et al., 2014).

Acetogenesis

In this phase, substrates from previous steps (higher organic acids, propionate and butyrate, and alcohols) are further digested by acetogens to produce mainly acetic acid as well as formic acid, CO_2 and H_2.

This conversion is controlled to a large extent by the partial pressure of H_2 in the mixture (Appels et al., 2008). Indeed, low hydrogen concentrations are required for the free energy change associated with the conversion of propionate and butyrate to acetate and hydrogen; otherwise, the process will not occur spontaneously. If methanogenic bacteria keep H_2 levels low, acetate will be the predominant byproduct, and the process will not be inhibited (Metcalf & Eddy I AECOM, 2014).

Methanogenesis

The anaerobic trophic chain ends with the production of CH_4.

The microorganisms involved are called methanogens; they are crucial to AD processes because they grow slowly and are extremely sensitive to changes in the environment.

Methane-producing bacteria can be divided in two groups: hydrogenophilic and acetophilic methanogens. The first group splits acetate into methane and carbon dioxide and the second group uses hydrogen as electron donor and carbon dioxide as acceptor to produce methane (Appels et al., 2008). Generally, about 2/3 of the methane produced in anaerobic digestion comes from acetoclastic methanogenesis. The two methanogenic strains perform two important functions through their activity: on the one hand, they degrade acetic and formic acid to CH_4 by removing acids from the medium, preventing acidity from inhibiting the degradation of organic substrates, and on the other

hand, they keep the H_2 concentration low to allow the conversion of long-chain fatty acids and alcohols to acetate and H_2 (Cecchi et al., 2005).

2.1.2. Kinetics of Anaerobic Digestion

Growth kinetics

The bacterial growth is often described by a series of mathematical expressions according to the equation *(2. 1)*:

$$r_X = \mu \cdot X$$

(2. 1)

Where:

- μ symbolizes the specific growth rate of the microorganisms $\left[\frac{1}{d}\right]$;
- X is the concentration of microorganisms $\left[\frac{kg}{m^3}\right]$.

Monod suggested the following equation *(2. 2)* for the specific growth rate:

$$\mu = \frac{\mu_{max} \cdot S}{K_S + S}$$

(2. 2)

Where:

- μ_{max} is the maximum specific growth rate achievable when $S \gg K_S$ $\left[\frac{1}{d}\right]$;
- S is the concentration of soluble substrate $\left[\frac{kg}{m^3}\right]$;
- K_S symbolizes the half-saturation constant, meaning the value of the limiting nutrient (substrate) concentration at which the specific growth rate is half its maximum value $\left[\frac{kg}{m^3}\right]$.

By combining equations *(2. 1)* and *(2. 2)*, the microbial growth rate is as follows:

$$r_X = \frac{\mu_{max} \cdot S}{K_S + S} \cdot X$$

(2. 3)

Whereas the substrate consumption rate, r_S, follows the equation (2. 4):

$$r_S = \frac{1}{Y} \cdot \frac{\mu_{max} \cdot S}{K_S + S} \cdot X$$

(2. 4)

Where Y is the biomass yield factor [-].

However, Monod's equation is incapable of predicting the decrease of the biomass concentration that is due to the endogenous respiration and the cell lysis. McCarty developed the following modified Monod equation taking into consideration the endogenous respiration and the cell lysis (2. 5):

$$r_X = \frac{\mu_{max} \cdot S}{K_S + S} \cdot X - k_d \cdot X$$

(2. 5)

Where k_d is the decay coefficient $\left[\frac{1}{d}\right]$.

Both reactions involved in the growth and decay mechanisms are described by first-order kinetics.

The above expressions are incapable of describing the bacterial growth when an inhibitory factor is present. In anaerobic digestion, many factors could inhibit the whole process and especially the methanogenesis step (Gavala et al., 2003).

The most common inhibition types used in anaerobic models are expressed according to equations (2. 6) and (2. 7) and are those of Haldane first used by Andrews and the non-competitive inhibition type, first introduced by Ierusalimsky, respectively (Gavala et al., 2003).

$$\mu = \mu_{max} \cdot \frac{1}{\frac{K_S}{S} + \frac{I}{K_I} + 1}$$

(2. 6)

$$\mu = \mu_{max} \cdot \frac{S}{K_S + S} \cdot \frac{K_I}{K_I + I}$$

(2. 7)

Where:

- K_I is the inhibition constant $\left[\frac{kg}{m^3}\right]$;
- I symbolizes the concentration of the inhibitor $\left[\frac{kg}{m^3}\right]$.

Hydrolysis of biopolymers

It is extremely difficult to characterize the entire process using reliable kinetics because hydrolysis of a complex, insoluble substrate is dependent on numerous characteristics such as particle size, pH, production of enzymes, diffusion and adsorption of enzymes to particles.

Hydrolysis of organic polymers is often described by a first-order kinetic model (2. 8) since the enzymatic activity is not directly coupled to the bacterial growth (Gavala et al., 2003).

$$r_S = K_h \cdot S$$

(2. 8)

Where K_h is the hydrolytic constant $\left[\frac{1}{d}\right]$.

Acidogenesis and Acetogenesis

Both phases of acidogenesis and acetogenesis are described by Monod kinetics, with a limitation on the concentration of the corresponding organic substrate. The inhibiting factors related to hydrogen (H_2) and pH could be included in the analytical expression (Bonomo, 2014).

Methanogenesis

Acetoclastic methanogenesis is well described by a Monod kinetics, in whose analytical expression terms referring to the concentrations of acetate and inorganic nitrogen, a pH inhibition function and a non-competitive inhibition function by ammonia can be considered (Bonomo, 2014), while hydrogenotrophic bacteria kinetics is a two substrates Monod-type kinetics (H_2 and CO_2, respectively) (Cecchi et al., 2005).

2.1.3. Parameters affecting Anaerobic Digestion process

Many factors affect the performance of anaerobic digestion. Indeed, some parameters have a significant impact on the process' metabolism. pH and alkalinity, VFA concentration, the VFA-to-alkalinity ratio, temperature, mixing, OLR (organic loading rate), HRT and SRT (solids and hydraulic retention time), availability of nutrients, the presence of toxic or inhibiting compounds are all key factors that must be considered (Cecchi et al., 2005). Therefore, constant monitoring of the above parameters is required to optimize biogas production.

pH and Alkalinity

The measurement of pH provides important information about the process's stability and correct performance in AD. Its variation is related both to the reaction medium ability to buffer the system and changes in the trophic chain's species balance (Cecchi et al., 2005). The optimal pH values for anaerobic metabolism differ depending on the stage of the process. Methanogenic bacteria are extremely sensitive to pH with an optimum range between 6.5 and 7.2, whereas fermentative microorganisms are somewhat less sensitive and can function in a wider range of pH between 4.0 and 8.5 (Dewil et al., 2008).

The pH value in a digester is mainly determined by the presence of CO_2 in the liquid medium, and therefore by its partial pressure in the biogas, and by the concentrations of volatile fatty acids and ammonia (Cecchi et al., 2005). pH fluctuations are important indicators of process balance, but they become apparent only after alkalinity has been completely depleted, when the latter no longer exerts its buffering action. It is therefore important to consider pH in conjunction with other key control parameters like medium alkalinity, volatile fatty acid concentration, and biogas composition, as well as their trends.

Alkalinity is a measure of a system's ability to neutralize protons, and it is usually measured in terms of $CaCO_3$ concentration. For anaerobic digesters operating under stable conditions, alkalinity values in the range of 3000-5000 mgCaCO$_3$/L are typical. The presence of a buffer system in an anaerobic digester is largely determined by the coexistence of ammonia, which results from protein degradation, and bicarbonate, which results from the dissolution of carbon dioxide in the medium (Cecchi et al., 2005). This parameter is extremely important in anaerobic processes. Indeed, as already mentioned above, the rate of production of volatile fatty acids is much higher than that of methane. The greatest risk for digester failure is a result of acid accumulation, which would occur if the amount of volatile solids loaded into the digester or produced by acidogenesis increase sharply. The acidogenic bacteria

would then flourish, producing high volumes of organic acids and further lowering the pH to below 5.0, which is lethal to methanogens (Lohani and Havukainen, 2017). In these cases, the system's buffering capacity is critical, as it must be able to neutralize the pH drop caused by the accumulation of organic acids.

Volatile fatty acids (VFA)

Volatile fatty acids are usually represented by the general formula R-COOH, where R is an alkyl group: $CH_3(CH_2)_n$.

In general, during the anaerobic digestion process, hydrolytic and acidifying bacteria produce volatile fatty acids with R containing 0 to 3 carbon atoms (short-chain fatty acids). The variation in concentration, rather than the absolute concentration, is usually used as a stability parameter: sudden changes with an increase in concentration indicate that the process is sliding towards acidogenic rather than methanogenic processes. In general, an increase in volatile acids is a consequence of organic overloading, which accelerates hydrolytic and acidogenic phenomena, resulting in an unbalanced trophic chain and a shift in the system towards low pH conditions after the medium's buffering capacity is depleted. Indeed, anaerobic digestion imbalances could arise when VFAs concentration exceeds the buffering capacity of the components in the digester.

VFA-to-alkalinity ratio

The concentration of volatile fatty acids and alkalinity are the two parameters that change more quickly when the system deviates from stable conditions. Since, in the case of acid accumulation, fatty acid concentration tends to increase while alkalinity tends to decrease, a useful parameter to consider is the ratio between these two quantities. Values around 0.3 $\frac{mgCH_3COOH}{mgCaCO_3}$ indicate stable digester operation, while higher values may indicate the occurrence of stability issues (Cecchi et al., 2005).

Long-chain fatty acids

LCFAs are generated during fat and lipid breakdown and are further reduced to acetate and hydrogen. LCFAs are known to be inhibitory at low concentrations and their toxicity is caused by adsorption onto the cell wall or cell membrane, which interferes with the cell's transport and/or protective activities. Furthermore, the sorption of an LCFA layer to the biomass results in sludge flotation

potentially leading to bacteria washout. Aceticlastic methanogenic bacteria have been found to be more sensitive to LCFA than hydrogenotrophic methanogens (Dewil et al., 2008).

Temperature

Temperature plays a key role in the growth of the microbial populations involved in the anaerobic digestion process, with a significant impact also on reaction kinetics; three different operating ranges are identified:

- psychrophilic range: 4-15 °C;
- mesophilic range: 20-40 °C, with the optimum temperature of 35 °C;
- thermophilic range: 45-70 °C, with the optimum temperature of 55 °C.

Bacterial populations in each interval are specifically adapted to the corresponding temperature range and are unable to operate efficiently outside of it. Within each interval, an increase in process kinetics is observed with a trend reflecting the Vant'Hoff-Arrhenius relationship, with a subsequent slowdown near the optimum value, followed by a rapid decrease (Bonomo, 2014). Comparing the three ranges, from psychrophilic to thermophilic, it can be observed: an increase in process kinetics, a decrease in the values of the half-saturation constants and a faster bacterial decay. In the mesophilic field, the process is more stable and less sensitive to changes in operating conditions. In the thermophilic field, high temperatures also exert a sanitizing effect against pathogenic microorganisms. However, the temperature must be chosen based on both energy and kinetic considerations, which make the thermophilic process inconvenient in most cases (Bonomo, 2014).

Mixing

Mixing or agitation is required in the digester to maintain homogeneity and process stability. Mixing helps to combine the fresh incoming material with microorganisms and prevents from thermal stratification and scum formation in the digester. Mixing maintains uniformity in substrate concentration, temperature and other environmental factors. In addition, it prevents solid deposition at the bottom of the digester. Mixing can be done either by using mechanical stirrers or by recirculation using centrifugal pumps (Deepanraj et al., 2014).

OLR

Organic loading rate (OLR) is an important parameter, which affects the biogas production in anaerobic digestion. It can be expressed as the amount of raw material (kg of volatile solids) fed to the digester per unit of volume per day:

$$OLR = \frac{C}{HRT} \left[\frac{kgSV}{m^3 \cdot d}\right]$$

(2. 9)

Where:

- C is the substrate concentration in the feed as VS $\left[\frac{kgSV}{m^3}\right]$;
- HRT is the hydraulic retention time $[d]$.

Increases in OLR result in higher biogas production, lower conversion efficiencies, and higher risks for process stability. However, when OLR is increased beyond optimum levels, a decrease in the performance of the biogas production is observed. High OLR can also have a negative impact on process performance by inhibiting microbial growth and inducing washout. Conversion efficiencies are generally high at low OLR, though too low OLR may also result in the death or inactivation of microorganisms due to inadequate nutrients supply for microbial metabolism. Consequently, it is crucial to find an optimum OLR that guarantees elevated production while avoiding the AD process failure.

The optimal loading rate is between 0.5 and 2 kg of VS per m^3 of the digester per day, which can be determined by the type of raw material, retention time, and process temperature (Deepanraj et al., 2014).

HRT and SRT

The ratio between the volume of the reactor and its volumetric feeding rate is known as the average hydraulic retention time (HRT):

$$HRT = \frac{V}{Q}$$

(2. 10)

Where:

- V is the volume of the reactor $[m^3]$;

- Q is the flow rate withdrawn $\left[\frac{m^3}{d}\right]$.

It represents the average time the liquid and soluble components in the sludge are held in the digester.

The solids retention time (SRT) is the average time the solids (bacteria and particulate matter) spend in the digester and it is expressed as the ratio between the solids present in the digester and the solids flow rate extracted from the reactor:

$$SRT = \frac{X \cdot V}{X \cdot Q} = \frac{V}{Q}$$

(2. 11)

Where:

- X is the biomass concentration $\left[\frac{kg}{m^3}\right]$;

- V is the volume of the reactor $[m^3]$;

- Q is the flow rate withdrawn $\left[\frac{m^3}{d}\right]$.

As shown in the formula, if the reactor is well mixed and there is no recirculation, the biomass concentration in the reactor will be the same as that of the flow rate withdrawn.

The SRT is a fundamental design and operating parameter for all biological processes. Indeed, the subsequent steps of the digestion process are directly related to the SRT. An increase or decrease in SRT results in an increase or decrease in the extent of each reaction. There is a minimum SRT for each reaction. If the SRT is less than the minimum SRT, bacteria cannot grow rapidly enough and the digestion process will fail eventually (Metcalf & Eddy I AECOM, 2014).

The influence of the retention time on the breakdown efficiency is mostly studied at laboratory scale and the observed relationship between gas production and retention time in a CSTR indicates that (i) retention times shorter than 5 days are insufficient for a stable digestion: VFA concentrations are increasing due to a washout of methanogenic bacteria, (ii) VFA concentrations are still relatively high for SRT of 5–8 days: there is an incomplete breakdown of compounds, especially of the lipids, (iii) stable digestion is obtained for SRT higher than 8–10 days corresponding to low VFA concentrations and to the breakdown of lipids, and (iv) the breakdown curve stabilizes at SRT>10 days when all sludge compounds are significantly reduced (Dewil et al., 2008).

Nutrients demand

Macronutrients including (C, H, N, O, and S) have a significant impact on the metabolic activity of microorganisms. Microorganisms require sulphur during the methanogenesis phase, nitrogen for protein production, and carbon for cell construction. CH_4 and CO_2 are mainly the byproducts of the conversion of C, H, and O during AD. N and S, on the other hand, are normally converted to ammonia and H_2S, respectively. As already stated above, process buffering can be accomplished with ammonia. It was observed that a high level of nitrogen in the feedstock might inhibit methanogens growth, whereas too little nitrogen may negatively affect the process since it is insufficient to meet the required level of growth of microorganisms.

The performance of the AD process may be enhanced by the use of micronutrients, also referred to as trace elements. Zinc, iron, cobalt, tungsten, and molybdenum are examples of commonly used trace elements. Even though it has been discovered that adding trace elements can help methanogenic bacteria grow more effectively, at higher concentrations they can cause methane inhibition (Sibiya et al., 2015).

Inhibitory substances

One of the main reasons why the anaerobic process is unstable or fails completely is the presence of inhibiting substances. In particular, high concentrations of substances such as ammonia, H_2S, heavy metals, sulfide, nitrogen compounds and, in general, specific organic substances can compromise normal metabolic activity with consequent negative impacts on specific biogas production.

Ammonia, which is produced during the degradation of nitrogenous compounds (mainly proteins and urea), is one of the most important inhibitory compounds for AD. Ammonium (NH_4^+) and free ammonia (NH_3) are the two forms of inorganic nitrogen. NH_3 has been suggested to be the main cause of inhibition as it is freely-membrane permeable and passively diffuses into the cell, causing a proton imbalance and/or potassium deficiency. Among the four types of anaerobic microorganisms, the methanogens are the least tolerant and the most likely to cease growth due to ammonia inhibition (Chen et al., 2008). The free ammonia concentration mainly depends on three parameters: total ammonia concentration, temperature and pH. The microbial growth rate is found to be positively affected by high temperatures (such as those of thermophilic conditions), but this is also associated with a rise in the concentration of free ammonia. Similarly, as pH rises, the ratio of free to ionized ammonia rises, resulting in increased toxicity (Dewil et al., 2008). Because nitrogen is an essential nutrient for the microorganisms, ammonia levels below 200 mg/L are advantageous for AD (Dewil

et al., 2008). When the ammonia concentration is between 200 and 1000 mg/L, no antagonistic effect is observed. However, inhibition is evident between 1500 and 3000 mg/L at higher pH levels and complete inhibition cannot be avoided when the ammonia concentration is above 3000 mg/L at any pH (Rajagopal et al., 2013).

Sulfate is a common component of many industrial wastewaters and its presence is associated with another type of inhibition. In anaerobic reactors, sulfate is reduced to sulfide by the sulfate reducing bacteria (SRB). Two stages of inhibition exist because of sulfate reduction. Primary inhibition is due to competition for common organic and inorganic substrates from SRB, which suppresses methane production. Secondary inhibition results from the toxicity of sulfide to various bacteria groups (Chen et al., 2007).

Heavy metals can also have an inhibitory effect on the AD process. These compounds can be present in significant concentrations in municipal sewage and sludge. The heavy metals identified to be of particular concern include chromium, iron, cobalt, copper, zinc, cadmium, and nickel. A distinguishing feature of heavy metals is that, unlike many other toxic substances, they are not biodegradable and can accumulate to potentially toxic concentrations (Chen et al., 2007). Many studies in the literature reported that heavy metal toxicity is one of the major causes of digester upset or failure.

Biogas production and composition

Monitoring the amount and composition of the biogas is essential for controlling the anaerobic digestion process's stability. Biogas production and composition are constant when the reactor is operating under stable conditions. A decrease in overall biogas production and an increase in CO_2 percentage may indicate inhibition phenomena affecting the methanogenic bacteria due, for instance, to volatile fatty acids' accumulation. As a result, the analysis of biogas production and percentage composition should always be associated with the control of parameters such as volatile fatty acid concentration and the alkalinity of the medium. It can be observed that in the presence of high OLR, the percentage of CO_2 tends to increase, as well as VFA concentrations (Cecchi et al., 2005).

2.2. *Co-digestion*

Anaerobic digestion has been applied traditionally as a single substrate, single-purpose treatment process and is commonly used in municipal, industrial, and agricultural treatment facilities (Metcalf

& Eddy I AECOM, 2014). Currently, mono-digestion systems are used by many AD plants (Karki et al., 2021) (i.e., AD systems using one feedstock). However, AD of single substrates (mono-digestion) presents some drawbacks linked to substrate properties. For instance, wastewater sludge in quite diluted, limiting the OLR; in fact, most municipal wastewater treatment plants have reported an excess digestion capacity of 15 to 30% (Metcalf & Eddy I AECOM, 2014). Animal manures have low organic loadings and high N concentrations, which may inhibit methanogens. The organic fraction of municipal solid waste (OFMSW) contains extraneous materials as well as a relatively high concentration of heavy metals. Crops and agro-industrial wastes are seasonal substrates, which might lack N, and slaughterhouse wastes (SHW), which are high proteinaceous substances, can result in the generation of toxic compounds such as ammonia (NH_3), a potential inhibitor of methanogenic activity.

Most of these problems can be solved by the addition of a co-substrate in what has been recently called anaerobic co-digestion (AcoD) (Mata-Alvarez et al., 2014).

Anaerobic co-digestion provides an opportunity to overcome the drawbacks of mono-digestion by simultaneously digesting two or more feedstocks. Blending organic substrates can result in synergistic, antagonistic, or neutral effects based upon degradation efficiency and methane production, which can be higher, less, or equal to those found when each material is digested alone (Metcalf & Eddy I AECOM, 2014). The major benefits of co-digestion include enhanced system stability and methane yield through the synergistic effects of promoting a more versatile and robust microbial community (Mata-Alvarez et al., 2014), better nutrient balance (proper carbon-to-nitrogen (C/N) ratio and supplementation of trace elements) and dilution of toxic compounds including heavy metals (Xie et al., 2018), improved buffering capacity (Bolzonella et al., 2006), and safe and better quality digestate for agricultural applications.

Despite the numerous advantages of co-digestion, many researchers have encountered difficulties in performing co-digestion, which has occasionally resulted in system upset, mainly due to inappropriate substrate blending and operating conditions (Chow et al., 2020).

2.2.1. Factors influencing Co-Digestion performance

As previously stated, AD is a process that is significantly influenced by multiple factors. These parameters, which affect the functioning of anaerobic digesters and the feasibility of co-digestion, need sufficient control to prevent reactor failure. A few of the major influences that greatly affect digester performance in co-digestion are mixing, co-substrate mixing ratio, nutrient balance,

operating temperature, organic loading rates (OLR), and hydraulic retention time (HRT) in the digester (Chow et al., 2020).

2.2.2. Co-feedstocks for AcoD

Co-substrates are broadly classified as carbohydrate-rich, protein-rich, and lipid-rich organic materials (Xie et al., 2018), and their selection is strictly related to the need to counterbalance nutrient insufficiency in the main substrate as well as to reduce the toxic and inhibiting effects of substances present above threshold levels.

Food waste is a substrate rich in sugars with high biodegradability and suitable C/N ratio (Chow et al., 2020).

A major drawback of food waste mono-digestion is the rapid hydrolysis rate, resulting in pH drops due to VFA accumulation. However, food waste is usually considered as an attractive option for AcoD due to its high biogas potential.

Hence, co-digestion of food waste with recalcitrant feedstocks, such as lignocellulosic biomass, can help reducing the accumulation of VFA and slowing the rate of hydrolysis.

It has also been reported that co-digesting food waste with cattle manure or sewage sludge provides an additional source of alkalinity and micronutrients. However, ammonia inhibition caused by free ammonia nitrogen (FAN) is one of the major concerns for co-digestion with these waste streams. Therefore, it is crucial to select suitable co-substrate combinations based on FAN and VFA accumulation for effective digestion (Karki et al., 2021).

Co-digestion of sewage sludge with rapidly biodegradable feedstocks with a higher C/N ratio (such as OFMSW) has resulted in improved specific methane yield (BMP), provided supplemental alkalinity and trace elements, and diluted pathogens and heavy metals present in sewage sludge (Mata-Alvarez et al., 2014). For instance, Bolzonella et al. (2006) observed a two-fold increase in SMY when sewage sludge was co-digested with the organic fraction of municipal solid wastes compared to sewage sludge mono-digestion.

Fat, oil, and grease (FOG) waste are also reported as co-feedstocks as they provide a high-energy source. Indeed, lipids have the highest biochemical methane potential (BMP) compared to carbohydrates and proteins (Elalami et al., 2019), and their blending with sewage sludge may improve specific methane production compared to sewage sludge mono-digestion.

However, the accumulation of long-chain fatty acids (LCFAs), which are produced during lipids' breaking down, and foaming are the main issues with FOG co-feedstocks (Karki et al., 2021).

The main characteristics of manures are frequently related to high nitrogen content, as they are protein-rich materials, and the presence of easily formed sulphur, ammonia, and hydrogen sulphide gases. Because of the lower C/N ratio, mono-digestion of animal manure often leads to ammonia toxicity and subsequent process instability, thus inhibiting methane production. One of the most effective methods to prevent such toxicity is co-digestion with carbon-rich feedstocks.

One of the most significant benefit of using animal manure as a co-substrate is its high buffering capacity against potential accumulation of VFA (Karki et al., 2021). Furthermore, because of its high nutrient concentration, it is a suitable co-feedstock for the main substrate, which has a low nutrient content, such as sewage sludge (Chow et al., 2020).

2.2.3. Applications

Currently, the treatment and disposal of MSW still poses a significant problem in both small and large towns. Although food waste is potentially an appealing material for biogas production, many anaerobic digesters have reported unstable operation and even process cessation when food waste is treated as the mono-substrate (Borowski et al., 2018).

It was also reported that most digestion installations working at WWTPs are underloaded and oversized. These facilities may be able to process with their existing digester capacity a wide range of organic material thus increasing their biogas production (Metcalf & Eddy I AECOM, 2014).

As suggested by many studies, co-digestion of sludge and food waste presents many technological and economic opportunities.

For instance, Borowski et al. (2018) performed anaerobic mesophilic (35 °C) co-digestion of food waste (FW) with municipal sewage sludge (MSS). The test was conducted in a reactor with a working volume of 50 L operated in semi-continuous conditions. The C/N ratio below 10, which is far from the optimal range of 15-30, was not taken into account in this study.

Food waste was mixed with sewage sludge in a proportion of 70:30 based on TS content; a similar mixture composition was also demonstrated to have the best stability and efficiency in previous reports.

At the start-up, the reactor was filled with inoculum (anaerobically digested municipal sewage sludge) and then operated at an SRT of 25 days during the entire experimental period. The co-digestion of

food waste with sewage sludge was performed with an OLR of 2.40 kgVS/m^3/d. Simultaneously, a MSS mono-digestion was carried out in a second reactor with the same characteristics.

In the first reactor (R1), the specific methane production (BMP) was 449 mLCH$_4$/gVS$_{fed}$, with a VS reduction of 64%; several authors, who reported similar methane yields from full-scale digester or during laboratory batch tests, observed similar findings. In the second reactor (R2), where MSS mono-digestion was performed, a specific methane production of 288 mLCH$_4$/gVS$_{fed}$ and a VS reduction of 45% were achieved. As expected, co-digestion showed a BMP and a VS reduction significantly higher than the corresponding values obtained for sewage sludge.

Animal manure is another attractive substrate, which was investigated for overcoming the challenges due to process inhibition during mono-digestion of food waste.

An interesting case of such an approach is that of Chuenchart et al. (2020), who evaluated the performance of bench-scale thermophilic (55°C) anaerobic mono and co-digestion of food waste with chicken manure. In this study the effect of organic loading rates (OLR) during mono and co-digestion were investigated, and the performance of the anaerobic systems was evaluated in terms of stability, productivity and efficiency at steady state. BMP tests found the optimal C/N ratio to be 20, and a mixing ratio (FW:CM) of 70:30 (based on VS content) was adopted according to previous studies. The tests were conducted in a CSTR with a working volume of 60 L. The feedstock was fed for both mono and co-digestion at the organic loading rates of 1, 2, 3 and 4 kgVS/m^3/d.

Food waste mono-digestion posed challenges due to process inhibition owing to VFA accumulation at higher organic loading rate (>3 kgVS/m^3/d). To overcome this challenge, chicken manure was co-digested with food waste for synergistic effect in anaerobic system, which resulted in improved performance throughout the experimental period.

During the co-digestion, specific methane yields tended to decrease when the loading rate was increased; BMPs of 795, 666, 601, and 655 mLCH$_4$/gVS$_{fed}$ were obtained at OLRs of 1, 2, 3, and 4 kgVS/m^3/d, respectively. The pH value during co-digestion was maintained higher than 7, even when the OLR was higher than 3 kgVS/m^3/d, unlike in mono-digestion where it decreased to sub-optimal conditions and led to process failure. The authors hypothesized that this failure could be due to acidification in the system, which led to methanogenic inhibition. FOS/TAC higher than the optimum range also indicated the overloading of the system. The stability of the process during co-digestion was also monitored through the FOS/TAC parameter, whose value indicated the higher capacity of loading for the anaerobic system due to alkalinity from ammonia in chicken manure and nutrient balance by C/N adjustment in the feedstock. The percentage increase of specific methane yields in

co-digestion compared with mono-digestion was found to be 33.2, 10.4, 12.1 and 89.9% at OLR of 1, 2, 3, and 4 kgVS/m^3/d, respectively.

2.2.4. Kinetic modelling of Co-Digestion

Various conventional mono-digestion models, such as first-order, logistic, modified Gompertz, cone, etc., have been tested to examine the kinetics of co-digestion in batch studies. However, these models have not succeeded in properly fitting methane or biogas production kinetics in co-digestion.

In batch tests, biogas production during co-digestion of complex organics typically exhibits two peaks. The readily biodegradable fraction of the combined feedstock is responsible for a first peak in the cumulative biogas production curve, whereas the second peak is characteristic of the slowly biodegradable portion.

One of the models that have been developed specifically to describe this phenomenon is the superimposed model (the modified Gompertz model coupled with the first-order kinetic model), which describes a two-peak methane production during co-digestion.

Some studies have also reported a two-phase model that separates the rate constant into two-equation terms (e.g., rapid and slow rate constants).

However, further development of these models to fit the cumulative BMP is essential to facilitate progress with the understanding of two-peak or two-phase anaerobic degradation due to different feedstock combinations. In addition, the application of more complex modelling such as Anaerobic Digestion Model No. 1 (ADM1) based on a two-phase kinetic model needs to be further investigated (Karki et al., 2021).

Anaerobic co-digestion is a promising waste management and resource recovery technique that promotes economic and environmental sustainability. However, further research should focus on developing new methods to characterize the complex feedstocks and quantify different hydrolysis rates, thus improving mathematical models to better predict the multitude of interactions, and studying the dynamics of the microbial community and the associated pathways in substrate degradation.

2.3. BMP tests

Biochemical methane potential (BMP) tests are a means of evaluating the anaerobic biodegradability and the methane potential of complex organic compounds. This test is carried out at laboratory scale and is based on batch assays where an aliquot of substrate is digested by an appropriate inoculum, typically taken from an active digester. The substrate and the anaerobic bacteria culture are stored in lab-scale batch reactors, which are kept at a constant temperature of either 35 °C or 55 °C for about 30 days while being constantly mixed (Filer et al., 2019).

The BMP is the maximum amount of methane that can be recovered from a substrate per mass of substrate organic matter expressed as volatile solids (VS) or chemical oxygen demand (COD). Therefore, providing optimal conditions for the AD process is crucial in order to achieve the highest possible degree of degradation. For instance, this includes using inoculum from a well-functioning digester, selecting a suitable inoculum-to-substrate ratio (ISR) to prevent over- or under-loading of the process, maintaining an appropriate and constant temperature along with gentle mixing, and removing oxygen from the headspace before incubation.

Additionally, in order to avoid underestimation of the BMP due to incomplete degradation of slowly degradable substrates, tests must continue until the methane production rate is very low (Kock et al., 2020).

Related to the BMP is the anaerobic biodegradability of a substrate. It is obtained by dividing the experimental BMP by a corresponding theoretical value (Kock et al., 2020), which is obtained from the chemical ratio of 1 gCOD = 0.35 mLCH$_4$ at standard temperature and pressure conditions (Filer et al., 2019).

According to a realistic estimate of anaerobic biodegradability, even if the organic material is completely anaerobically biodegradable, only around 90% of it will be converted into methane because about 10% will be used to produce microbial biomass.

The information gathered from batch tests has been found to reasonably predict the full-scale behavior. Kock et al. (2020) have stressed the importance of BMP tests, as kinetic parameters estimated from BMP tests, such as the hydrolysis constant, allow for a qualitative evaluation of the process kinetics.

Furthermore, different components of full-scale anaerobic digestion systems, such as digester capacity and biogas capturing/conversion systems may be designed using the BMPs of the substrates to be digested and their specific OLRs. For example, Hooliger et al. (2017) found out that the methane

production calculated from BMPs of the digested substrates and their specific organic loads compared well with the methane production measured on site.

To date, there is yet a lack of standardized BMP testing procedure, resulting in a lack of comparable BMP values due to the differences in equipment, experimental conditions, and procedures (Filer et al., 2019).

Despite the fact that several detailed international and national guidelines for BMP tests exist, inter-laboratory tests frequently reveal high variability of BMPs values for the same substrate.

In order to reach an agreement on potential solutions to the issue of inconsistent BMP test results, a workshop was held in June 2015, in Leysin, Switzerland, that included researchers from 30 laboratories around the world. Some of the compulsory elements for the validation of BMP results that were defined are (Holliger et al., 2016):

- all tests must be carried out in triplicate;
- besides the BMP of the substrate, blank essays (background methane production from the inoculum) and positive controls must be carried out;
- the duration of the BMP tests should not be fixed in advance, but should only be terminated when daily methane production during three consecutive days is <1% of the accumulated volume of methane;
- the BMP is expressed as the volume of dry methane gas under standard conditions per mass of volatile solids added, with the unit $NLCH_4$/kg VS;
- the BMP of the substrate and the positive control is determined by subtracting the methane production of the blanks from the gross methane production of the substrate/positive control.

2.3.1. Recommendations to obtain validated BMP test results

According to the compulsory elements mentioned above, recommendations should be made in order to increase the probability of obtaining validated and reproducible BMP test results.

Factors that strongly influence the outcome of BMP tests are:

- Inoculum. It should be collected from an operating anaerobic digester that is digesting complex organic materials and is at steady-state at the time of sampling. This results in a highly varied microbial population able to digest a wide range of organic compounds. The BMP test temperature is usually the same as the inoculum digester's working temperature (Holliger et al., 2016). It is often advised to use an inoculum that has already been acclimated

to the substrate, since a differently sourced inoculum might result in different substrate biodegradability and incorrect results due to diverse bacterial populations and substrate adaptation (Filer et al., 2019). Quality checks that can be carried out are analysis of pH, volatile fatty acids (VFA), ammonium, and alkalinity. The pH should always be measured before setting up a BMP test, and the other parameters can be analyzed on a less regular basis if the inoculum source is always the same. Indicative values for operational parameters of the digester providing an inoculum of good quality are indicated in Table 2. 1. Another quality check is to test its activity (biomass activity tests) with various standard substrates such as glucose, acetate, butyrate, etc. (Holliger et al., 2016). Lastly, the inoculum should have a low endogenous methane production, meaning that little residual substrate that can still be transformed into biogas should be present. The most common recommendation is to pre-incubate the inoculum for 1 to 5 days at 35 °C in order to degas and reduce the impact of its methane production (Filer et al., 2019).

Table 2. 1 - Recommended inoculum conditions for BMP tests (Holliger et al., 2016)

Parameter	Recommended range	Units
pH	7 - 8.5	-
VFA	< 1	gCH_3COOH/L
NH_4^+	< 2.5	$gN\text{-}NH_4/L$
Alkalinity	> 3	$gCaCO_3/L$

- Substrate. The substrate samples to be tested must be as representative as possible of the substrate to be digested at full scale and the sample preparation should be minimal in order to avoid alteration of its properties and digestibility. All particles must be no larger than 10 mm in any dimension (diameter, length). To accomplish this, the substrate sample can be sieved to separate the fraction >10 mm, which can then be ground and re-mixed with the fraction < 10 mm. Substrate samples should be used as fresh as possible. They can be stored at 4 °C, but only for two to five days. TS and VS are compulsory parameters for substrate as well as inoculum analysis. Substrate properties such as pH, VFA, Total Kjeldahl Nitrogen,

ammonium, and alkalinity should all be measured, since they may be used to assess possible inhibition issues during BMP tests (Holliger et al., 2016).

- Test setup. The volume of the batch reactors depends on the homogeneity of the substrate. Smaller volumes (125–500 mL) can be used for homogenous substrates, while large volumes (500 to 2000 mL) are more appropriate for heterogeneous substrates. While the substrate bottle is filled with water, nutrients, substrate and inoculum, in the blank no substrate is added in order to provide the background methane generation from the organic material in the inoculum. Control bottles can also be set up; they are filled with inoculum, the control substrate, and nutrients. For test and statistical analysis reproducibility, all groups should be done in triplicate (Filer et al., 2019).

- VS content and ISR. A total VS concentration of 20 to 60 gVS/L is usually recommended, and the amount of VS added by the inoculum should be the same in all batches. The ISR, the ratio of VS from the inoculum to VS from the substrate, is a key parameter of BMP tests. In order to minimize acidification or inhibition problems, an ISR between 2 and 4 is recommended. For easily biodegradable substrates, which easily lead to VFA buildup, an ISR greater than or equal to 4 should be set. A lower ISR can be applied when dealing with less degradable substrates (Holliger et al., 2016).

- Incubation conditions. Temperature can influence the growth rate and metabolism of microorganisms, but also affects factors such as gas transfer rates and chemical equilibria (Filer et al., 2019). BMP tests can be carried out under either mesophilic or thermophilic conditions, whose typical temperatures are 37 °C and 55 °C, respectively. The vessels should be incubated in a temperature-controlled environment with maximum variations of ±2 °C (Holliger et al., 2016). Mixing is another key parameter that influences the distribution of microorganisms, nutrients, substrate, alkalinity, prevents sedimentation of particulate material, and keeps the temperature distribution uniform inside the digester. Static incubation without any mixing should be avoided, as it can lead to inhibition due to toxic by-product accumulation (Filer et al., 2019).

2.3.2. Models describing methane production kinetics in batch AD

As previously stated, the data from BMP essays, which are frequently supplied as final values of substrate methane yields, lack a common baseline for comparison.

However, the methane production curves obtained from these studies provide additional relevant information on substrate degradation kinetics that is rarely used.

A basic comprehension of the kinetics of the biogas process could be the first step toward a consolidation of assay methodologies (Brulè et al., 2014).

The models that describe the kinetics of methane production in batch anaerobic digestion are generally derived from Monod kinetics. This kinetics accounts for a saturation effect. Under certain conditions, saturation effects may be neglected, and the Monod equation can be simplified to a first-order kinetics and used to design simpler models. In these models, the variable monitored would not necessarily be the rate of bacterial growth, but rather the kinetics of substrate degradation or product formation (Brulè et al., 2014).

The first-order model assumes the rate of substrate utilization to be proportional to the amount of substrate available in the medium:

$$r = k \cdot S_t$$

(2. 12)

Where:

- k is the first-order kinetics constant;
- S_t is the amount of undegraded substrate remaining at time t.

By integrating along time, an exponential equation is obtained, which gives the undegraded substrate at time t (S_t):

$$S_t = S \cdot e^{-kt}$$

(2. 13)

Where:

- S is the total amount of degradable substrate;
- k is the first-order kinetics constant;
- t is the time after experiment start-up.

If the product formation kinetics is applied to batch anaerobic digestion, the cumulated methane produced can be expressed as:

$$M_t = BMP \cdot (1 - e^{-kt})$$

(2. 14)

42

From an experimental point of view, BMP represents the ultimate methane yield, i.e., the cumulated methane yield at t = ∞.

2.4. *Anaerobic digestion model (ADM1)*

The Anaerobic Digestion Model No. 1 (ADM1) is the most widely recognized and popular mathematical model for anaerobic digestion processes.

The generic Anaerobic Digestion Model No. 1 was developed by the IWA Task Group for Mathematical Modelling of Anaerobic Digestion in response to the need for a standard model (Batstone et al., 2002), providing a common basis for further model development and comparisons of different studies.

In its original version, the model describes the dynamics of 7 biomass groups, 12 soluble compounds, 5 particulate compounds, interrelated by 19 biochemical kinetic processes, 7 physicochemical equilibrium processes, and 3 gas-liquid mass transfer processes.

The main issue with such a structured model is the large number of parameters and, therefore, the related identifiability problem (Poggio et al., 2015).

2.4.1. *Reaction system*

An anaerobic digester has a complex reaction system with numerous sequential and parallel steps. Two major categories of reactions can be distinguished:

- Biochemical reactions;
- Physico-chemical reactions.

Biochemical processes

These reactions are generally catalyzed by intracellular or extracellular enzymes and deal with biologically available organic material. In ADM1, extracellular steps (disintegration and hydrolysis) are assumed to be first-order, while intracellular reactions are described by Monod-type substrate-based uptake (acidogenesis, acetogenesis and methanogenesis). Biochemical reactions are described as substrate uptake and not as biomass growth. Biomass growth is implicit in substrate uptake, since they are related through a yield coefficient (Poggio et al., 2015). The death of biomass is described by first-order kinetics, and dead biomass is maintained in the system as a composite particulate

material. In the model, inhibition functions include pH (all groups), hydrogen (acetogenic groups), and free ammonia (aceticlastic methanogens) (Batstone et al., 2002). The biochemical processes considered in ADM1 are represented in Figure 2. 1.
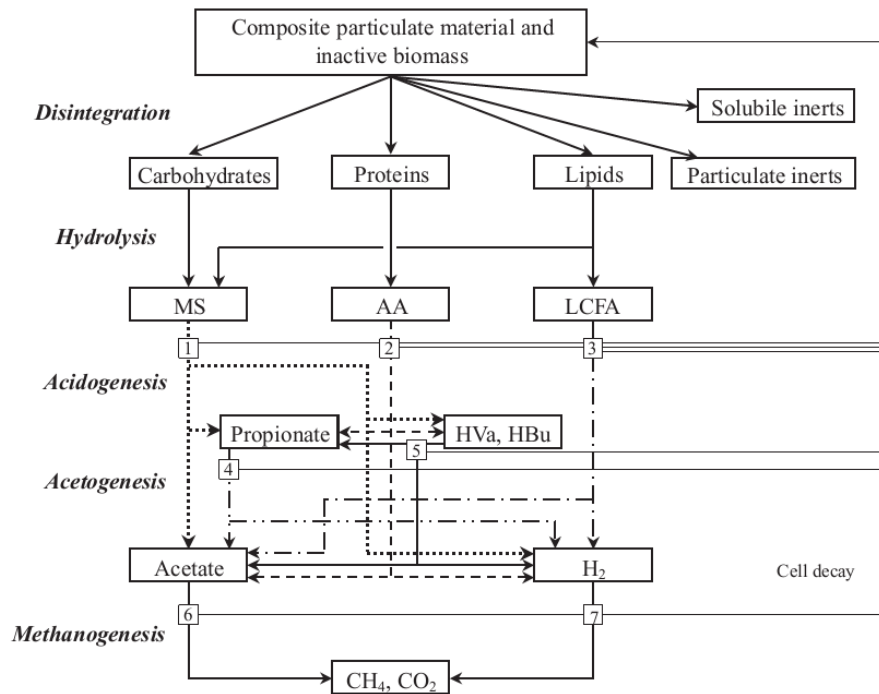
Figure 2. 1 - ADM1 including biochemical processes: acidogenesis from sugars (1), acidogenesis from amino acids (2), acetogenesis from LCFA (3), acetogenesis from propionate (4), acetogenesis from butyrate and valerate (5), aceticlastic methanogenesis (6) and hydrogenotrophic methanogenesis (7) (Batstone et al., 2002).

As shown in Figure 2. 1, the biochemical reaction pathway includes:

- an extracellular disintegration step converting composite particulate matter into carbohydrates, lipids and proteins;
- an extracellular enzymatic hydrolysis step converting the degradation products into their chemical building blocks, i.e. monosaccharides (MS), long chain fatty acids (LCFA) and amino acids (AA);
- acidogenesis or fermentation of the building blocks into hydrogen, acetate and volatile fatty acids (VFA), i.e. propionate, butyrate and valerate;
- acetogenesis of VFA to acetate;
- aceticlastic and hydrogenotrophic methanogenesis.

Additionally, the death of biomass is taken into account (Ramíres-Rivas, 2013).

In order to address these mechanisms, the model employs both soluble (expressed by a capital "S") and particulate components (represented by a capital "X"). All these terms are quantified in terms of

their COD. In addition, the model addresses inorganic carbon species (CO_2 and HCO_3^-) and nitrogenous species (NH_4^+ and NH_3), which are represented in terms of their molar concentrations.

In ADM1, the Petersen matrix is often employed to represent biochemical reactions. In this matrix, biological kinetic rate expressions and stoichiometric coefficients are shown (APPENDIX A).

The matrix can be modified by adding a new state variable and any associated stoichiometric and kinetic parameters when, for instance, the substrate contains a particular component whose degradation dynamics is of interest (Poggio et al., 2015).

Physico-chemical reactions

These reactions are not biologically mediated and involve ion association/dissociation in the liquid phase and gas-liquid mass transfer. Precipitation is not covered in the ADM1. The physico-chemical system is very important when modelling anaerobic systems because:

- it allows expressing biological inhibition factors (e.g. inhibition caused by pH, free acids and bases, etc.);
- major performance variables such as gas flow and carbonate alkalinity are dependent on the correct estimation of physico-chemical transformations.

2.4.2. *ADM1 limitations*

Although ADM1 does represent a better model structure with respect to simpler models, the first idea was to develop a tool for general modelling of AD, leaving the opportunity to implement the model for specific applications. The idea of process and component inclusion was to maximize applicability while maintaining a reasonably simple model structure (Batstone et al., 2002).

For instance, one of the ADM1 basic version's limitations is glucose fermentation modelling. The ADM1 considers glucose as the model monomer for fermentation. Acetate, propionate and butyrate have been considered as the only fermentation products, given the possibility to analyze them simultaneously in GC analysis and their different downstream degradation paths. Other fermentation products, such as ethanol and lactate, have been omitted in the original formulation of ADM1, as their concentration as fermentation intermediates is usually low in most anaerobic digesters (Poggio et al., 2015).

With a better understanding of the digester's metabolic pathways, users would be able to predict system performance, manipulate systems towards new products, and increase yields. Monitoring

different intermediate levels and learning how they affect AD, including inhibitory effects, could be a beneficial supplement to current optimization strategies. (Hunter et al., 2020).

Metabolic pathways of glucose fermentation

Out of all the four phases of AD, the acidogenic phase is the most crucial for deciding the metabolic pathway of biomass conversion (Zhou et al., 2018). Indeed, multiple distinct pathways coexist in the digester, and the dominant pathway changes depending on the conditions, influencing VFA production and distribution. (Zhou et al., 2018).

Fermentation products are predominantly produced from the metabolic intermediate pyruvate. Pyruvate is the primary intermediate resulting from the initial carbohydrate oxidation step (Hoelzle, 2016). Pyruvate can be converted into a variety of products including formate, acetate, propionate, butyrate, ethanol, propanol, butanol, H_2, and CO_2 (Chen et al., 2013) (Figure 2. 2).

Figure 2. 2 - Metabolic pathways of acidogenic fermentation. (AET, acetate-ethanol type fermentation; ABE, acetone-butanol-ethanol; PTF, propionate-type fermentation; BTF, butyrate-type fermentation; MAF, mixed-acids fermentation; LTF, lactate-type fermentation) (Zhou et al., 2018).

The amount of pyruvate sent to each pathway is determined by the substrate, environmental conditions, and strain characteristics. According to the end product, acidogenic metabolic pathways may be categorized as acetate-ethanol type, propionate-type, butyrate-type, mixed-acid, and lactate-type metabolic pathway (Zhou et al., 2018).

46

Acetate-ethanol fermentation (AEF) is a metabolic pathway that produces acetate (CH_3COOH) and ethanol (CH_3CH_2COOH). Acetate can be obtained not only from pyruvate through the acetyl-CoA pathway, but also from the syntrophic oxidation of ethanol or longer chain fatty acids like propionate and butyrate (Zhou et al., 2018).

$$C_6H_{12}O_6 + 2H_2O \rightarrow 2CH_3COOH + 2CO_2 + 4H_2$$

(2. 15)

$$CH_3CH_2COOH + 2H_2O \rightarrow CH_3COOH + CO_2 + 3H_2$$

(2. 16)

$$CH_3CH_2CH_2COOH + 2H_2O \rightarrow 2CH_3COOH + 2H_2$$

(2. 17)

$$CH_3CH_2OH + 2H_2O \rightarrow CH_3COOH + 2H_2$$

(2. 18)
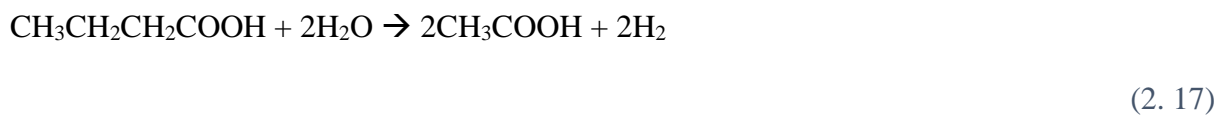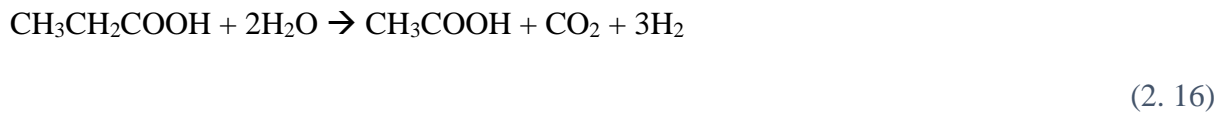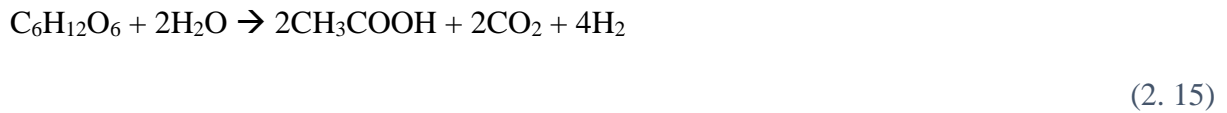
Ethanol is another common product of glucose or other organic materials fermentation (Zhou et al., 2018).

$$C_6H_{12}O_6 + H_2O \rightarrow CH_3CH_2OH + CH_3COOH + 2H_2 + 2\ CO_2$$

(2. 19)
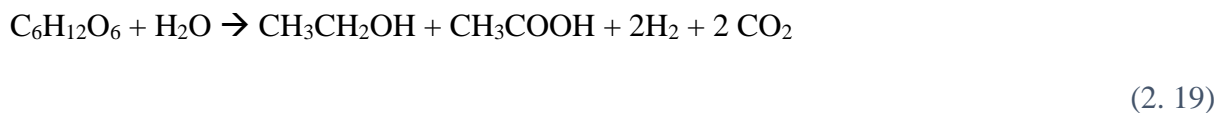
Ethanol is usually obtained through a two-step process of pyruvate decarboxylation, which generates acetaldehyde, followed by acetaldehyde reduction, resulting in ethanol synthesis. However, some bacteria convert pyruvate to ethanol through a three-step process, including the production of acetyl-CoA and acetaldehyde as intermediates (Zhou et al., 2018). Parameters in the digester, such as substrate type, inoculum, pH, temperature, configuration, organic loading rate (OLR), hydraulic retention time (HRT), operational modes, and headspace H_2 pressure, are all important factors in acetate production (Zhou et al., 2018). Feedstock composition influences the distribution of acetate and ethanol through AEF. For instance, a larger carbohydrate content in the feedstock encourages the production of acetate (Shin and Youn, 2005). The acidogenic metabolic pathway shift is always influenced by pH. The literature studies revealed that ethanol production increased as the pH value dropped below 5.5 (Ren et al., 1997; Rodriguez et al., 2006). The ethanol-type fermentation is characterized by a simultaneous production of acetic acid and unionized ethanol (Ren et al., 1997). Fang and Liu (2002) also reported that increased pH from 4 to 7 could lead to an increase in acetate production while decreasing butyrate production, but in the pH range of 6.5–7.0, both acetate and

butyrate production became equally abundant. Ethanol production could be enhanced under certain conditions, such as increased H_2 partial pressure. However, ethanol accumulation in the digester would be toxic to the microorganisms (Zhou et al., 2018). Some Clostridium species can produce acetone and butanol from glucose during the ethanol production process, which is known as acetone-butanol-ethanol (ABE) fermentation (Zhou et al., 2018).

$$C_6H_{12}O_6 + H_2O \rightarrow CH_3COCH_3 + 4H_2 + 3CO_2$$

(2. 20)

$$C_6H_{12}O_6 \rightarrow 2CH_3CH_2OH + 2CO_2$$

(2. 21)

$$C_6H_{12}O_6 \rightarrow CH_3CH_2CH_2\ CH_2OH + H_2O + 2CO_2$$

(2. 22)
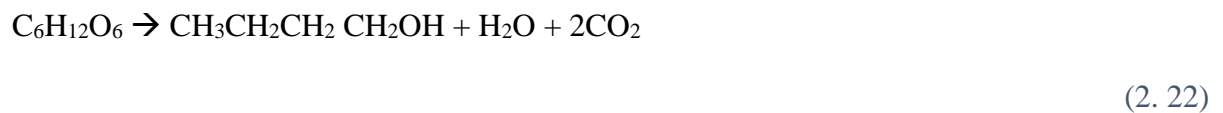
Solvent biosynthesis follows the same metabolic pathway from glucose to acetyl-CoA, but then diverges into distinct processes.

Biphasic fermentation is commonly performed by solvent-producing bacteria. Organic acids are produced and stored in the first phase; as the pH lowers in the second phase, solvents become the predominant products. The accumulation of acids and a drop in pH usually encourage the production of solvents (Zhou et al., 2018).

Propionate-type fermentation is an acidogenic metabolic pathway with propionate as the main product (PTF).

$$C_6H_{12}O_6 + 2H_2 \rightarrow 2CH_3CH_2COOH + 2H_2$$

(2. 23)

$$3C_6H_{12}O_6 \rightarrow 4CH_3CH_2COOH + 2CH_3COOH + 2CO_2 + 2H_2O$$

(2. 24)
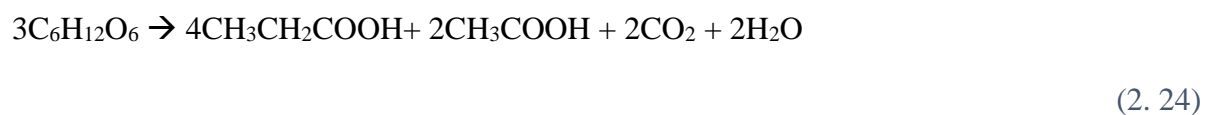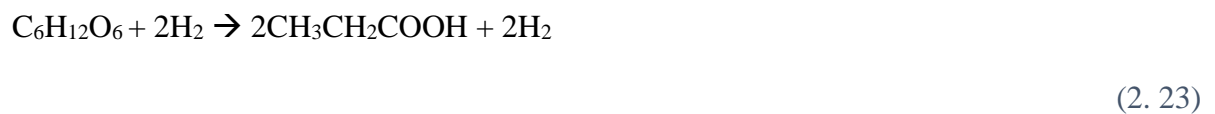
Propionate is obtained in two ways (Figure 2. 2). In the first pathway, propionate is produced by pyruvate reduction, which results in the formation of lactate as intermediate. Lactate production catalyzed by lactate dehydrogenase is followed by lactate reduction to propionate in presence of propionate dehydrogenase. The transcarboxylase cycle, which produces propionate through a series of intermediates such as oxaloacetate, succinate, fumarate, and propionyl CoA, is the second pathway for propionate production (Zhou et al., 2018).

There are many factors, which influence propionate production, including pH, inoculum type, and product inhibition (Yadav et al., 2021). Reported pH values of 4.0-4.5 have been shown to favor acidogenic propionate production (Wang et al., 2014). The typical byproducts of the propionate-type metabolic pathway are acetate and CO_2, which could further reduce the carbon substrate for propionate synthesis (Jin and Yang, 1998).

Butyrate ($CH_3CH_2CH_2COOH$) and acetate are the major products of the butyrate-forming pathway, and H_2 is always produced as a by-product.

Metabolic reactions for butyrate production from glucose are:

$$C_6H_{12}O_6 \rightarrow CH_3CH_2CH_2COOH + 2CO_2 + 2H_2$$

(2. 25)

$$4C_6H_{12}O_6 \rightarrow 8H_2 + 8CO_2 + 2CH_3COOH + 3CH_3CH_2CH_2COOH$$

(2. 26)
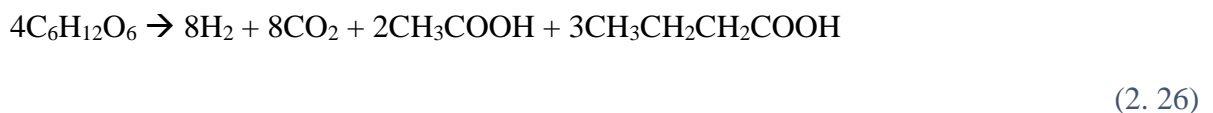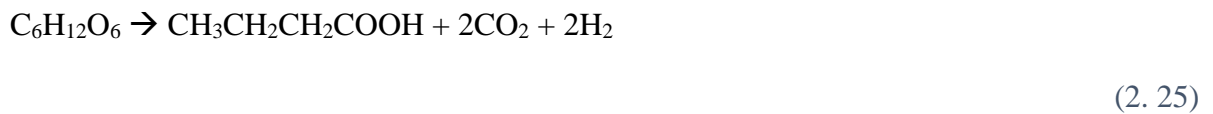
Butyrate type metabolic pathways produce butyrate by reduction and decarboxylation of pyruvate with the consumption of acetate via acetyl-CoA, acetoacetyl-CoA, 3-hydroxybutryl-CoA, crotonyl-CoA and butyryl-CoA (Zhou et al., 2018). The optimal pH for butyrate generation from mixed acid fermentation has been reported to be between 6 and 6.5 (Lee et al., 2014), with thermophilic (55 °C) being the best temperature (Zhou et al., 2018).

In mixed-acid fermentation (MAF), acidogenic bacteria could convert simple organic substrate (such as glucose) to a mixture of acetate, propionate, butyrate, and valerate, etc., equally distributed, with the possibility of biogas formation (CO_2 and H_2).

$$\text{Glucose} \rightarrow \text{acetate} + \text{propionate} + \text{butyrate} + \text{valerate} + CO_2 + H_2$$

(2. 27)
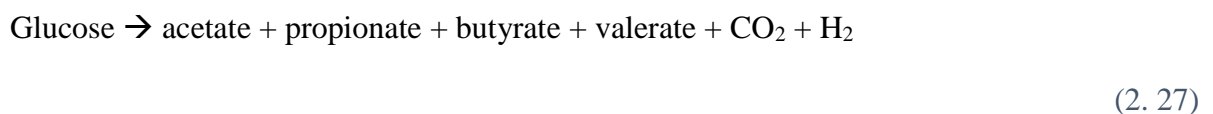
Various factors, such as the concentration and characteristics of the substrates, pH and redox potential can affect the abundance of individual components in mixed acids (Zhou et al., 2018). Zhu et al. (2009) reported how pH influences the composition of the VFA's mixture. For instance, low pH (<4.5) leads to the production of acetate, butyrate and ethanol as the primary products, while a pH of >6.5 would increase the ethanol production and decrease acid formation. Furthermore, the distribution of these metabolic products is influenced by the kind of inoculum used (Zhou et al., 2018).

Lactate-type fermentation (LTF) is a metabolic route for producing lactic acid from glucose or other organic molecules. The pyruvate produced by glycolysis is converted to lactate by lactate dehydrogenase. According to the products, lactate-producing mechanism can be classified into two types of fermentation, homolactate fermentation in which one mole of glucose is converted to two moles of lactic acid:

$$C_6H_{12}O_6 \rightarrow 2CH_3CH(OH)COOH$$

(2. 28)

and heterolactate fermentation in which one mole of lactic acid is produced along with other co-products such as CO_2, ethanol and/or acetic acid (Castillo Martinez et al., 2013):

$$C_6H_{12}O_6 \rightarrow CH_3CH(OH)COOH + CO_2 + CH_3CH_2OH$$

(2. 29)

$$C_6H_{12}O_6 \rightarrow CH_3CH(OH)COOH + CO_2 + CH_3COOH$$

(2. 30)
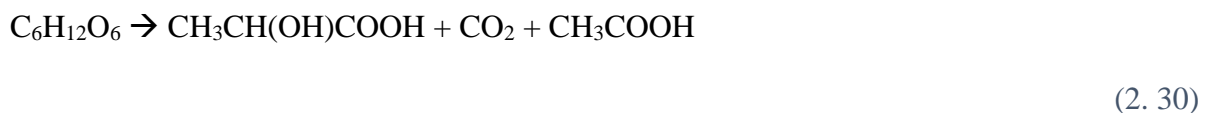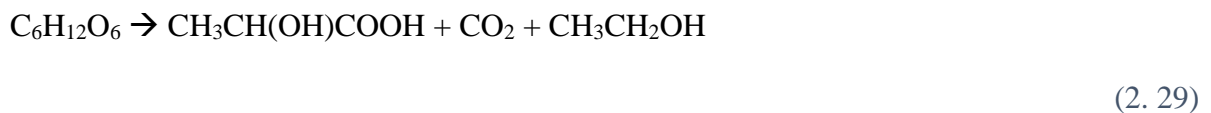
Glucose fermentation modelling

ADM1 and the majority of existing models of anaerobic digestion take into account conversion processes with fixed stoichiometry (Kleerebezem and van Loosdrecht, 2006). Indeed, in many studies of carbohydrate acidogenesis in ADM1, the recommended stoichiometric coefficient values from the technical report of IWA have been employed. These coefficients are based on the assumption that all the products of carbohydrate acidogenesis are produced in constant proportions; because of this incorrect assumption, they did not adequately reproduce the experimental results. Many of these models employ kinetic-based approaches to fit the experimental behavior and have inherited their structure from the ASM models' family. The latter were originally developed for aerobic systems whose processes are more clearly kinetically controlled, provide high-energy yields, and proceed far from thermodynamic equilibrium.

Anaerobic processes, however, as opposed to aerobic processes, provide low energy yields and their conversions can proceed very close to thermodynamic equilibrium. This suggests that anaerobic processes may be controlled thermodynamically rather than kinetically (Rodriguez et al., 2006).

Rodriguez et al. (2006) and Zhang et al. (2013) used this approach with moderate success for modelling product formation in anaerobic carbohydrate fermentation. These models, known as

bioenergetics-based models, are based on thermodynamics constraints on the process, limiting the possible reactions that may occur in the system and on the assumption that microbial populations tend to maximize growth. This is a key hypothesis that allows for the connection of the reaction stoichiometry in the process with the maximization of biomass growth. As this relationship is established, a variable stoichiometry capable of describing variations in catabolic yields of products when operating conditions vary is possible (Gonzalez-Cabaleiro, PhD thesis, 2015).

As already pointed out, the carbohydrate fermentation stage generates a wide spectrum of products, and variations in environmental conditions influence the type and distribution of fermentation products produced. More than 20 years ago, Mosey (1983) already stressed the importance of a more realistic approach, which would include a regulation function that changes the relative yield depending on influential environmental factors (principally pH and H_2 concentration). For instance, a low hydrogen concentration is expected to promote hydrogen-rich processes such as acetate formation, whereas a low pH is expected to boost ethanol production. In this regard, Rodriguez et al. (2006) updated the ADM1 with variable stoichiometric coefficients for glucose fermentation, based on the Gibbs free energy variations of the different fermentative pathways. First, all the COD state variables of the ADM1 were redefined into molar units and the corresponding kinetic and stoichiometric parameter values properly adapted and a function changing dynamically the stoichiometry matrix was also implemented.

To keep the model as simple as possible, the stoichiometry change between butyrate and acetate was only considered. The values of the butyrate and acetate catabolic yields of glucose fermentation were made dependent on the hydrogen concentration and the reactor pH (Figure 2. 3), according to the predictions of a previously developed mixed culture fermentation (MCF) model based on thermodynamic considerations. The MCF model considers a virtual microorganism with the most common fermentation pathways and their bioenergetics, implemented in a metabolic network (Rodriguez et al., 2006).
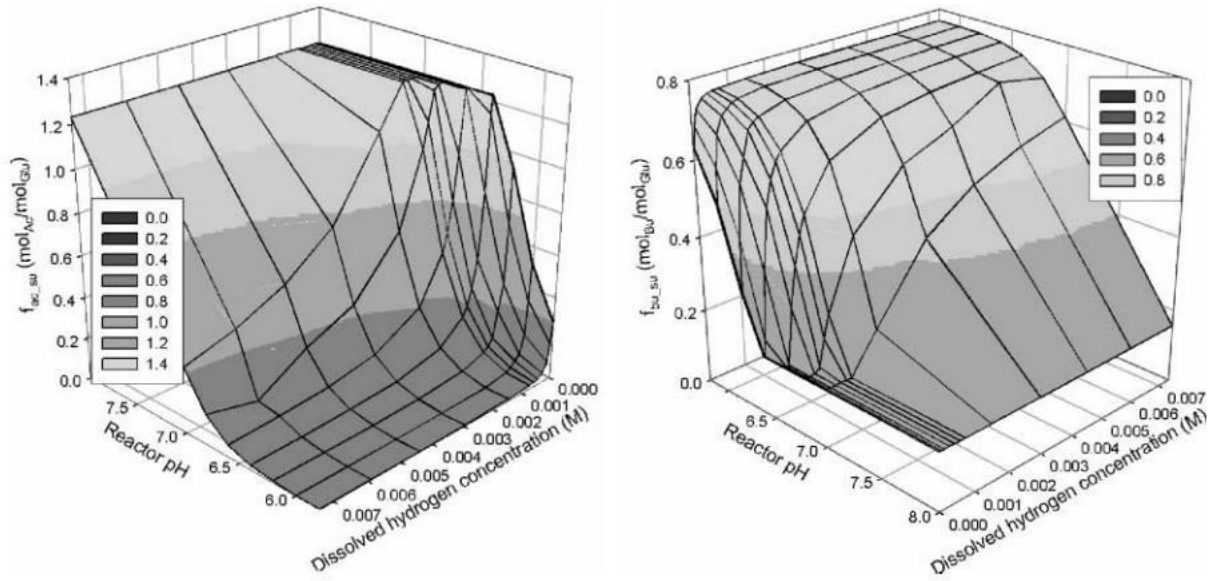
Figure 2. 3 - ADM1 catabolic stoichiometry coefficients of acetate and butyrate as a function of the dissolved hydrogen concentration and the reactor pH during mixed culture fermentation of glucose (Rodriguez et al., 2006).

To analyze the influence of the changing stoichiometry, the system was overloaded, resulting in a situation in which the stoichiometry varied depending on the functions implemented.

The fast dynamics observed showed that the acidogenic and acetogenic conversions remain close to thermodynamic equilibrium and are regulated thermodynamically rather than kinetically. Furthermore, in methanogenic reactors where both acidogenic and oxidative acetogens are present, the effect of shifting acidogenic stoichiometry is immediately compensated by acetogenic activity, according to ADM1 structure and parameters, and the effluent characteristics remain almost unchanged. Therefore, under steady-state conditions, no significant differences between fixed and variable stoichiometry were observed in methanogenic systems, while differences appeared in the effluent composition during the transient period, suggesting that this approach should be used when simulating an acidogenic reactor for bio hydrogen production or when a better estimation of the composition of the fermentation products is required.

Although these first energy-based models (Rodriguez et al., 2006; Zhang et al., 2013) made significant improvements over prior versions, they fell short of accurately predicting specific important shifts in product yields.

Gonzalez-Cabaleiro et al. (2015) and Regueira et al. (2018) identified the major limits of these models in the incompletely defined roles of electron carriers, the use of incomplete metabolic networks, and thus, an insufficiently comprehensive description of the reactions that take place and the specific modelling approaches used for the transport processes across the cell membrane.

52

Gonzalez-Cabaleiro et al. (2015) developed a model with an approach in line with that described by Rodriguez et al. (2006), considering one single microbial population in a CSTR capable of performing all the most important known metabolic fermentation pathways from glucose, that addressed and partially overcame the abovementioned limitations. The results showed that the mechanistic tool was able to successfully predict the observed shifts in major fermentation products (acetate, propionate, butyrate and ethanol) with external pH, including the shift between CO_2/H_2 and formate production.

Among the researchers who have recently addressed the stoichiometry variability of the glucose fermentation paths and used a similar approach, it is worth mentioning Shi et al. (2019). The objective of their study was to investigate and extend the applicability of ADM1 to butyric acid, propionic acid, mixed acid, and ethanol-type fermentative systems. For this purpose, the authors modified ADM1 using a variable stoichiometric approach, which predicts and controls the acidogenic process using the hydrogen partial pressure (p_{H2}) and pH. Since ADM1 does not foreseen for ethanol as a byproduct of glucose acidogenesis, its production and uptake rates were introduced into the model structure. The stoichiometry parameters derived from the p_{H2} were integrated into the biological kinetic rate expressions, which are shown in the Peterson matrix.

The control of butyric acid, propionic acid, and ethanol-type fermentation in a CSTR case study (Li et al., 2009) was used to validate the approach.

The results indicated that the p_{H2} and pH clearly influenced the stoichiometry parameters of carbohydrate fermentation in the CSTR case study. Although the VFA and ethanol concentrations showed great variations during the three types of fermentation, the deviation expressed as the SSE (sum of squared error) of the experimental data from the predicted data for butyric acid, propionic acid, acetic acid, and ethanol was small. This suggested that the developed model could be applied to simulate butyric acid, propionic acid, and ethanol-type fermentation in the CSTR.

2.5. *Biomass activity tests*

Biomass activity tests are a methodology for measuring the activity of the biomass by the addition of specific substrates (glucose, acetate, propionate, butyrate, etc.) to the biomass followed by the measurement of the gas production (de Zeeuw, 1984).

This methodology provides several opportunities, including the monitoring reactor performance, the characterization of biomass prior to its use as an inoculum for starting a new reactor, and thus its potential for that specific process. (Sørensen & Ahring, 1993). Volumetric or manometric methods,

which assess the volume of biogas produced and the pressure increase due to gas production respectively, can be employed to assess the activity of individual metabolic steps, such as glucose fermentation, providing that they are rate limiting the whole process (Rozzi & Remigi, 2004). The SMA (specific methanogenic activity) can generally be measured both as the specific rate of substrate consumption and the specific rate of CH_4 production, referred to either the total biomass (expressed as VSS) or the specific microbial population; it is quantified as the slope of the curve of substrate utilization or methane production (Rozzi & Remigi, 2004). Inhibition can be easily recognized by the patterns of the cumulated biogas production curves; two kind of patterns have been mostly reported when assessing activity.
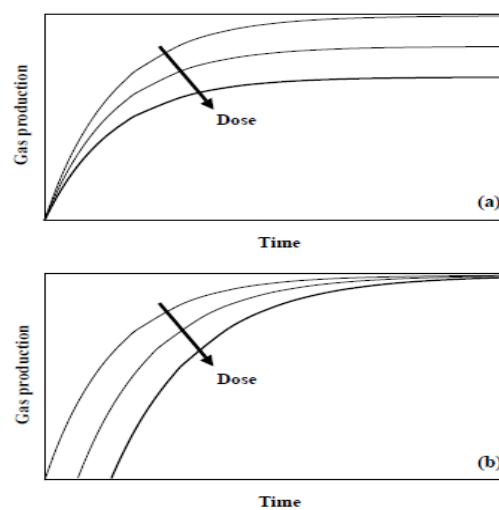
Figure 2. 4 - Possible toxicity patterns, detected at increasing doses of the inhibitory substance (from Young & Tabak, 1993): (a) absence of adaptation to the toxicant; (b) initial lag-phase, followed by acclimation to the toxicant.

Figure 2. 4 (a) represents the case where the inhibition increases as the substance increases, but no adaptation to the toxicant occurs, while Figure 2. 4 (b) shows a situation where inhibition occurs in the early stages, but a recover is shown when biomass adapts to the toxic compound by recovering its base activity (Young & Tabak, 1993).

SMA tests can be highly influenced by some factors such as biomass concentration, substrate type (acetic acid or a mixture of acetic, propionic and butyric acids) and concentration, and mixing intensity. In this respect, Cho et al. (2005) reported that COD added to SMA test reactors should be high enough to provide kinetic saturation ($S \gg K_S$) and optimum biomass concentrations should be employed in order to minimize the time required for the reaction to go to completion. Mixing is another critical parameter; when the mixing rate is too low, substrate mass transfer limits can occur (Cho et al., 2005).

Activity tests should be carried out in conditions that closely reflect the environment (e.g., pH, temperature, and mixing) of a given system. They generally require 10–25 days, even though shorter times have been reported.

As already pointed out by Sørensen & Ahring (1993), Hussain & Dubey (2017) have reiterated the importance of the SMA test as a tool that can be used to outline the operating conditions for anaerobic digesters and better understand the system performance and stability. For instance, determination of SMA can be useful for estimation of initial organic loading rate during the start-up period of a reactor, but it also provides information about the development of sludge in further phases. Indeed, a change in sludge activity (SMA) may be an indication that inhibition or accumulation of slowly degradable or even no biodegradable organic substrate is occurring.

In this regard, Zhang Bo et al. (2006) found that in a methanogenic reactor, high concentrations of lactic acid negatively affect the performance of methanogenesis due to propionic accumulation in the effluent. Indeed, lactic acid is usually considered the precursor of propionic acid during the anaerobic digestion process. The results were obtained by comparing the two reactors fed with lactic acid and glucose, respectively. The reactor fed with lactic acid had a higher effluent COD concentration, a lower biogas productivity rate and a higher effluent VFA concentration with an increase in the COD loading rate. The authors observed an obvious decrease in the SMA when the COD loading was increased.

According to Sørensen & Ahring (1993), the necessity for a standardized protocol activity test has been often pointed out in the literature, but no such test has been developed to date.

Chapter 3:   MATERIALS AND METHOD

3.1. Experimentation

3.1.1. Pilot plant configuration

The experimental phase of this study was carried out with a pilot plant consisting of 5 parts: pre-storage tank, anaerobic digester, hydraulic seals, gas meter and control panel. The plant as a whole was designed and built by the company Seam Engineering aimed at carrying out the research and development project called "PerFORM WATER 2030".

The pre-storage tank had a working volume of 25 L and was located on a balance and enveloped for its entire height by a silicone tube connected to a chiller capable of circulating water at a specific temperature. The temperature was maintained at 4 °C in the storage tank, although it increased to 8–10 °C in the hottest months. Inside the tank, there was a mixer (ARGO LAB AM40-D) to avoid sludge settling. The mixer could work at a speed range of 50–2200 rpm. It was set to work at 210 rpm.

The storage tank was connected via a pump to the pilot digester (NETZSCH CY15/15). The pump could operate with a flow rate range of 5-20 L/h. The flow rate was set at about 14 L/h. Downstream from the pump, a three-way valve determined if the sludge was fed to the digester or sent back to the tank. The pump and the digester inlet valve were programmed to operate during the same time interval. Outside of this time frame, the pump was turned off and the valve was opened in the direction of the storage tank's return pipe. The digester had an overall volume of 77 L. Two hydraulic seals regulated the liquid working volume. The experimentation was carried out with a liquid volume of 51 L and a headspace of 26 L. The digester was equipped with a mechanical mixer operating at 104 rpm. It was also equipped with a heating system to maintain the temperature at 37±0.5 °C and a set of sensors capable of measuring pH, temperature, pressure, and RedOx potential in real time. Finally, the digester was equipped with a bottom purge valve and a side valve for digestate sampling.

The pilot plant was also equipped with a biogas flow meter. Specifically, BPC® µFlow, which is a compact standalone volumetric gas flow meter. The µFlow is a flow meter for ultralow gas flow detection. It provides a large detection range, with high linearity from 4 to 850 mL/h with a 2 mL flow cell. This makes it highly suitable for most lab- and small pilot-scale applications. The µFlow automatically normalizes gas flow and volume measurements with real-time temperature and pressure compensation. The volumes are normalized to 0 °C and 1 atm.

Since the instrument used to measure biogas production was slightly undersized to measure the actual biogas flow rate, some biogas was often lost due to instrument overflow. To reduce the risk of gas losses, two 2 L bottles, each containing 1 L of 3M NaOH solution, were located upstream of the biogas-reading instrument and used to reduce the volume of biogas reaching the instrument. Indeed, the 3M NaOH solution was used to precipitate the CO_2 in the biogas mixture. As a result, the biogas read by the device had 99 % methane except when the CO_2 absorption capacity was exhausted. It was therefore critical to replace the solution within the bottles every 5 days. The bottles were placed upstream of the biogas-reading instrument.

Finally, a programmable logic controller (PLC) was available for signals storage and operation of the main equipment. This could also be managed remotely and had the purpose of allowing the user to check the operating conditions of the system, as well as to feed up the digester (by acting on the three-way valve) and check for malfunctions.

Figure 3. 1 shows a scheme of the pilot plant.
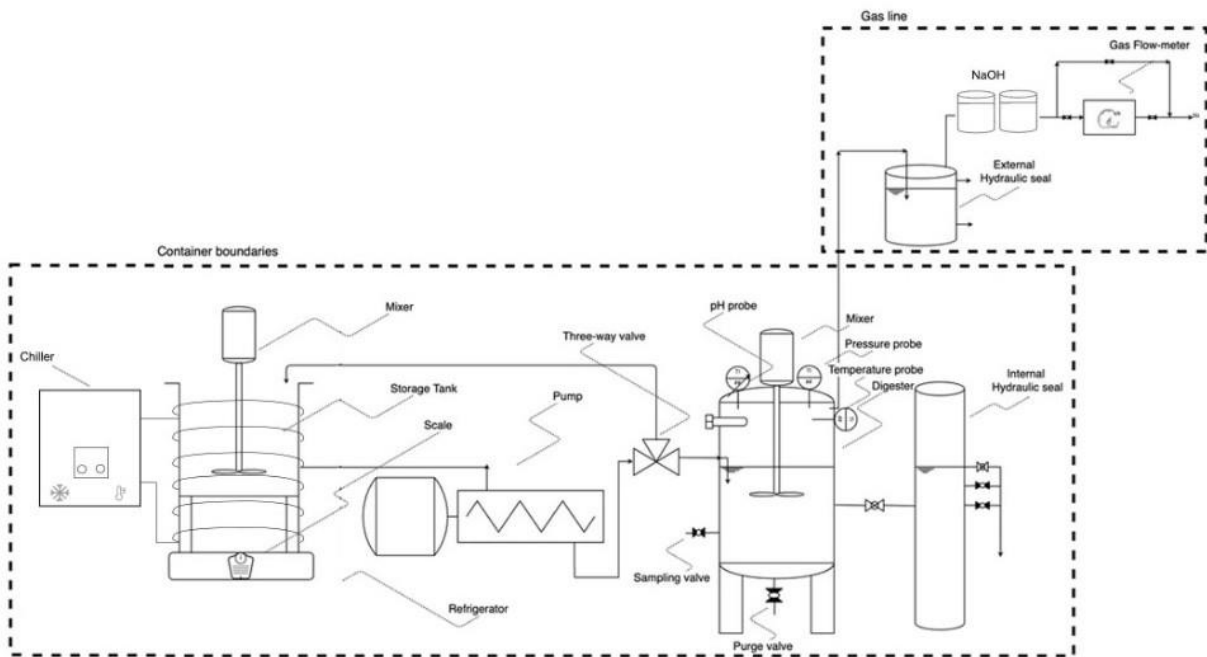
Figure 3. 1 - Scheme of the pilot plant.

Figure 3. 2 - Pictures of the anaerobic digester, the pump, the internal and external hydraulic seals and the container before the start-up.

3.1.2. Operating modes

The pilot plant was fed semi-continuously. In order to better mimic a continuous feeding, the PLC was set up to feed the digester for 2 minutes, during which time about 0.5 kg of sludge (or yogurt and sludge) were supplied to the reactor, 6 times per day (every 4 hours), for an overall daily feeding supply of 3 kg. The average OLR operated during mono-digestion of WS, where only sludge was fed, was 1.36 kgVS/m^3/d, but it was increased to a mean value of 1.67 kgVS/m^3/d, when AcoD of WS and yogurt was implemented. Concerning the hydraulic retention time (HRT), an average value of about 17.1 d was maintained throughout the whole period.

However, temporary deviations from the average values were observed due to occasional malfunctioning.

The liquid volume inside the reactor was significantly lowered from April 17 to April 22 due to a clogging and subsequent unblocking of the line connecting the digester to the internal hydraulic seal. The accident caused the pressure within the reactor to increase and then fall below the average value. The digester had to be re-inoculated following this event. From an operational point of view, the result was a decrease in hydraulic retention time and an increase in OLR compared to average values of mono-digestion.

Furthermore, due to a loss of biogas from the digester head, which resulted in an increase in liquid volume inside the digester and a drop in pressure, the feed flow rate was reduced from 7 to 18 May to avoid gas accumulation inside the container. As a result, as compared to the average situation of mono-digestion, higher HRT and lower OLR were observed.

3.1.3. Sampling and storage of digestate/feedstocks

The digestate used to inoculate the reactor and the waste sludge were collected from the full-scale WWTP of Peschiera Borromeo (Gruppo CAP-Amiacque). The WS was a pre-thickened sludge, the majority of which came from the primary sedimenter and a variable amount ranging from 15% to 20% from a biofiltration process (secondary sludge). The sludge was collected on a weekly basis and then stored in a fridge below 4 °C until its use.

Every week, the pre-storage tank was refilled with enough feedstock in order to prevent the minimum capacity from being met. This alert was necessary to guarantee that the digester was regularly fed and to prevent the pump from running dry. Before carrying out this operation, it was generally necessary to clean the mixer inside the tank from sludge biofilm.

Also, the digestate was taken every week through the appropriate sampling valve. During this operation, the biogas outlet valve directed to the external hydraulic seal and the connection valve to the internal hydraulic seal were always closed. This precaution was taken to prevent the water from the external hydraulic seal or the digestate contained in the internal hydraulic seal from entering the digester. These two valves were therefore reopened only after the pressure inside the digester had been re-established at 35 mbar, generally following the feeding of the sludge.

The yogurt used as co-substrate during co-digestion was previously supplied by Gruppo Cap and collected from the WWTP of Sesto San Giovanni. The yogurt packages that had been improperly

preserved or expired belonged to well-known brands and were labelled with the carbohydrate, protein, and lipid content. The yogurt was stored in a refrigerator at a temperature below 4 °C.

3.1.4. Monitoring plan

In order to identify the characteristics of digestate and sludge, a simplified monitoring plan and a comprehensive monitoring plan for the digestate sampled from the pilot plant digester were carried out every week on Monday and Friday, respectively, and a comprehensive monitoring plan for the sludge collected from the WWTP was carried out every week on Thursday.

The digestate simplified plan included the following analyses:

- pH and alkalinity;
- VFA;
- Volatile (VS) and total solids (TS);
- Ammonium (NH_4^+);
- Phosphate (PO_4^{3-}).

The following analyses were included in the WS and digestate comprehensive plans:

- pH and alkalinity;
- VFA;
- Volatile (VS) and total solids (TS);
- Ammonium (NH_4^+);
- Phosphate (PO_4^{3-});
- Total COD;
- Total TKN;
- Total carbohydrates and proteins;
- Particulate lipids;
- VS and TS of soluble and particulate solids;
- BMP tests.

BMP tests were performed approximately every 3 weeks. Overall, 3 BMP tests were performed during the first phase of mono-digestion and 2 BMP tests during the second phase of co-digestion with yogurt.

Concerning yogurt, since it is a commercial product and therefore standardized, just one characterization was obtained at the start of the experimentation. The following analyses were carried out:

- pH and alkalinity;
- VFA;
- Volatile (VS) and total solids (TS);
- VS and TS of soluble and particulate solids;
- Total COD;
- Total TKN;
- Total carbohydrates and proteins;
- Particulate lipids;
- Soluble COD;
- Soluble carbohydrates and proteins;
- Ammonium (NH_4^+);
- Phosphate (PO_4^{3-});
- BMP tests.

The biogas was sampled every week through a gas-sampling bag directly from the pilot's gas line to study its composition.

3.1.5. Analytical methods

pH/alkalinity

The pH was directly measured in liquid samples by means of a portable multi-probe meter (Hach-Lange, HQ40d).

The alkalinity was determined in the A. Rozzi laboratory in Cremona. Total alkalinity (corresponding to TAC in German) was measured by means of the FOS/TAC instrument (Hach Lange BIOGAS Tritation Manager). Samples were always diluted 1:10 with deionized water. Then, titration was performed with Sulfuric acid (H_2SO_4) to pH 8.3 and 4.3.

Total alkalinity was calculated as the product of the volume of acid used to reach the pH end point, the normality of the acid and the conversion coefficient of Calcium carbonate ($CaCO_3$) to equivalent (50 $mgCaCO_3$/eq), divided by the volume of the sample.

Ammoniacal nitrogen

The ammoniacal nitrogen determination ($NH_3+NH_4^+$) was carried out on filtered samples at 0.45 μm and analyzed using the HACH-Lange colorimetric kit (LCK302 and LCK303).

Phosphate

The phosphate determination (PO_4^{3-}) was carried out on a filtered sample at 0.45 μm and analyzed using the HACH-Lange colorimetric kit (LCK348 and LCK350).

COD

The determinations of the total COD $\left(\frac{g_{COD}}{kg_{t.q.}}\right)$ were performed at the A. Rozzi laboratory according to Standard Methods 5220 (APHA 2005). Determinations of dissolved COD were carried out using HACH-Lange colorimetric kits on the soluble fraction.

Biogas

This analysis was carried out using the tool Inficon Micro GC fusion. The composition of the biogas was obtained in terms of methane, carbon dioxide, hydrogen, oxygen and nitrogen. Biogas sampling was carried out both upstream and downstream of the biogas-reading instrument.

Particulate lipids

The lipid analyses were conducted at the environmental engineering laboratory of Politecnico di Milano. Particulate lipids were measured. The samples were prepared by centrifugation for 15-30 minutes at 5000 rpm to separate the solid fraction from the liquid fraction. Samples were stored in the refrigerator at 4-6 °C after being acidified to pH 2 by concentrated H_2SO_4.

The analysis of the particulate lipids was carried out using the Soxhlet solvent extractor of Velp SER 148 shown in Figure 3. 3. The SER 148 can be used to separate a substance or a group of elements from solid and semi-solid samples according to the Randall technique (consisting of immersion, washing, and solvent recovery). The fast solubilization by hot solvent permits a considerable reduction of the extraction time (approximately 90 minutes). The extraction is made by immersion of the sample in the boiling solvent, followed by a rinsing phase with cold solvent.

The sample must be dried before it can be analyzed. This procedure was carried out using anhydrous sodium sulfate (Na_2SO_4). Specifically, about 20-25 g of anhydrous sodium sulfate is dosed on a sample of about 3-5 g. After the addition of Na_2SO_4, the sample has been stirred to a smooth paste and spread on the sides of the beaker to facilitate subsequent sample removal. It was let stand until solidification (15 to 30 min). Then, the solids were removed and grinded in a porcelain mortar into a powder. The powder was then added to a paper extraction thimble. In addition, the beaker and mortar were wiped with small pieces of filter paper moistened with n-hexane and added to the thimble. Then the thimble was covered with cotton wool. For each thimble, a SER 148 specific Velp beaker was filled with 60-70 mL of n-hexane (used as a solvent) and small glass beads. At the end of the procedure, oil and grease extracted are transferred to a 25 mL vial using n-hexane for precise measurement of their weight. Before being weighed, they were kept in an oven at 40 ° C for about 2 hours. A blank test was also carried out in which the paper extraction thimble is filled with small pieces of filter paper moistened with n-hexane and covered with cotton wool. The blank results are then subtracted from the tests.

Another important step in determining the relative mass of lipids is the extraction of hydrocarbons. These hydrocarbons must be isolated and quantified to obtain an exact measurement of the lipids. This is done using syringes containing florisil. If the solution of hydrocarbons and fatty materials in a non-polar solvent passes through florisil, the fatty acids are removed selectively from the solution. The materials that are not removed are defined as hydrocarbons.

Figure 3. 3 - Soxhlet solvent extractor VELP SER 148.

TKN

TKN (Total Kjeldahl Nitrogen) is defined by the sum of ammoniacal nitrogen and organic nitrogen present in a sludge $\left(\frac{mg_N}{kg_{t.q.}}\right)$. Its determination was carried out in the A. Rozzi laboratory according to ISO 5663-1984 Method.

VFA

In this analysis, 25 mL of fresh sample was stabilized with 1 mL of 3M NaOH solution, subsequently centrifuged, and filtered at 0.45 μm in San Giuliano Ovest laboratory. Then about 3-5 ml of stabilized sample was stored in the refrigerator below 6°C and analyzed for VFA at the A. Rozzi laboratory in Cremona.

In particular, the VFAs (Volatile Fatty Acids) were determined by quantifying each single volatile fatty acid (acetic, propionic, isobutyric, butyric, isovaleric and valeric) by gas chromatography, according to Standard Method n. 5560 (APHA, 2005). Specifically, a gas chromatograph (DANI Master GC) was used coupled to a flame ionization detector (FID Nukol fused silica).

Determination of the total content of carbohydrates and proteins

In order to determine the total content of carbohydrates (CH$_{tot}$) and proteins (PT$_{tot}$), the following pre-treatment procedure of the sludge sample was adopted, previously developed and selected at the A. Rozzi laboratory in Cremona. This procedure involves the following steps:

- freezing of about 30 mL of sample as it is;
- defrosting;
- sonication for 1h;
- dilution with deionized water (variable according to the type of analysis-proteins or carbohydrates-, in order to fall within the range of concentrations defined by the calibration line and the type of sample).

This is followed by the analysis of carbohydrates and proteins using Dubois and BCA methods directly on the diluted sample. These analyses were performed in duplicate for each collected sample.

The BCA (Bicinchoninic Acid) method was selected to determine the protein content. Concentrations are expressed in mg of Bovine Serum Albumin (BSA) equivalent per liter of solution and the kit provided by Thermo Fisher Scientific was used. The method involves the dosage of 2 ml of BCA

reagent and 0.1 ml of sample. The samples to be analyzed for proteins were incubated at 37 °C for 30 minutes, following the "standard" procedure. After cooling to room temperature, the absorbance at 562 nm was measured using a UV-VIS spectrophotometer. For the determination of the calibration curve, bovine serum albumin (BSA) was used as a standard. The range of validity is 20−2000 $\frac{mg_{BSA}}{L}$.

Carbohydrate content analysis was conducted using the Dubois colorimetric method using a 5% w/v solution of phenol and pure sulfuric acid (≥ 97%). The results are expressed in mg of glucose equivalent per liter of sample $\left(\frac{mg_{Glu}}{L}\right)$. Specifically, 1 mL of phenol solution is added to 1 mL of sample. Then 5 mL of H_2SO_4 is added and 10 minutes are allowed to pass. At this point, the sample can be mixed and allowed to cool down to room temperature for further 30 minutes. The absorbance reading at 490 nm is then carried out using a spectrophotometer. Glucose was used as a standard for the determination of the calibration curve. The validity range for the calibration curve is 0−200 $\frac{mg_{Glu}}{L}$.

Total and volatile solids

Total and volatile solids were determined in duplicate according to Standard Methods 2540 (APHA, 2005).

3.1.6. Batch essays

The apparatus used to perform these batch essays is the Nautilus Anaerotech model by Anaero Technologies, which is shown in Figure 3. 4. It includes 15 batch reactors, which are mixed through a gearbox using one motor to mix all reactors through stainless/silicone paddles. By immersion in a water bath with a tight water lid, the temperature is kept constant at 37 °C for all reactors, and evaporation is minimized. The reactor features a high volume of 1 L. Gas generation is measured using the liquid displacement method. The gas flow meter is a single Perspex block with 15 cells of 0.2 L and Perspex tumbling buckets of around 9 mL of gas volume. A spare cell is used for the automatic monitoring of temperature. The liquid in all cells is interconnected to maintain an equal head pressure in all reactors. The liquid used is a 3M NaOH solution in order to remove CO_2 from the gas. Each cell has a tumbling bucket with an active volume of around 9 mL (easily calibrated). The data is constantly monitored through an Arduino-based system that consists of an Arduino 2560 Mega microcontroller, which acts as the main controller for the data logger.
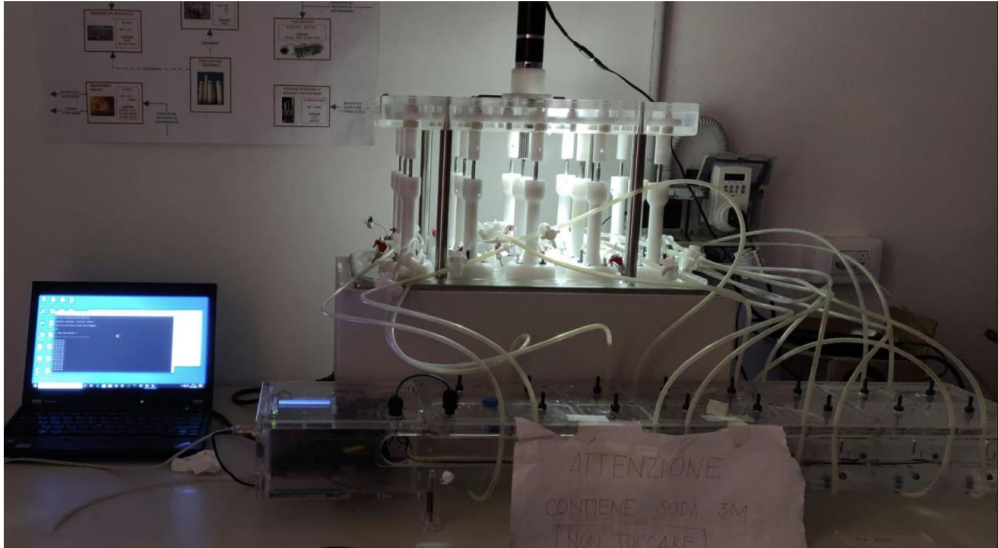
Figure 3. 4 - Nautilus Anaerotech model by Anaero technologies.

BMP tests

The following tests were carried out in duplicate:

- blank BMP test containing inoculum (degassed digestate), water and nutrients;
- sludge BMP test containing inoculum, sludge, water and nutrients;
- yogurt BMP test containing inoculum, yogurt, water and nutrients (only at the start of the experimentation);
- co-digestion BMP test containing both sludge and yogurt, inoculum, water and nutrients (only during the co-digestion phase).

A degassing phase of the inoculum was always carried out before running BMP tests. After sampling, the digestate was stored in a thermostat at 37 °C and left to degas for about 7 days. The BMP tests were prepared by dosing inoculum and substrate, as well as water and nutrients, into 1 L Anaerotech reactors. The tests were carried out with a working volume of 800 mL. The BMP tests of sludge, yogurt and co-digestion (sludge and yoghurt) were set up assuming a VS-based inoculum/substrate (I/S) ratio. Table 3. 1 shows the BMP tests performed and the relevant test conditions.

Table 3. 1 - Summary of BMP test conditions.

BMP test	Number of tests	Date	Inoculum dosed [g]	I/S ratio [$g_{VS,I}$/$g_{VS,s}$]	Y/S ratio [$g_{VS,yogurt}$/$g_{VS,sludge}$]
Blank	5	13/04/2022	550	-	-
		29/04/2022	530		
		25/05/2022	480		
		17/06/2022	500		
		06/07/2022	480		
Sludge	5	13/04/2022	550	3	-
		29/04/2022	530	2	
		25/05/2022	480	2.5	
		17/06/2022	500	2	
		06/07/2022	480	2	
Yogurt	1	13/04/2022	550	3	-
Co-digestion	2	17/06/2022	500	2	0.55
		06/07/2022	480	2	0.25

Three nutrient solutions were supplied to each BMP test for a total volume of 88 mL. APPENDIX G details the composition of various nutritional solutions. Finally, once the amount of inoculum and substrate to be dosed in the test was determined, the dilution water was calculated as the difference between a working volume of 0.8 L and the sum of the substrate, inoculum, and the nutrients volumes. The blank test was carried out by providing the same quantity of inoculum as the BMPs to be compared with. Also in this case, nutrients and a volume of water were added to get the working volume to 0.8 mL.

During the BMP setting process, the total solids in the batch were verified to ensure that the ST concentration was between 10 and 50 gTS/L.

Volatile and total solids of inoculum and substrates were measured for each test. In addition, the pH was measured at the beginning and at the end of the test.

BMP tests were only discontinued when the methane production increased by less than 1% of the cumulated volume for three straight days. According to this criterion, the tests lasted between 19 and 26 days.

Activity tests

Activity tests were carried out supplementing different substrates: acetate, glucose and propionate.

As opposed to BMPs, activity tests were performed using fresh inoculum obtained directly from the digester. The tests were always carried out in duplicate and the time required varied between 5 and 10 days, according to the same 1% term-criterion of BMP tests.

A 100 gCOD/L solution of acetate, glucose, and propionate was used for all activity tests.

In activity tests, several concentrations of substrate and inoculum were tested. Table 3. 2 summarizes each test's setup.

Table 3. 2 - Summary of biomass activity test conditions.

Biomass activity tests	Number of tests	Date	Inoculum concentration [$g_{vs,I}$/L]	Substrate concentration [g_{COD}/L]
Acetate	6	01/04/2022	6	0.5 2
		06/05/2022	7.5	2
		20/06/2022 29/06/2022 07/07/2022	8.25	0.5 1.5 3
Glucose	5	01/04/2022	6	2.5
		06/05/2022	7.5	3
		20/06/2022 06/07/2022 18/07/2022	8.25	2.5 0.5 3.5
Propionate	7	01/04/2022	6	0.5 1 2
		06/05/2022	7.5	1
		20/06/2022 29/06/2022 07/07/2022	8.25	0.5 2 3

In order to investigate potential inhibitions in glucose fermentation, activity tests were also performed using another approach. As opposed to activity tests performed in Nautilus Anaerotech, in these types of tests biogas production was not measured. In this approach, the activity test was carried out using 1 L bottle with a working volume of 800 mL placed in a thermostat, where the temperature was kept at 37 °C. The bottle was equipped with a sampling point and a biogas outlet.

Since previous results of glucose activity tests had shown a lag phase in the first 10 hours from the beginning of the trial, probably due to inhibition/adaptation, 5 mL samples were taken every 60–90 minutes for a total of 7-8 samplings, in order to examine the VFA composition. After sampling, 5 mL of water was injected into the bottle to keep constant the working volume. The same kind of test was also performed with propionate.

3.2. Modelling

3.2.1. Model implementation

Both the continuous reactor and the batch tests were modelled using the ADM1 according to the implementation described by Rosen and Jeppsson (2006). As a simulation tool, the OpenModelica platform was employed, and the DASSL (Differential/Algebraic System Solver) code was used for the numerical solution of the systems of differential/algebraic equations.

Initial values of the stoichiometric and kinetic parameters are the result of the previous modelling and calibration work carried out by Soderino and Nunziata (2021), which started adopting literature values (Rosen & Jeppsson, 2006) of the above mentioned parameters.
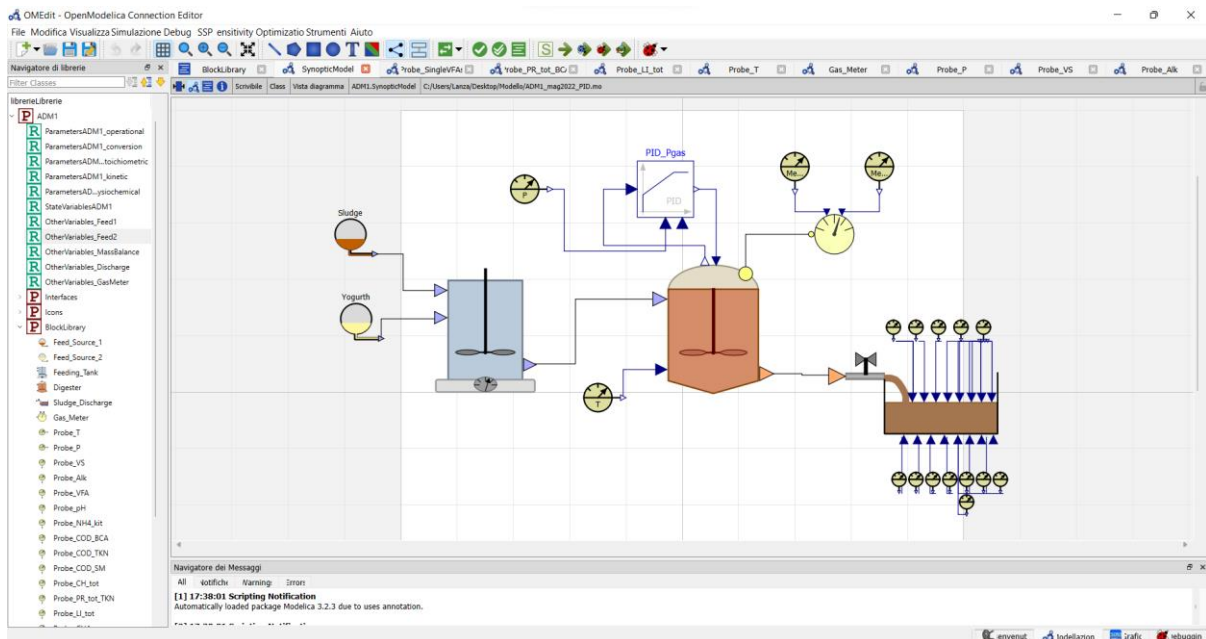
Figure 3. 5 - User interface of the OpenModelica platform.

The OpenModelica user interface is shown in Figure 3. 5. All variables and parameters were defined in the "Record" panels (R), whereas all equations characterizing the system were given in the "Package" panels (P) in accordance with Rosen and Jeppsson description (2006).

Starting from the Soderino and Nunziata setting of the model, some modifications were made.

Since the overpressure inside the reactor was almost steady, a fixed working volume associated with this overpressure was calculated and set in the operational "Record" panel.

The diagram representing the pilot plant system includes a storage tank, where sludge and yogurt inflow are mixed, a digester and a storage tank for the digestate. In addition to the already existing meters in the digestate storage tank, probes retrieving the simulated values of total carbohydrates, proteins, lipids, total COD, and single VFAs were introduced in order to compare experimental and simulated data. The validity of the model was further assessed by comparing simulated and experimental data on biogas composition and related CH_4 and CO_2 flow rates.

The batch tests (BMP and activity tests) were also simulated using the OpenModelica system. The digestate characterization derived from the pilot plant simulation was transferred to the batch tests' model. As concerns activity tests' simulation, the digestate was used as it was, while the BMP tests' simulation was carried out after the digestate was degassed using the same batch tests' model.

In the latest release of the models, different volume-specific liquid-gas transfer coefficients ($K_L a$) for methane, carbon dioxide and hydrogen were taken into account. They were calculated using their respective diffusivities, whose values were taken from the literature (Pauss et al., 1990), and the diffusivity and $K_L a$ of oxygen.

$$K_L a_{gas} = K_L a_{O2} \cdot \left(\frac{D_{gas}}{D_{O2}}\right)^{\frac{1}{2}}$$

(3. 1)

Where:

- $K_L a_{O2}$ is the volume-specific liquid-gas transfer coefficient for oxygen $\left[\frac{1}{d}\right]$;
- D_{O2} is the diffusivity of oxygen $\left[\frac{cm^2}{s}\right]$;
- D_{gas} is the diffusivity of a gas $\left[\frac{cm^2}{s}\right]$.

As concerns acetate and propionate uptake, the Haldane inhibition type was considered instead of the original Monod-type model.

$$r_S = k_m \cdot \frac{S}{(S + K_S + \frac{S^2}{K_{Hald}})} \cdot X \cdot I$$

(3. 2)

Where:

- K_{Hald} is the Haldane's inhibition constant for the specific degrading organisms $\left[\frac{kg}{m^3}\right]$;

- k_m is the maximum uptake rate for the specific degrading organisms $\left[\frac{1}{d}\right]$;

- I is the inhibition function;

- K_S is the half saturation constant for the specific degrading organisms $\left[\frac{kg}{m^3}\right]$;

- S is the substrate concentration $\left[\frac{kg}{m^3}\right]$;

- X is the biomass concentration $\left[\frac{kg}{m^3}\right]$.

3.2.2. Input state variables' determination

Sludge

One of the model's main issue to be addressed is the accurate and realistic identification of the model's input state variables. The identification of all individual parameters, as well as a valid analytical evaluation of all model input components, are neither simple nor practical.

For this reason, it was frequently necessary to make assumptions about data that could not be directly assessed and to neglect those that were considered irrelevant.

The concentration of the 7 biomasses ($X_{ac}, X_{pro}, X_{c4}, X_{h2}, X_{su}, X_{aa}, X_{fa}$) were considered as being negligible in the feeding substrates. As concerns sludge, the concentration of the two dissolved gases ($S_{ch4} \; and \; S_{h2}$) were taken from Rosen and Jeppsson (2006), while they were assumed as negligible for yogurt.

The base unit of measurement for all state variables is $\frac{g_{COD}}{L}$, except for those compounds such as inorganic carbon, inorganic nitrogen and ions, whose unit of measurement is expressed as $\frac{mol}{L}$.

The concentration of hydrogen ions $S_{h_{ion}}$ is calculated by means of the experimental value of the pH as:

$$S_{h_{ion}} = 10^{-pH}$$

(3. 3)

71

$$S_{oh_{ion}} = \frac{K_w}{S_{h_{ion}}}$$

$$(3.4)$$

The concentration of total inorganic nitrogen was calculated using the measured value of ammoniacal nitrogen in the samples:

$$S_{IN} = \frac{(TAN)_{measured} \left[\frac{mg_N}{L}\right]}{14 \left[\frac{g}{mol}\right] \cdot 1000}$$

$$(3.5)$$

The measured concentrations of the single volatile fatty acids were expressed in $\frac{mol}{L}$ through their molecular weight (S_{Ac}, S_{Pro}, S_{Bu} and S_{Va}).

By means of the acid-base equilibrium equations included in the ADM1, the following variables were estimated:

$$S_{nh4_{ion}} = \frac{S_{IN} \cdot S_{h_{ion}}}{K_{a,nh4} + S_{h_{ion}}} \left[\frac{mol}{L}\right]$$

$$(3.6)$$

$$S_{nh3} = S_{IN} - S_{nh4_{ion}} \left[\frac{mol}{L}\right]$$

$$(3.7)$$

$$S_{Ac_{ion}} = \frac{S_{Ac} \cdot K_{a,Ac}}{K_{a,Ac} + S_{h_{ion}}} \left[\frac{mol}{L}\right]$$

$$(3.8)$$

$$S_{Pro_{ion}} = \frac{S_{Pro} \cdot K_{a,Pro}}{K_{a,Pro} + S_{h_{ion}}} \left[\frac{mol}{L}\right]$$

$$(3.9)$$

$$S_{Bu_{ion}} = \frac{S_{Bu} \cdot K_{a,Bu}}{K_{a,Bu} + S_{h_{ion}}} \left[\frac{mol}{L}\right]$$

$$(3.10)$$

$$S_{Va_{ion}} = \frac{S_{Va} \cdot K_{a,Va}}{K_{a,Va} + S_{h_{ion}}} \left[\frac{mol}{L}\right]$$

(3. 11)

Conversion factors (kgCOD/kmol) were used in the model to convert the molar concentrations of S_{Ac}, S_{Pro}, S_{Bu} and S_{Va} to $\frac{g_{COD}}{L}$.

The concentration of bicarbonate ($S_{hco3_{ion}}$) was calculated as the difference between the measured alkalinity (expressed as $\frac{mol}{L}$) and the sum of the dissociate fractions of each VFA, the free ammonia concentration and the concentration of hydroxide ions:

$$S_{hco3_{ion}} = Alk - (S_{Ac_{ion}} + S_{Pro_{ion}} + S_{Bu_{ion}} + S_{Va_{ion}} + S_{nh3} + S_{oh_{ion}}) \left[\frac{mol}{L}\right]$$

(3. 12)

The concentration of bicarbonate was necessary in order to calculate the concentration of inorganic carbon (S_{IC}) according to the acid-base equilibrium, and the carbon dioxide concentration (S_{co2}) as the difference of the latter:

$$S_{IC} = S_{hco3_{ion}} \cdot \frac{S_{h_{ion}} + K_{a,co2}}{K_{a,co2}}$$

(3. 13)

$$S_{co2} = S_{IC} - S_{hco3_{ion}}$$

(3. 14)

The value of the net charge of all other ions ($S_{delta,ions}$) was calculated from the charge balance:

$$S_{delta,ions} = -S_{nh4_{ion}} - S_{h_{ion}} + S_{hco3_{ion}} + S_{oh_{ion}} + S_{Ac_{ion}} + S_{Pro_{ion}} + S_{Bu_{ion}} + S_{Va_{ion}}$$

(3. 15)

Total COD was calculated by adding the contributions of total carbohydrates, proteins, lipids, and all VFA species present in the sludge. Different conversion factors for determining COD were considered for influent and effluent carbohydrates, proteins and lipids, as shown in Table 3. 3.

Table 3. 3 - COD conversion factors for carbohydrates, proteins and lipids.

CH_CONV$_{IN}$	1.07	gCOD/gGlu	COD conversion factor for influent carbohydrates
PR_TKN_CONV_$_{IN}$	1.42	gCOD/gVS	COD conversion factor for influent proteins (TKN)
N_PR_CONV$_{IN}$	6.5	gVS/gN	Conversion factor influent proteins to N$_{org}$
LIP_CONV$_{IN}$	2.9	gCOD/gVS(lip)	COD conversion factor for influent lipids
CH_CONV$_{OUT}$	1.07	gCOD/gGlu	COD conversion factor for effluent carbohydrates
PR_TKN_CONV$_{OUT}$	1.42	gCOD/gVS	COD conversion factor for effluent proteins (TKN)
PR_BCA_ CONV$_{OUT}$	1.58	gCOD/gVS	COD conversion factor for effluent proteins (BCA)
N_PR_CONV$_{OUT}$	7.5	gVS/gN	Conversion factor effluent proteins to N$_{org}$
LIP_CONV$_{OUT}$	1.9	gCOD/gVS(lip)	COD conversion factor for effluent lipids

The COD associated with the particulate fraction of the substrate was calculated as the difference between the total COD and the COD of soluble volatile fatty acids.

$$COD_P = COD_{tot} - COD_{VFA}$$

(3. 16)

The COD relating to carbohydrates, proteins and lipids was assumed to be mainly associated to the particulate form.

Since the waste sludge was a mixture of primary (90% on VS base) and secondary sludge (10% on VS base), the 10% of the secondary sludge was assumed to enter the digester as complex particulate (X_C), while the remaining part (90% of primary sludge) as already disintegrated variables ($X_{ch}, X_{pr}, X_{li}, X_i$).

The concentration of substrate entering the digester in the aggregated form (X_C) was calculated as the product between the particulate fraction of substrate and the percentage of substrate not yet disintegrated:

$$X_C = COD_P \cdot \%_{aggr}$$

(3. 17)

The BMP value obtained for the total fraction of waste sludge was used in order to derive the inert particulate fraction (X_i) entering the digester, assuming that the soluble inert fraction (S_i) was considered as being negligible. It was also hypothesized that the percentage of COD used for cell growth during the BMP test was 8% of the total COD.

$$\%COD_{CH4} = \frac{BMP_{tot}\left[\frac{NmL_{CH4}}{gCOD}\right]}{350}$$

(3. 18)

From the percentage of the total COD converted into methane and that for cell growth, the percentage of total COD anaerobically undegradable was derived.

$$\%COD_{undegradable,sub} = 1 - \%COD_{CH4} - \%COD_{new,bio}$$

(3. 19)

The inert particulate fraction was computed as:

$$X_i = COD_{tot} \cdot \%_{undegradable,sub} \cdot (1 - \%_{aggr})$$

(3. 20)

The inert fraction was necessary in order to evaluate the concentration of carbohydrates, proteins and lipids associated to the degradable particulate COD.

$$COD_{P,degr} = COD_P - X_i$$

(3. 21)

$$X_{ch} = COD_{P,degr} \cdot \frac{C_{ch,tot}}{COD_P}$$

(3. 22)

$$X_{pr} = COD_{P,degr} \cdot \frac{C_{pr,tot}}{COD_P}$$

(3. 23)

$$X_{li} = COD_{P,degr} \cdot \frac{C_{li,tot}}{COD_P}$$

(3. 24)

Since the BCA method for quantifying proteins provided extremely high values that were inconsistent with total COD measurements, the protein concentration was determined using the TKN method. Protein concentration was calculated as the difference between the total TKN value (mgN/kg) and the ammoniacal nitrogen content (mgN/L) in the sludge sample.

$$C_{pr,tot} = TKN_{TOT} - NH_4^+$$

<div align="right">(3. 25)</div>

As already mentioned above, the concentrations of soluble carbohydrates, proteins and lipids (S_{su}, S_{aa}, S_{fa}) were assumed as negligible.

As concerns the substrate entering the digester in a complex form (X_C), the percentages of the fractions resulting from the disintegration of the composite were hypothesized $(f_{Xc,ch}, f_{Xc,pr}, f_{Xc,li}, f_{Xc,Xi}, f_{Xc,Si})$.

A scheme representing substrate fractionation used to determine the input variables is reported below (Figure 3. 6).
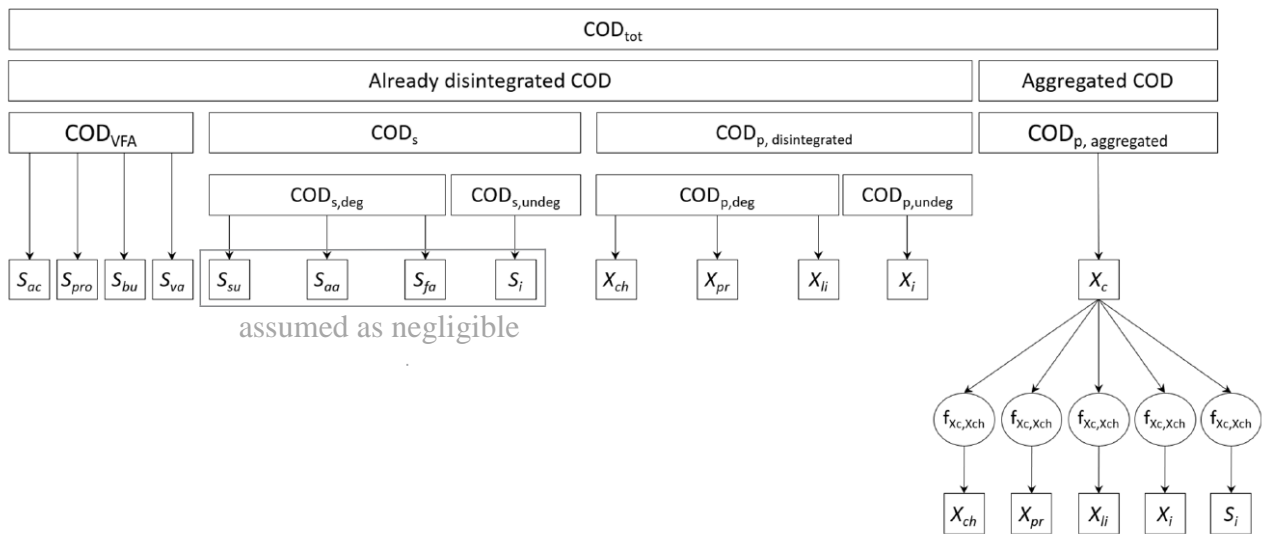
Figure 3. 6 - Input COD fractionation scheme

Yogurt

As concerns yogurt, the same characterization approach was used. As opposed to sludge, it was assumed that it was already disintegrated before it entered the digester $(X_C \cong 0)$ and it was completely degradable $(X_i = S_i \cong 0)$. In this case, analyses for determining the soluble concentrations of carbohydrates, proteins and lipids were carried out and their respective input state

variables (S_{su}, S_{aa}, S_{fa}) were implemented in the model using the COD conversion factors reported above.

3.2.3. Calibration

To take advantage of the synergy between batch and pilot-scale reactor results, kinetic parameters were calibrated iteratively in order to optimize batch and continuous tests simultaneously. As already pointed out, this iterative process consisted of using the characteristics of digestate provided by the pilot plant modelling as initial conditions for batch tests. The values of the kinetic parameters were identified by comparing the simulated methane production in these batch essays to the experimental one, such that the difference between the curves was minimized. Estimates of parameters were fed back into the pilot plant model to obtain more precise values for digestate state variables. This iterative procedure was carried on until no major changes were required.

A conceptual scheme of the iterative procedure is given below (Figure 3. 7).
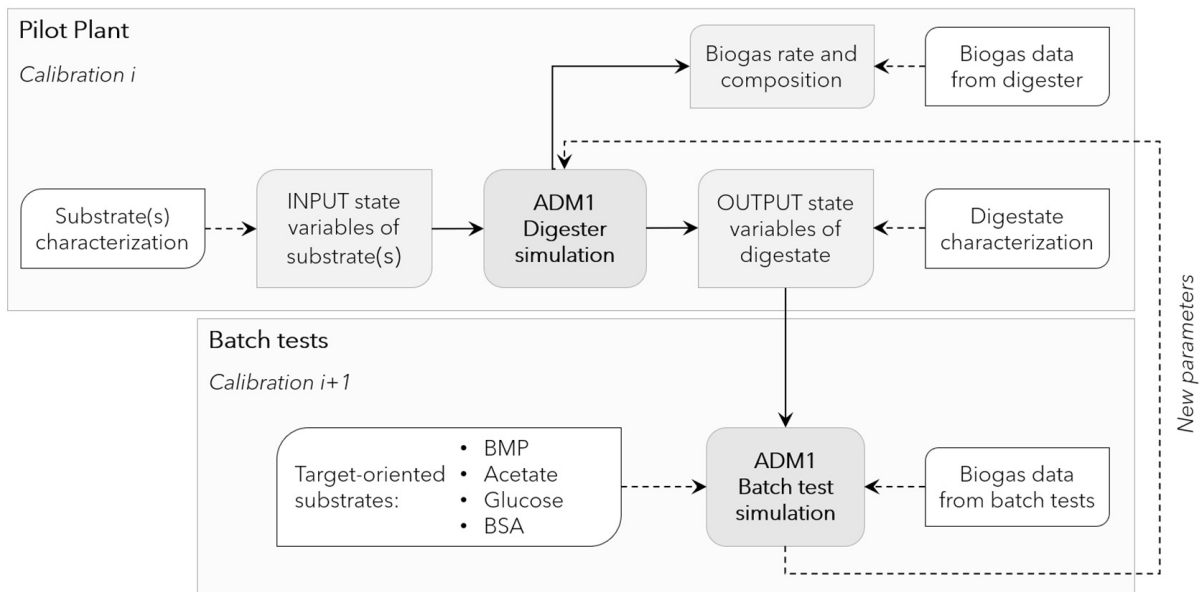
Figure 3. 7 - Schematic representation of the iterative process for the calibration of the ADM1 model.

3.2.4. Model performance

Model predictive accuracy was assessed through the modified Theil's Inequality Coefficient, TIC (Decostere at al. 2016) and the modified Mean Absolute Relative Error, MARE (Hauduc et al.,

2015) as reported in the equations (3. 26) and (3. 27):

$$TIC = \frac{\sqrt{\Sigma_i(y_{s,i} - y_{m,i})^2}}{\sqrt{\Sigma_i y_{s,i}^2} + \sqrt{\Sigma_i y_{m,i}^2}}$$

(3. 26)

$$MARE = \frac{1}{n} \cdot \sum_{i=1}^{n} \frac{|y_{m,i} - y_{s,i}|}{y_{m,i} + \varphi}$$

(3. 27)

Where:

- $y_{s,i}$ represents the value of the variable experimentally measured;
- $y_{m,i}$ represents the model estimated value;
- φ (0.1) is a small correction factor, which was applied to avoid division by zero.

Both criteria quantify the difference between model predictions and experimental values and normalize them according to the magnitude of the considered variable. TIC <0.3 represents a good simulation result. In general, for both criteria, the closer the value is to zero, the better the model performance.

Chapter 4: RESULTS & DISCUSSION

4.1. Sludge characterization

4.1.1. Analytical characterizations

In Table 4. 1, the results obtained from the analyses carried out on waste sludge samples are presented. Analyses were performed on the total, particulate (after centrifugation), and soluble (after centrifugation) fractions. The table shows the average and standard deviation values of the 11 sludge samples collected throughout the experimentation.

Table 4. 1 - Results of sludge characterization analyses.

Parameter	Unit	Average	Standard Deviation
Total Fraction			
pH	-	5.61	0.2
Alkalinity	$mgCaCO_3/L$	2613	338
TS	gTS/kg	30.7	4.4
VS	gVS/kg	21.9	3
Total COD	gCOD/kg	29.9	3.2
Total TKN	gN/kg	1.44	0.4
Total Carbohydrates	gGlu/kg	3.88	0.7
Total Proteins	gN/kg	1.41	0.4
BMP Total	$NmLCH_4/gVS$	318	20
Particulate Fraction			
Particulate Lipids	g/kgVS,p	180.3	17
Particulate Lipids	g/kgVS	174.0	17
TS - particulate fraction	gTS,p/kg,p	125.9	11
VS - particulate fraction	gVS,p/kg,p	90.2	8
Soluble Fraction			
VFA: acetic acid	mg/L	704	198
VFA: propionic acid	mg/L	216	44
VFA: iso-butyiric acid	mg/L	35	12
VFA: butyric acid	mg/L	53	20
VFA: iso-valeric acid	mg/L	23	13
VFA: valeric acid	mg/L	13	5
TS - soluble fraction	gTS,s/L	2.1	0.3
VS - soluble fraction	gVS,s/L	1	0.2
Ammoniacal nitrogen	mgN/L	72.1	22
Phosphate	mgP/L	31.2	6

A complete table of all individual values is given APPENDIX C.

The VFAs, pH, alkalinity, ammoniacal nitrogen and phosphate trends are represented in Figure 4. 1, Figure 4. 2 and Figure 4. 3, respectively.
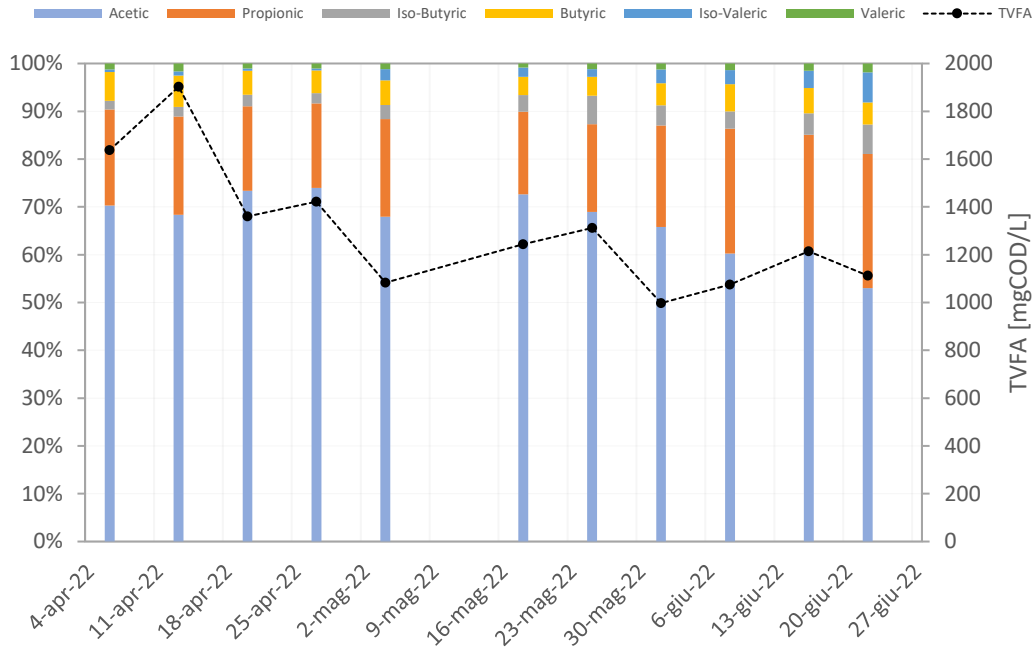

Figure 4. 1 - TVFA trend and VFA speciation of sludge samples.
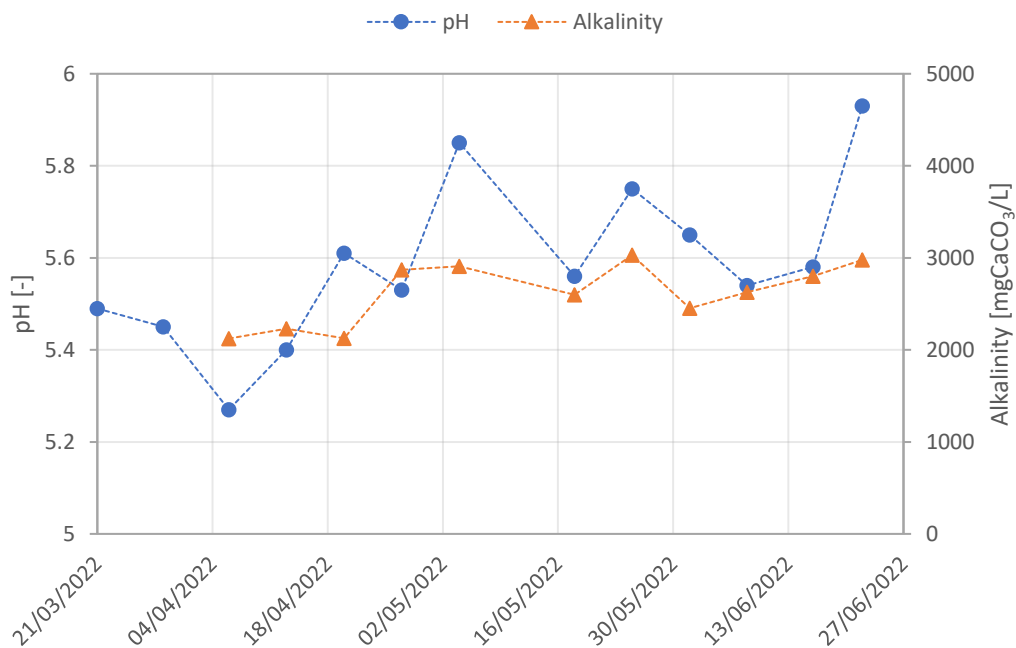
Figure 4. 2 - pH and alkalinity trend of sludge samples.
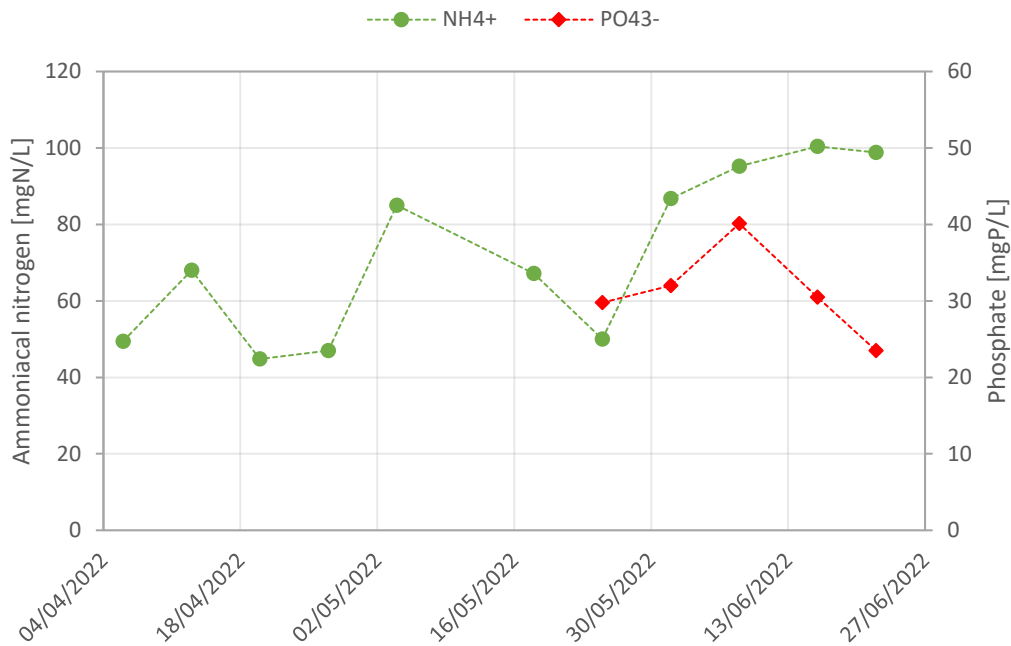
Figure 4. 3 - Ammonium and phosphate concentration trend of sludge samples.

The VFAs in the sludge samples collected throughout the experiment were predominantly acetic and propionic, with an average value of 1325 mgCOD/L.

The pH and alkalinity values of the sampled sludge revealed a constant trend.

The ammoniacal nitrogen concentration was likewise pretty steady until the end of May, with an average value of 60 mgN/L. Higher NH_4^+ concentrations resulted in an average value of 98 mgN/L in June. Phosphate was found in low concentrations.

Table 4. 2 presents data analysis on sludge measurements. Three additional variables were obtained as two-variable ratios (VS/TS, N/COD and COD/VS). It can be observed that the measured COD is very similar to the COD estimated as the sum of the contributions of proteins, carbohydrates, lipids and VFAs. In this case, the COD/VS and N/COD ratios were computed from the estimated total COD due to the limited set of COD measures available.

Table 4. 2 - Data analysis of sludge analytical measurements.

Parameter	Unit	Average	Standard Deviation
Total Carbohydrates	gCOD/L	4.17	0.8
Total Proteins	gCOD/L	12.99	3.5
Total Lipids	gCOD/L	11.33	2.4
Carbohydrates/CODtot	-	14%	2%
Proteins/CODtot	-	43%	4%
Lipids/CODtot	-	38%	3%
Estimated total COD	gCOD/L	29.8	5.8
VS/TS	gVS/gTS	0.72	0.03
TVFA	gCOD/L	1.31	0.27
COD/VS	gCOD/gVS	1.32	0.15
N/COD	gN/gCOD	0.0025	0.001

Figure 4. 4 shows boxplots of the percentage of total COD associated with carbohydrates, proteins, and lipids in the sludge, and they indicate how the values in the data are spread out.
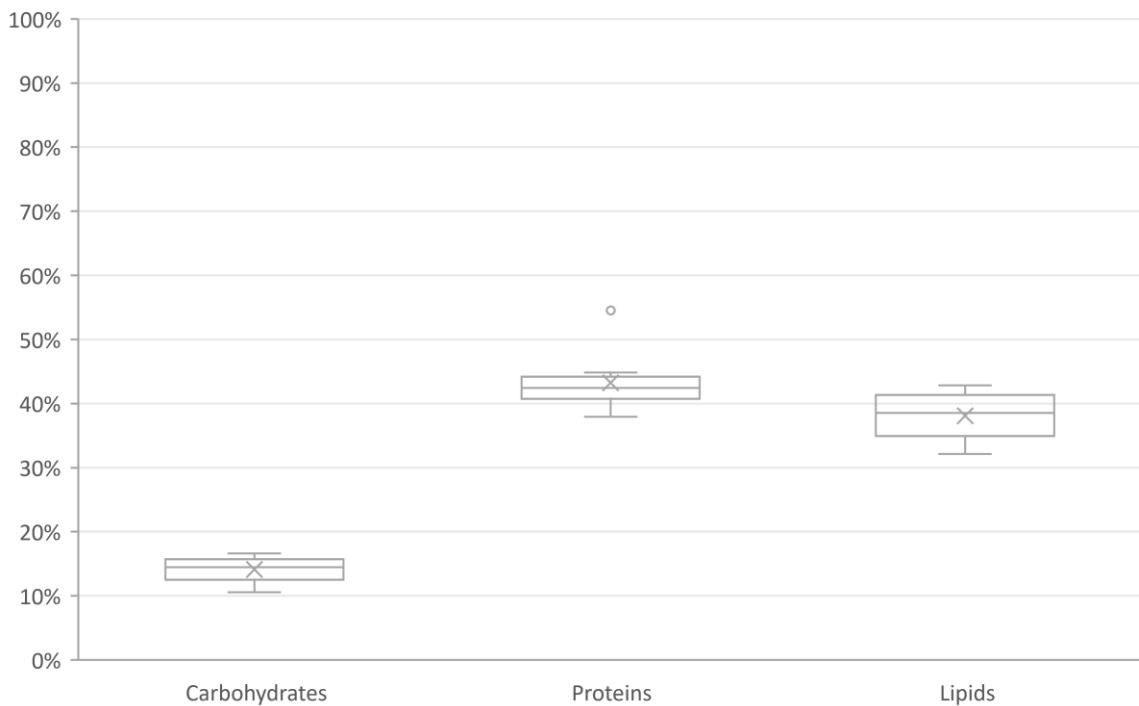
Figure 4. 4 - Percentage of total COD associated with carbohydrates, proteins and lipids in the sludge.

Table 4. 3 summarises literature measurements of major sludge properties. The data gathered in this study appear to be comparable to those collected in previous studies. The sludge used in this work presents a higher lipid content compared to those that have been reported in the literature.

The analyses performed on VFA, COD, TS, VS, TKN, and TAN in the current work reveal very similar results to those found in Soderino and Nunziata's study (2021), with the same order of magnitude. Indeed, both sludges come from WWTPs in the province of Milan.

Table 4. 3 - Sludge characterizations comparison.

Sludge type	Carbs	Proteins	Lipids	VS/TS	VFA/CODs	CODs/COD	TAN	TKN	TS	VS	CODs	COD	VFA	Bibliographic reference
	gCOD/L	gCOD/L	gCOD/L	-	-	-	mgN/L	gN/kg	gTS/kgFM	gVS/kgFM	gCOD/L	gCOD/kg	gCOD/L	
Primary sludge	0.59	2.16	1.41	0.7	0.52	0.05	77.4	1.37	32.1	22.6	1.83	34.7	1.03	Catenacci et al., 2019
Primary sludge	N.A.	N.A.	N.A.	0.82	N.A.	N.A.	N.A.	3.8	31.8	26.2	N.A.	61.3	N.A.	Villamil et al., 2019
Primary sludge	N.A.	N.A.	N.A.	0.68	N.A.	0.13	N.A.	N.A.	49.3	33.6	11.2	87	N.A.	Damtie et al., 2020
Activated sludge	2.13	13.5	3.19	0.65	N.A.	N.A.	130	N.A.	26.7	17.3	0.35	24.8	0.61	Chen et al., 2020
Activated sludge	8	13.3	N.A.	0.77	N.A.	0.02	121	N.A.	55.7	42.8	1.4	68.7	N.A.	Zhen et al., 2015
Mixed sludge	9.61	13.4	8.55	0.79	0.61	0.07	79	1.53	28.9	22.7	2.44	33.6	1.5	Soderino & Nunziata, 2021
Experimental values	4.17	12.99	11.33	0.72	N.A.	N.A.	72	1.44	30.7	22	N.A.	29.9	1.3	

4.1.2. ADM1 characterization

As already explained in paragraph 3.2.2, the information obtained from sludge analyses was then processed to provide the input state variables needed by the ADM1 model. Only the non-zero variables are shown in Table 4. 4.

Table 4. 4 - ADM1 sludge characterization.

Variable	Unit	Average	Standard deviation
S_{va}	gCOD/L	0.07	0.03
S_{bu}	gCOD/L	0.18	0.06
S_{pro}	gCOD/L	0.34	0.09
S_{ac}	gCOD/L	0.82	0.28
S_{ic}	M	0.25	0.06
S_{in}	M	0.01	0.00
S_{cat}	M	0.07	0.01
S_{an}	M	0.02	0.00
X_c	gCOD/L	2.86	0.51
X_{ch}	gCOD/L	2.84	0.69
X_{pr}	gCOD/L	8.97	1.58
X_{li}	gCOD/L	7.50	1.43
X_i	gCOD/L	6.45	2.84

The table only provides the averages and standard deviations of all characterizations. A detailed table of all individual values is reported in APPENDIX C.

As already stated in paragraph 3.2.2, many assumptions were made. Some data could not be directly measured and hence had to be derived from the literature, while others were set to zero because they were assumed to be negligible according to previous sludge sample analyses, thus reducing the number of analyses to be carried out on the influent.

4.2. Yogurt characterization

4.2.1. Analytical characterizations

Table 4. 5 shows the results of the analyses carried out on a blend of two well-known yogurt brands.

As previously stated in paragraph 3.1.4, the analyses on yogurt samples were performed only once since its characterization was assumed to be constant in each package.

Table 4. 5 - Results of yogurt characterization analyses.

Parameter	Unit	Value
Total Fraction		
pH	-	3.72
TS	gTS/kg	153.1
VS	gVS/kg	109
Total COD	gCOD/kg	212
Total TKN	gN/kg	4.9
Total Carbohydrates	gGlu/kg	132.3
Total Proteins	gBSA/kg	43.8
BMP Total	$NmLCH_4/gVS$	705
Particulate Fraction		
Particulate Lipids	g/kgVS,p	137
Particulate Lipids	g/kgVS	77
TS - particulate fraction	gTS,p/kg,p	192
VS - particulate fraction	gVS,p/kg,p	141
Soluble Fraction		
VFA: acetic acid	mg/L	4471
VFA: propionic acid	mg/L	47
VFA: iso-butyiric acid	mg/L	285
VFA: butyric acid	mg/L	137
VFA: iso-valeric acid	mg/L	34
VFA: valeric acid	mg/L	0
TS - soluble fraction	gTS,s/L	123
VS - soluble fraction	gVS,s/L	87
Soluble COD	gCOD/L	166
Soluble Carbohydrates	gGlu/L	137
Soluble Proteins	gBSA/L	20
Ammoniacal nitrogen	mgN/L	105
Phosphate	mgP/L	508

The data analysis on yogurt measurements is shown in Table 4. 6. It can be observed that the analytically measured COD and the COD estimated as the sum of proteins, carbohydrates, lipids and VFAs as COD are quite different. The estimated COD value is 10% higher than the measured value. For this reason, the derived variables were computed from the total COD, which was calculated as the sum of the contributions from proteins, carbohydrates, lipids, and VFAs. As it can be seen from the yogurt composition, it is mostly constituted of carbohydrates. The yogurt COD/VS ratio is higher than that found in sludge samples, while sludge and yogurt VS/TS ratios are comparable. The TVFA concentration of yogurt is five times higher than that observed in waste sludge.

Table 4. 6 - Data analysis of yogurt analytical measurements.

Parameter	Unit	Value
Total Carbohydrates	gCOD/L	146
Total Proteins	gCOD/L	64
Total Lipids	gCOD/L	25
Carbohydrates/CODtot	-	60%
Proteins/CODtot	-	27%
Lipids/CODtot	-	10%
Estimated total COD	gCOD/L	241
TVFA	gCOD/L	5.7
VS/TS	gVS/gTS	0.71
COD/VS	gCOD/gVS	2.14
N/COD	gN/gCOD	0.0004

A comparison between carbohydrates and proteins' analyses and the values reported on the yogurt label was made. Table 4. 7 provides the analysis's overestimation with respect to the values displayed on the yogurt package.

Table 4. 7 - Comparison of analysis' results with measures reported on the yogurt label.

Measure	Error
Carbohydrates	9.48%
Proteins (TKN)	1.74%
Proteins (BSA)	43.15%
Lipids	10.52%

As concerns proteins, the table shows that the results varied significantly depending on the measurement method; with the TKN method, the values measured substantially corresponded with the label, whereas with the BCA method, the proteins' content indicated on the package was

overestimated by 43%. The measurements of carbohydrates and particulate lipids were comparable to the average values reported on the label, with a 10% overestimation.

Because the estimated COD accounted for the protein contribution measured with the BCA method, the discrepancy between the measured and estimated COD values might be attributed to protein overestimation with the BCA method.

More analyses should be carried out on the carbohydrates, proteins and lipids of yogurt in order to have a better characterization of the feedstock.

4.2.2. ADM1 characterization

Since both the yogurt's analysis and label indicated that carbohydrates were mostly present as sugars, it was assumed that they entered the model as soluble components (S_{su}). The analyses of lipids and the soluble COD, on the other hand, revealed that fats were mostly present in particulate form and therefore included in the model as particulate (X_{li}). Proteins, instead, were included in the model both as soluble and insoluble components (S_{aa} and X_{pr}) since proteins' analyses revealed that soluble proteins accounted for half of total protein composition. Only the non-zero variables are reported in Table 4. 8.

Table 4. 8 - ADM1 yogurt characterization.

Variable	Unit	Value
S_{su}	gCOD/L	145.69
S_{aa}	gCOD/L	28.59
S_{va}	gCOD/L	0.07
S_{bu}	gCOD/L	0.77
S_{pro}	gCOD/L	0.07
S_{ac}	gCOD/L	4.77
S_{ic}	M	0.00
S_{in}	M	0.01
S_{cat}	M	0.02
S_{an}	M	0.02
X_{pr}	gCOD/L	35.65
X_{li}	gCOD/L	25.23

4.3. Digestate characterization

4.3.1. Analytical characterizations

In Table 4. 9, the results obtained from the analyses carried out on digestate samples are present. Analyses were performed on the total, particulate (after centrifugation), and soluble fraction (after centrifugation). Both the average and standard deviation are shown for all digestate samples collected throughout the experimentation. A complete table of all individual values is given in APPENDIX C.

Table 4. 9 - Results of digestate characterization analyses.

Parameter	Unit	Average	Standard Deviation
Total Fraction			
pH	-	7.11	0.04
Alkalinity	$mgCaCO_3/L$	4817	376
TS	gTS/kg	25.3	2.5
VS	gVS/kg	15.6	1.4
Total COD	gCOD/kg	13.9	3.1
Total TKN	gN/kg	1.45	0.2
Total Carbohydrates	gGlu/kg	2.36	0.4
Total Proteins	gN/kg	0.92	0.2
Particulate Fraction			
Particulate Lipids	g/kgVS,p	75.90	13
Particulate Lipids	g/kgVS	71.03	12
TS - particulate fraction	gTS,p/kg,p	125.9	2.4
VS - particulate fraction	gVS,p/kg,p	79	1.4
Soluble Fraction			
VFA: acetic acid	mg/L	83.50	16.9
VFA: propionic acid	mg/L	0.19	1
VFA: iso-butyiric acid	mg/L	10.38	4.3
VFA: butyric acid	mg/L	0	0
VFA: iso-valeric acid	mg/L	0	0
VFA: valeric acid	mg/L	0	0
TS - soluble fraction	gTS,s/L	2.5	0.3
VS - soluble fraction	gVS,s/L	1.2	0.1
Ammoniacal nitrogen	mgN/L	527	28
Phosphate	mgP/L	15	4

Table 4. 10 provides the data analysis on digestate measurements. Also in this case, the analytically measured COD and the COD calculated as the sum of proteins, carbohydrates, lipids and VFAs as COD are very similar.

Table 4. 10 - Data analysis of digestate analytical measurements.

Parameter	Unit	Average	Standard Deviation
Total Carbohydrates	gCOD/L	2.5	0.4
Total Proteins	gCOD/L	9.9	2
Total Lipids	gCOD/L	2.1	0.4
Carbohydrates/CODtot	-	17%	2%
Proteins/CODtot	-	67%	4%
Lipids/CODtot	-	15%	3%
Estimated total COD	gCOD/L	14.6	2.0
VS/TS	gVS/gTS	0.61	0.02
TVFA	mgCOD/L	105	22.65
COD/VS	gCOD/gVS	0.9	0.2
N/COD	gN/gCOD	0.040	0.013

Figure 4. 5 shows boxplots of the percentage of total COD associated with carbohydrates, proteins, and lipids in the digestate, and they indicate how the values in the data are spread out.
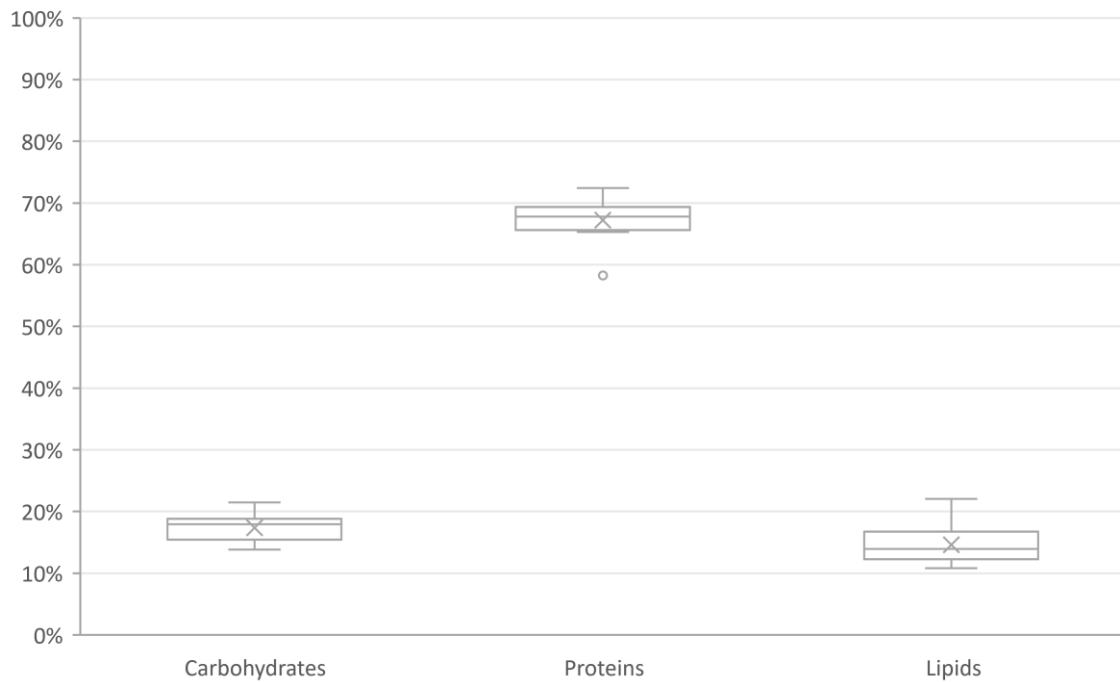

Figure 4. 5 - Percentage of total COD associated with carbohydrates, proteins and lipids in the digestate.

4.4. Pilot plant performance

4.4.1. HRT & OLR

Figure 4. 6 and Figure 4. 7 show the trend over time of the pilot plant's hydraulic retention time and OLR, respectively. As previously stated in paragraph, variations from the average target HRT of 17.1 d were observed between the 17th and 22nd of April and between the 7th and 18th of May. In the same periods, deviations from the mono-digestion OLR average value are observed. During mono-digestion, the reactor was operated at an average OLR of 1.36 $kgVS/m^3/d$. In the co-digestion phase, the average OLR was increased by 15%, 20%, 40% and finally 60% by adding yogurt, resulting in an average OLR of 1.67 $kgVS/m^3/d$. The OLR was modified by changing the yogurt and waste sludge contributions in the mixture entering the digester while maintaining the overall feed flow rate constant and equal to the flow rate during the mono-digestion phase. The red dotted line represents the start of the co-digestion phase.
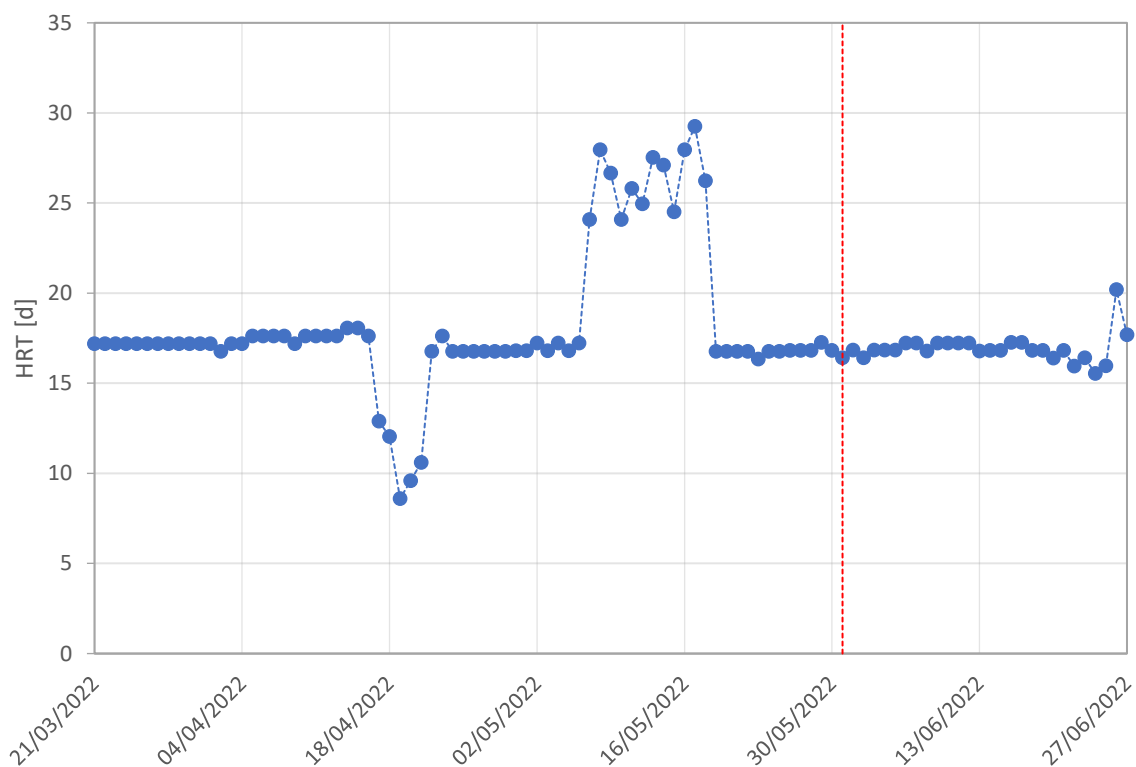

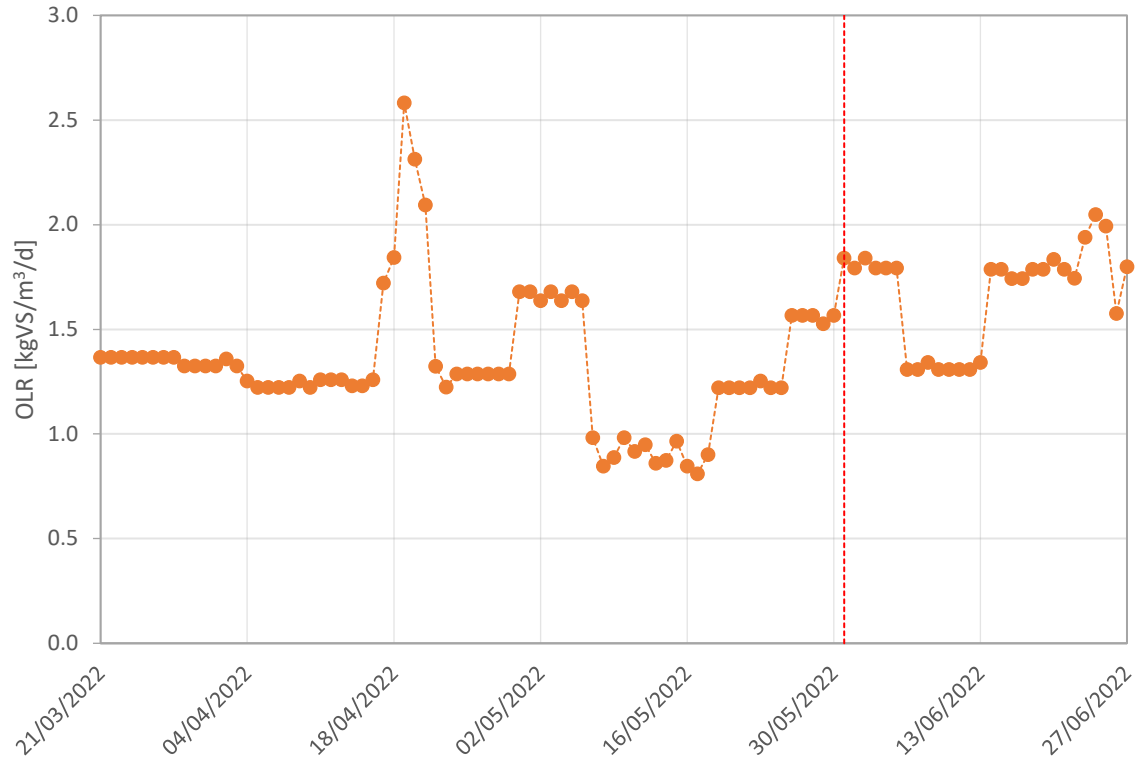Figure 4. 6 - Pilot plant hydraulic retention time (HRT).

Figure 4. 7 - Pilot plant organic loading rate (OLR).

4.4.2. Volatile solids reduction

In Figure 4. 8, the cumulative trends of VS entering and exiting the digester are reported. The red dotted line denotes the end of the mono-digestion phase and the beginning of the co-digestion phase, and hence the incoming volatile solids loading refers to the sludge and yogurt mixture.
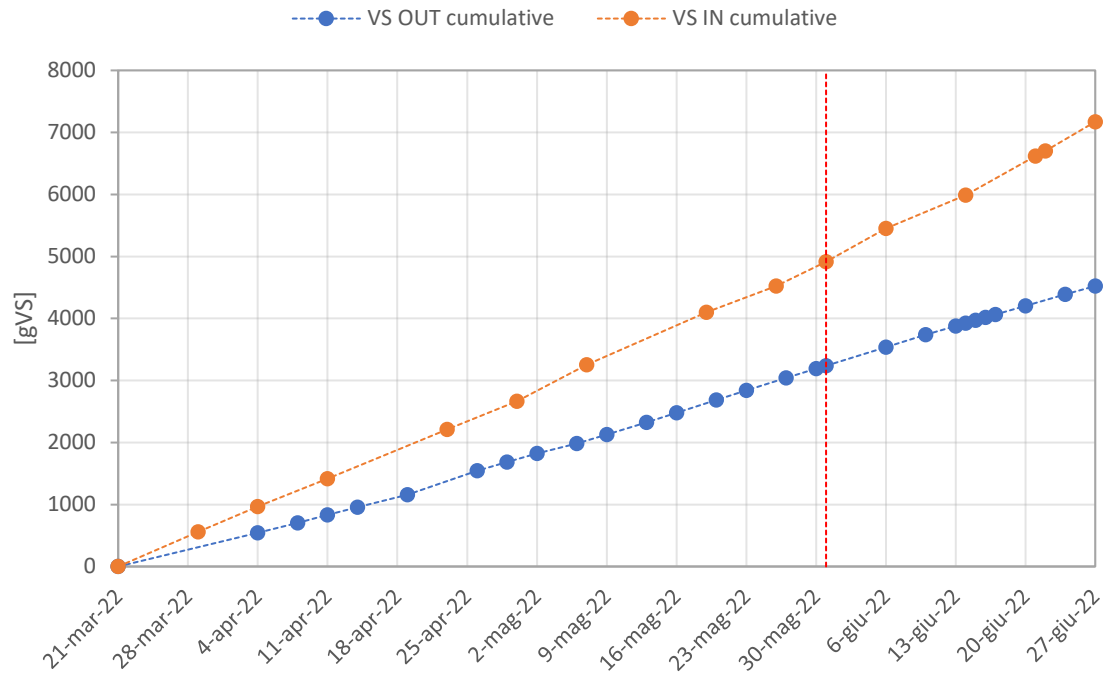
Figure 4. 8 - Comparison between influent and effluent cumulated VS.

By comparing the trend of the curves in the two periods, it is evident that the slope of the cumulative curve of VS going out of the digester is quite constant, while the slope of the cumulative curve of VS entering the reactor increases when both sludge and yogurt are fed.

Based on what has been shown, co-digestion tends to promote an increase in the reduction efficiency of volatile solids. Indeed, during the mono-digestion period, the average VS removal efficiency is 34%, while it goes up to 43% during the co-digestion phase.

4.4.3. pH and alkalinity

Figure 4. 9 show the pH and alkalinity trend. These parameters remained sufficiently stable throughout the experimentation.
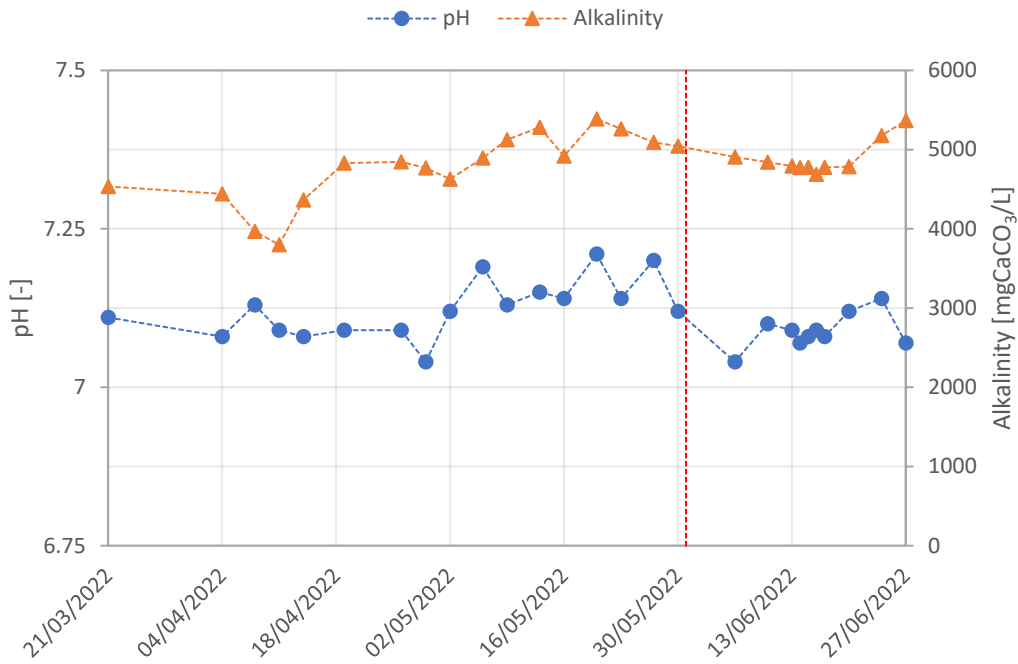
Figure 4. 9 - Measurements of pH and alkalinity for the digestate.

4.4.4. Ammonium and phosphate concentrations

The trend of the ammonium and phosphate concentrations is shown in Figure 4. 10. No significant variations in NH_4^+ and PO_4^{3-} concentrations were observed throughout the experimentation.
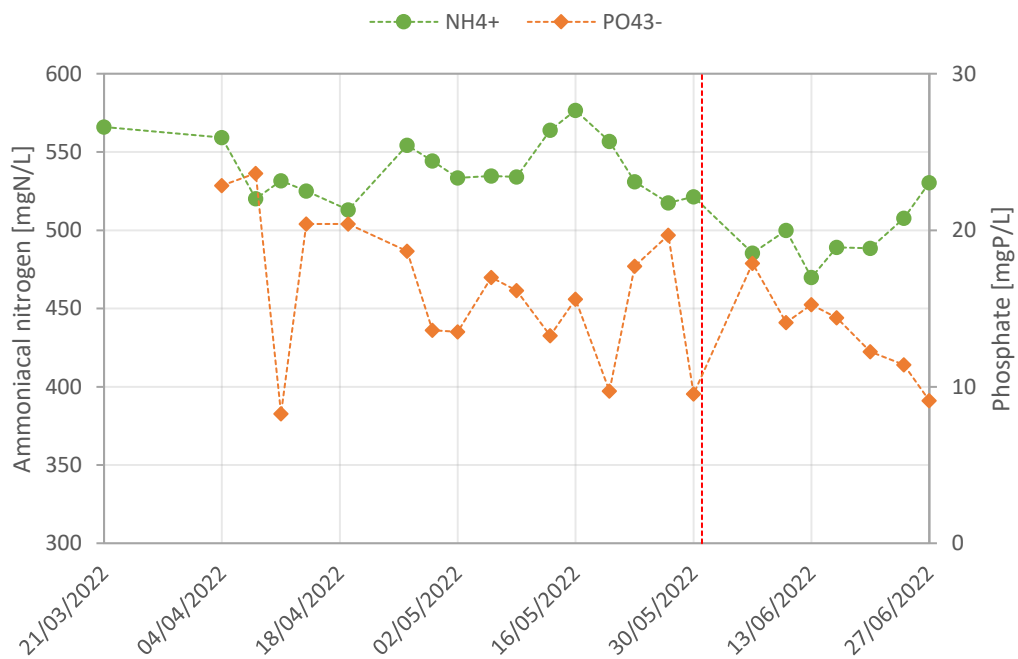

Figure 4. 10 - Measurements of the ammonium and phosphate concentrations in the digestate.

4.4.5. Volatile fatty acids

Figure 4. 11 shows the volatile fatty acids' trend in the digestate. The only acids detected in the digestate samples were acetic acid and iso-butyric acid. Also in this case, no significant variations in VFA concentration were observed during the co-digestion period compared with the mono-digestion one.
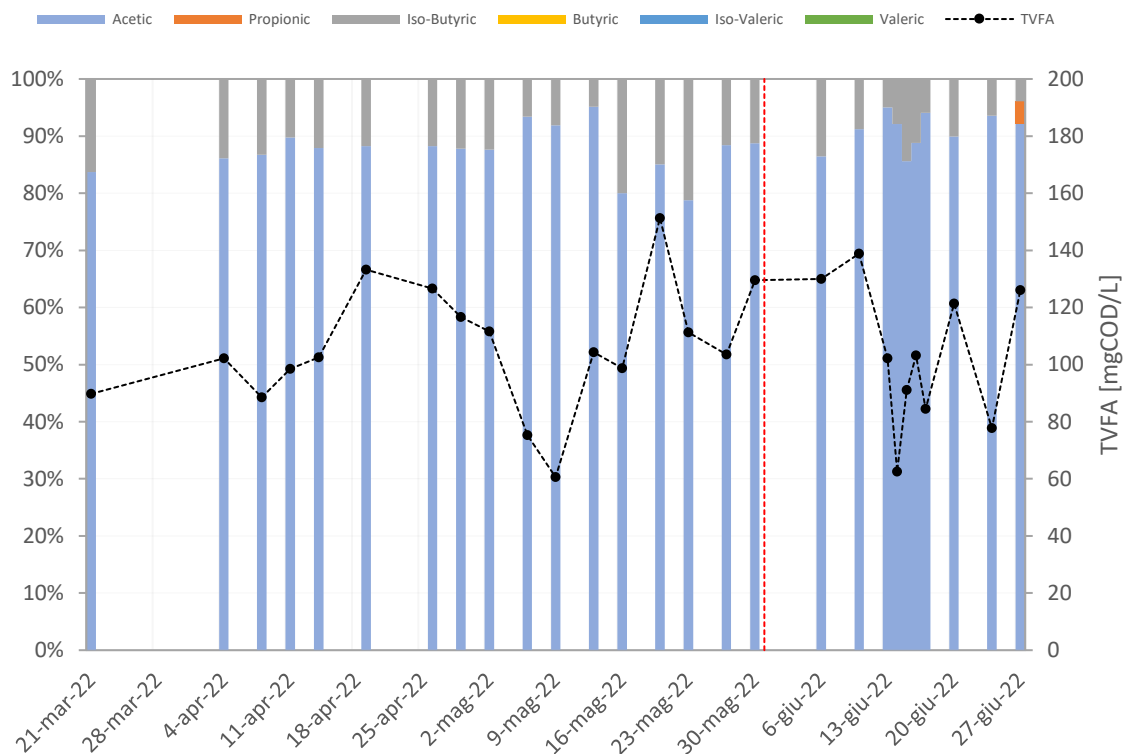

Figure 4. 11 - TVFA trend and VFA speciation of digestate samples.

4.4.6. Biogas

Biogas production

Figure 4. 12 shows the pilot plant average specific methane production expressed as $NmLCH_4$ per gVS fed to the digester. Measurements of the specific methane production were significantly underestimated when the deterioration of a seal on the reactor head caused large biogas leaks, as evidenced by the first three weeks of May. An increasing trend was observed when co-digestion was implemented. The graph shows that the measurements from the pilot plant were almost 100% of the BMP values. This suggests that the hydrolysis and methanation processes achieved very high efficiencies.
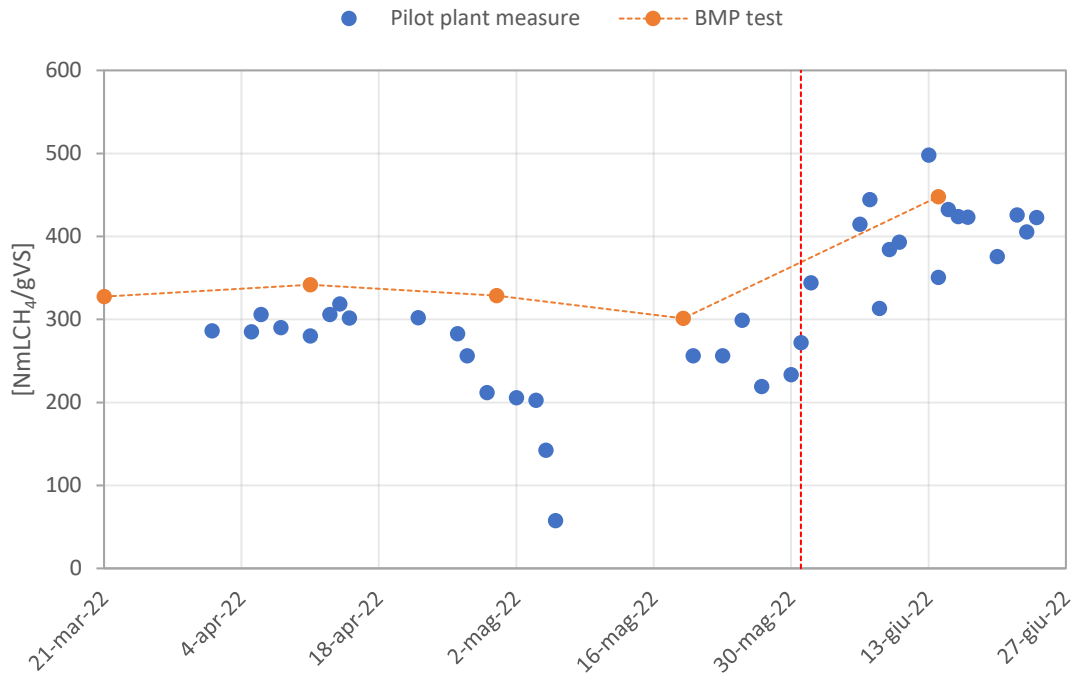
95

Figure 4. 12 - Pilot plant average specific methane production.

Figure 4. 13 shows the average methane production rate of the pilot plant. The addition of yogurt to waste sludge resulted in an increase of the methane production rate. When the OLR was increased by 40% during co-digestion, the average methane production rate nearly doubled compared to the mono-digestion period, whose average production rate was 20 $NLCH_4/d$.
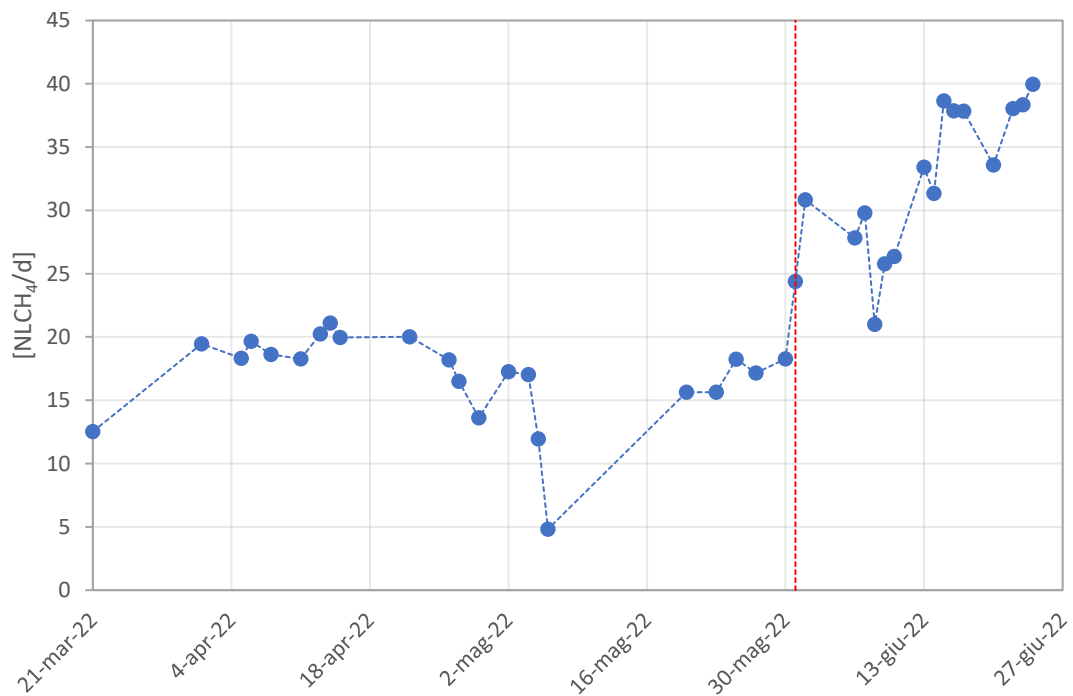

Figure 4. 13 - Pilot plant average methane production rate.

96

Biogas composition

Figure 4. 14 shows the composition of the biogas samples collected throughout the experimentation. The gathered biogas data revealed an average methane composition of 67.9 % and a carbon dioxide composition of 32.1 %. These values fall within the typical range of biogas composition (Metcalf & Eddy I AECOM, 2014). There were no significant changes in the percentages of methane and carbon dioxide during the co-digestion phase compared to the mono-digestion phase.
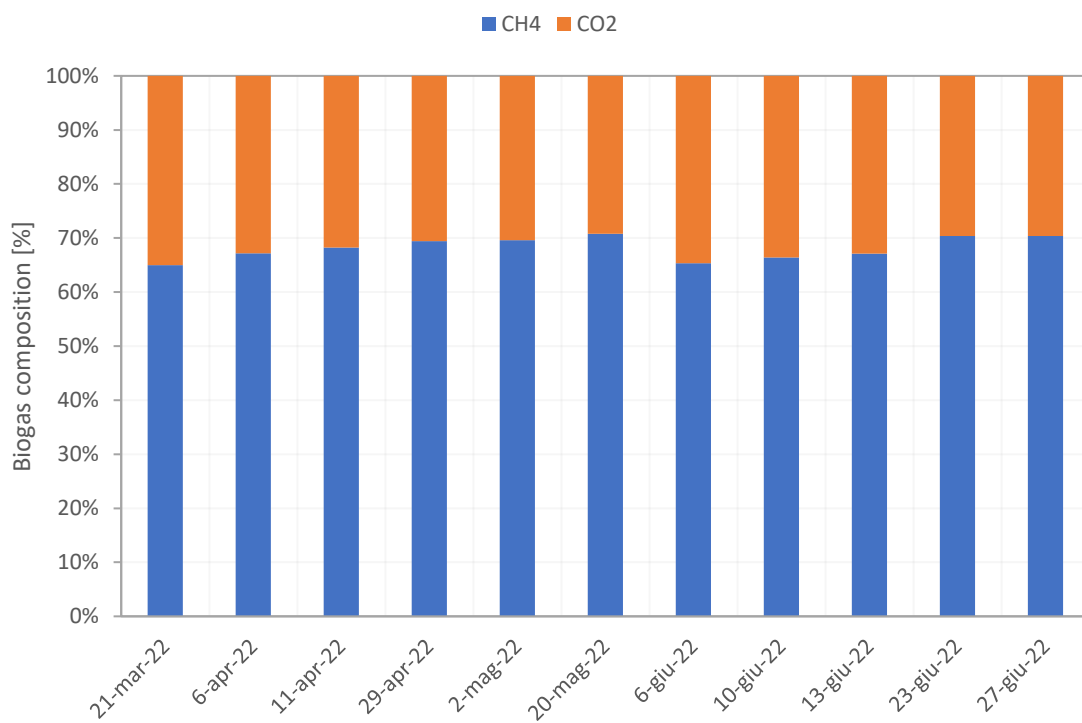

Figure 4. 14 - Dry biogas composition.

4.5. BMP tests

The results of the BMP tests are shown in this paragraph. For each test, the net cumulative methane production per gram of volatile solid of the dosed substrate is given. For blank BMP tests, the cumulative methane production is reported as $NmLCH_4$ per gram of volatile solid of the dosed inoculum. Since the tests were performed in duplicate, the graphs display the average of the duplicates and their standard deviation.

4.5.1. Blank BMP tests

Figure 4. 15 compares the methane production obtained for the various blank BMP tests. The blank tests were carried out on the inoculum alone, with no substrate addition. This test shows how much methane may be produced per gram of volatile solids in the degassed digestate used as inoculum. The figure reveals some variability, which might be explained by both differences in the digestate exiting the pilot plant and the length of the degassing process.
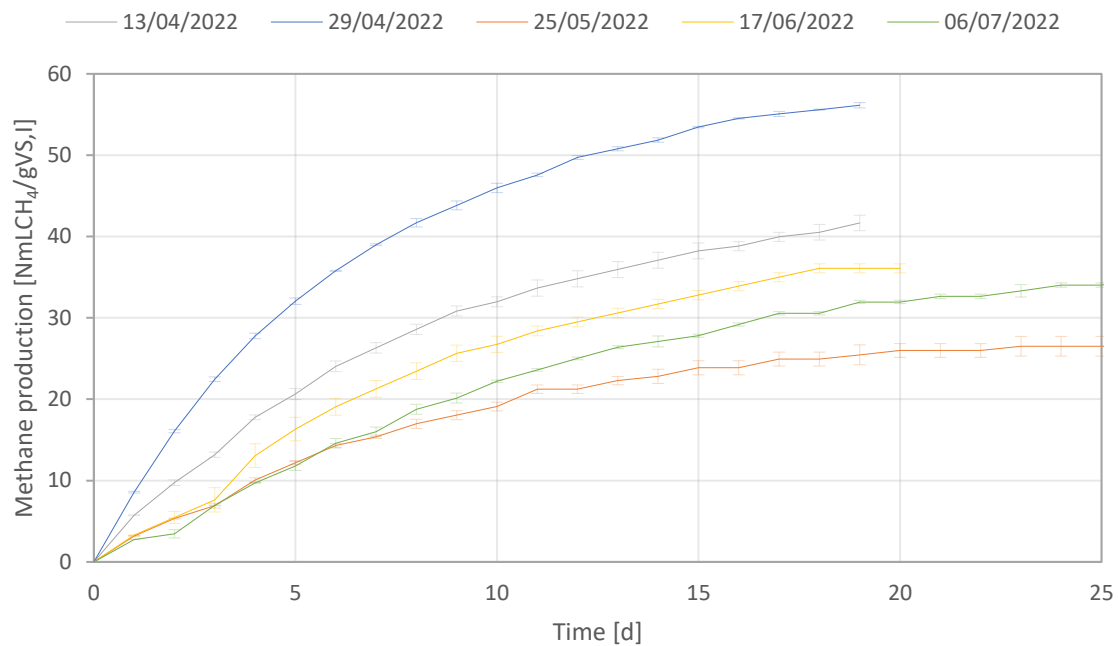

Figure 4. 15 - Methane production comparison between blank BMP tests carried out.

4.5.2. Sludge BMP tests

In Figure 4. 16, the curve of the cumulative methane production is shown for each sludge BMP test. A typical BMP curve is characterised by an initial phase of rapid production, which slows down within the first 5 days. The amount of solids to be digested decreases as the digestion process progresses, as well as the bio-methanation rate. All the curves seem to follow first-order kinetics. Keeping all operational conditions constant, the greater the bio-degradability of the substrate, the higher the bio-methanation rate.
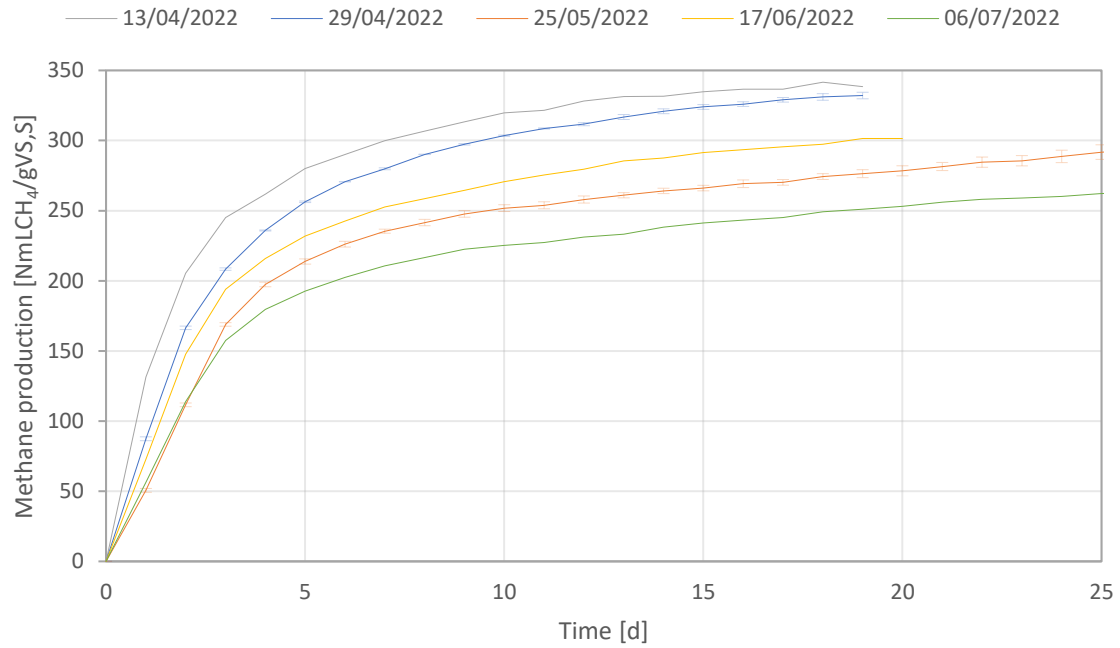
Figure 4. 16 - Methane production comparison between sludge BMP tests carried out.

The curves do not exhibit high variability. However, the tests performed on May 25 and July 6 show slightly slower kinetics. For each sludge BMP test, the hydrolytic constant (k_{hyd}) calculated by interpolation using first-order kinetics is shown in Table 4. 11, with an average value of 0.27 d^{-1}.

Table 4. 11 - Hydrolysis constant estimation by interpolation with a first-order kinetics.

Parameter	Unit	13/04/2022	29/04/2022	25/05/2022	17/06/2022	06/07/2022
k_{hyd}	1/d	0.37	0.27	0.21	0.28	0.23

4.5.3. Yogurt BMP test

Figure 4. 17 shows the methane production reported during the BMP tests on yogurt. Compared to sludge BMP tests, which had an I/S ratio of around 2, this test was carried out with an I/S ratio of about 3. The choice was made in light of earlier experiences on this substrate, which indicated pH inhibition phenomena brought on by yogurt's increased initial concentration. Yogurt exhibited a faster hydrolysis kinetics than sludge according to the hydrolytic constant of 0.52 d^{-1} obtained by first-order kinetics interpolation.
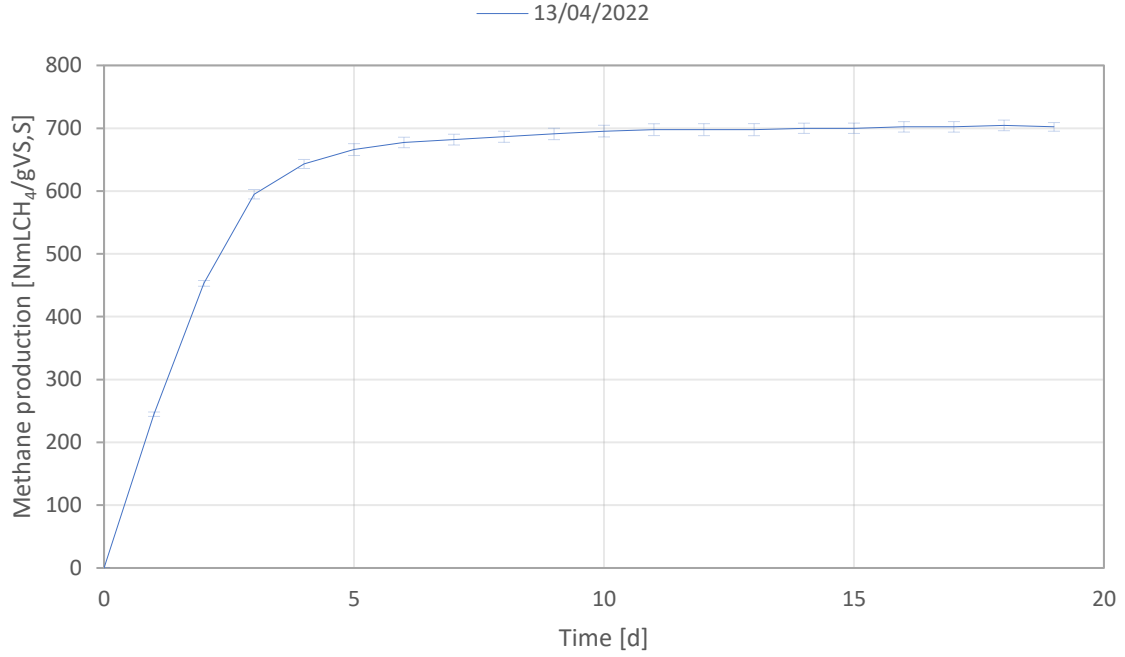
Figure 4. 17 - Methane production of yogurt BMP test carried out.

4.5.4. Co-digestion BMP tests

Figure 4. 18 shows the curves of the cumulative methane production for the co-digestion BMP tests that were carried out. The amount of yogurt (as VS) dosed with respect to waste sludge (as VS) dosed in each co-digestion BMP test carried out is shown in Table 4. 12 (Y/S Ratio), along with the expected increase in methane production as a result of adding the results of the yogurt and sludge BMP tests together. Due to possible synergistic effects, the methane production increases in co-digestion BMP tests. The expected methane production in the co-digestion BMP test was calculated using the following Equation:

$$BMP_{co-dig,expected}\left[\frac{NmLCH_4}{g_{VS,co-substrates}}\right]=$$

$$\frac{BMP_{sludge}\left[\frac{NmLCH_4}{g_{VS,sludge}}\right]\times VS_{sludge,co-dig,BMP}\left[g_{VS,sludge,co-dig}\right]+BMP_{yogurt}\left[\frac{NmLCH_4}{g_{VS,yogurt}}\right]\times VS_{yogurt,co-dig,BMP}\left[g_{VS,yogurt,co-dig.}\right]}{VS_{sludge+yogurt,co-dig,BMP}\left[g_{VS,co-substrates}\right]}$$

$$(4.1)$$

Due to possible synergistic effects, the methane production increases in co-digestion BMP tests. The expected methane production and the kinetics increase as the Y/S ratio rises.
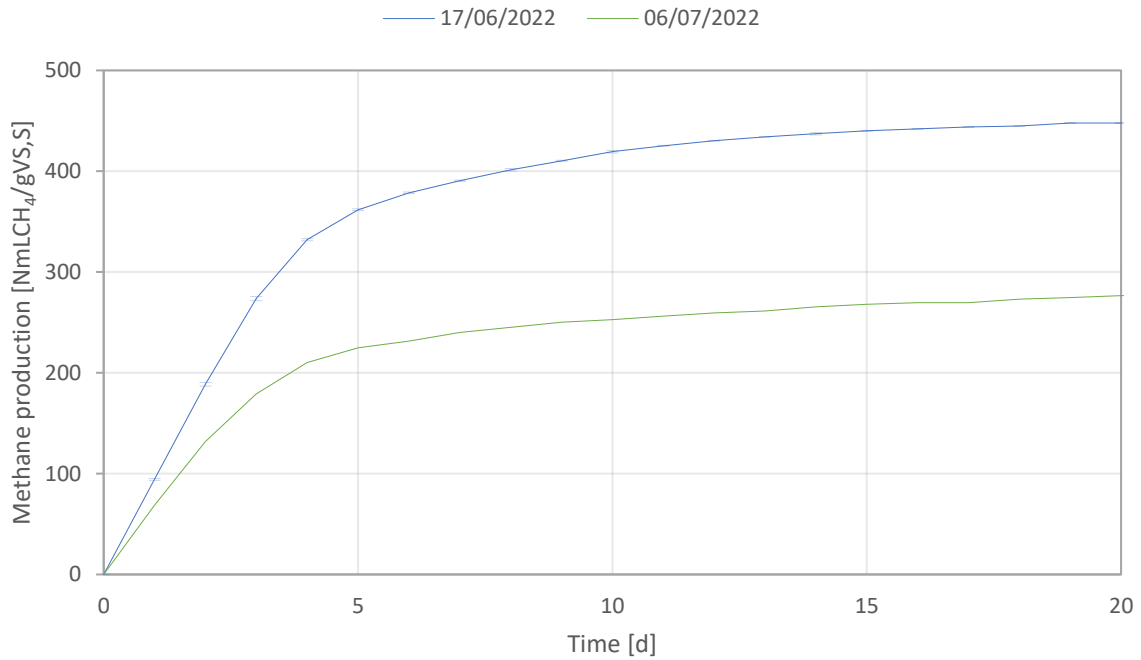
Figure 4. 18 - Methane production comparison between co-digestion BMP tests carried out.

Table 4. 12 - BMP increase in co-digestion.

Co-digestion BMP test	Y/S Ratio [gVS,Y/gVS,S]	BMP increase [%]
17/06/2022	0.55	48%
06/07/2022	0.25	34%

The hydrolytic constant was calculated for both co-digestion BMP tests and was found to be 0.3 d^{-1} for a Y/S ratio of 0.55 and 0.28 d^{-1} for a Y/S ratio of 0.25.

4.5.5. Residual BMP tests

Figure 4. 19 represents a comparison of the specific methane production (NmLCH$_4$ per gram of volatile solid of inoculum) of the various residual BMP tests. This test shows a moderate

slope and slow kinetics. Fresh digestate is used as inoculum for residual BMP tests. The residual BMP tests can be used to calculate the net production of the biomass activity tests having the same inoculum.
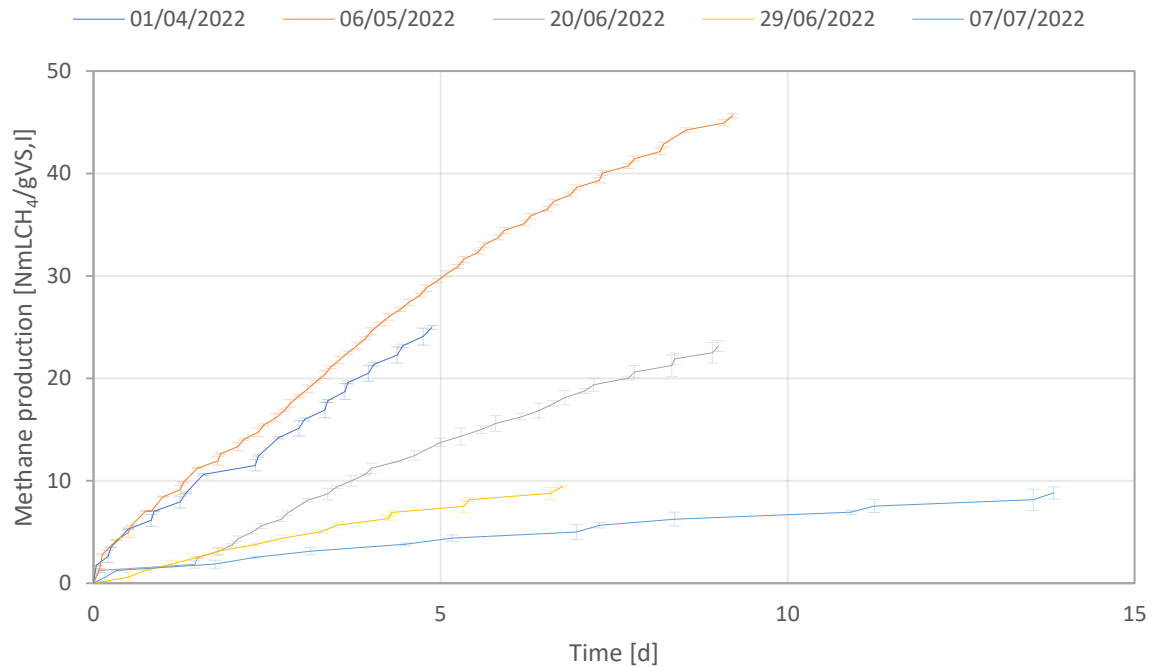

Figure 4. 19 - Methane production comparison between residual BMP tests performed.

4.6. Biomass activity tests

This paragraph discusses the results of the biomass activity tests. The results of a single representative test are provided and discussed for each type of test. In APPENDIX E, all the other results are reported, along with a table outlining the percentage of dosed COD converted into methane in each biomass activity test. Since the tests were carried out in duplicate, the graphs display the average of the duplicates and their standard deviation. These figures represent the gross methane production per gram of COD dosed of a specific substrate.

4.6.1. Acetate activity test

Figure 4. 20 shows the results of a test conducted on May 6, 2022, using acetate at a concentration of 2.0 gCOD/L. The curve is characterized by a first phase in which the substrate is degraded more slowly than a second phase, which is highlighted by the vertical dashed red

lines. This slower degradation rate in the initial phase is reproduced in all the tests, even when the substrate concentration is lower. In the interval indicated by the vertical dashed red lines, the linear slope is associated with the degradation of the acetate. The slope of the last part of the curve, on the other hand, indicates methane production as a result of the degradation of the residual organic component contained in the fresh digestate used as inoculum. Through an iterative procedure, these curves are used to estimate the model parameters $k_{m,ac}$ and $K_{s,ac}$.
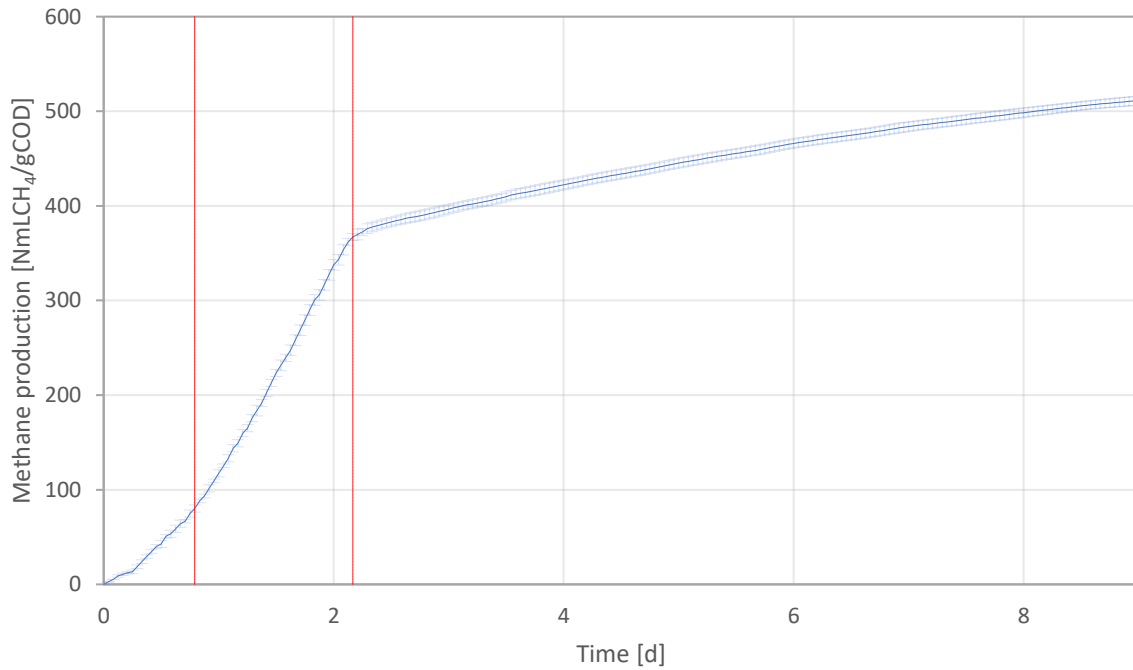

Figure 4. 20 - Methane production of acetate activity test (06/05/2022).

Table 4. 13 shows the percentage of COD associated with the acetate dosage, which is converted into methane at the end of the test and at the curve's elbow.

Table 4. 13 - Fraction of COD associated with acetate converted into methane.

	End of the test	Curve's elbow
%COD-CH$_4$	98.6%	90.1%

4.6.2. Glucose activity test

The results of a glucose activity test at a concentration of 3 gCOD/L performed on May 6, 2022, are shown in Figure 4. 21. There is a twofold change in slope in the area of the graph enclosed by the dashed red lines. There is a first slope, then a more vertical slope, indicating fast methane production associated with rapid substrate consumption. The slope then changes again, becoming almost parallel to the first one. The aforementioned behaviour might be explained by the hypothesis that the glucose dosage causes an initial pH drop. This lowering may be attributed to VFA accumulation, which is not capable of causing inhibition but may be responsible for the initial slowdown. The pH rises as soon as the methanogens begin to breakdown the VFA, and rapid biogas production is observed. The COD converted into methane at the end of the test is 85.4% and 66.8% at the curve's elbow. The residual COD is partially used for biomass synthesis, and a fraction may be involved in metabolic pathways that do not lead to methane formation.

The tests with glucose were performed at various initial COD concentrations, as anticipated in the previous chapter. Figure 4. 22 shows the results of a glucose activity test at a concentration of 0.5 gCOD/L carried out on July 6, 2022. The same previously described trend is observed, with a double change in slope, even though it is significantly attenuated when compared to tests performed with a higher glucose concentration. However, a higher COD conversion to methane is observed at a lower glucose concentration. Indeed, this test results in a 100% COD conversion to methane at the end of the test and an 89% conversion is achieved at the curve's elbow.
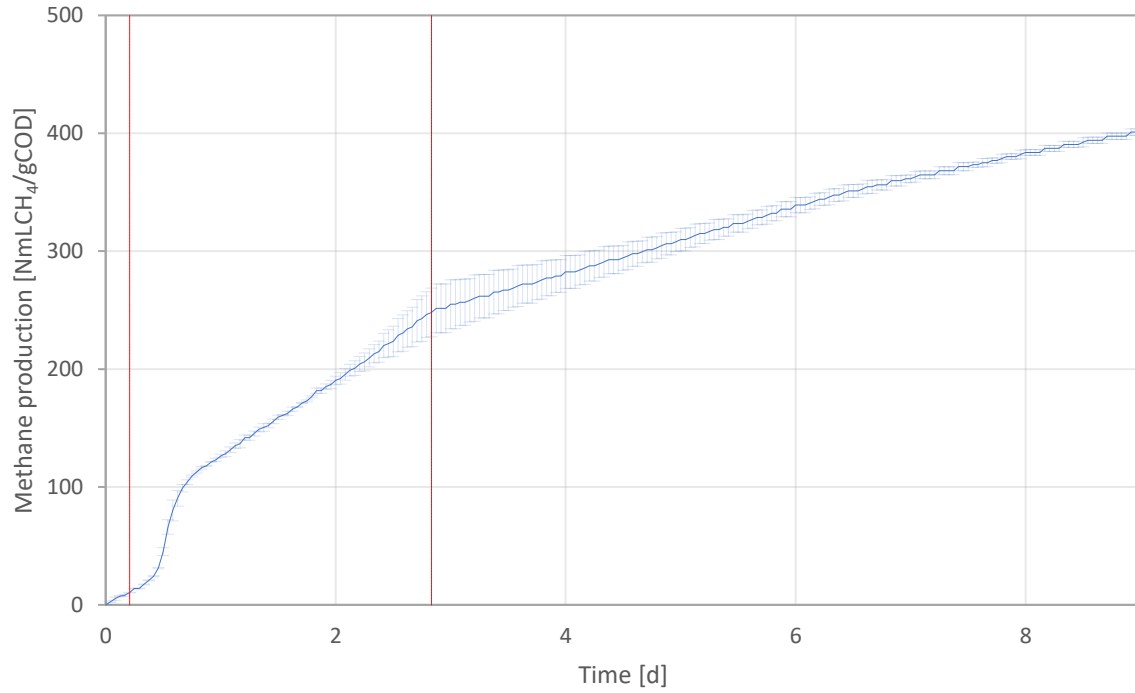
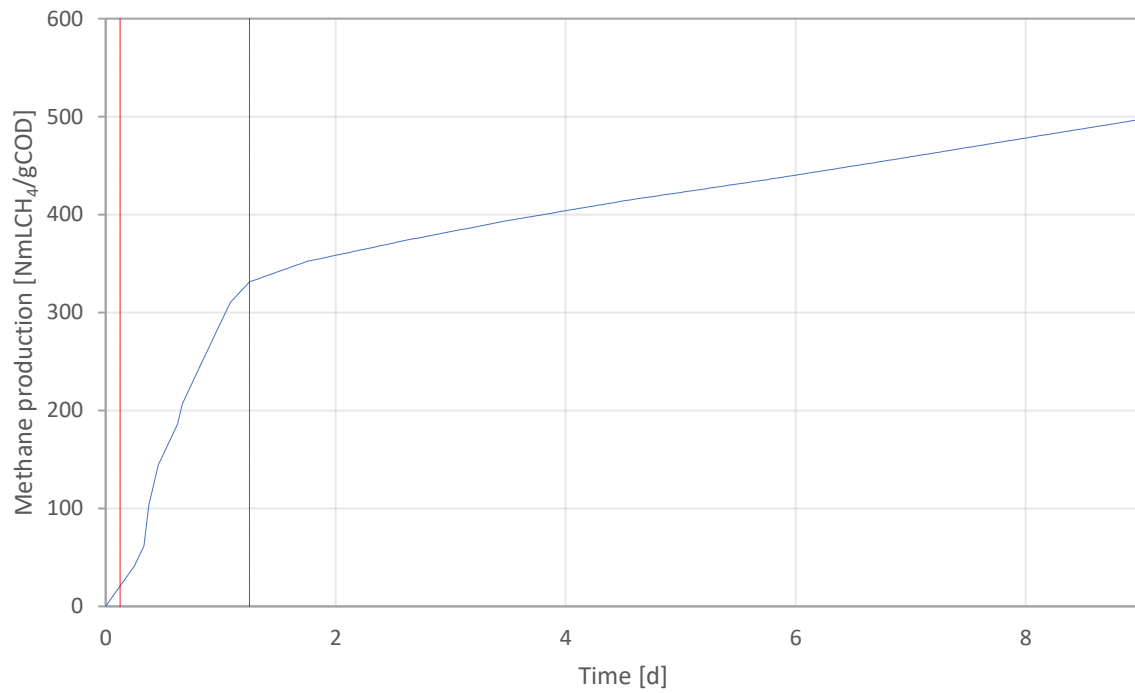Figure 4. 21 - Methane production of glucose activity test (06/05/2022).

Figure 4. 22 - Methane production of glucose activity test (06/07/2022).

These tests are used in the ADM1 calibration phase to identify the parameters of $k_{m,su}$ and $K_{s,su}$.

4.6.3. Propionate activity test

Figure 4. 23 shows the results of a test conducted on July 7, 2022, using propionate at a concentration of 3.0 gCOD/L. As shown in acetate activity tests, the curve reveals a first phase of slow methane production, which is followed by an increased linear slope associated with propionate degradation. Almost all of the propionate as COD is used when the elbow's curve is reached. The last part of the curve is associated with the degradation of the residual organic content present in the fresh digestate. Table 4. 14 shows the percentage of COD associated with the propionate dosage that is converted into methane at the end of the test and at the curve's elbow.

Table 4. 14 - Fraction of COD associated with propionate converted into methane.

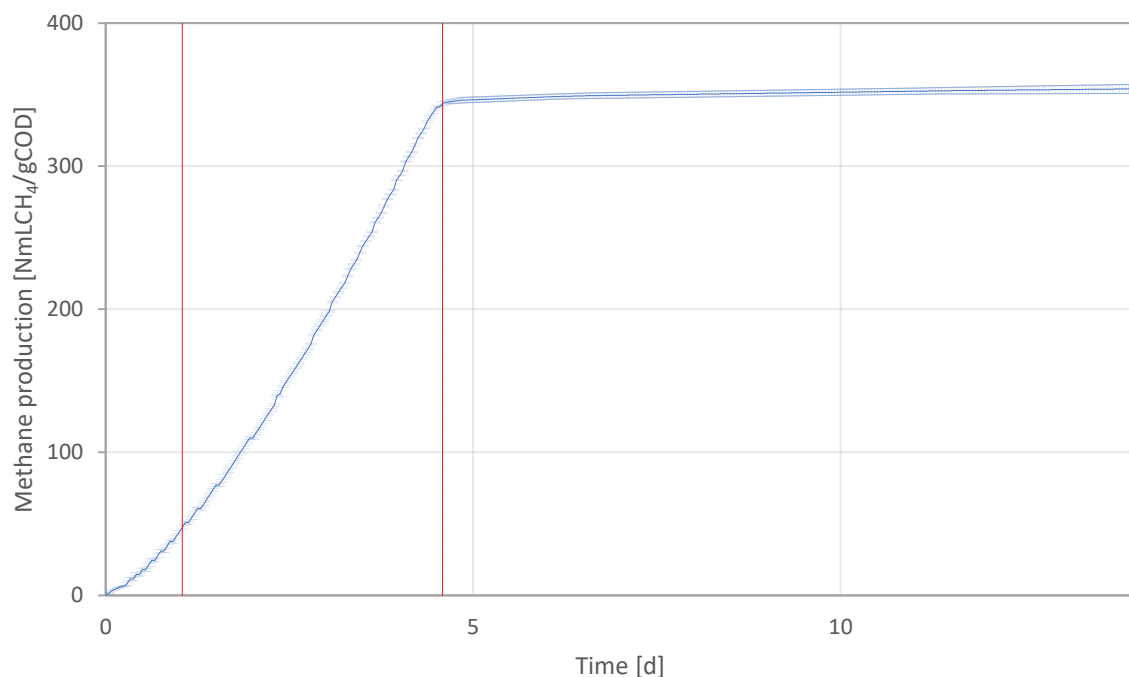|	End of the test	Curve's elbow
%COD-CH$_4$	96.0%	95.4%

Figure 4. 23 - Methane production of propionate activity test (07/07/2022).

Figure 4. 24 shows the results of a test performed on May 6, 2022, with a propionate concentration of 1 gCOD/L. When testing lower concentrations, it is observed that the trend remains similar. At the end of the test, 95% of the COD associated with propionate is converted into methane, compared to 87.5% at the curve's elbow.

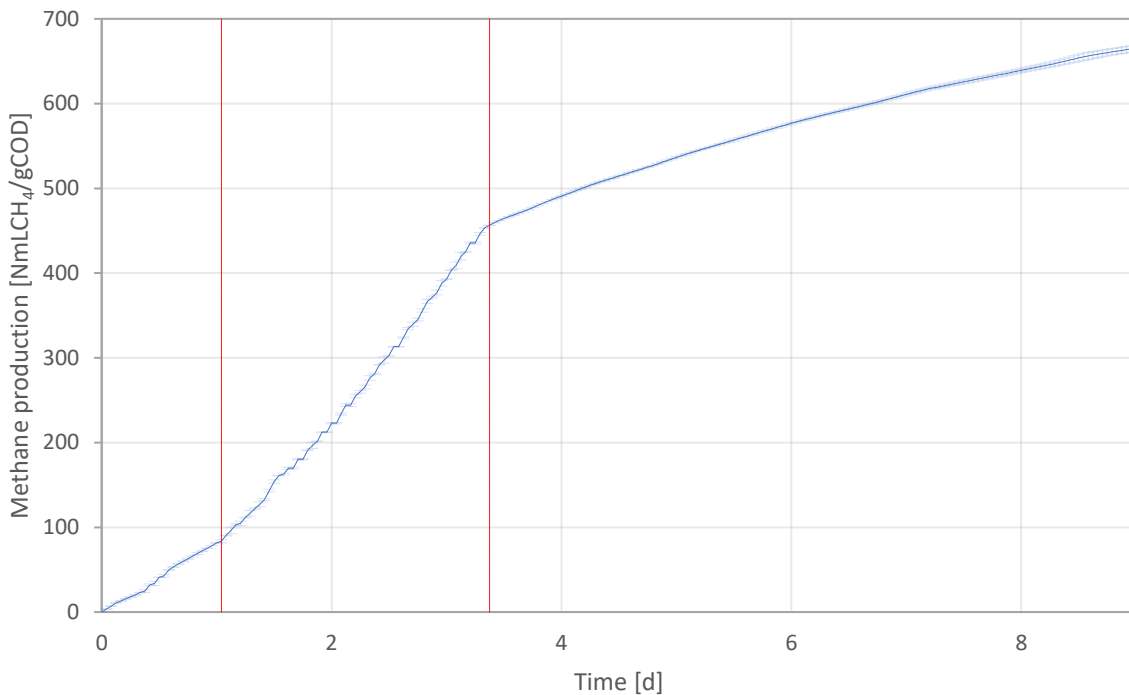These tests are used in the ADM1 calibration phase to identify the parameters of $k_{m,pro}$ and $K_{s,pro}$.

Figure 4. 24 - Methane production of propionate activity test (06/05/2022).

4.7. ADM1 dynamic simulations

4.7.1. Calibration

The outcomes of the iterative calibration procedure and the values of the kinetic parameters estimated through the various iterations are shown in Table 4. 15.

Since the waste sludge and digestate used in this study revealed similar characteristics to those of Nunziata and Soderino's experimentation, the current model was initialized with the same values of the calibrating parameters.

The iterative process stopped at the second iteration. However, a third iteration was carried out because, as evidenced by Nunziata and Soderino's study, different hydrolysis constants might be considered when dealing with different substrates. Also in this case, a higher $k_{H,Pr}$ was used to predict methane production in the yogurt and co-digestion BMP tests.

As evidenced by the values of the TIC and MARE coefficients (from Table 4. 16 to Table 4. 22), the simulation of the batch tests produced satisfactory results. No significant improvements in simulating the pilot plant monitoring parameters, such as total COD, alkalinity, pH, ammoniacal nitrogen, VS and methane and carbon dioxide percentages in the biogas were observed (Table 4. 23).

Table 4. 15 - ADM1 kinetics parameters estimated during each iterative step of the calibration process.

Parameters	UM	Initial	1st iteration	2nd iteration	3rd iteration (yogurt)
k_{dis}	d^{-1}	1.5	1.2	1.2	1.2
$k_{H,Ch}$	d^{-1}	0.3	0.2	0.3	0.3
$k_{H,Pr}$	d^{-1}	0.2	0.2	0.2	0.3
$k_{H,Li}$	d^{-1}	0.5	0.3	0.3	0.3
$k_{m,su}$	d^{-1}	8	20	6	6
$k_{m,ac}$	d^{-1}	8	8	8.2	8.2
$k_{m,pro}$	d^{-1}	20	14	13	13
$K_{S,su}$	gCOD/L	0.3	0.3	0.5	0.5
$K_{S,ac}$	gCOD/L	0.01	0.01	0.15	0.15
$K_{S,pro}$	gCOD/L	0.3	0.2	0.1	0.1
$K_{ac,Hald}$	gCOD/L	0.65	3	3	3
$K_{pro,Hald}$	gCOD/L	3	3.8	3.8	3.8

4.7.2. Batch tests simulation

Blank BMP tests simulation

Figure 4. 25 shows the simulation of a blank BMP test performed on June 17, 2022. The graph refers to the production of methane expressed as $NmLCH_4$ per bottle. This test exhibits a particular behaviour in the initial phase (as shown in Figure 4. 25), which the model cannot

predict accurately. This behaviour is characterized by changes in slope. Nevertheless, the second half of the curve is better estimated.

As anticipated in paragraph 3.2.3, the BMP tests were simulated using the pilot plant model's output digestate; a degassing step was also considered by simulating an extra batch digestion phase.

However, since the digestate sampling for BMPs required several days due to the pilot plant feeding mode, the degassing phase for each sample was different. Consequently, this phase was simulated by assuming an average degassing time. Moreover, the degassing phase was carried out without any mixing during the experimentation, while it was simulated by assuming complete mixing conditions. These assumptions introduced additional uncertainties into the modelling of BMP tests. Another reason for the difficulties in simulating blank BMP tests might be the instrument's reduced accuracy because of the lower methane production in this test.
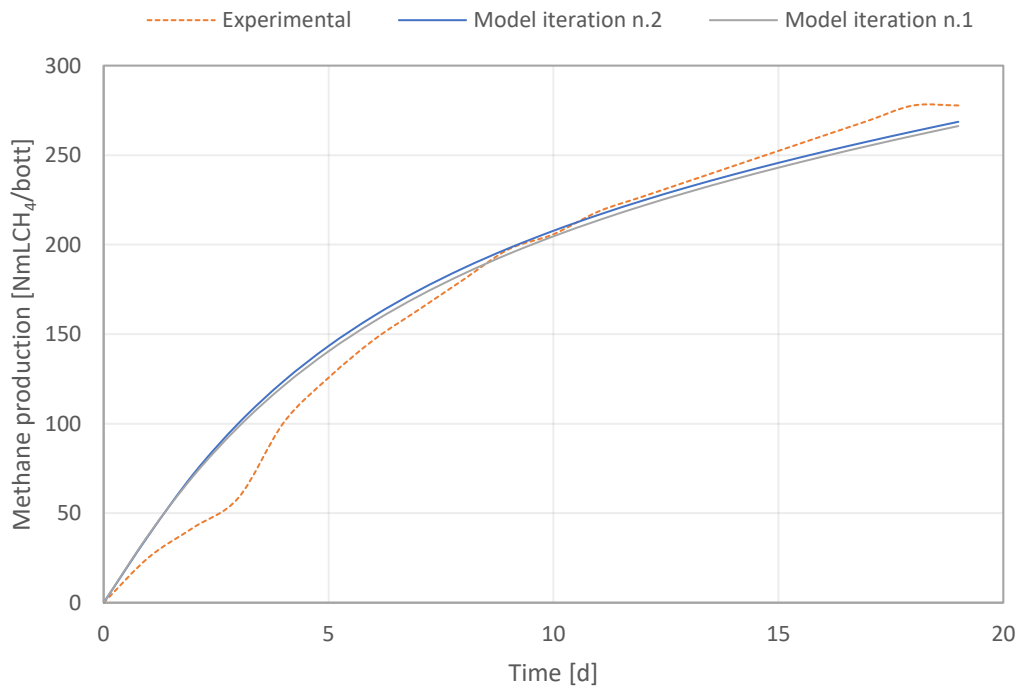

Figure 4. 25 - Blank BMP test simulation (17/06/2022).

Table 4. 16 shows the model fitting criteria. No significant improvement was obtained from the first to the second iteration. However, the blank methane production was satisfactory predicted by the model.

Table 4. 16 - Model prediction performances for blank BMP test simulation (17/06/2022).

Model fitting criteria	1st iteration	2nd iteration
TIC	0.038	0.039
MARE	0.096	0.095

Sludge BMP tests simulation

Figure 4. 26 shows the comparison between the simulations of a Sludge BMP test (carried out on 29/04/22) at the first and second iteration with the experimental results. The graph refers to the gross production of methane expressed as NmLCH$_4$ per bottle.
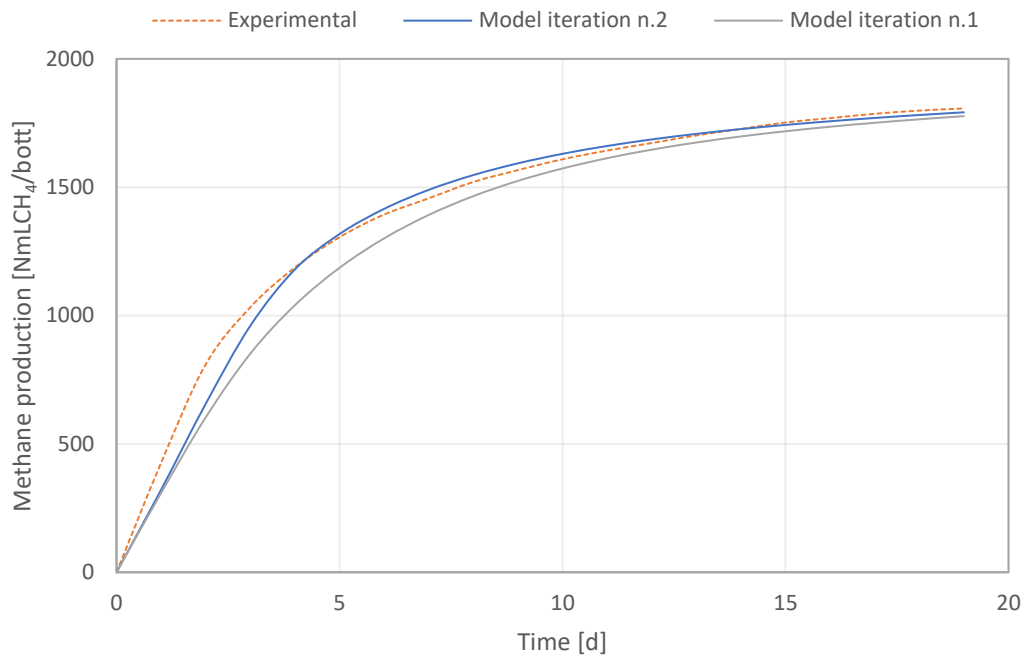

Figure 4. 26 - Sludge BMP test simulation (29/04/2022).

The fitting of the experimental data was better in the second iteration than in the first, which was also confirmed by the model fitting criteria, whose values were closer to zero in the second iteration (Table 4. 17).

Model fitting criteria	1st iteration	2nd iteration
TIC	0.03	0.016
MARE	0.077	0.040

Yogurt BMP test simulation

Figure 4. 27 shows the gross methane production per bottle at the first, second and third model iteration and the experimental data of the yogurt BMP test (carried out on 13/04/2022).
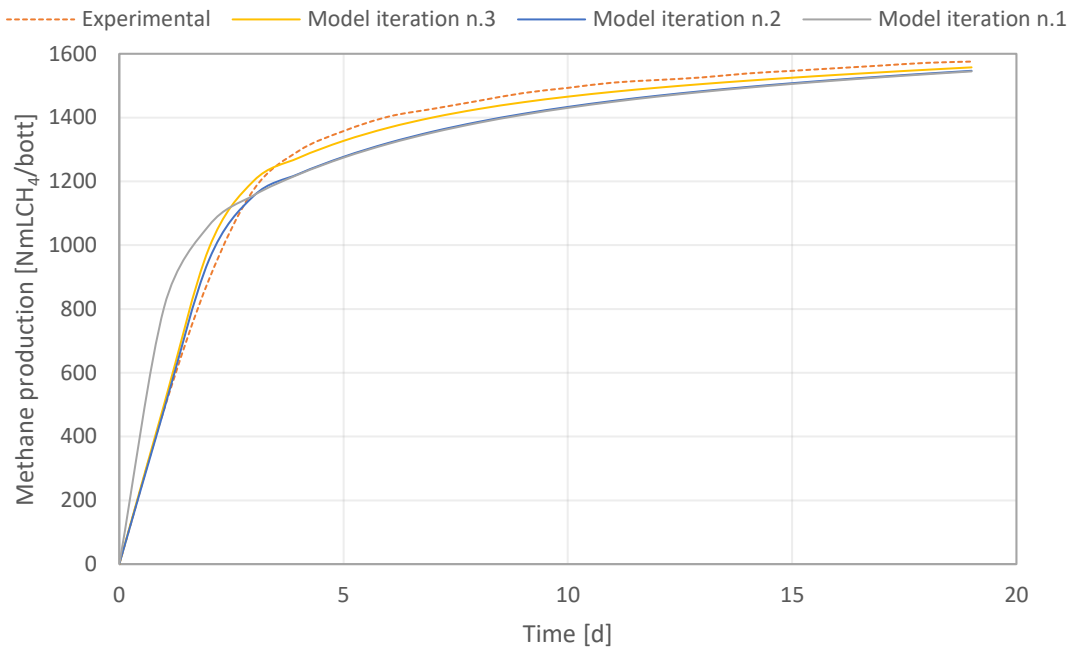

Figure 4. 27 - Yogurt BMP test simulation (13/04/2022).

The simulation clearly shows an improvement from the first to the second iteration.

However, as Nunziata and Soderino demonstrated in their study, increasing the protein hydrolysis constant in the third iteration (from 0.2 d^{-1} to 0.3 d^{-1}) resulted in a further improvement in fitting the experimental data of the yogurt BMP test, as evidenced by the model prediction performance reported in Table 4. 18.

Table 4. 18 - Model prediction performances for yogurt BMP test simulation (13/04/2022).

Model fitting criteria	1st iteration	2nd iteration	3rd iteration
TIC	0.036	0.019	0.012
MARE	0.061	0.035	0.021

Co-digestion BMP tests simulation

Figure 4. 28 shows the results of the co-digestion BMP test carried out on 17/06/2022 and its simulation at the first and second iteration.
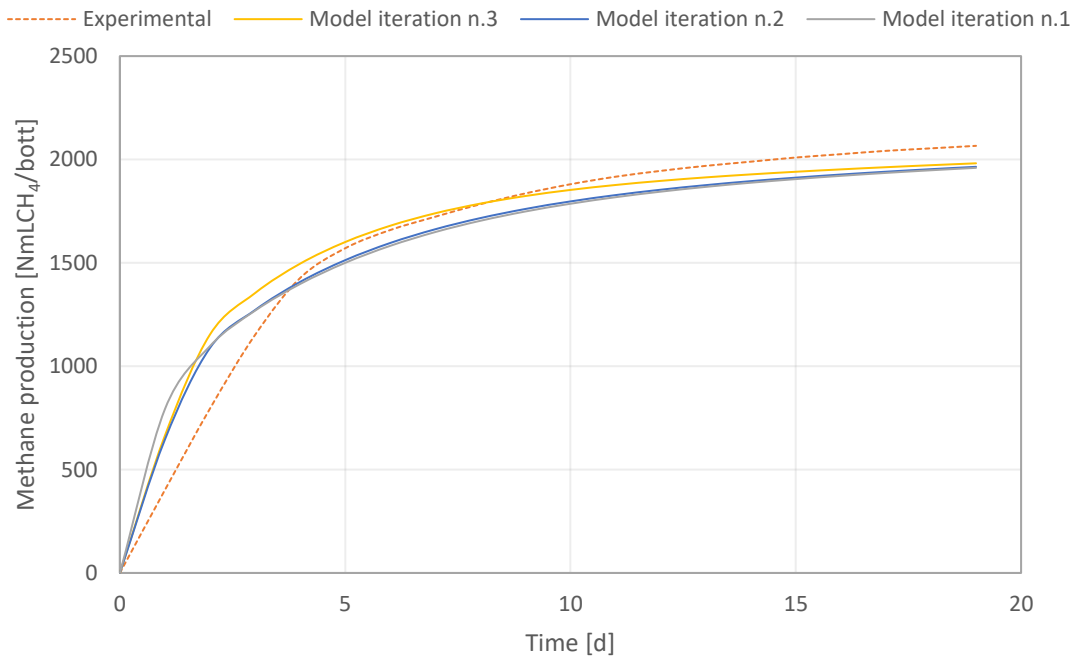

Figure 4. 28 - Co-digestion BMP test simulation (17/06/2022).

Despite the presence of yogurt in co-digestion BMP tests, the adjustment of the protein hydrolysis kinetic constant did not result in a significant improvement of the simulation in the third iteration. In this case, the simulation appeared to have degradative kinetics faster than reality. Table 4. 19 shows the values of TIC and MARE for the various model iterations' results.

Model fitting criteria	1st iteration	2nd iteration	3rd iteration
TIC	0.042	0.035	0.035
MARE	0.083	0.073	0.064

Table 4. 19 - Model prediction performances for co-digestion BMP test simulation (13/04/2022).

Residual BMP tests simulation

Although the digestate used in the residual and biomass activity tests was not degassed in the experimentation, a 4-day degassing phase simulation was also considered in the modelling of these tests. This choice was made because the pilot plant model's output digestate was characterised by an overestimated content of degradable proteins, carbohydrates and lipids. The model calibration and the lowering of the conversion factor for influent proteins to organic nitrogen (kgVS/kgN) resulted in a minimal improvement, which, however, was not sufficient to exclude the simulation of a degassing step.

Figure 4. 29 shows the simulation of a residual BMP test performed on April 1, 2022. The experimental data were well fitted by the model and no improvement was observed from the first to the second iteration.
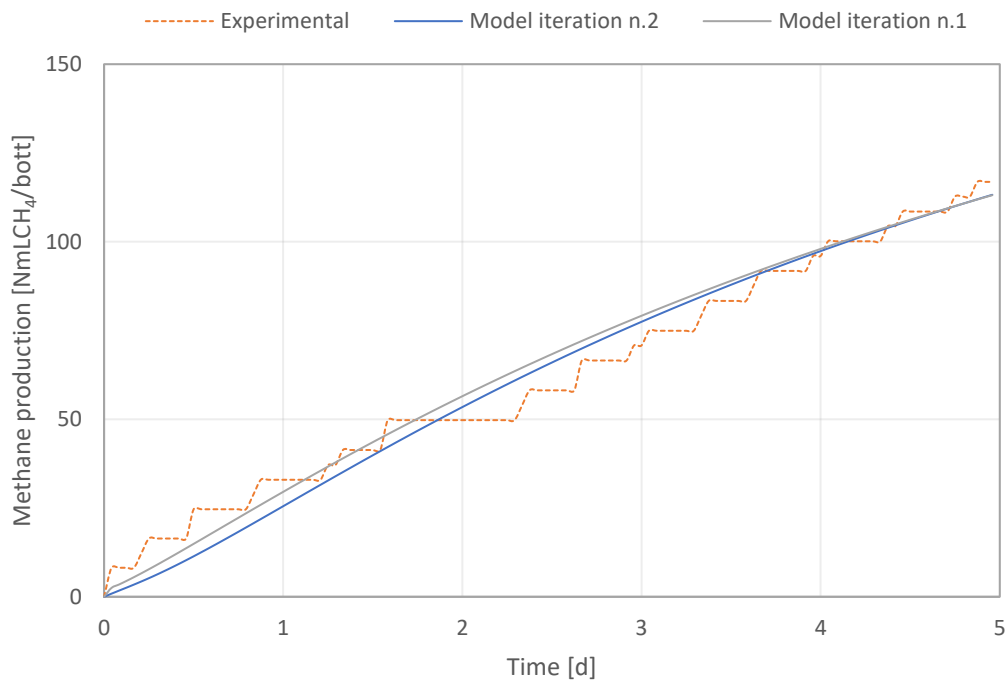

Figure 4. 29 - Residual BMP test simulation (01/04/2022).

Acetate activity tests simulation

Figure 4. 30 shows the result of a simulation of an acetate activity test performed on April 1, 2022. The simulation slightly overestimated the methane production in the acetate degradation phase, while the endogenous methane production was well replicated.

However, the incorporation of the Haldane inhibition kinetics ($K_{ac,Hald}$) into the model proved to be very successful in replicating the behaviour of the methane production curve in acetate activity tests. This is evident when the curves' trends are compared. Furthermore, the adjustment of the $k_{m,ac}$ and $K_{S,ac}$ values from the first to the second iteration resulted in a further improvement in fitting the experimental curve. The TIC and MARE indicators supported this improvement (Table 4. 20).
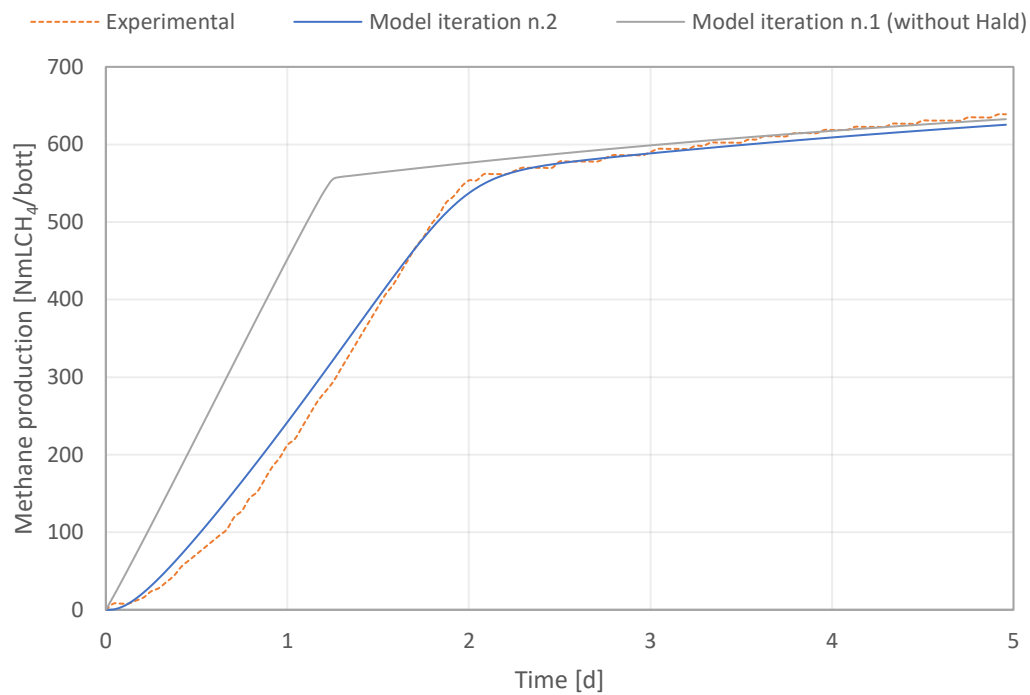

Figure 4. 30 - Acetate activity test simulation (01/04/2022).

Table 4. 20 - Model prediction performances for acetate activity test simulation (13/04/2022).

Model fitting criteria	1st iteration	2nd iteration
TIC	0.104	0.015
MARE	0.201	0.056

Glucose activity tests simulation

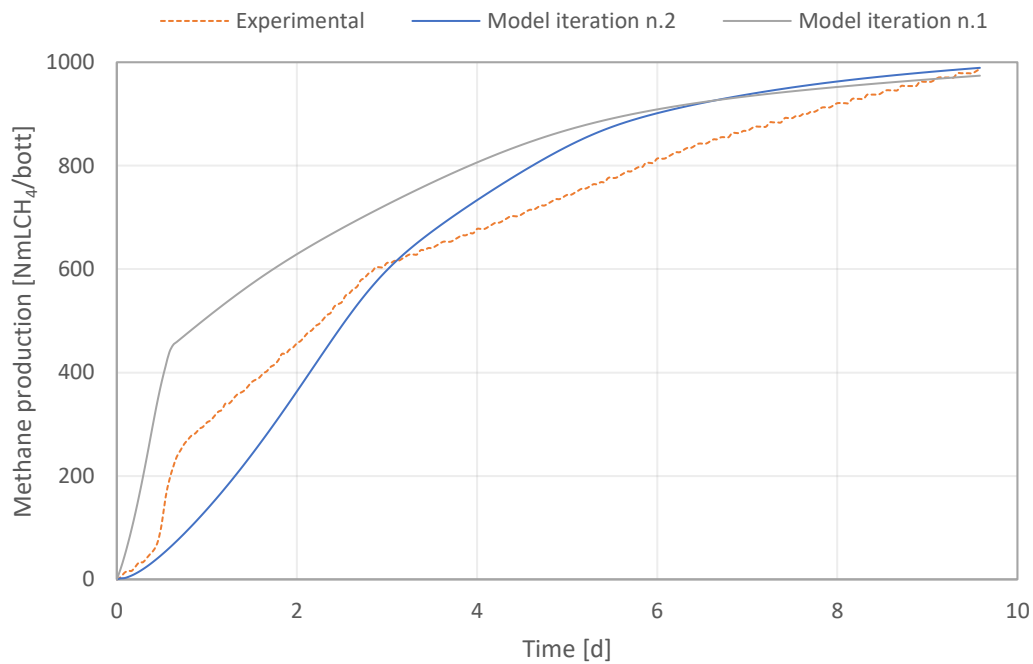Figure 4. 31 illustrates the simulation of a glucose activity test performed on May 6, 2022.

Figure 4. 31 - Glucose activity test simulation (06/05/2022).

As previously stated in paragraph 4.6.2, the experimental curve exhibits a twofold change in slope in the initial phase, which the model finds extremely difficult to replicate. This particular behaviour is most likely related to an inhibitory phenomenon involving the first slowdown and subsequent fast production of methane (i.e. the inhibition from VFA accumulation). Therefore, for an accurate simulation of the real trend, the calibration of inhibitory kinetics parameters seems to be crucial.

Nevertheless, by adjusting the $k_{m,su}$ and $K_{S,su}$ a minimal improvement in the simulation was obtained, supported by the model prediction performance reported in Table 4. 21.

Table 4. 21 - Model prediction performances for glucose activity test simulation (06/05/2022).

Model fitting criteria	1st iteration	2nd iteration
TIC	0.065	0.055
MARE	0.241	0.239

Propionate activity tests simulation

Figure 4. 32 presents the results of a simulation of propionate activity test performed on April 1, 2022.

Also in this case, the simulation improved significantly when the Monod type kinetics was replaced by the Haldane inhibition kinetics ($K_{pro,Hald}$). The modification had a positive impact on the fitting of the propionate degradation phase.

Through the adjustment of the kinetic constants, the simulation improved from the first to the second iteration. Table 4. 22 shows the simulation improvement through the values of TIC and MARE.
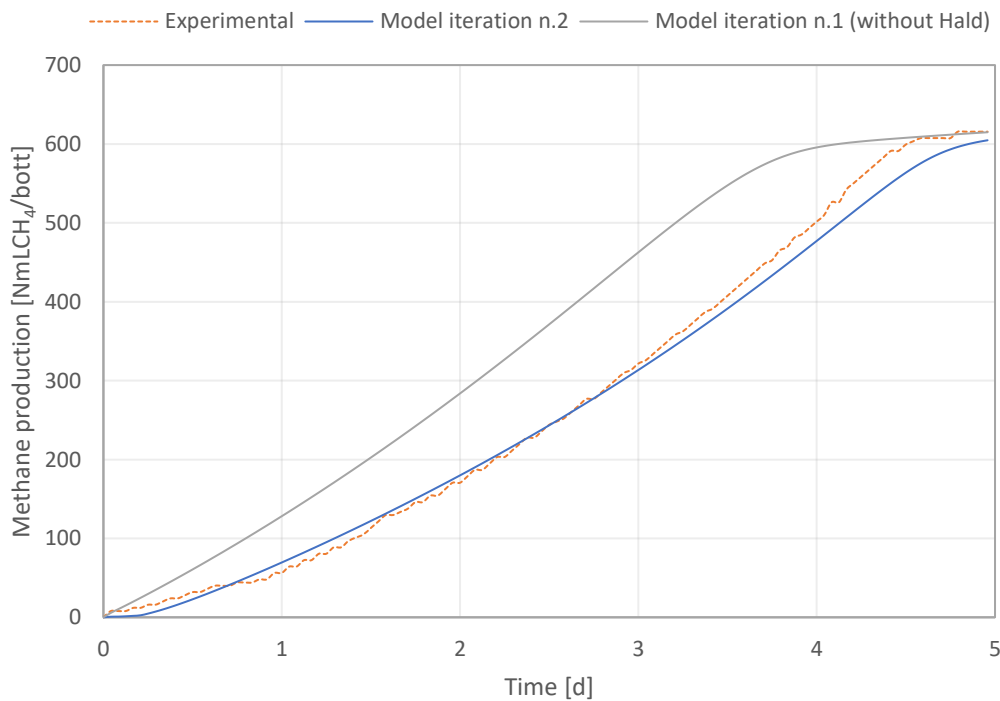

Figure 4. 32 - Propionate activity test simulation (01/04/2022).

Table 4. 22 - Model prediction performances for propionate activity test simulation (01/04/2022).

Model fitting criteria	1st iteration	2nd iteration
TIC	0.127	0.027
MARE	0.314	0.137

4.7.3. Pilot plant simulations

Although the identification of the kinetic constants led to a satisfactory simulation of the batch tests, the iterative procedure did not produce significant improvements in the modelling of the pilot plant's monitoring parameters. The main causes of model inefficiency in predicting the pilot-plant behaviour have been identified in the inability of the available experimental measures of feedstock characterization to properly apportion their organic content into the ADM1 state variables and the introduction of strong hypotheses that, in some cases, may lead to errors.

In order to accurately reflect the time period between 21/03/2022 and 27/06/2022 in which the monitoring of the pilot plant was conducted, the simulation of the pilot plant was performed for 98 days. Phases of mono- and co-digestion were included in the simulation, and the simulation complied with the real time intervals during which they were implemented. The feeding was simulated in semi-continuous mode, as in reality, and during the co-digestion phase, yogurt was added to increase the OLR first to 20%, then to 40% and finally to 60%, as was done in the real pilot plant.

The graphs from Figure 4. 33 to Figure 4. 41 illustrate the simulations' results obtained during the calibration process. To highlight how effective the model's calibration was, the trends of the variables predicted by the model at the first and second iterations are represented and compared to the experimental data. Each graph shows the trend of the simulated variable at the second iteration in blue, the simulations produced at the first iteration in grey, and the experimental data in orange. The red dotted line denotes the beginning of the co-digestion phase.

The simulation curve of the alkalinity is represented in Figure 4. 33. Although the simulation seems to follow the experimental data trend, the model significantly underestimates the alkalinity of the output digestate and no improvements are observed from the first to the second iteration. This underestimation is due to a manipulation of pH and alkalinity input data. These variables were modified because of an incomplete identification of the anionic species that could serve as proton acceptors and thus contribute to the alkalinity, which initially led to an overestimated production of carbon dioxide. Indeed, $S_{hco3_{ion}}$ is calculated in the model as the difference between the measured alkalinity and the proton-accepting species and its value, in turns, determines the percentage of CO_2. The high measured values of the input alkalinity determined high HCO_3^- concentrations and thus high CO_2 percentages in the biogas, which

117

were not comparable with those observed experimentally. The procedure was therefore to reduce the sludge alkalinity by 40% and increase pH by 10%, which enhanced the contribution of the anionic species considered, resulting in a lower $S_{hco3_{ion}}$. This reduction in the input alkalinity led to a consequent worsening of the fit on the digestate data. However, it is highly likely that some anionic species, which were not measured in the experimentation, contributed to the alkalinity of the input sludge and hence to the alkalinity of the output digestate. The identification of these components, which contribute to the alkalinity and can be subtracted from the computation of bicarbonate, would then result in a lower HCO_3^- and therefore a lower CO_2. Furthermore, the determination of these anions would allow the real input alkalinity data to be used without overestimating the CO_2 percentages, thus obtaining output alkalinity values that are comparable to those measured.

As a first attempt in this direction, the determination of PO_4^{3-} was carried out in this study, but its contribution to alkalinity was shown to be negligible. However, its experimental measurement may have been underestimated due to the analytical method employed. As can be seen from Table 4. 23, the coefficients TIC and MARE do not improve from the first to the second iteration.
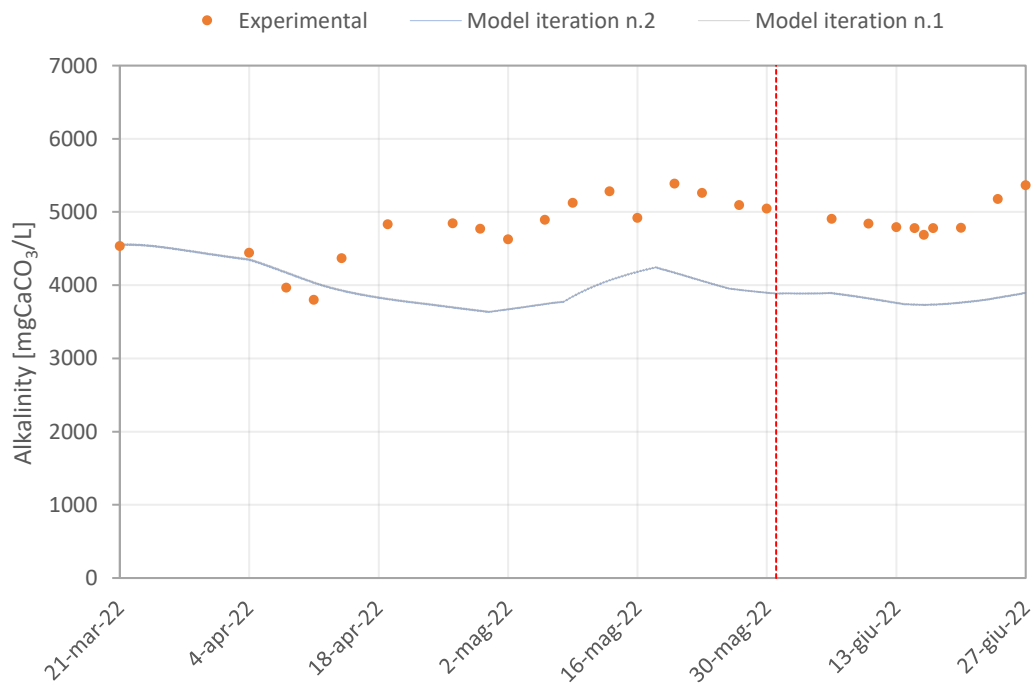

Figure 4. 33 - Digestate alkalinity simulation.

118

Figure 4. 34 shows the digestate pH simulation. The measured data appear to be more properly fitted in the final phase of the experimentation than in the first one, which corresponds to the last part of co-digestion. The slight overestimation might be explained by the pH manipulation of the input sludge. The green line represents the online data collected by the pH-probe of the pilot plant. In the first part of mono-digestion, these data are quite similar to those collected in the lab (represent by the orange dots), while the pilot plant probe appears to have been out of calibration since April 21.

Nevertheless, the simulations show a good fit of the real data as also demonstrated by the TIC and MARE indices in Table 4. 23.
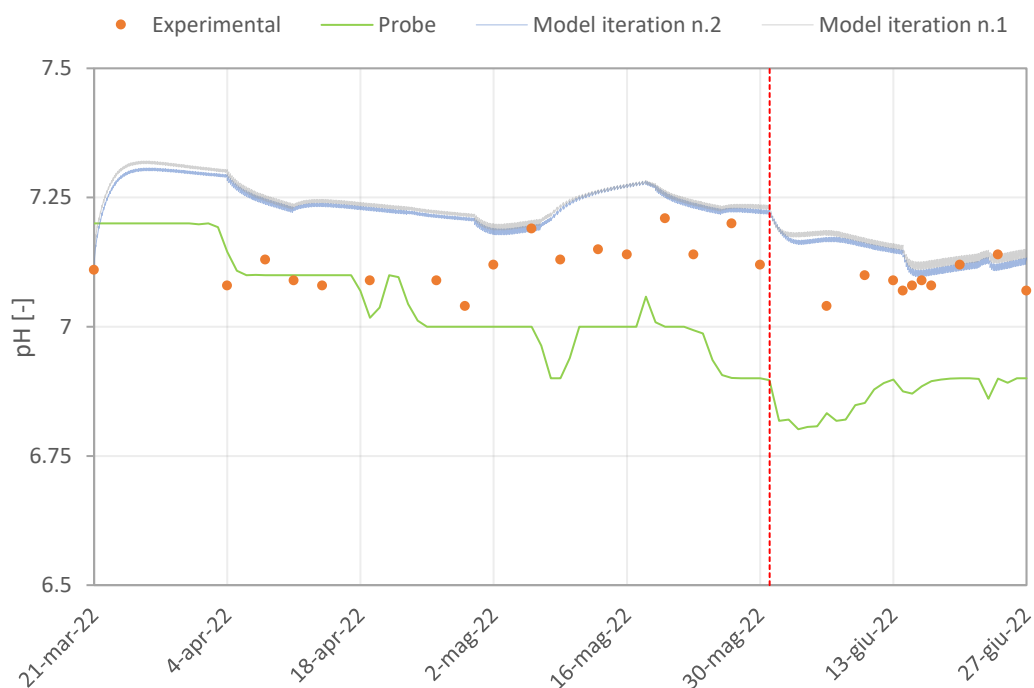

Figure 4. 34 - Digestate pH simulation.

The simulation curve of the VFAs, represented in Figure 4. 35, has a noticeable improvement from the first to the second iteration of the calibration process. In fact, the model clearly simulates the experimental data much better in the second iteration compared to the first. However, it is evident that the model is not very accurate in following the real trend. As can be seen from Table 4. 23, the TIC has a significant improvement: from 0.396 in the first iteration to 0.149 in the second iteration. The MARE index also went from 1.403 to 0.29 indicating that the calibration was very effective.
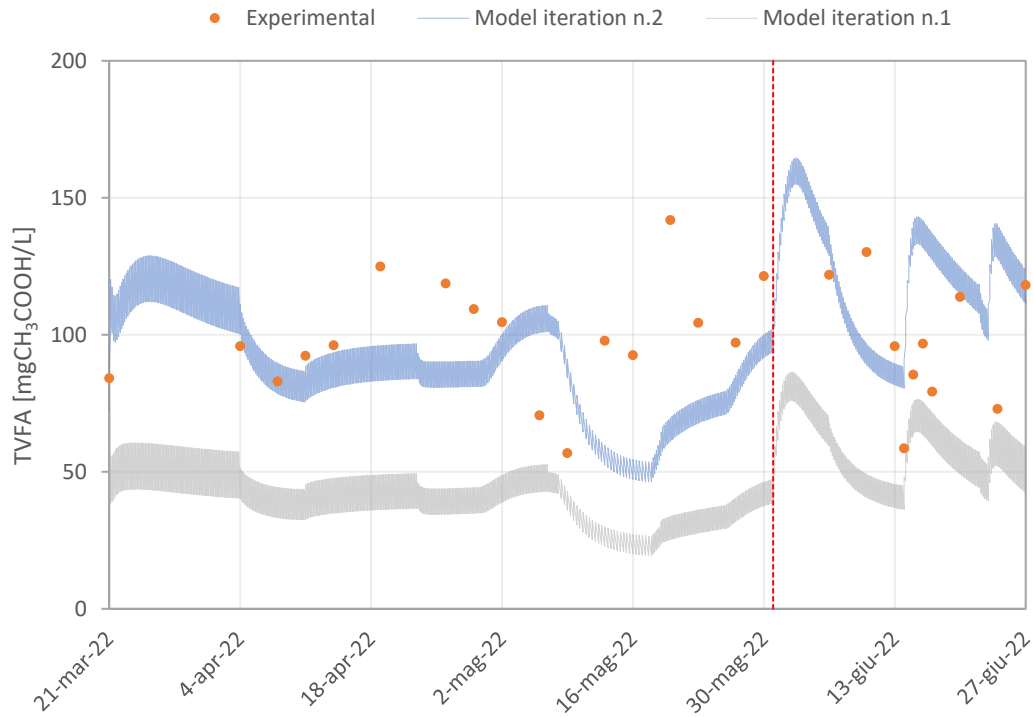
Figure 4. 35 - Digestate VFA simulation.

Figure 4. 36 shows the simulation curve of the digestate VS content. The calibration procedure was ineffective at improving the simulation.
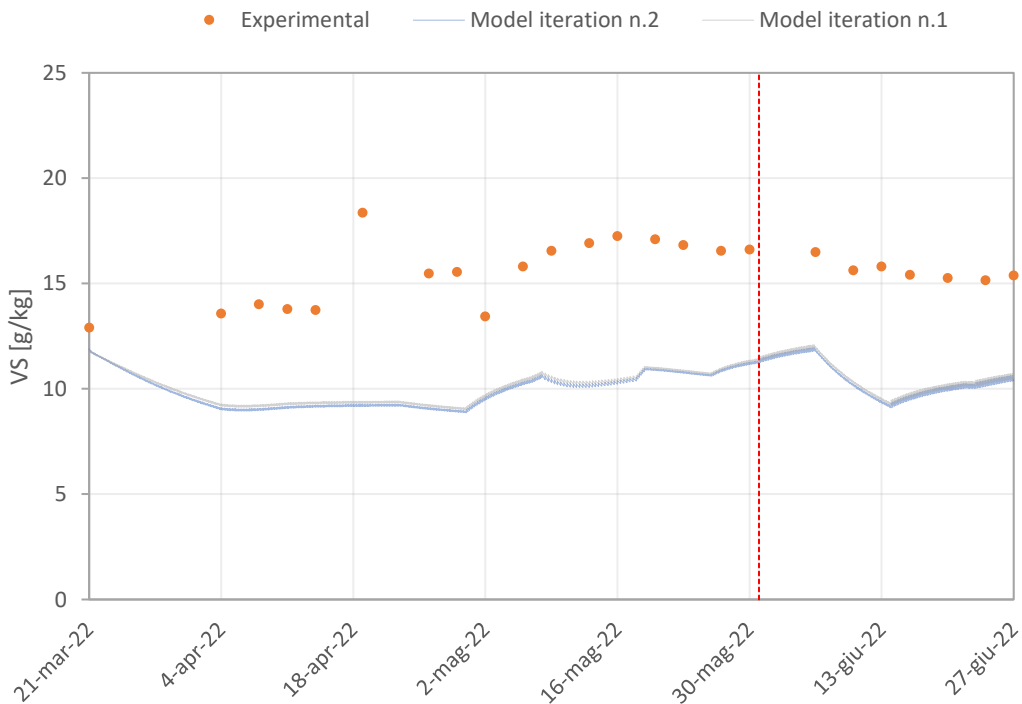

Figure 4. 36 - Digestate VS simulation.

As already observed by Nunziata and Soderino in their study, the VS calculation of the outgoing digestate is very complex, as it accounts for different aggregate measures and COD conversion factors, which are hypothesized. On the other hand, the model seems to be able to estimate the VS order of magnitude. Table 4. 23 shows a TIC value lower than 0.3, which is the maximum threshold for having a model that represents an acceptable fitting.

The simulation of the ammoniacal nitrogen is shown in Figure 4. 37. The model seems to follow the trend of the experimental data, but they are highly overestimated. The graph shows a comparison between two simulations in which the coefficient for converting the influent protein to organic nitrogen (Nc) assumes a value of 6.5 and 7.5 kgVS/kgN. The simulation represented by the blue line (Nc=6.5 kgVS/kgN) appears to better estimate the experimental data, although the deviation remains significant. A lower Nc coefficient determines a lower degradable influent proteins' concentration and thus, a lower ammoniacal nitrogen concentration in the digestate.
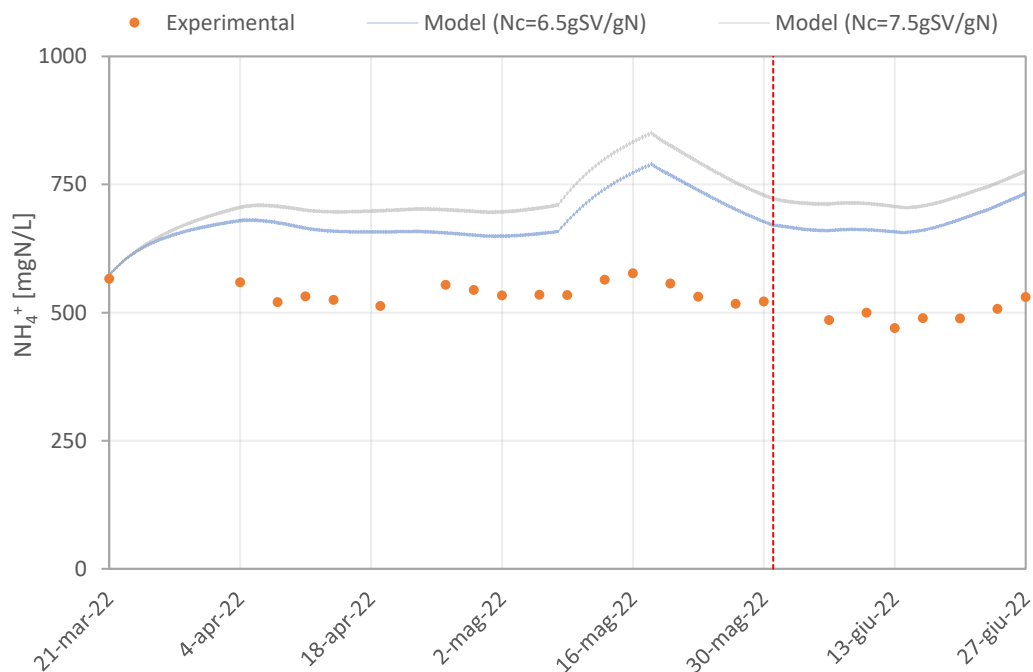

Figure 4. 37 - Digestate ammoniacal nitrogen simulation.

Furthermore, the model is based on the strong hypothesis that the undegradable fractions (proteins, carbohydrates and lipids) associated with the input inert particulate (X_i) are distributed exactly as they are in the total COD and in the X_c. This is a strong assumption that may lead to errors, as it seems in this case. This simulation, indeed, suggests that a larger portion of proteins may be considered as non-degradable, thus not contributing to the

ammonium formation. Knowing the nature of the input proteins would allow for a more precise estimation of the input concentration of degradable and non-degradable proteins. Table 4. 23 reports the TIC and MARE values for both the simulations.

Concerning the modelling of total COD, as illustrated in Figure 4. 38, the model fits the total COD experimental data quite well.

Also in this case, the simulation was carried out with two different conversion factors for converting the influent proteins to organic nitrogen. Hypothesizing a lower conversion parameter (Nc=6.5 gVS/gN) and thus, a lower fraction of degradable proteins, the model seems to more accurately predict the COD values calculated as the sum of measured proteins, carbohydrates and lipids (orange dots). The model, on the other hand, appears to better follow the trend of the measured COD values (purple dots) with an Nc value of 7.5 gVS/gN.
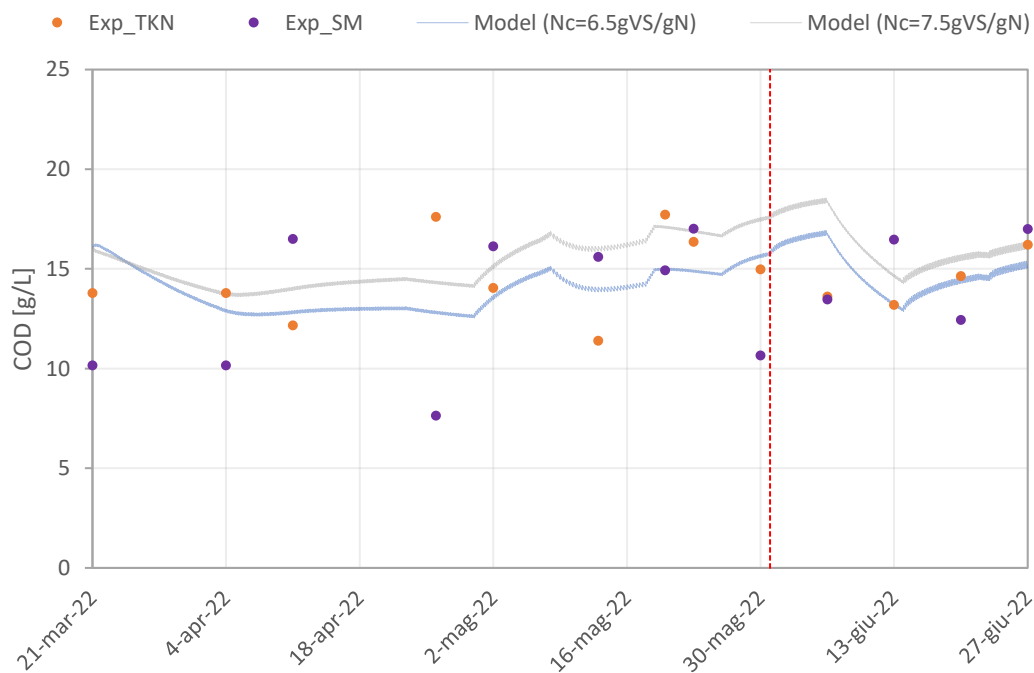

Figure 4. 38 - Digestate COD simulation.

Considering the sum of the various aggregates as a more reliable measure of total COD, the simulation improves when a conversion factor of 6.5 gVS/gN is assumed, as indicated by the TIC and MARE statistical indices in Table 4. 23.

Regarding the simulation of methane production, as shown in Figure 4. 39, the model excellently predicts the trend of the experimental data in both mono- and co-digestion phases. As expected, the model prediction gets worse when operational difficulties are encountered during the experimentation. For instance, as stated in paragraph 3.1.2, there was a loss of biogas

from the digester head at the beginning of May, which the graph clearly shows. The methane production simulation shows great deviation from the experimental data when this malfunctioning occurs.

Nevertheless, the calibration procedure seems to be effective in improving the curve's trend, especially in the co-digestion phase. TIC and MARE performance quality indices also confirm this better data fit (Table 4. 23).
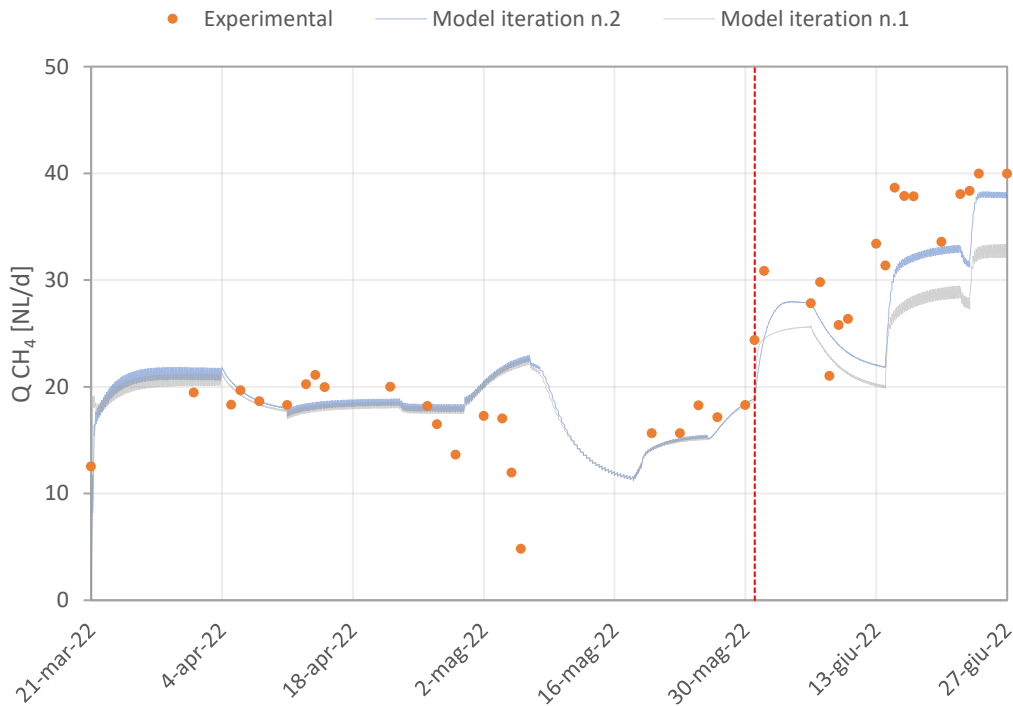

Figure 4. 39 - Methane production simulation.

Figure 4. 40 and Figure 4. 41 represent the simulations of methane and carbon dioxide content in the biogas. The biogas composition is sufficiently well predicted by the model. Errors can be due to the manipulation on total alkalinity, as described before.

Despite the manipulation of pH and alkalinity data, the CO_2 percentages still appear to be slightly too high. Other components may be present, which would determine a lower $S_{hco3_{ion}}$ and thus, lower CO_2 percentage.
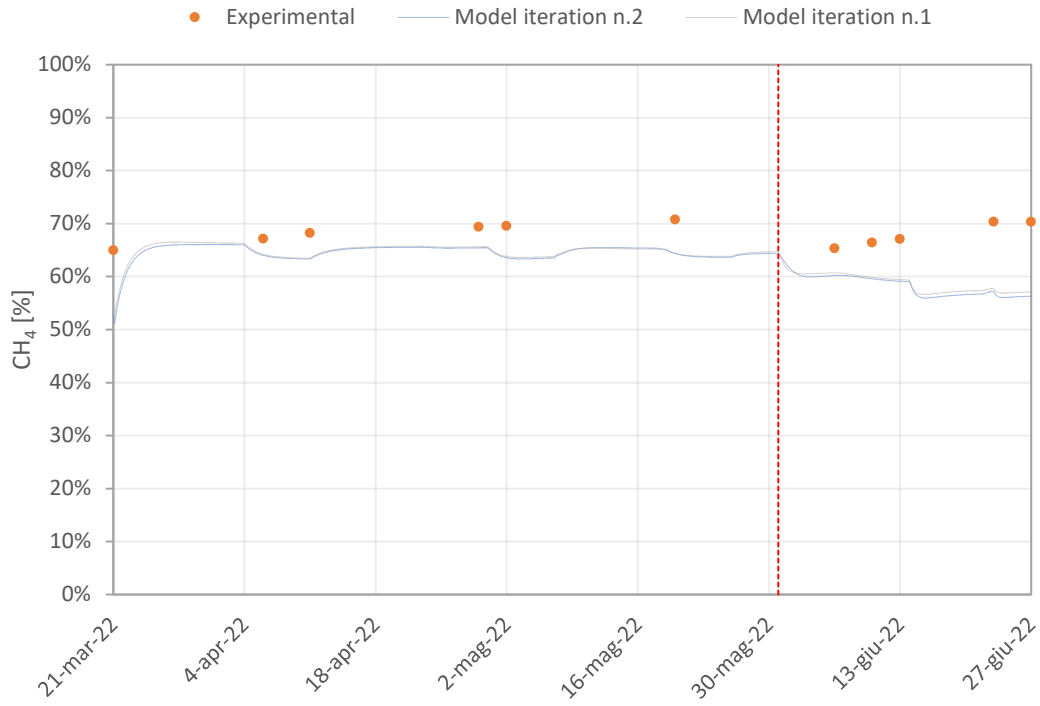
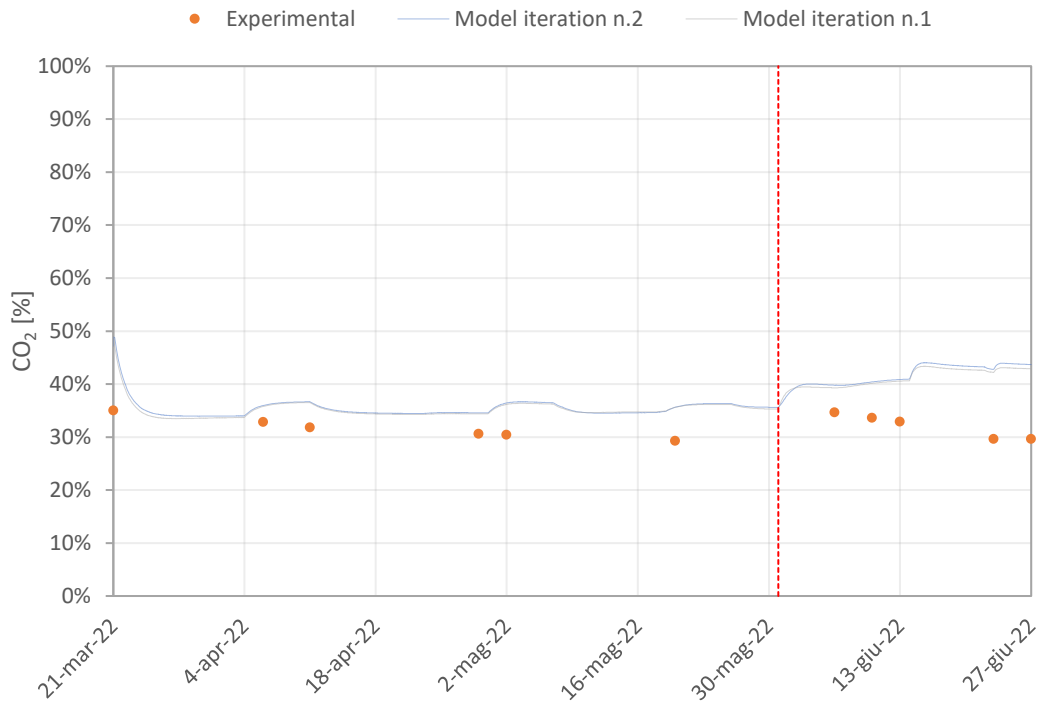Figure 4. 40 - Biogas methane content simulation.

Figure 4. 41 - Biogas carbon dioxide content simulation.

Table 4. 23 - TIC and MARE results for pilot plant simulations.

	Model fitting criteria	1st iteration or Nc=7.5	2nd iteration or Nc=6.5
Alkalinity	TIC	0.108	0.108
	MARE	0.214	0.214
pH	TIC	0.009	0.008
	MARE	0.015	0.014
VFA	TIC	0.396	0.149
	MARE	1.403	0.29
VS	TIC	0.216	0.216
	MARE	0.534	0.534
Ammoniacal nitrogen	TIC	0.158	0.127
	MARE	0.259	0.216
COD	TIC	0.068	0.061
	MARE	0.101	0.095
Q CH$_4$	TIC	0.142	0.11
	MARE	0.224	0.17
% CH$_4$	TIC	0.065	0.064
	MARE	0.111	0.11

Chapter 5: CONCLUSIONS

The experimentation was conducted on a pilot plant, first implementing a mono-digestion phase of sludge, then with a co-digestion-phase of yogurt and sludge. The major purpose of this work was to refine and recalibrate the co-digestion model previously developed and employed in the work of Soderino and Nunziata, using the analytical data from the pilot plant and the results obtained from the BMP and biomass activity tests.

5.1. Main achievements

The experimentation conducted in this study revealed an excellent response by the pilot plant to phase transitions, especially the transition from mono- to co-digestion. The plant adapted well to the higher organic loading rate due to the contribution of yogurt, which reached an increase of 60% in the final phase of co-digestion. Despite the increasing fraction of yogurt in the feeding during this step, parameters such as pH, alkalinity, ammonium and VFA were not affected and remained quite stable throughout the experimentation.

The implementation of co-digestion resulted in an increase of VS reduction and methane production rate. Indeed, the VS removal efficiency raised from 34% to 43%, shifting from mono- to co-digestion, while the methane production rate, whose average value was 20 NL/d during mono-digestion, almost doubled when the OLR was increased by 40%.

Co-digestion BMP tests also showed a higher methane production, which can be explained by potential synergistic effects between sludge and yogurt.

Biomass activity tests with propionate and acetate were useful in estimating the kinetic constants $k_{m,ac}$, $k_{m,pro}$, $K_{S,ac}$ and $K_{S,pro}$ thorough an iterative process.

Biomass activity tests with different glucose concentrations were carried out, highlighting the fact that the particular behavior characterized by an initial inhibition appeared even when low concentrations were tested.

Furthermore, incorporating Haldane inhibition kinetics into the batch ADM1 model improved significantly the simulation trend in propionate and acetate activity tests.

5.2. *Future developments*

New elements have emerged from the current investigation, which are outlined below and might be further investigated in future research.

- To improve the glucose fermentation modelling, a more realistic approach might be that of including in the ADM1 a variable stoichiometry capable of describing variations in catabolic yields of products when operating conditions vary. Indeed, these coefficients are based on the assumption that all the products of carbohydrates acidogenesis are produced in constant proportions; because of this incorrect assumption, they do not adequately reproduce the experimental results. The addition of a regulatory function that changes the relative yield depending on influential environmental parameters (mostly pH and H_2 concentration) may have a considerable impact.

- In order to better understand the digester's metabolic pathways and learn how they affect AD, including inhibitory effects, specific biomass activity tests may be carried out and a sampling procedure may be developed. These tests would aim to periodically sample small quantities of digestate and, through VFA analysis, comprehend which are the acidogenesis products that can contribute to inhibition phenomena and in what concentration.

- In order to identify the acids that might be produced by glucose fermentation, such as pyruvic acid, formic acid, lactic acid and so on, specific kits may be used.

- Further investigations may be carried out in order to identify all the anionic species that contribute to the alkalinity of sludge and digestate. In this study, a partial identification of these components led to an overestimation of $S_{hco3_{ion}}$, resulting in the model's prediction of high CO_2 percentages. Since previous analyses revealed irrelevant phosphate concentrations, the PO_4^{3-} measure was omitted from $S_{hco3_{ion}}$ calculation. However, it is possible that the analytical procedure used resulted in an underestimation of this component. Indeed, sample centrifugation can affect CO_2 stripping and pH variation, which in turn determine phosphate precipitation. In this way, solid-state phosphate is not measured, and the measurement is thus underestimated. Repeating these analyses might result in a more accurate phosphate measure.

- A correct estimation of $S_{hco3_{ion}}$ was found to be critical in the model. There are analytical methods available for determining the total inorganic carbon (TIC). On a modelling level, this provides advantages since gross errors may be avoided; nevertheless, this parameter is not frequently tested and the alkalinity measure is usually preferred.

- The model considerably overestimated the output ammonium concentration. In order to better predict the ammonium concentration, the non-degradable fractions (carbohydrates, proteins and lipids) associated with the input inert particulate (X_i) may be modified. The model relies on the strong assumption that the non-degradable fractions associated with the input inert particle (X_i) are distributed in the same way as they are in the total COD. This hypothesis may lead to errors, as it seems in this case. An alternative method for decreasing the input degradable proteins and thus the output ammonium concentration is the model calibration with respect to the parameter for converting protein to organic nitrogen (kgVS/kgN) and the COD conversion parameter (kgCOD/kgVS).

- The pilot plant's specific methane production measurements were nearly 100% of the BMP values, indicating that the hydrolysis and methanation processes were extremely efficient. This suggests that the digestate's proteins, carbohydrates, and lipids fractions were mostly non-degradable. The digestate composition may provide information regarding the X_i composition, allowing for a more accurate estimation of the input components.

BIBLIOGRAPHY

Anukam, A., Mohammadi, A., Naqvi, M., & Granström, K. (2019). A review of the chemistry of anaerobic digestion: Methods of accelerating and optimizing process efficiency. *Processes*, *7*(8), 504.

Appels, L., Baeyens, J., Degrève, J., & Dewil, R. (2008). Principles and potential of the anaerobic digestion of waste-activated sludge. *Progress in energy and combustion science*, *34*(6), 755-781.

Batstone, D. J., Keller, J., Angelidaki, I., Kalyuzhnyi, S. V., Pavlostathis, S. G., Rozzi, A., Sanders, W. T., Siegrist, H., & Vavilin, V. A. (2002). The IWA Anaerobic Digestion Model No 1 (ADM1). *Water Science and Technology : A Journal of the International Association on Water Pollution Research*, *45*(10), 65–73.

Bo, Z., Wei-min, C. A. I., & Pin-Jing, H. E. (2007). Influence of lactic acid on the two-phase anaerobic digestion of kitchen wastes. *Journal of Environmental Sciences*, *19*(2), 244-249.

Bolzonella, D., Battistoni, P., Susini, C., & Cecchi, F. (2006). Anaerobic codigestion of waste activated sludge and OFMSW: the experiences of Viareggio and Treviso plants (Italy). *Water Science and Technology*, *53*(8), 203-211.

Bonomo, L. (2014). *Trattamenti delle acque reflue*. McGraw-Hill Companies, S.r.l.

Borowski, S., Boniecki, P., Kubacki, P., & Czyżowska, A. (2018). Food waste co-digestion with slaughterhouse waste and sewage sludge: digestate conditioning and supernatant quality. *Waste Management*, *74*, 158-167.

Brulé, M., Oechsner, H., & Jungbluth, T. (2014). Exponential model describing methane production kinetics in batch anaerobic digestion: a tool for evaluation of biochemical methane potential assays. *Bioprocess and biosystems engineering*, *37*(9), 1759-1770.

Cabaleiro, R.G. (2015). Bioenergetics-based modelling of microbial ecosystems for biotechnological applications. UNIVERSIDADE DE SANTIAGO DE COMPOSTELA DEPARTAMENTO DE ENXEÑARÍA QUÍMICA.

Cecchi, F., Battistoni, P., Pavan, P., Bolzonella, D., & Innocenti, L. (2005). *APAT - Digestione anaerobica della frazione organica dei rifiuti solidi*.

Chen, Y., & Cheng, J. J. i Creamer KS 2008. *Inhibition of anaerobic digestion process: a review*, 4044-4064.

Chen, Y., Luo, J., Yan, Y., & Feng, L. (2013). Enhanced production of short-chain fatty acid by co-fermentation of waste activated sludge and kitchen waste under alkaline conditions and its application to microbial fuel cells. *Applied Energy*, *102*, 1197-1204.

Cho, Y. T., Young, J. C., Jordan, J. A., & Moon, H. M. (2005). Factors affecting measurement of specific methanogenic activity. *Water Science and technology*, *52*(1-2), 435-440.

Chow, W. L., Chong, S., Lim, J. W., Chan, Y. J., Chong, M. F., Tiong, T. J., Chin K. J. & Pan, G. T. (2020). Anaerobic co-digestion of wastewater sludge: A review of potential co-substrates and operating factors for improved methane yield. *Processes*, *8*(1), 39.

Chuenchart, W., Logan, M., Leelayouthayotin, C., & Visvanathan, C. (2020). Enhancement of food waste thermophilic anaerobic digestion through synergistic effect with chicken manure. *Biomass and bioenergy*, *136*, 105541.

Deepanraj, B., Sivasubramanian, V., & Jayaraj, S. (2014). Biogas generation through anaerobic digestion process-an overview. *Research Journal of Chemistry and Environment*, *18*, 5.

Elalami, D., Carrere, H., Monlau, F., Abdelouahdi, K., Oukarroum, A., & Barakat, A. (2019). Pretreatment and co-digestion of wastewater sludge for biogas production: Recent research advances and trends. *Renewable and Sustainable Energy Reviews*, *114*, 109287.

Fang, H. H., & Liu, H. (2002). Effect of pH on hydrogen production from glucose by a mixed culture. *Bioresource technology*, *82*(1), 87-93.

Filer, J., Ding, H. H., & Chang, S. (2019). Biochemical methane potential (BMP) assay method for anaerobic digestion research. *Water*, *11*(5), 921.

Gavala, H. N., Angelidaki, I., & Ahring, B. K. (2003). Kinetics and modeling of anaerobic digestion process. *Biomethanation I*, 57-93.

González-Cabaleiro, R., Lema, J. M., & Rodríguez, J. (2015). Metabolic energy-based modelling explains product yielding in anaerobic mixed culture fermentations. *Plos one*, *10*(5), e0126739.

Hoelzle, R. D. (2017). Metabolic mechanisms and regulation of mixed culture fermentation.

Holliger, C., Alves, M., Andrade, D., Angelidaki, I., Astals, S., Baier, U., Bougrier, C., Buffière, P., Carballa, M., De Wilde, V., Ebertseder, F., Fernández, B., Ficara, E., Fotidis, I., Frigon, J. C., De Laclos, H. F., Ghasimi, D. S. M., Hack, G., Hartel, M., … Wierinck, I. (2016). Towards a standardization of biomethane potential tests. *Water Science and Technology*, *74*(11), 2515–2522.

Holliger, C., de Laclos, H. F., & Hack, G. (2017). Methane production of full-scale anaerobic digestion plants calculated from substrate's biomethane potentials compares well with the one measured on-site. *Frontiers in Energy Research*, *5*(JUN), 1–9.

Hunter, S. M., Blanco, E., & Borrion, A. (2021). Expanding the anaerobic digestion map: A review of intermediates in the digestion of food waste. *Science of The Total Environment*, *767*, 144265.

Hussain, A., & Dubey, S. K. (2017). Specific methanogenic activity test for anaerobic degradation of influents. *Applied water science*, *7*(2), 535-542.

Jin, Z., & Yang, S. T. (1998). Extractive fermentation for enhanced propionic acid production from lactose by Propionibacterium acidipropionici. *Biotechnology progress*, *14*(3), 457-465.

Karki, R., Chuenchart, W., Surendra, K. C., Shrestha, S., Raskin, L., Sung, S., ... & Khanal, S. K. (2021). Anaerobic co-digestion: Current status and perspectives. *Bioresource Technology*, *330*, 125001.

Kleerebezem, R., & Van Loosdrecht, M. C. M. (2006). Critical analysis of some concepts proposed in ADM1. *Water Science and Technology*, *54*(4), 51-57.

Koch, K., Hafner, S. D., Weinrich, S., Astals, S., & Holliger, C. (2020). Power and limitations of biochemical methane potential (BMP) tests. *Frontiers in Energy Research*, *8*, 63.

Lee, W. S., Chua, A. S. M., Yeoh, H. K., & Ngoh, G. C. (2014). A review of the production and applications of waste-derived volatile fatty acids. *Chemical Engineering Journal*, *235*, 83-99.

Li, J., Zheng, G., He, J., Chang, S., & Qin, Z. (2009). Hydrogen-producing capability of anaerobic activated sludge in three types of fermentations in a continuous stirred-tank reactor. *Biotechnology Advances*, *27*(5), 573-577.

Martinez, F. A. C., Balciunas, E. M., Salgado, J. M., González, J. M. D., Converti, A., & de Souza Oliveira, R. P. (2013). Lactic acid properties, applications and production: A review. *Trends in food science & technology*, *30*(1), 70-83.

Mata-Alvarez, J., Dosta, J., Romero-Güiza, M. S., Fonoll, X., Peces, M., & Astals, S. (2014). A critical review on anaerobic co-digestion achievements between 2010 and 2013. *Renewable and sustainable energy reviews*, *36*, 412-427.

Metcalf & Eddy I AECOM. (2014). *Wastewater Engineering: Treatment and Resource Recovery, Fifth Edition* (McGraw-Hill Education (ed.); 5th ed.). McGraw-Hill Education.

Poggio, D. A. (2015). *Modification and experimental calibration of ADM1 for modelling the anaerobic digestion of solid wastes in demand driven applications* (Doctoral dissertation, University of Leeds).

Rajagopal, R., Massé, D. I., & Singh, G. (2013). A critical review on inhibition of anaerobic digestion process by excess ammonia. *Bioresource technology*, *143*, 632-641.

Ramírez-Rivas, I. D. (2013). Anaerobic digestion modeling: from one to several bacterial populations. *TecnoLógicas*, (31), 181-201.

Regueira, A., González-Cabaleiro, R., Ofiţeru, I. D., Rodríguez, J., & Lema, J. M. (2018). Electron bifurcation mechanism and homoacetogenesis explain products yields in mixed culture anaerobic fermentations. *Water Research*, *141*, 349-356.

Ren, N., Wang, B., & Huang, J. C. (1997). Ethanol-type fermentation from carbohydrate in high rate acidogenic reactor. *Biotechnology and bioengineering*, *54*(5), 428-433.

Rodríguez, J., Lema, J. M., Van Loosdrecht, M. C. M., & Kleerebezem, R. (2006). Variable stoichiometry with thermodynamic control in ADM1. *Water Science and Technology*, *54*(4), 101-110.

Rozzi, A., & Remigi, E. (2004). Methods of assessing microbial activity and inhibition under anaerobic conditions: a literature review. *Re/Views in Environmental Science & Bio/Technology*, *3*(2), 93-115.

Shi, E., Li, J., & Zhang, M. (2019). Application of IWA Anaerobic Digestion Model No. 1 to simulate butyric acid, propionic acid, mixed acid, and ethanol type fermentative systems using a variable acidogenic stoichiometric approach. *Water research*, *161*, 242-250.

Shin, H. S., & Youn, J. H. (2005). Conversion of food waste into hydrogen by thermophilic acidogenesis. *Biodegradation*, *16*(1), 33-44.

Sibiya, N. T., Tesfagiorgis, H. B., & Muzenda, E. (2015). Influence of nutrients addition for enhanced biogas production from energy crops: A review. *Magnesium*, *1*(1.5).

Sørensen, A. H., & Ahring, B. K. (1993). Measurements of the specific methanogenic activity of anaerobic digestor biomass. *Applied microbiology and biotechnology*, *40*(2), 427-431.

Wang, K., Yin, J., Shen, D., & Li, N. (2014). Anaerobic digestion of food waste for volatile fatty acids (VFAs) production with different types of inoculum: effect of pH. *Bioresource technology*, *161*, 395-401.

Xie, S., Higgins, M. J., Bustamante, H., Galway, B., & Nghiem, L. D. (2018). Current status and perspectives on anaerobic co-digestion and associated downstream processes. *Environmental Science: Water Research & Technology*, *4*(11), 1759-1770.

Yadav, M., Joshi, C., Paritosh, K., Thakur, J., Pareek, N., Masakapalli, S. K., & Vivekanand, V. (2021). Organic waste conversion through anaerobic digestion: A critical insight into the metabolic pathways and microbial interactions. *Metabolic Engineering*.

Zhang, F., Zhang, Y., Chen, M., van Loosdrecht, M. C., & Zeng, R. J. (2013). A modified metabolic model for mixed culture fermentation with energy conserving electron bifurcation reaction and metabolite transport energy. *Biotechnology and Bioengineering*, *110*(7), 1884-1894.

Zhou, M., Yan, B., Wong, J. W., & Zhang, Y. (2018). Enhanced volatile fatty acids production from anaerobic fermentation of food waste: A mini-review focusing on acidogenic metabolic pathways. *Bioresource technology*, *248*, 68-78.

Zhu, H., Parker, W., Basnar, R., Proracki, A., Falletta, P., Béland, M., & Seto, P. (2009). Buffer requirements for enhanced hydrogen production in acidogenic digestion of food wastes. *Bioresource technology*, *100*(21), 5097-5102.

APPENDIX A

All the biochemical rate coefficients and the kinetic rate equations for soluble and particulate components of the ADM1 model are shown in the Petersen matrix (Table A. 2 and Table A. 3). Table A. 1 summarizes the nomenclatures and units used in the ADM1 and in the current work.

Table A. 1 - Nomenclature and units used.

C_i	carbon content of component i	$kmoleC \cdot kgCOD^{-1}$
i	component index	
I	inhibition function	
j	process index	
$k_{A/B,i}$	acid-base rate constant for component i	$M^{-1} \cdot d^{-1}$
k_{dec}	first order decay rate for biomass death	d^{-1}
$k_L a$	gas–liquid transfer coefficient	d^{-1}
k_m	specific Monod maximum uptake rate	$kgCOD \cdot m^{-3}\_S \cdot kgCOD \cdot m^{-3}\_X \cdot d^{-1}$
K_a	acid-base equilibrium constant	$M\ (kmole \cdot m^{-3})$
K_H	Henry's law coefficient	$M.bar^{-1}$
K_I	inhibition constant	nominally $kgCOD \cdot m^{-3}$
K_S	Monod half saturation constant	$kgCOD \cdot m^{-3}$
N_i	nitrogen content of component I	$kmoleN \cdot kg\ COD^{-1}$
p_{gas}	pressure of gas	bar
pH	$-log_{10}[S_{H^+}]$	
pK_a	$-log_{10}[K_a]$	
q	flow	m^3
S_i	soluble component i (dynamic or algebraic variable)	nominally $kgCOD \cdot m^{-3}$
S_I	inhibitory component	nominally $kgCOD \cdot m^{-3}$
t	time	d
T	temperature	K
V	volume	m^3
X_i	particulate component i	$kgCOD \cdot m^{-3}$
$Y_{substrate}$	yield of biomass on substrate	$kgCOD\_X \cdot kgCOD\_S$
$v_{i,j}$	rate coefficients for component i on process j	nominally $kgCOD \cdot m^{-3}$
$f_{product,substrate}$	yield (catabolism only) of product on substrate	$kgCOD \cdot kgCOD^{-1}$
ρ_i	rate for process j	$kgCOD.m^{-3}$

The inhibition functions in the Petersen matrix are as follows:

$$I_{pH} = \begin{cases} exp\left(-3\left(\dfrac{pH - pH_{UL}}{pH_{UL} - pH_{LL}}\right)^2\right) & if\ pH < pH_{UL} \\ \\ 1\ otherwise \end{cases}$$

$$I_{IN,lim} = \frac{1}{1 + K_{S,IN}/S_{IN}}$$

$$I_{h2} = \frac{1}{1 + S_{h2}/K_I}$$

$$I_{NH3,Xac} = \frac{1}{1 + S_{nh3}/K_{I,nh3}}$$

Table A. 2 - Biochemical rate coefficients ($v_{i,j}$) and the kinetic rate equations (ρ_j) for soluble components (i = 1-12).

j	Component → i / Process ↓	1 S_{su}	2 S_{aa}	3 S_{fa}	4 S_{va}	5 S_{bu}	6 S_{pro}	7 S_{ac}	8 S_{h2}	9 S_{ch4}	10 S_{IC}	11 S_{IN}	12 S_I	Rate (ρ_j, kg COD.m^{-3}.d^{-1})
1	Disintegration												$f_{sI,xc}$	$k_{dis}X_c$
2	Hydrolysis carbohydrates	1												$k_{hyd,ch}X_{ch}$
3	Hydrolysis of proteins		1											$k_{hyd,pr}X_{pr}$
4	Hydrolysis of lipids	$1-f_{fa,li}$		$1-f_{fa,li}$										$k_{hyd,li}X_{li}$
5	Uptake of sugars	-1				$(1-Y_{su})f_{bu,su}$	$(1-Y_{su})f_{pro,su}$	$(1-Y_{su})f_{ac,su}$	$(1-Y_{su})f_{h2,su}$		$-\sum_{i=9,11-24} C_i v_{i,5}$	$-(Y_{su})N_{bac}$		$k_{m,su}\dfrac{S_{su}}{K_S+S}X_{su}I_1$
6	Uptake of amino acids		-1		$(1-Y_{aa})f_{va,aa}$	$(1-Y_{aa})f_{bu,aa}$	$(1-Y_{aa})f_{pro,aa}$	$(1-Y_{aa})f_{ac,aa}$	$(1-Y_{aa})f_{h2,aa}$		$-\sum_{i=1-9,11-24} C_i v_{i,6}$	$N_{aa}-(Y_{aa})N_{bac}$		$k_{m,aa}\dfrac{S_{aa}}{K_S+S_{aa}}X_{aa}I_1$
7	Uptake of LCFA			-1				$(1-Y_{fa})0.7$	$(1-Y_{fa})0.3$			$-(Y_{fa})N_{bac}$		$k_{m,fa}\dfrac{S_{fa}}{K_S+S_{fa}}X_{fa}I_2$
8	Uptake of valerate				-1		$(1-Y_{c4})0.54$	$(1-Y_{c4})0.31$	$(1-Y_{c4})0.15$			$-(Y_{c4})N_{bac}$		$k_{m,c4}\dfrac{S_{va}}{K_S+S_{va}}X_{c4}\dfrac{1}{1+S_{bu}/S_{va}}I$
9	Uptake of butyrate					-1		$(1-Y_{c4})0.8$	$(1-Y_{c4})0.2$			$-(Y_{c4})N_{bac}$		$k_{m,c4}\dfrac{S_{bu}}{K_S+S_{bu}}X_{c4}\dfrac{1}{1+S_{va}/S_{bu}}I$
10	Uptake of propionate						-1	$(1-Y_{pro})0.57$	$(1-Y_{pro})0.43$		$-\sum_{i=1-9,11-24} C_i v_{j,10}$	$-(Y_{pro})N_{bac}$		$k_{m,pr}\dfrac{S_{pro}}{K_S+S_{pro}}X_{pro}I_2$
11	Uptake of acetate							-1		$(1-Y_{ac})$	$-\sum_{i=1-9,11-24} C_i v_{j,11}$	$-(Y_{ac})N_{bac}$		$k_{m,ac}\dfrac{S_{ac}}{K_S+S_{ac}}X_{ac}I_3$
12	Uptake of hydrogen								-1	$(1-Y_{h2})$	$-\sum_{i=1-9,11-24} C_i v_{j,12}$	$-(Y_{h2})N_{bac}$		$k_{m,h2}\dfrac{S_{h2}}{K_S+S_{h2}}X_{h2}I_1$
13	Decay of X_{su}													$k_{dec,Xsu}X_{su}$
14	Decay of X_{aa}													$k_{dec,Xaa}X_{aa}$
15	Decay of X_{fa}													$k_{dec,Xfa}X_{fa}$
16	Decay of X_{c4}													$k_{dec,Xc4}X_{c4}$
17	Decay of X_{pro}													$k_{dec,Xpro}X_{pro}$
18	Decay of X_{ac}													$k_{dec,Xac}X_{ac}$
19	Decay of X_{h2}													$k_{dec,Xh2}X_{h2}$

| Monosaccharides (kgCOD·m^{-3}) | Amino acids (kgCOD·m^{-3}) | Long chain fatty acids (kgCOD·m^{-3}) | Total valerate (kgCOD·m^{-3}) | Total butyrate (kgCOD·m^{-3}) | Total propionate (kgCOD·m^{-3}) | Total acetate (kgCOD·m^{-3}) | Hydrogen gas (kgCOD·m^{-3}) | Methane gas (kgCOD·m^{-3}) | Inorganic carbon (kmoleC·m^{-3}) | Inorganic nitrogen (kmoleN·m^{-3}) | Soluble inerts (kgCOD·m^{-3}) | Inhibition factors: $I_1 = I_{pH}I_{IN,lim}$, $I_2 = I_{pH}I_{IN,lim}I_{h2}$, $I_3 = I_{pH}I_{IN,lim}I_{NH3,Xac}$ |

Table A. 3 - Biochemical rate coefficients (vi,j) and the kinetic rate equations (ρj) for particulate components (i = 13-24).

j	Component → \ Process ↓	i	13 X_c	14 X_{ch}	15 X_{pr}	16 X_{li}	17 X_{su}	18 X_{aa}	19 X_{fa}	20 X_{c4}	21 X_{pro}	22 X_{ac}	23 X_{h2}	24 X_I	Rate (ρ_j, kg COD·m^{-3}·d^{-1})
1	Disintegration		-1	$f_{ch,xc}$	$f_{pr,xc}$	$f_{li,xc}$								$f_{xI,xc}$	$k_{dis}X_c$
2	Hydrolysis carbohydrates			-1											$k_{hyd,ch}X_{ch}$
3	Hydrolysis of proteins				-1										$k_{hyd,pr}X_{pr}$
4	Hydrolysis of lipids					-1									$k_{hyd,li}X_{li}$
5	Uptake of sugars						Y_{su}								$k_{m,su}\dfrac{S_{su}}{K_S+S}X_{su}I_1$
6	Uptake of amino acids							Y_{aa}							$k_{m,aa}\dfrac{S_{aa}}{K_S+S_{aa}}X_{aa}I_1$
7	Uptake of LCFA								Y_{fa}						$k_{m,fa}\dfrac{S_{fa}}{K_S+S_{fa}}X_{fa}I_2$
8	Uptake of valerate									Y_{c4}					$k_{m,c4}\dfrac{S_{va}}{K_S+S_{va}}X_{c4}\dfrac{1}{1+S_{bu}/S_{va}}I$
9	Uptake of butyrate									Y_{c4}					$k_{m,c4}\dfrac{S_{bu}}{K_S+S_{bu}}X_{c4}\dfrac{1}{1+S_{va}/S_{bu}}I$
10	Uptake of propionate										Y_{pro}				$k_{m,pr}\dfrac{S_{pro}}{K_S+S_{pro}}X_{pro}I_2$
11	Uptake of acetate											Y_{ac}			$k_{m,ac}\dfrac{S_{ac}}{K_S+S_{ac}}X_{ac}I_3$
12	Uptake of hydrogen												Y_{h2}		$k_{m,h2}\dfrac{S_{h2}}{K_S+S_{h2}}X_{h2}I_1$
13	Decay of X_{su}		1				-1								$k_{dec,Xsu}X_{su}$
14	Decay of X_{aa}		1					-1							$k_{dec,Xaa}X_{aa}$
15	Decay of X_{fa}		1						-1						$k_{dec,Xfa}X_{fa}$
16	Decay of X_{c4}		1							-1					$k_{dec,Xc4}X_{c4}$
17	Decay of X_{pro}		1								-1				$k_{dec,Xpro}X_{pro}$
18	Decay of X_{ac}		1									-1			$k_{dec,Xac}X_{ac}$
19	Decay of X_{h2}		1										-1		$k_{dec,Xh2}X_{h2}$

Composites (kgCOD·m^{-3})

Carbohydrates (kgCOD·m^{-3})

Proteins (kgCOD·m^{-3})

Lipids (kgCOD·m^{-3})

Sugar degraders (kgCOD·m^{-3})

Amino acid degraders (kgCOD·m^{-3})

LCFA degraders (kgCOD·m^{-3})

Valerate and butyrate degraders (kgCOD·m^{-3})

Propionate degraders (kgCOD·m^{-3})

Acetate degraders (kgCOD·m^{-3})

Hydrogen degraders (kgCOD·m^{-3})

Particulate inerts (kgCOD·m^{-3})

Inhibition factors:
$I_1 = I_{pH}\cdot I_{IN,lim}$
$I_2 = I_{pH}\cdot I_{IN,lim}\cdot I_{h2}$
$I_3 = I_{pH}\cdot I_{IN,lim}\cdot I_{NH3,Xac}$

APPENDIX B

List of all the parameters that have been assumed as default from Rosen and Jeppsson (2006) and Nunziata and Soderino (2021).

Table B. 1 - ADM1 stoichiometric parameter values (on the left of the table) and biochemical parameter values (on the right).

Parameter	Value	Unit	Parameter	Value	Unit
N_Xc	0.0027	$kmol_N/kg_{COD}$	kdec_h2	0.02	d^{-1}
C_aa	0.03	$kmol_C/kg_{COD}$	kdec_Xaa	0.02	d^{-1}
C_ac	0.0313	$kmol_C/kg_{COD}$	kdec_Xac	0.02	d^{-1}
C_biom	0.0313	$kmol_C/kg_{COD}$	kdec_Xc4	0.02	d^{-1}
C_bu	0.025	$kmol_C/kg_{COD}$	kdec_Xfa	0.02	d^{-1}
C_ch	0.0313	$kmol_C/kg_{COD}$	kdec_Xpro	0.02	d^{-1}
C_ch4	0.0156	$kmol_C/kg_{COD}$	kdec_Xsu	0.02	d^{-1}
C_fa	0.0217	$kmol_C/kg_{COD}$	kdis	1.5	d^{-1}
C_li	0.022	$kmol_C/kg_{COD}$	khyd_ch	0.3	d^{-1}
C_pr	0.03	$kmol_C/kg_{COD}$	khyd_li	0.5	d^{-1}
C_pro	0.0268	$kmol_C/kg_{COD}$	khyd_pr	0.2	d^{-1}
C_SI	0.03	$kmol_C/kg_{COD}$	KI_h2_c4	1E-05	d^{-1}
C_su	0.0313	$kmol_C/kg_{COD}$	KI_h2_fa	5E-06	$kgCOD/m^3$
C_va	0.024	$kmol_C/kg_{COD}$	KI_h2_pro	3.5E-06	$kgCOD/m^3$
C_Xc	0.0279	$kmol_C/kg_{COD}$	KI_nh3	0.0018	M
C_XI	0.03	$kmol_C/kg_{COD}$	km_aa	8	d^{-1}
f_ac_aa	0.4	-	km_ac	8	d^{-1}
f_ac_su	0.41	-	km_c4	20	d^{-1}

Parameter	Value	Unit	Parameter	Value	Unit
f_bu_aa	0.26	-	**km_fa**	6	d^{-1}
f_bu_su	0.13	-	**km_h2**	35	d^{-1}
f_fa_li	0.95	-	**km_pro**	20	d^{-1}
f_h2_aa	0.06	-	**km_su**	8	d^{-1}
f_h2_su	0.19	-	**Ks_aa**	0.2	$kgCOD/m^3$
f_pro_aa	0.05	-	**Ks_ac**	0.01	$kgCOD/m^3$
f_pro_su	0.27	-	**Ks_c4**	0.2	M
f_va_aa	0.23	-	**Ks_fa**	0.4	$kgCOD/m^3$
N_aa	0.007	$kmol_N/kg_{COD}$	**Ks_h2**	7E-06	$kgCOD/m^3$
N_biom	0.006	$kmol_N/kg_{COD}$	**Ks_IN**	2.5E-05	M
N_I	0.004	$kmol_N/kg_{COD}$	**Ks_pro**	0.1	$kgCOD/m^3$
Y_aa	0.08	-	**Ks_su**	0.3	$kgCOD/m^3$
Y_ac	0.05	-	**pH_LL_aa**	4	-
Y_c4	0.06	-	**pH_LL_ac**	6	-
Y_fa	0.06	-	**pH_LL_h2**	5	-
Y_h2	0.06	-	**pH_UL_aa**	5.5	-
Y_pro	0.04	-	**pH_UL_ac**	7	-
Y_su	0.1	-	**pH_UL_h2**	6	-

Table B. 2 - ADM1 physiochemical parameter values; Van't Hoff temperature correction has been applied if required.

Parameter	Value	Unit
R	0.08314	bar M^{-1} K^{-1}
T_op	310.15	K
Ka_ac	10^ (-4.76)	M
Ka_bu	10^ (-4.82)	M
Ka_pro	10^ (-4.88)	M
Ka_va	10^ (-4.86)	M
Ka_co2	$10^{-6.35}\exp\left(\dfrac{7646}{R*100}\left(\dfrac{1}{298}-\dfrac{1}{T}\right)\right)$	M
Ka_IN	$10^{-9.25}\exp\left(\dfrac{51965}{R*100}\left(\dfrac{1}{298}-\dfrac{1}{T}\right)\right)$	M
Ka_h20	$10^{-14}\exp\left(\dfrac{55900}{R*100}\left(\dfrac{1}{298}-\dfrac{1}{T}\right)\right)$	M
KH_ch4	$0.0014\cdot\exp\left(\dfrac{-14240}{R*100}\left(\dfrac{1}{298}-\dfrac{1}{T}\right)\right)$	M$_{liq}$ bar^{-1}
KH_co2	$0.035\cdot\exp\left(\dfrac{-19410}{R*100}\left(\dfrac{1}{298}-\dfrac{1}{T}\right)\right)$	M$_{liq}$ bar^{-1}
KH_h2	$0.00078\cdot\exp\left(\dfrac{-4180}{R*100}\left(\dfrac{1}{298}-\dfrac{1}{T}\right)\right)$	M$_{liq}$ bar^{-1}
kLa_o2	150	d^{-1}
D_o2	2.8e-5	c^2 s^{-1}
D_ch4	1.57e-5	c^2 s^{-1}
D_co2	1.98e-5	c^2 s^{-1}

Parameter	Value	Unit
D_h2	4.65e-5	$c^2\ s^{-1}$
P_atm	1.013	bar
p_h2o	$0.0313 \cdot \exp\left(5290\left(\dfrac{1}{298} - \dfrac{1}{T}\right)\right)$	bar

APPENDIX C

The following tables show the analyses results for the characterization of sludge and digestate.

Table C. 1 - Analyses results for sludge characterization.

Parameter	Unit	Value											Average	St. Deviation
		06/04/2022	13/04/2022	20/04/2022	27/04/2022	04/05/2022	18/05/2022	25/05/2022	01/06/2022	08/06/2022	16/06/2022	22/06/2022		
Total Fraction														
pH	-	5.3	5.4	5.6	5.5	5.9	5.6	5.8	5.7	5.5	5.6	5.9	6	0.2
Alkalinity	$mgCaCO_3/L$	2123	2231	2127	2870	2907	2598	3029	2452	2627	2802	2978	2613	338
TS	gTS/kg	29	30	29	39	33	28	39	27	31	28	26	31	4
VS	gVS/kg	21	22	21	28	24	20	26	19	21	20	18	22	3
Total COD	gCOD/kg	27.6	29.0	28.6		34.6							30	3
Total TKN	gN/kg	1.42	1.52	1.38	1.71	2.35	1.37	1.45	0.92	1.31	1.23	1.12	1.44	0.4
Total Carbohydrates	gGlu/kg	4.63	4.07	3.78	4.91	3.79	3.01	4.92	2.99	3.66	3.04		3.88	0.7
Total Proteins	gN/kg	1.38	1.47	1.35	1.68	2.28	1.32	1.41	0.86	1.24	1.15		1.41	0.4
BMP Total	$NmLCH_4/gVS$		342		329		301			301			318	20
Particulate Fraction														
Particulate Lipids	g/kgVS,p	176	167	173	198	186	192	199	140	174	189	188	180	17
Particulate Lipids	g/kgVS	168	160	167	192	180	185	192	135	168	183	183	174	17
TS - particulate fraction	gTS,p/kg,p	131	126	124	136	124	120	153	115	127	115	113	126	11
VS - particulate fraction	gVS,p/kg,p	99	95	94	100	90	88	100	80	89	80	78	90	8
Soluble Fraction														
VFA: acetic acid	mg/L	934	1042	826	874	588	737	723	518	500	569	436	704	198
VFA: propionic acid	mg/L	266	314	200	209	176	176	193	167	217	227	231	216	44
VFA: iso-butyiric acid	mg/L	25	31	27	25	25	35	63	33	30	42	51	35	12
VFA: butyric acid	mg/L	80	100	56	56	45	39	41	37	47	50	38	53	20
VFA: iso-valeric acid	mg/L	7	13	5	5	20	20	17	23	25	33	52	20	14
VFA: valeric acid	mg/L	17	25	12	12	10	8	13	10	11	14	15	13	5
TS - soluble fraction	gTS,s/L	2.6	2.7	2.1	2.2	1.8	1.9	2.1	1.9	1.9	1.8	1.4	2	0.4
VS - soluble fraction	gVS,s/L	1.2	1.3	1.0	1.2	0.9	0.8	1.1	0.9	0.9	0.8	0.7	1	0.2
Ammoniacal nitrogen	mgN/L	49	68	45	47	85	67	50	87	95	100	99	72	22
Phosphate	mgP/L							30	32	40	31	24	31	6

Table C. 2 - Data analysis of sludge analytical measurements.

Parameter	Unit	Value										Average	St. Deviation
		06/04/2022	13/04/2022	20/04/2022	27/04/2022	04/05/2022	18/05/2022	25/05/2022	01/06/2022	08/06/2022	16/06/2022		
Total Carbohydrates	gCOD/L	4.96	4.37	4.06	5.28	4.07	3.23	5.29	3.21	3.94	3.26	4.17	0.8
Total Proteins	gCOD/L	12.75	13.47	12.43	15.49	21.01	12.12	13.03	7.78	11.28	10.51	12.99	3
Total Lipids	gCOD/L	10.51	10.29	10.43	15.71	12.37	11.01	14.70	7.33	10.46	10.53	11.33	2
Carbohydrates/CODtot	-	16.6%	14.6%	14.3%	13.9%	10.6%	11.7%	15.4%	16.6%	14.7%	12.8%	14%	2%
Proteins/CODtot	-	42.7%	44.9%	44.0%	40.9%	54.5%	43.9%	38.0%	40.3%	42.2%	41.2%	43%	4%
Lipids/CODtot	-	35.2%	34.3%	36.9%	41.4%	32.1%	39.9%	42.8%	37.9%	39.1%	41.3%	38%	3%
Estimated total COD	gCOD/L	29.9	30.0	28.3	37.9	38.5	27.6	34.3	19.3	26.7	25.5	29.8	6
VS/TS	gVS/gTS	0.74	0.74	0.75	0.73	0.72	0.72	0.66	0.69	0.69	0.69	0.71	0.03
TVFA	gCOD/L	1.6	1.9	1.4	1.4	1.1	1.2	1.3	1.0	1.1	1.2	1.3	0.3
COD/VS	gCOD/gVS	1.4	1.4	1.3	1.3	1.6	1.3	1.3	1.0	1.2	1.3	1.3	0.1
N/COD	gN/gCOD	0.0017	0.0023	0.0016	0.0012	0.0022	0.0024	0.0015	0.0045	0.0036	0.0039	0.0025	0.0011

Table C. 3 - ADM1 sludge characterization.

Parameter	Unit	Value											Average	St. Deviation
		21/03/2022	04/04/2022	11/04/2022	23/04/2022	30/04/2022	07/05/2022	19/05/2022	26/05/2022	06/06/2022	14/06/2022	22/06/2022		
S_{su}	gCOD/L	0.00	0.00	0.00	0.00	0.00	0.00	0.00	0.00	0.00	0.00	0.00	0.00	0.00
S_{aa}	gCOD/L	0.00	0.00	0.00	0.00	0.00	0.00	0.00	0.00	0.00	0.00	0.00	0.00	0.00
S_{fa}	gCOD/L	0.00	0.00	0.00	0.00	0.00	0.00	0.00	0.00	0.00	0.00	0.00	0.00	0.00
S_{va}	gCOD/L	0.10	0.05	0.08	0.02	0.03	0.06	0.06	0.06	0.07	0.07	0.10	0.07	0.03
S_{bu}	gCOD/L	0.33	0.19	0.24	0.15	0.15	0.13	0.13	0.19	0.13	0.14	0.17	0.18	0.06
S_{pro}	gCOD/L	0.55	0.40	0.48	0.30	0.32	0.27	0.27	0.29	0.25	0.33	0.34	0.34	0.09
S_{ac}	gCOD/L	1.49	1.00	1.11	0.88	0.93	0.63	0.79	0.77	0.55	0.53	0.61	0.82	0.28
S_{h2}	gCOD/L	1.00E-08	1.00E-08	1.00E-08	1.00E-08	1.00E-08	1.00E-08	1.00E-08	1.00E-08	1.00E-08	1.00E-08	1.00E-08	0.00	0.00
S_{ch4}	gCOD/L	1.00E-05	1.00E-05	1.00E-05	1.00E-05	1.00E-05	1.00E-05	1.00E-05	1.00E-05	1.00E-05	1.00E-05	1.00E-05	0.00	0.00
S_{ic}	M	3.60E-01	3.15E-01	2.30E-01	1.60E-01	2.87E-01	1.75E-01	2.49E-01	2.09E-01	2.10E-01	2.82E-01	2.74E-01	0.25	0.06
S_{in}	M	4.18E-03	3.53E-03	4.86E-03	3.20E-03	3.36E-03	6.07E-03	4.80E-03	3.57E-03	6.20E-03	6.80E-03	7.17E-03	0.01	0.00
S_i	gCOD/L	0.00	0.00	0.00	0.00	0.00	0.00	0.00	0.00	0.00	0.00	0.00	0.00	0.00
S_{cat}	M	0.07	0.06	0.06	0.06	0.07	0.07	0.07	0.08	0.06	0.07	0.07	0.07	0.01
S_{an}	M	0.02	0.02	0.02	0.02	0.02	0.02	0.02	0.02	0.02	0.02	0.02	0.02	0.00
X_c	gCOD/L	2.70	2.82	2.81	2.69	3.65	3.75	2.64	3.30	1.83	2.76	2.70	2.86	0.51
X_{ch}	gCOD/L	4.00	3.31	3.10	2.98	3.66	2.37	2.05	3.48	2.63	2.52	1.97	2.84	0.69
X_{pr}	gCOD/L	10.52	8.50	9.55	9.12	10.74	12.23	7.69	8.56	6.38	8.47	7.96	8.97	1.58
X_{li}	gCOD/L	7.82	7.00	7.30	7.65	10.89	7.20	6.98	9.66	6.01	6.71	6.37	7.50	1.43
X_{su}	gCOD/L	0.00	0.00	0.00	0.00	0.00	0.00	0.00	0.00	0.00	0.00	0.00	0.00	0.00
X_{aa}	gCOD/L	0.00	0.00	0.00	0.00	0.00	0.00	0.00	0.00	0.00	0.00	0.00	0.00	0.00
X_{fa}	gCOD/L	0.00	0.00	0.00	0.00	0.00	0.00	0.00	0.00	0.00	0.00	0.00	0.00	0.00
X_{c4}	gCOD/L	0.00	0.00	0.00	0.00	0.00	0.00	0.00	0.00	0.00	0.00	0.00	0.00	0.00
X_{pro}	gCOD/L	0.00	0.00	0.00	0.00	0.00	0.00	0.00	0.00	0.00	0.00	0.00	0.00	0.00
X_{ac}	gCOD/L	0.00	0.00	0.00	0.00	0.00	0.00	0.00	0.00	0.00	0.00	0.00	0.00	0.00
X_{h2}	gCOD/L	0.00	0.00	0.00	0.00	0.00	0.00	0.00	0.00	0.00	0.00	0.00	0.00	0.00
X_i	gCOD/L	1.94	6.59	5.36	4.47	7.53	11.90	7.00	8.02	1.48	7.14	7.96	6.45	2.84

Table C. 4 - Analyses results for digestate characterization.

Parameter	Unit	Value												Average	St. Deviation
		04/04/2022	11/04/2022	26/04/2022	02/05/2022	13/05/2022	20/05/2022	23/05/2022	30/05/2022	06/06/2022	13/06/2022	20/06/2022	27/06/2022		
Total Fraction															
pH	-	7.08	7.09	7.09	7.12	7.15	7.21	7.14	7.12	7.04	7.09	7.12	7.07	7.11	0.04
Alkalinity	mgCaCO₃/L	4441	3798	4845	4628	5282	5388	5262	5044	4906	4793	4784	5366	4878	455
TS	gTS/kg	22	22	25	21	27	28	27	27	27	26	26	26	25	2
VS	gVS/kg	14	14	15	13	17	17	17	17	16	16	15	15	16	1
Total COD	gCOD/kg	10.1	16.4	7.6	16.0	15.5	14.8	16.9	10.6	13.4	16.4	12.3	16.9	14	3
Total TKN	gN/kg	1.45	1.27	1.71	1.43	1.18	1.64	1.57	1.43	1.34	1.27	1.43	1.62	1.45	0.2
Total Carbohydrates	gGlu/kg	1.89	1.77	2.52	2.27	1.98	3.05	2.10	3.00	2.35	2.37	2.57	2.40	2.36	0.4
Total Proteins	gN/kg	0.89	0.74	1.16	0.90	0.62	1.09	1.04	0.92	0.85	0.80	0.95	1.10	0.92	0.2
Particulate Fraction															
Particulate Lipids	g/kgVS,p	88	88	84	79	83	85	93	61	61	68	59	64	76	13
Particulate Lipids	g/kgVS	82	83	78	73	78	80	88	57	57	63	55	60	71	12
TS - particulate fraction	gTS,p/kg,p	124	122	124	126	125	124	126	127	130	130	125	129	126	2
VS - particulate fraction	gVS,p/kg,p	80	78	79	81	79	78	79	80	80	80	76	79	79	1
Soluble Fraction															
VFA: acetic acid	mg/L	75	77	97	84	98	109	71	100	96	96	96	118	93	14
VFA: propionic acid	mg/L	0	0	0	0	0	0	0	0	0	0	0	5	0	1
VFA: iso-butyiric acid	mg/L	12	9	13	12	5	19	19	13	15	5	11	5	11	5
VFA: butyric acid	mg/L	0	0	0	0	0	0	0	0	0	0	0	0	0	0
VFA: iso-valeric acid	mg/L	0	0	0	0	0	0	0	0	0	0	0	0	0	0
VFA: valeric acid	mg/L	0	0	0	0	0	0	0	0	0	0	0	0	0	0
TS - soluble fraction	gTS,s/L	2.2	1.9	2.6	2.4	2.6	2.5	2.6	2.6	2.7	2.6	2.7	2.8	3	0.3
VS - soluble fraction	gVS,s/L	1.0	0.9	1.3	1.2	1.3	1.3	1.3	1.4	1.3	1.2	1.2	1.3	1	0.1
Ammoniacal nitrogen	mgN/L	559	532	554	533	564	557	531	521	485	470	488	530	527	31
Phosphate	mgP/L	23	8	19	14	13	10	18	10	18	15	12	9	14	5

Table C. 5 - Data analysis of digestate analytical measurements.

Parameter	Unit	Value												Average	St. Deviation
		04/04/2022	11/04/2022	26/04/2022	02/05/2022	13/05/2022	20/05/2022	23/05/2022	30/05/2022	06/06/2022	13/06/2022	20/06/2022	27/06/2022		
Total Carbohydrates	gCOD/L	2.03	1.90	2.71	2.44	2.13	3.28	2.26	3.22	2.53	2.55	2.76	2.57	3	0.4
Total Proteins	gCOD/L	9.53	7.98	12.45	9.62	6.64	11.68	11.18	9.83	9.17	8.61	10.17	11.75	10	2
Total Lipids	gCOD/L	2.13	2.18	2.32	1.87	2.51	2.61	2.82	1.80	1.79	1.92	1.60	1.75	2	0.4
Carbohydrates/CODtot	-	14.7%	15.6%	15.4%	17.4%	18.7%	18.5%	13.8%	21.5%	18.6%	19.3%	18.8%	15.9%	17%	2%
Proteins/CODtot	-	69.1%	65.6%	70.7%	68.5%	58.3%	65.9%	68.3%	65.7%	67.3%	65.3%	69.4%	72.4%	67%	4%
Lipids/CODtot	-	15.4%	17.9%	13.2%	13.3%	22.0%	14.7%	17.2%	12.0%	13.1%	14.5%	10.9%	10.8%	15%	3%
Estimated total COD	gCOD/L	13.8	12.2	17.6	14.0	11.4	17.7	16.4	15.0	13.6	13.2	14.6	16.2	14.6	2
VS/TS	gVS/gTS	0.63	0.62	0.62	0.65	0.62	0.61	0.62	0.62	0.60	0.60	0.59	0.59	0.61	0.02
TVFA	gCOD/L	0.1	0.1	0.1	0.1	0.1	0.2	0.1	0.1	0.1	0.1	0.1	0.1	0.1	0.0
COD/VS	gCOD/gVS	0.7	1.2	0.5	1.2	0.9	0.9	1.0	0.6	0.8	1.0	0.8	1.1	0.9	0.2
N/COD	gN/gCOD	0.055	0.032	0.073	0.033	0.036	0.037	0.031	0.049	0.036	0.029	0.039	0.031	0.040	0.013

APPENDIX D

In this appendix, the graphs of the BMP tests carried out are shown. For each test, the average and standard deviation of the results are presented. For some tests, problems were found with one of the duplicates; therefore, the standard deviation is not reported in these graphs, but only the value of the corrected test.

Blank
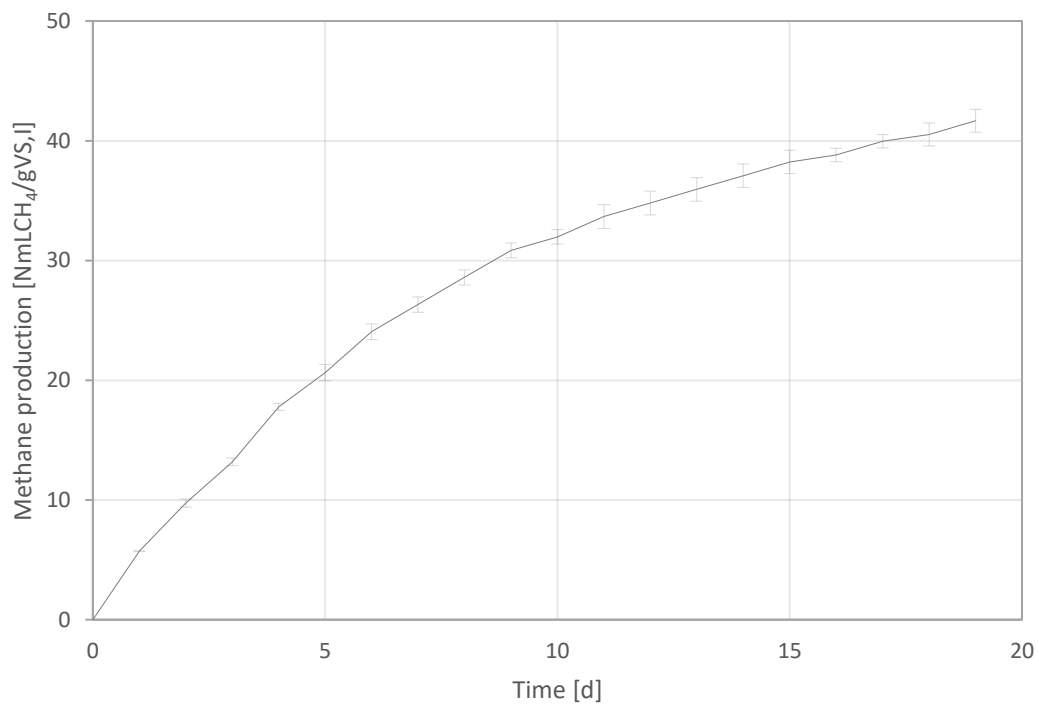
Figure D. 1 - Methane production of blank BMP test (13/04/2022).
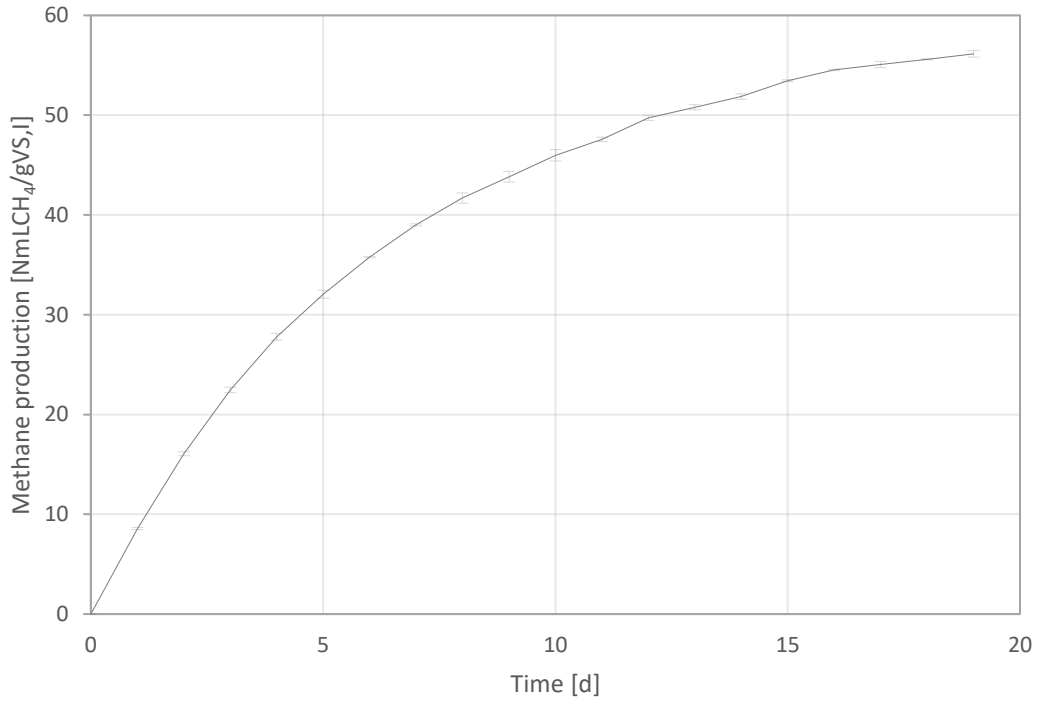
Figure D. 2 - Methane production of blank BMP test (29/04/2022).
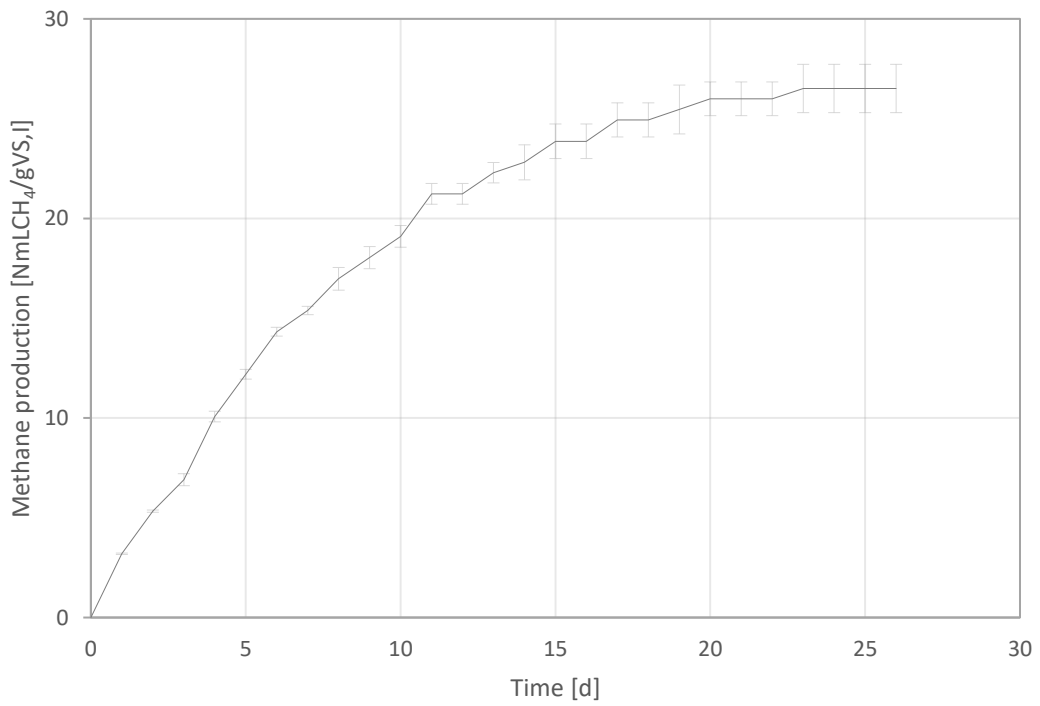
Figure D. 3 - Methane production of blank BMP test (25/05/2022).
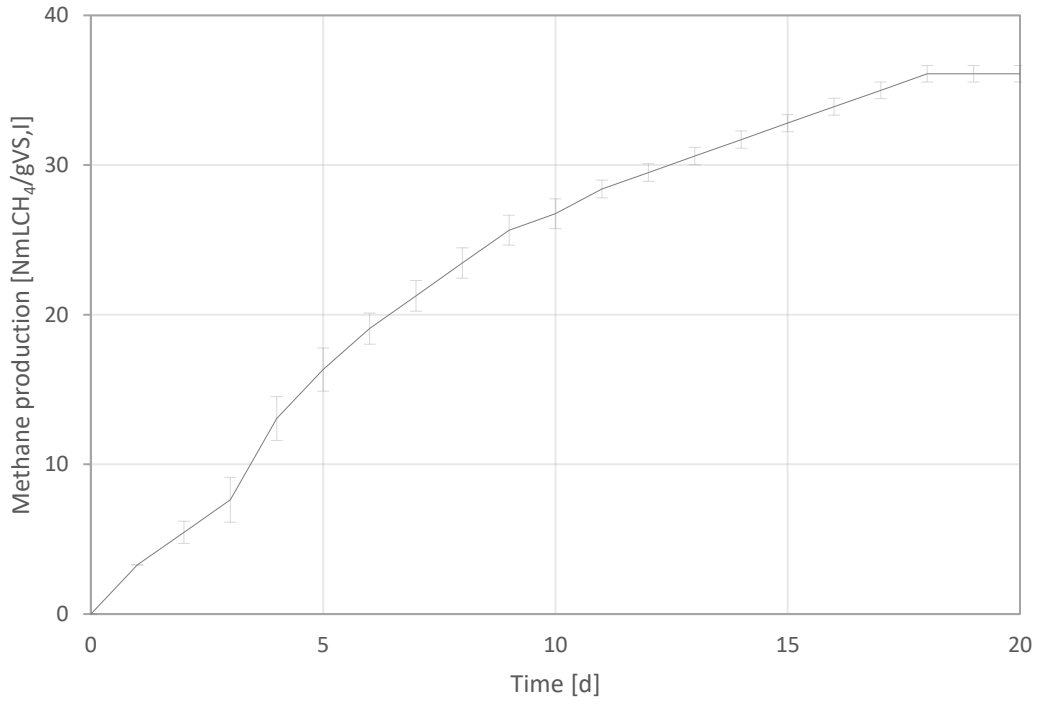
Figure D. 4 - Methane production of blank BMP test (17/06/2022).
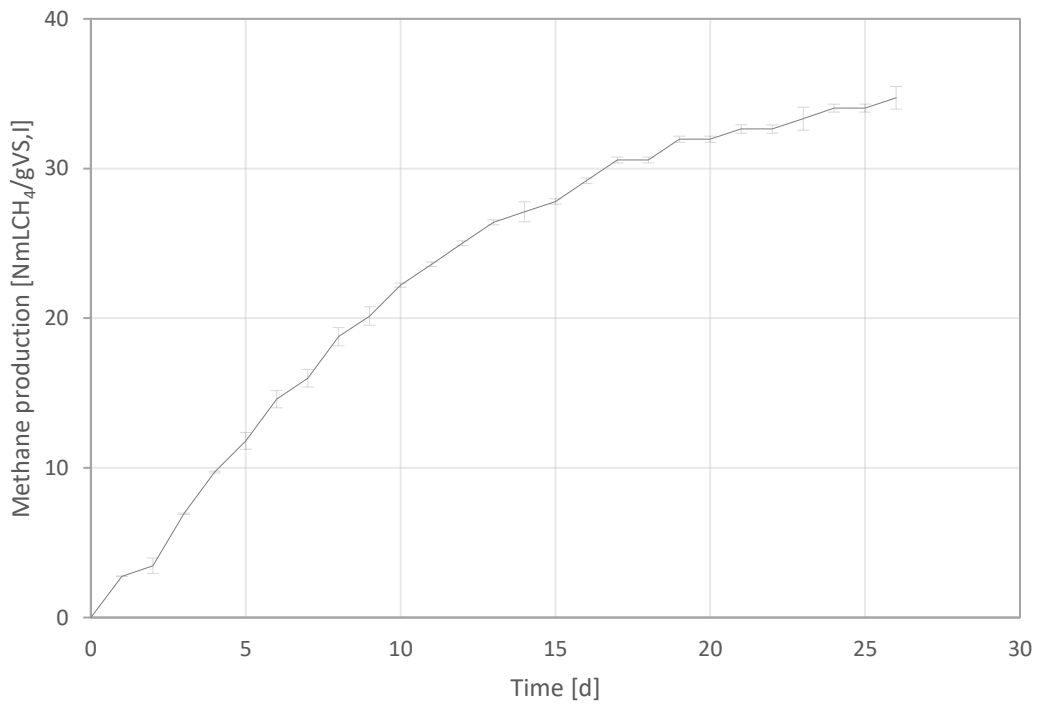
Figure D. 5 - Methane production of blank BMP test (06/07/2022).

Sludge
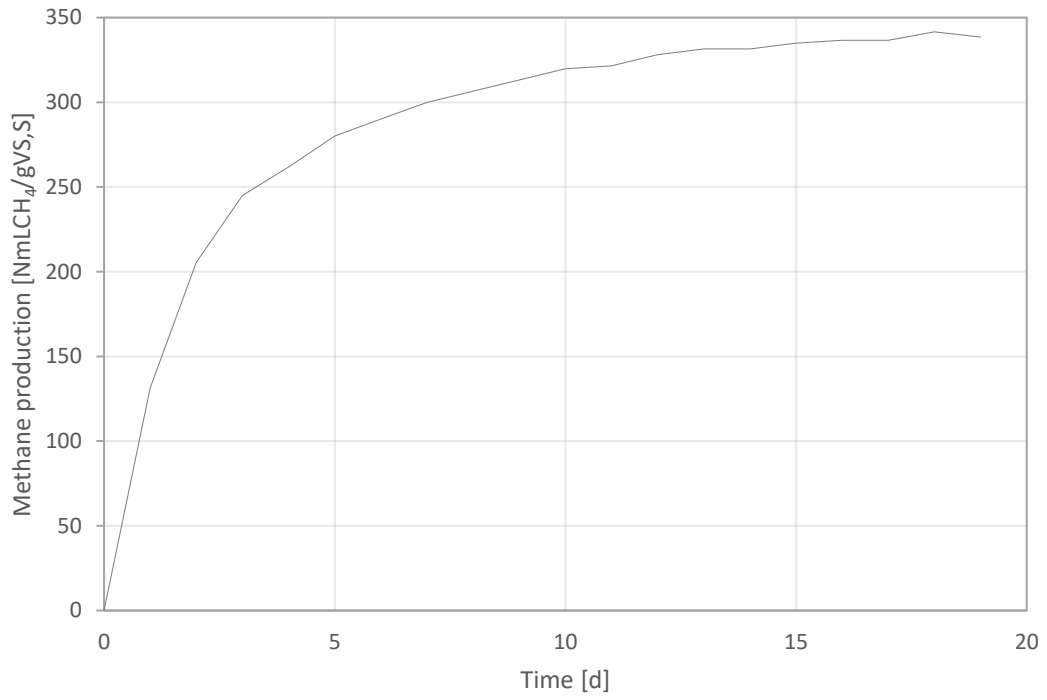
Figure D. 6 - Methane production of sludge BMP test (13/04/2022).
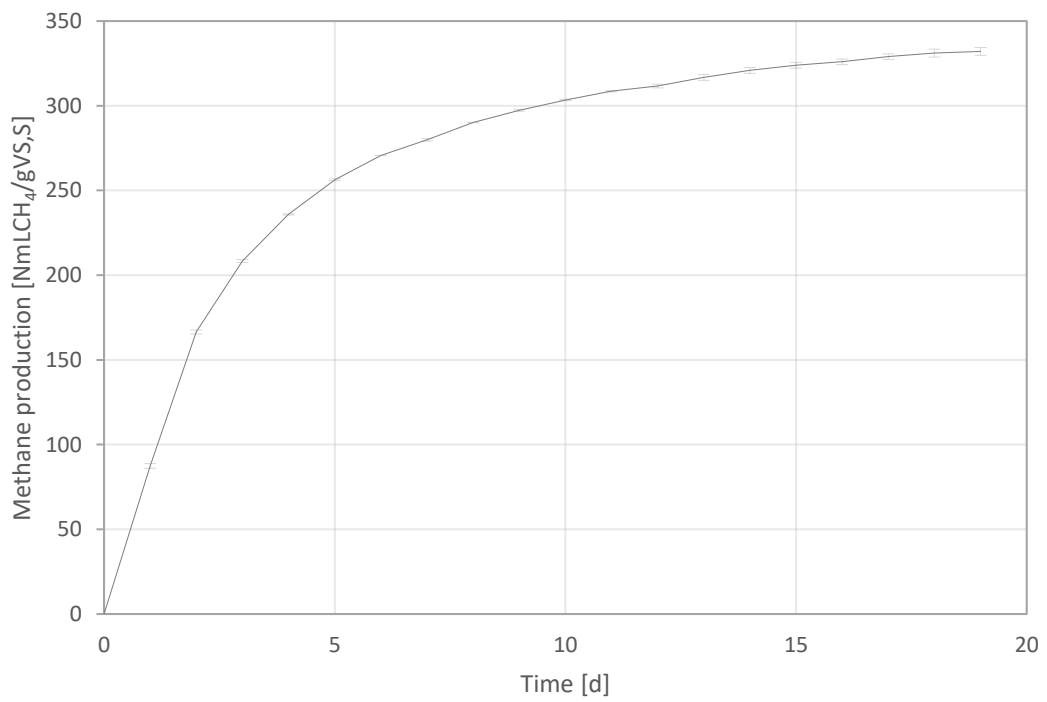
Figure D. 7 - Methane production of sludge BMP test (29/04/2022).
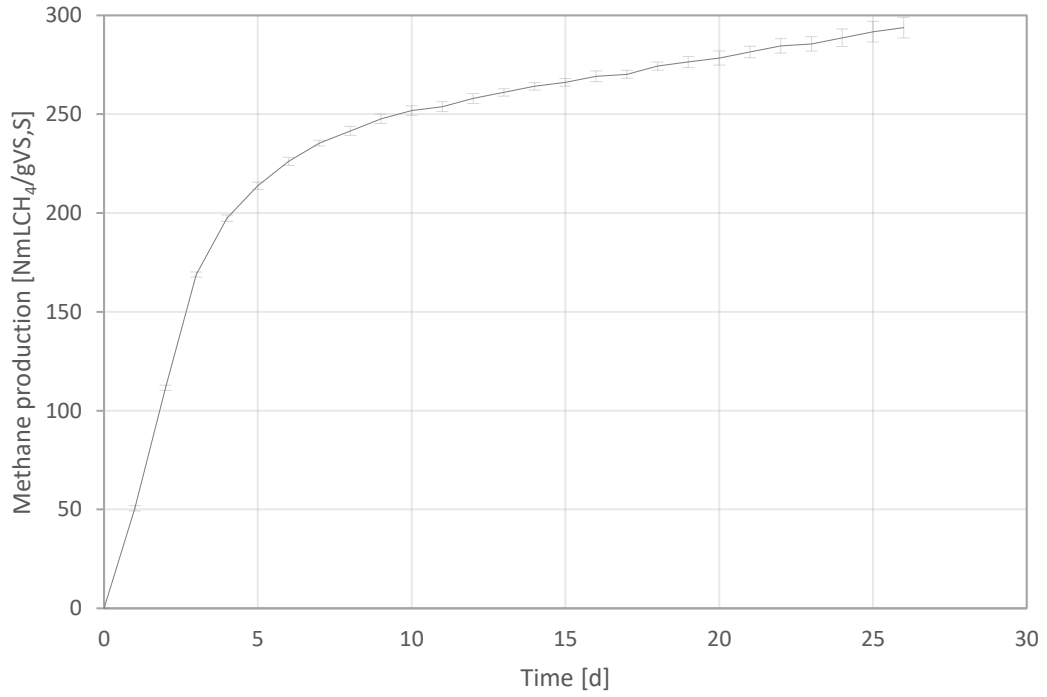
Figure D. 8 - Methane production of sludge BMP test (25/05/2022).
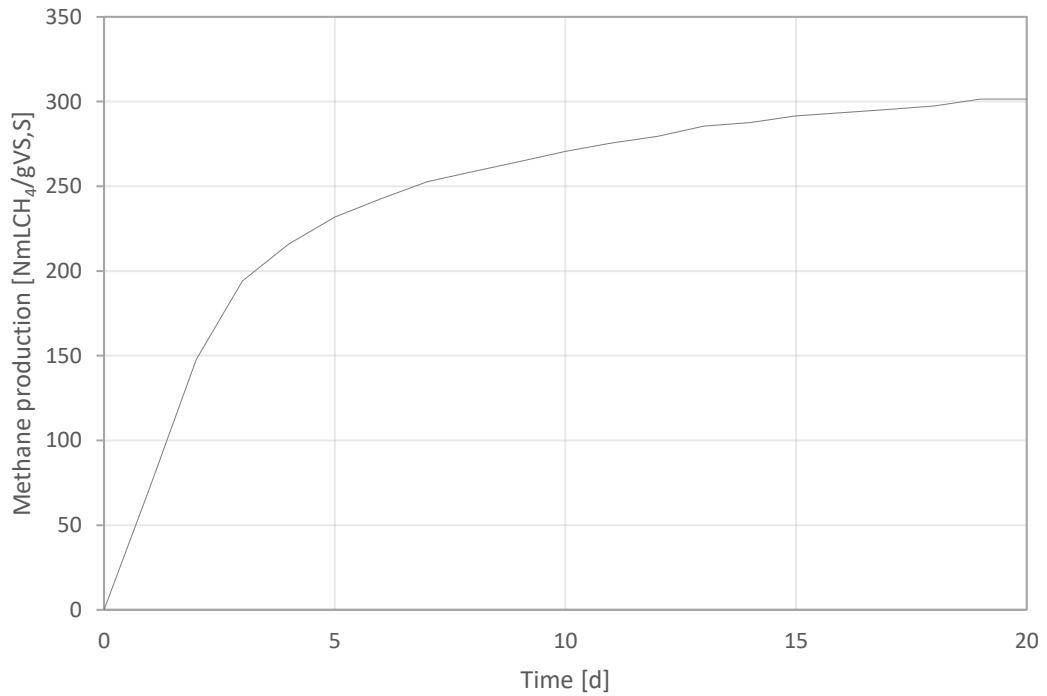
Figure D. 9 - Methane production of sludge BMP test (17/06/2022).

151
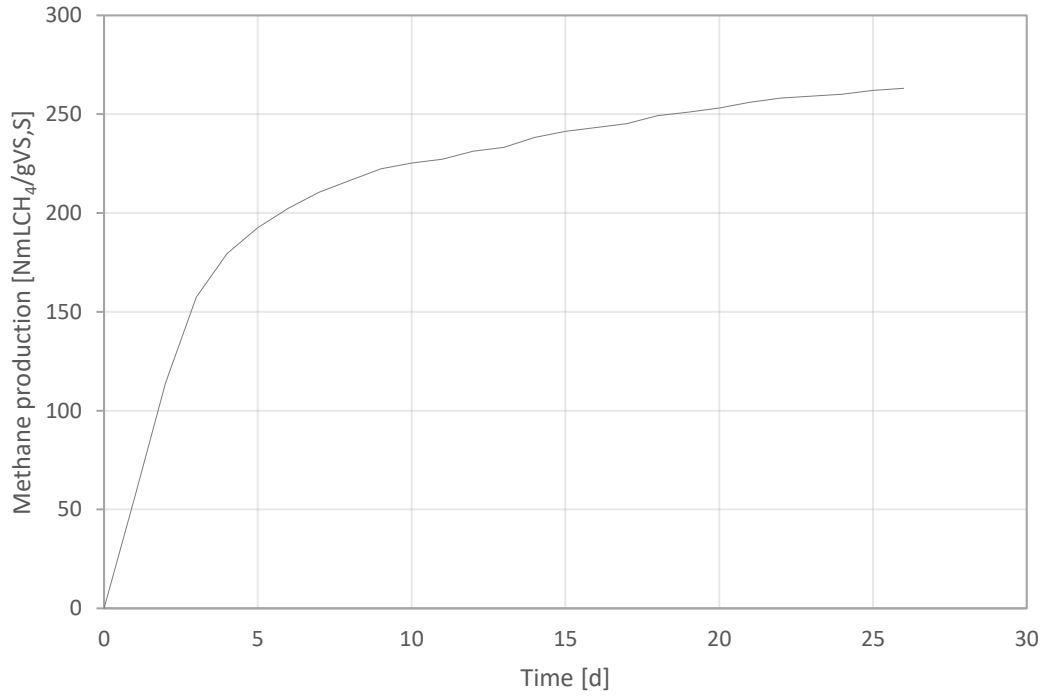
Figure D. 10 - Methane production of sludge BMP test (06/07/2022).

Yogurt
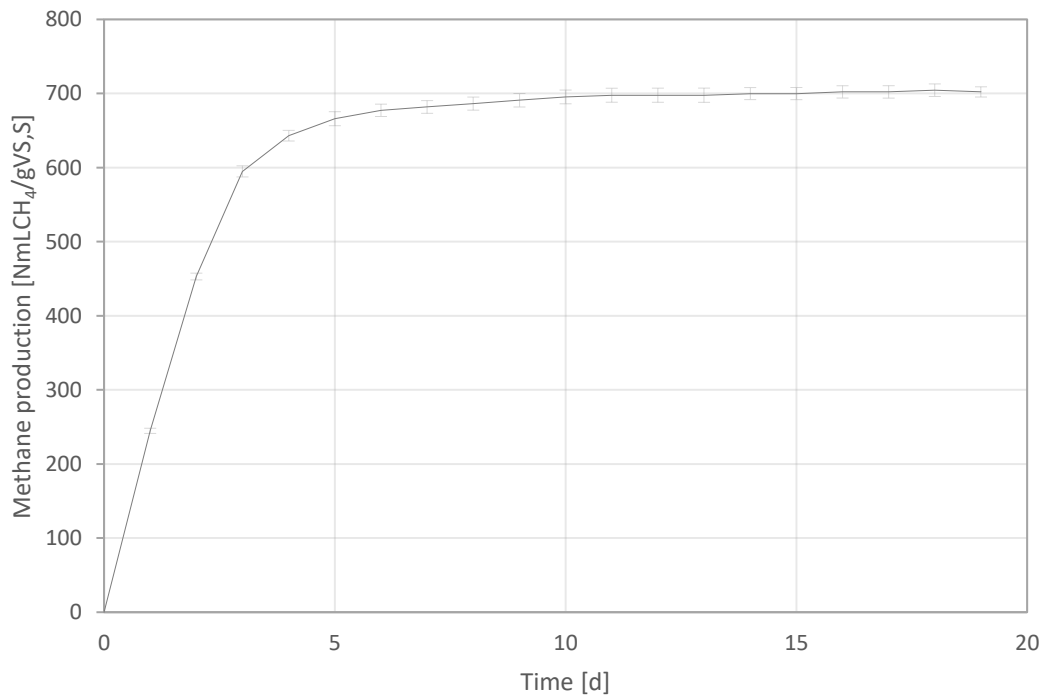
Figure D. 11 - Methane production of yogurt BMP test (13/04/2022).

Co-digestion
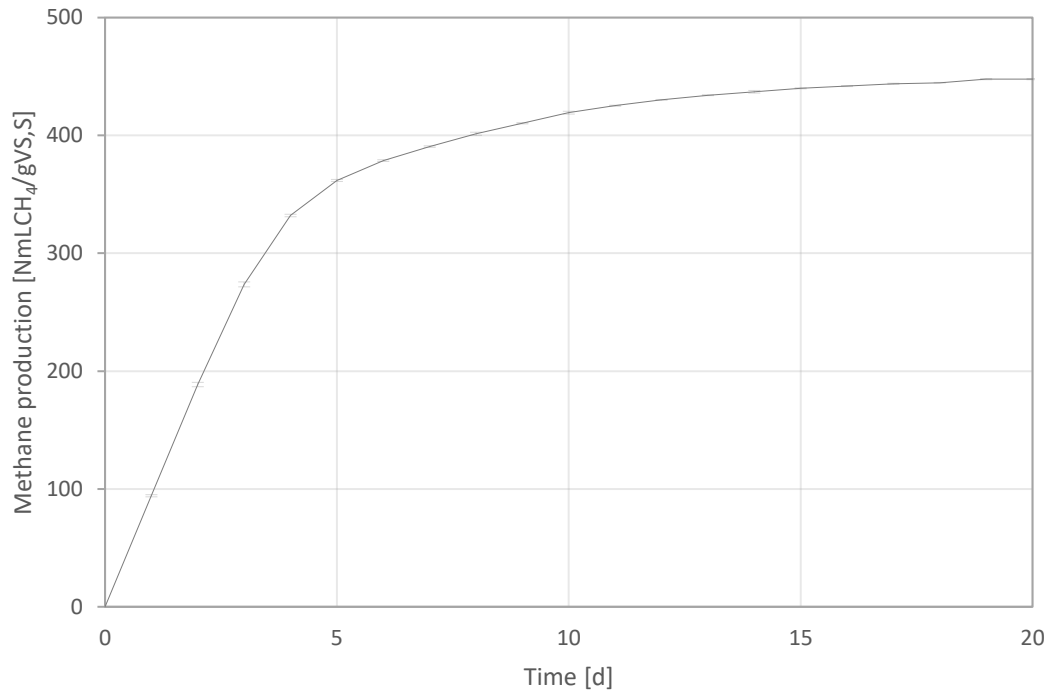
Figure D. 12 - Methane production of co-digestion BMP test (17/06/2022).
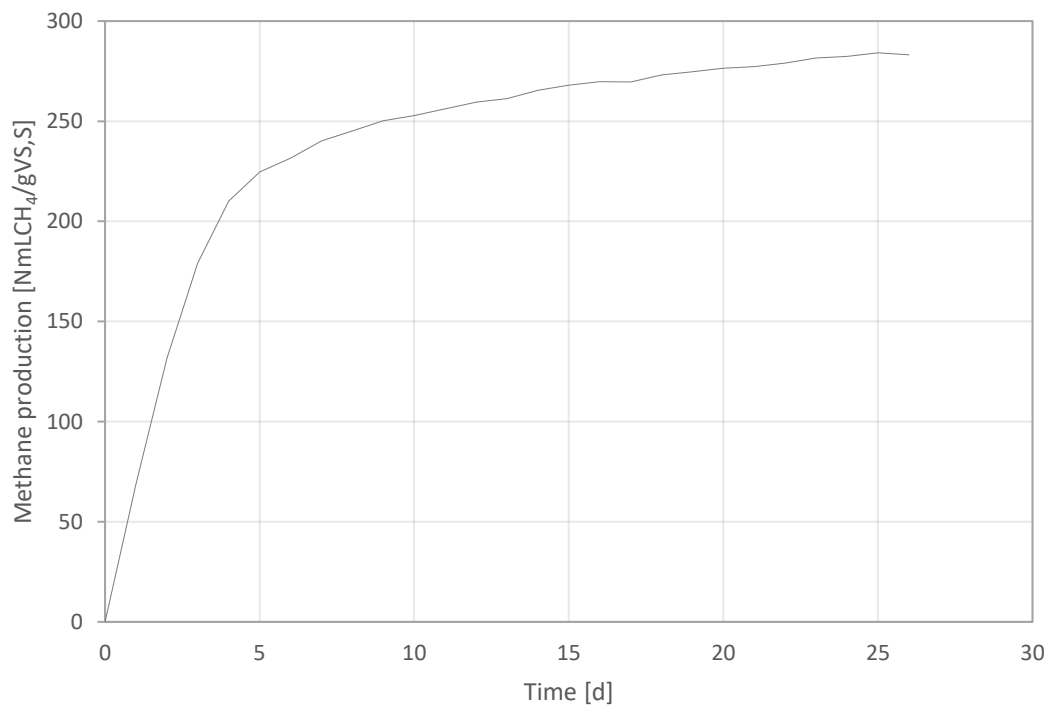
Figure D. 13 - Methane production of co-digestion BMP test (06/07/2022).

Residual
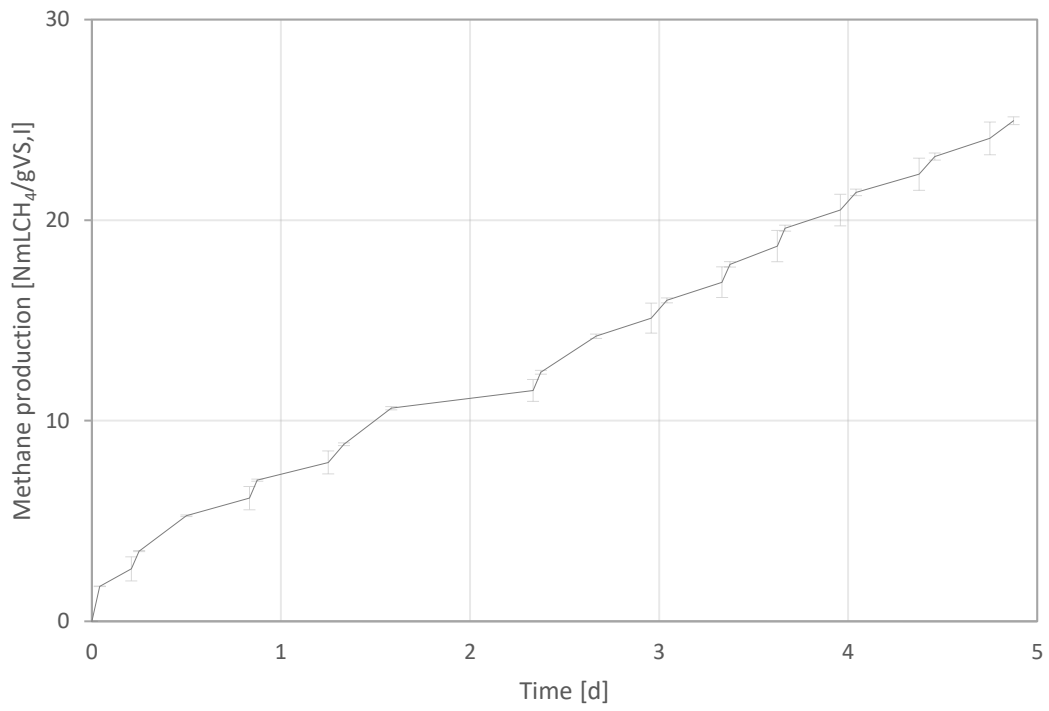
Figure D. 14 - Methane production of residual BMP test (01/04/2022).
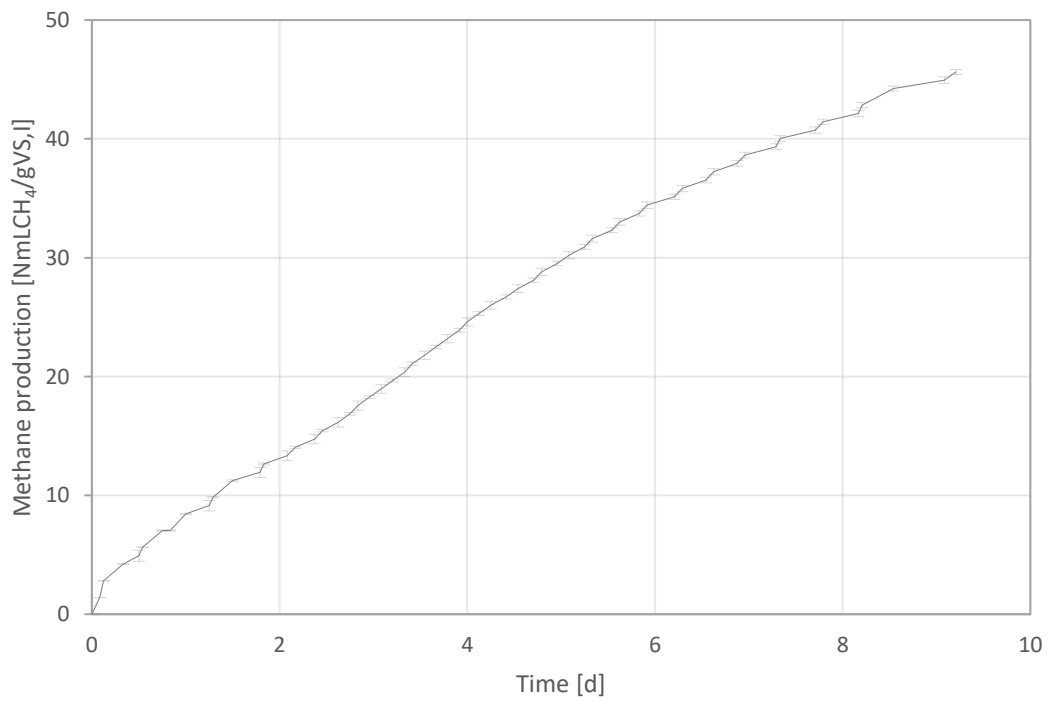
Figure D. 15 - Methane production of residual BMP test (06/05/2022).
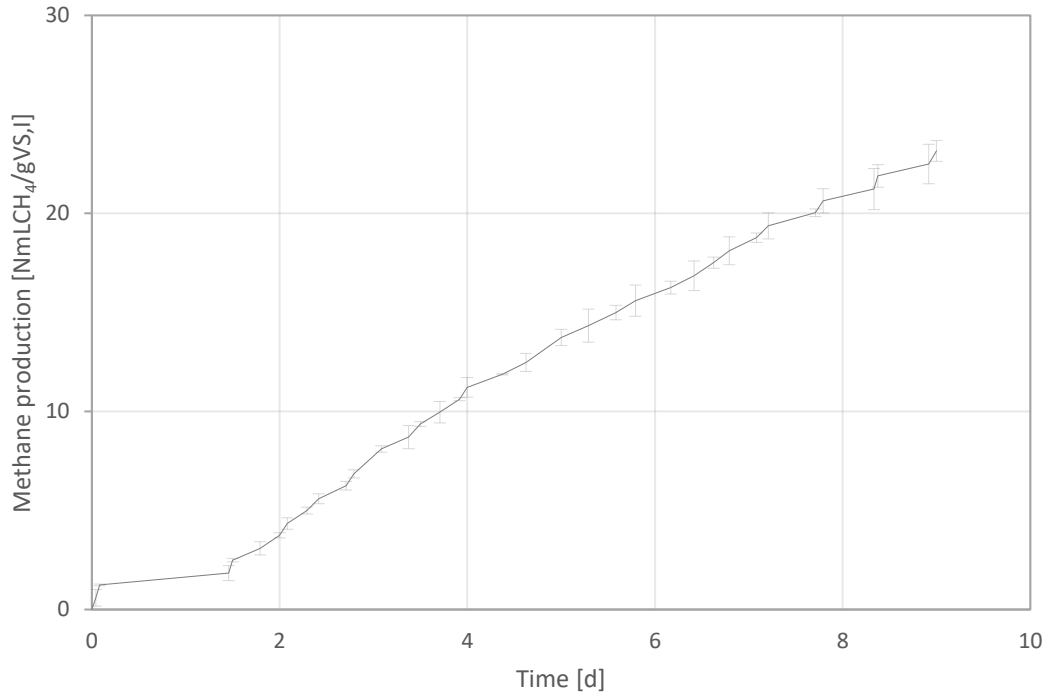
Figure D. 16 - Methane production of residual BMP test (20/06/2022).
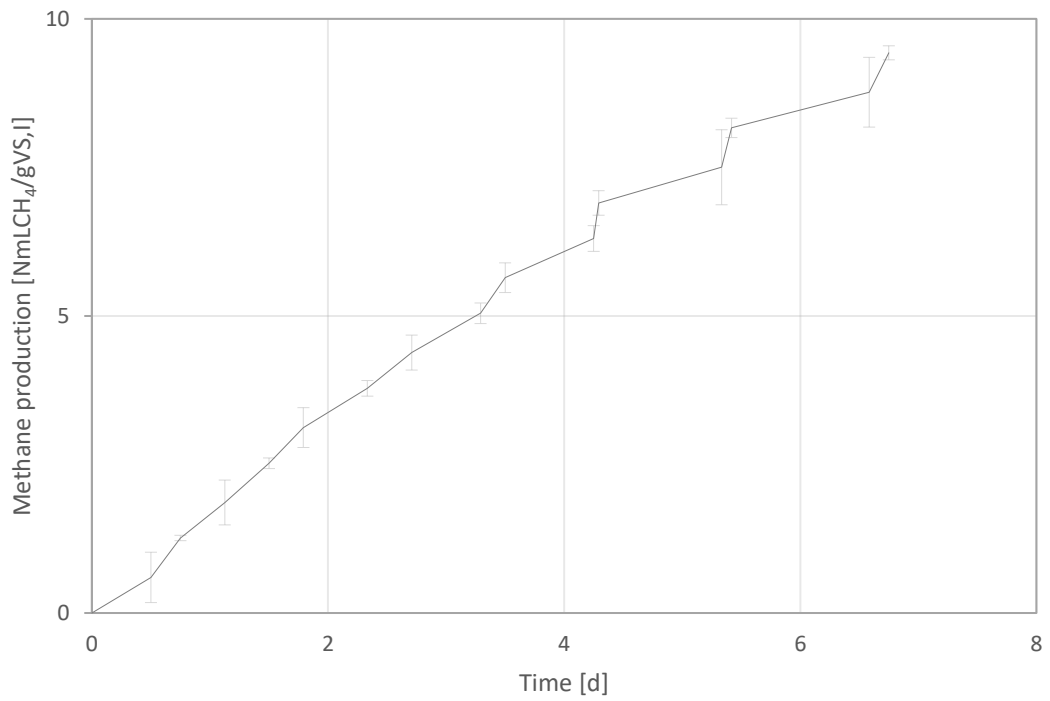
Figure D. 17 - Methane production of residual BMP test (29/06/2022).
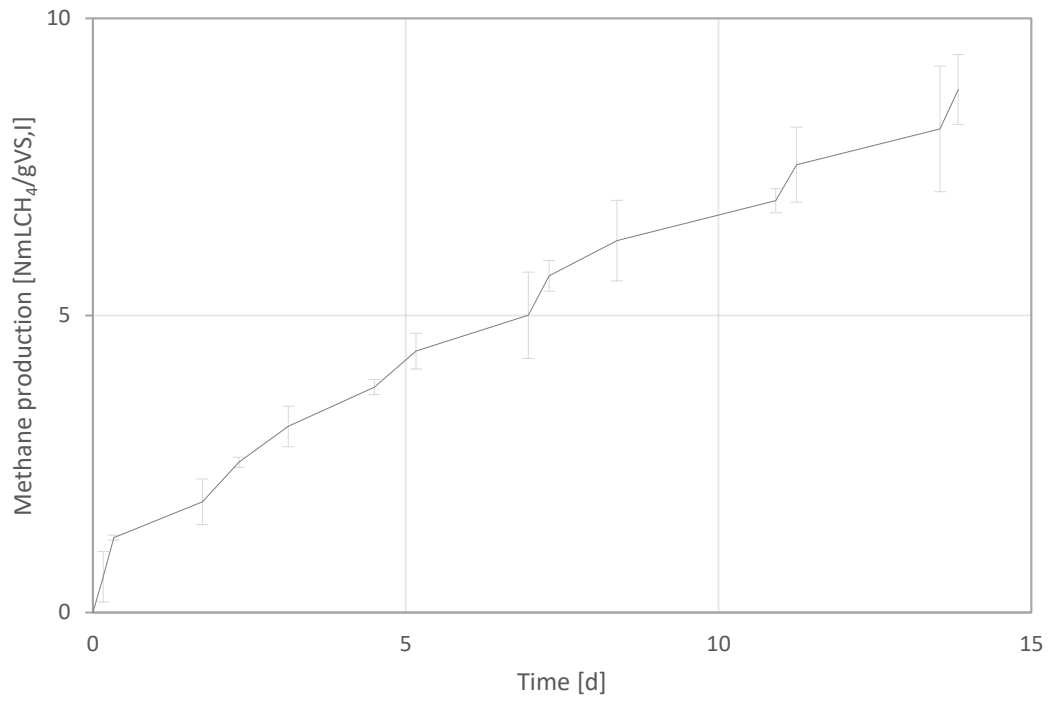
Figure D. 18 - Methane production of residual BMP test (07/07/2022).

APPENDIX E

This appendix shows the graphs of the specific gross production of methane (NmLCH$_4$/gCOD) of the biomass activity tests carried out during the experimentation. The average of the results obtained from the duplicates is reported in each graph. Table E. 1 shows the percentage of dosed COD converted into methane for each biomass activity test.

Acetate activity tests
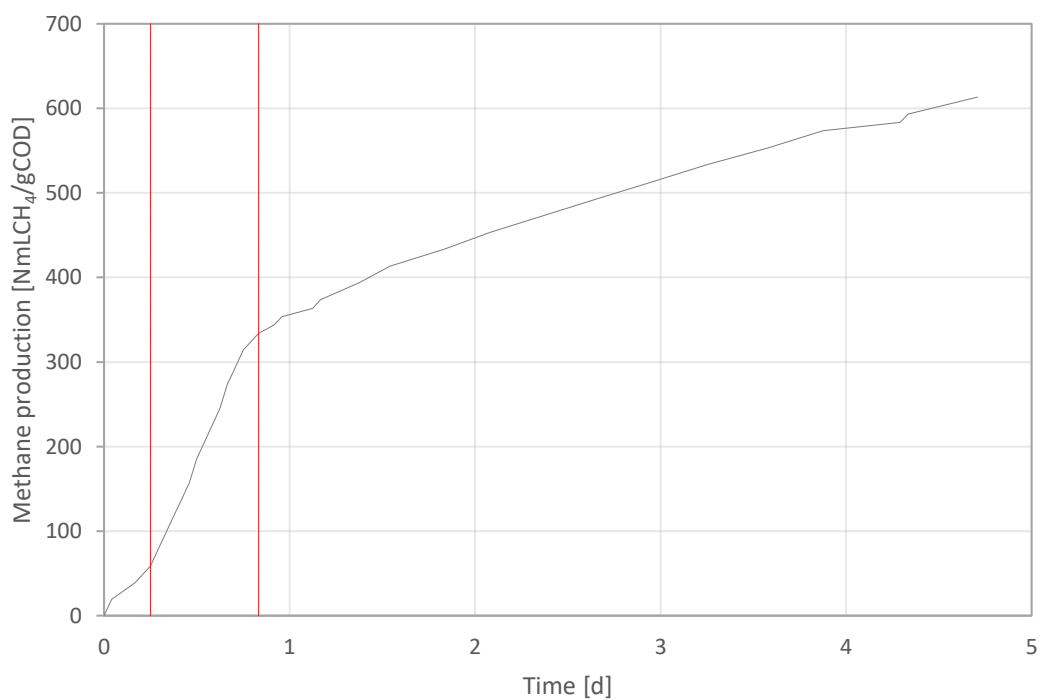
Figure E. 1 - Methane production of acetate activity test - 0.5 gCOD/L (01/04/2022).
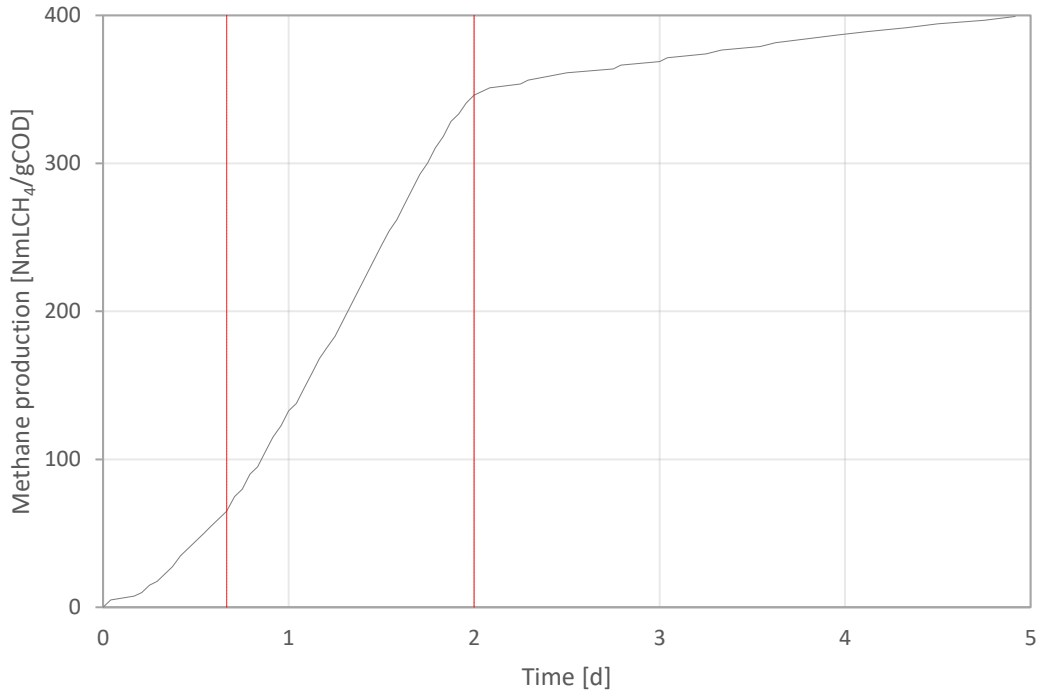
Figure E. 2 - Methane production of acetate activity test - 2 gCOD/L (01/04/2022).
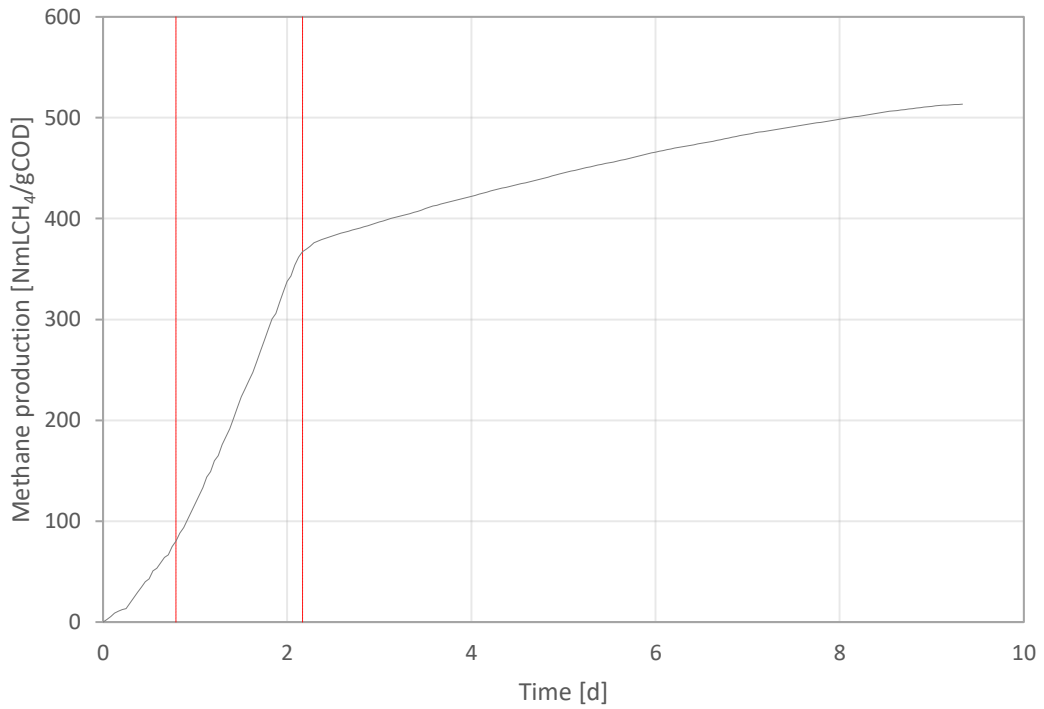
Figure E. 3 - Methane production of acetate activity test - 2 gCOD/L (06/05/2022).
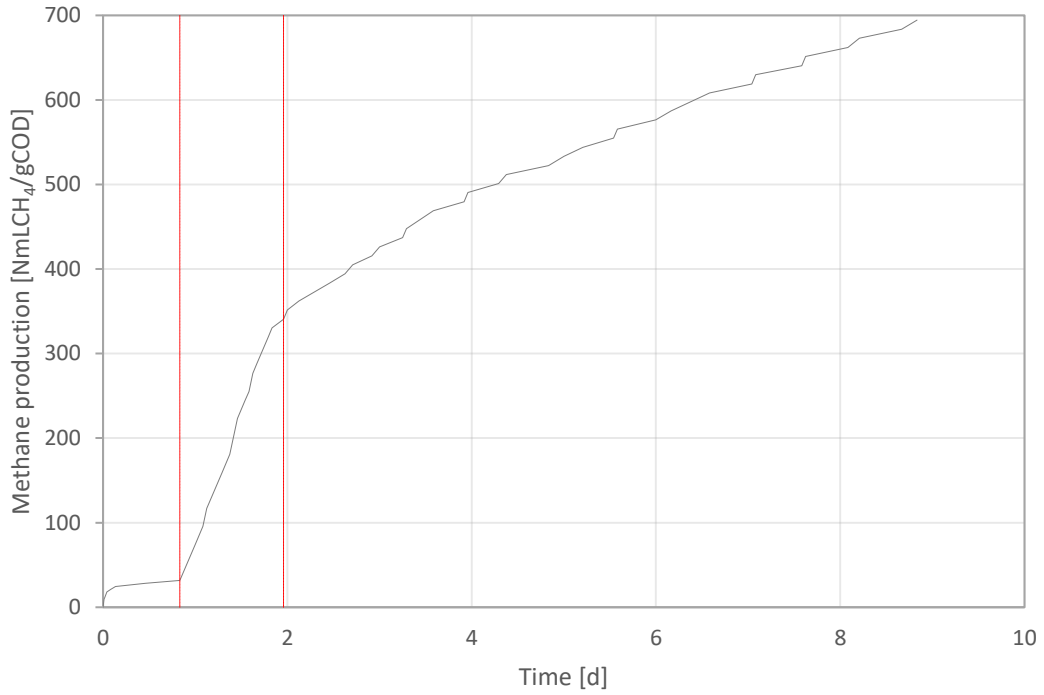
Figure E. 4 - Methane production of acetate activity test - 0.5 gCOD/L (20/06/2022).
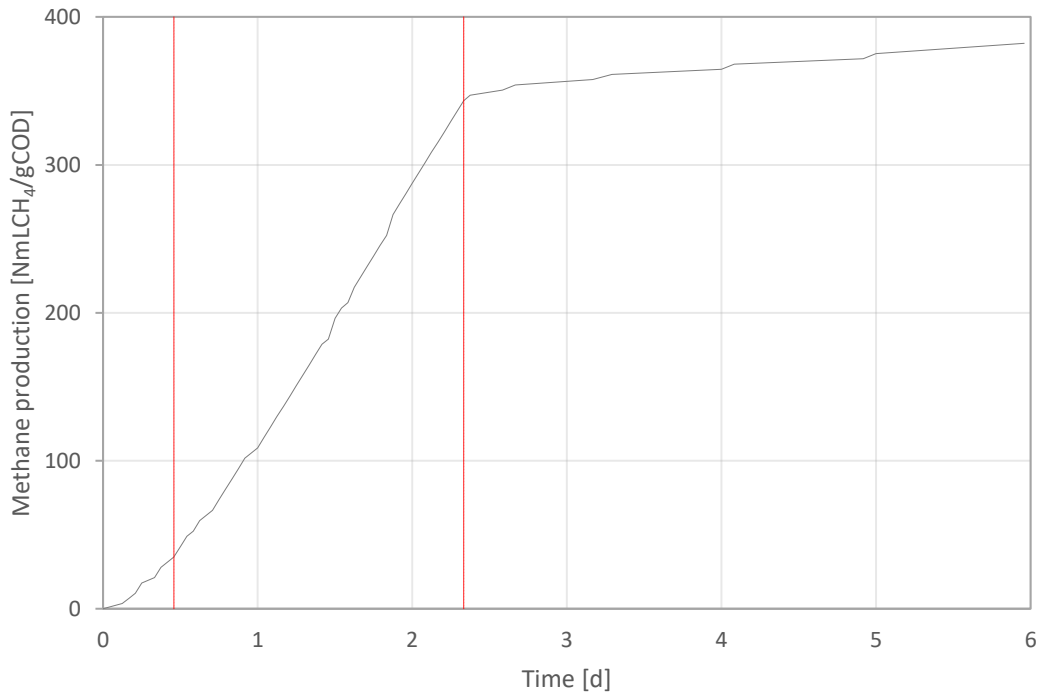
Figure E. 5 - Methane production of acetate activity test - 1.5 gCOD/L (29/06/2022).
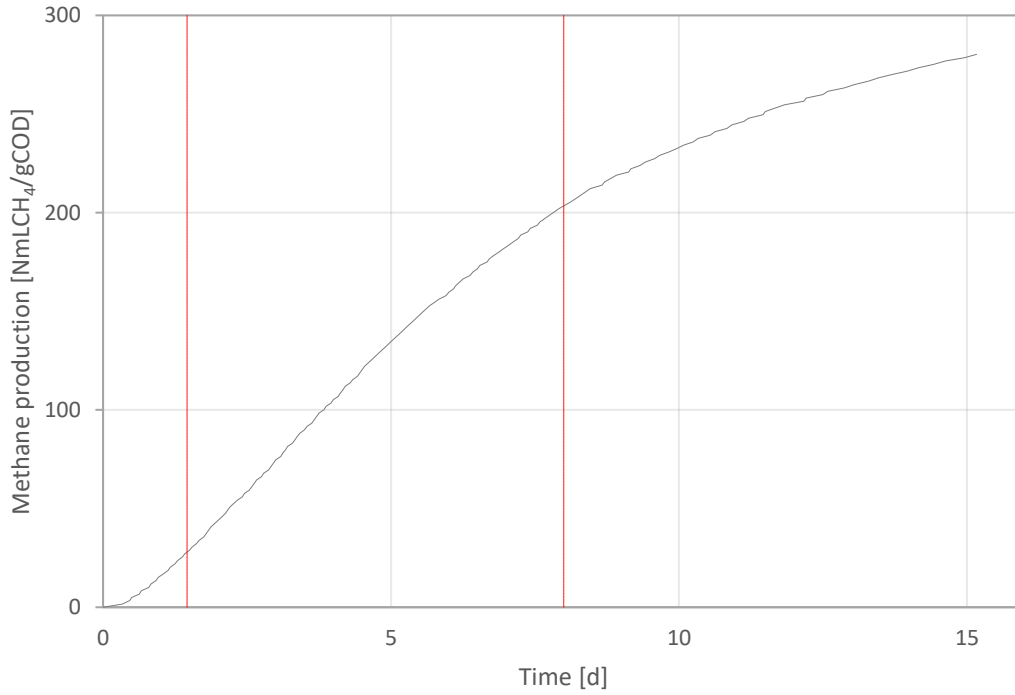
Figure E. 6 - Methane production of acetate activity test - 3 gCOD/L (07/07/2022).

Propionate activity tests
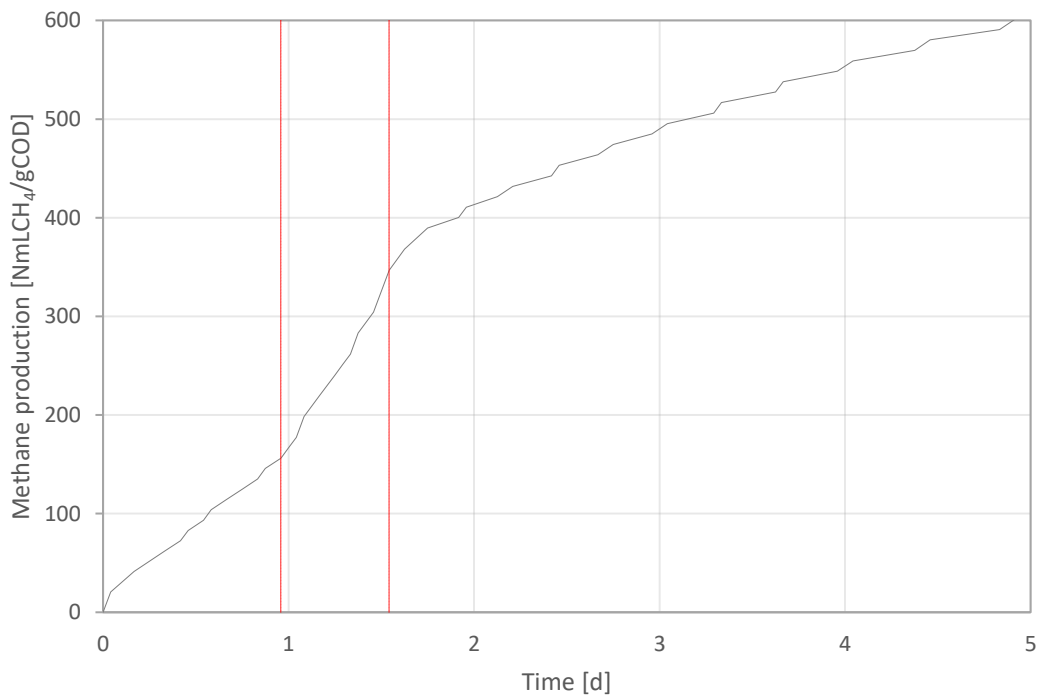
Figure E. 7 - Methane production of propionate activity test - 0.5 gCOD/L (01/04/2022).
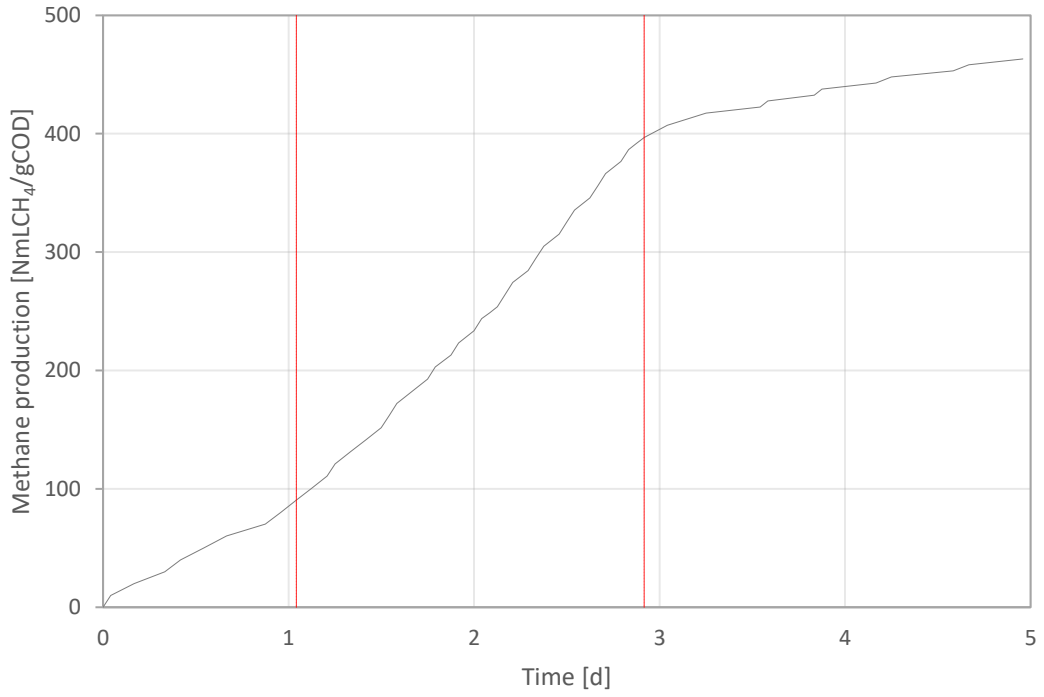
Figure E. 8 - Methane production of propionate activity test - 1 gCOD/L (01/04/2022).
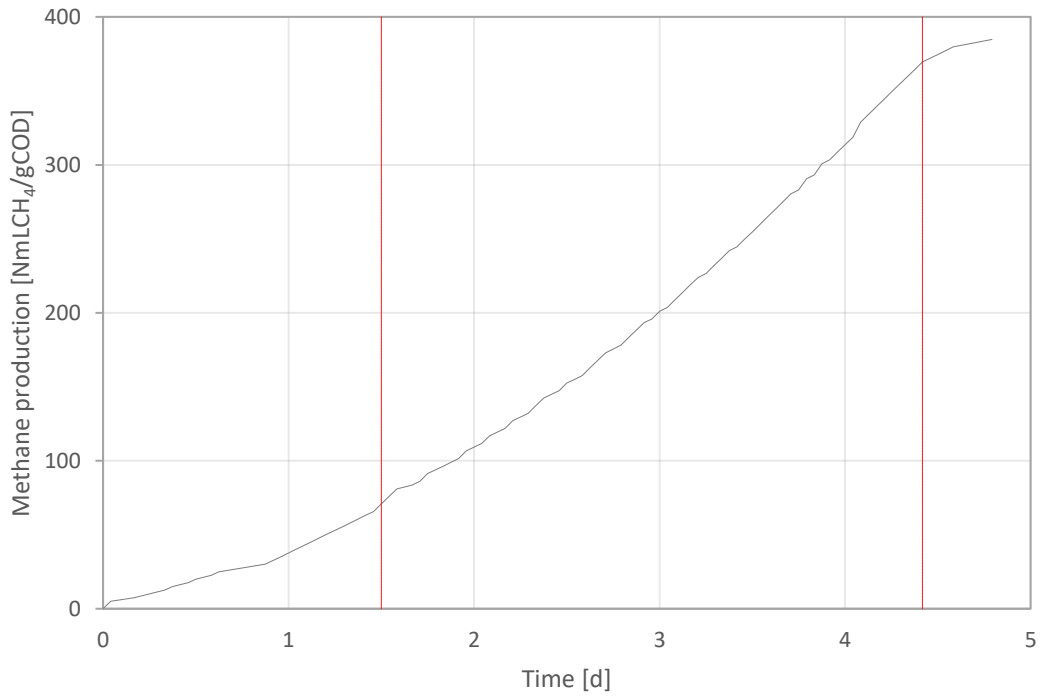
Figure E. 9 - Methane production of propionate activity test - 2 gCOD/L (01/04/2022).
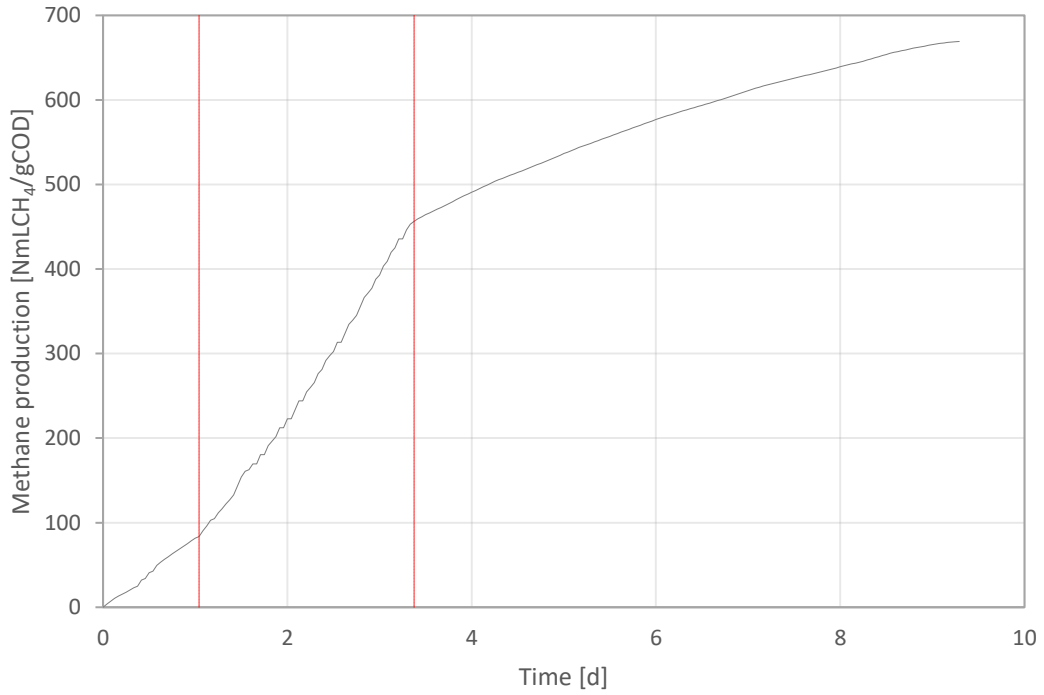
Figure E. 10 - Methane production of propionate activity test - 1 gCOD/L (06/05/2022).
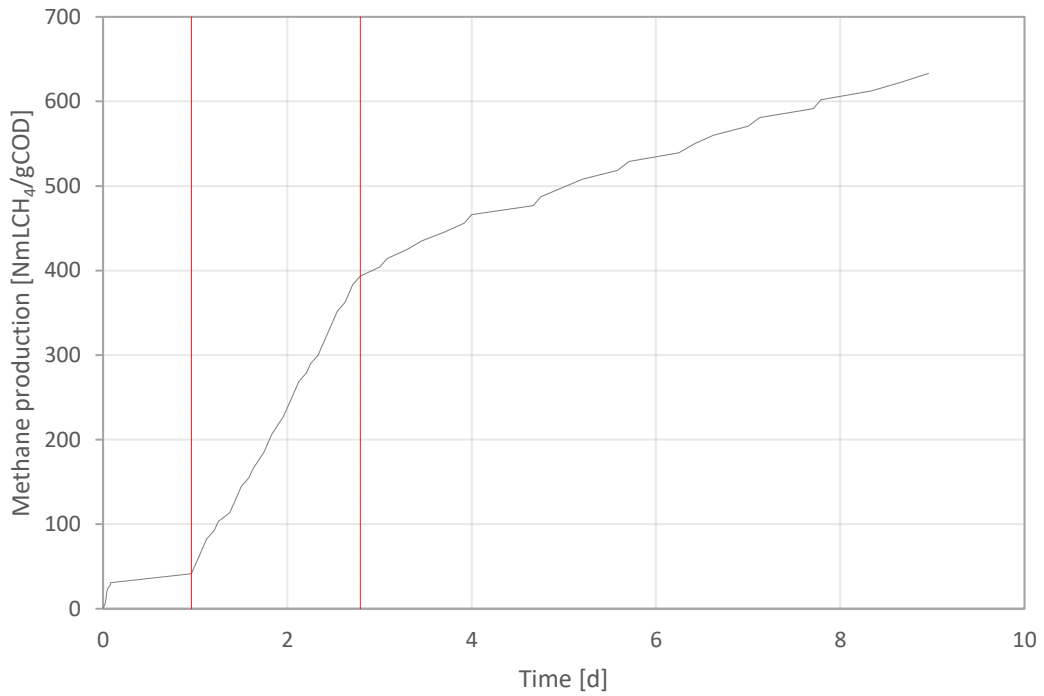
Figure E. 11 - Methane production of propionate activity test - 0.5 gCOD/L (20/06/2022).

162
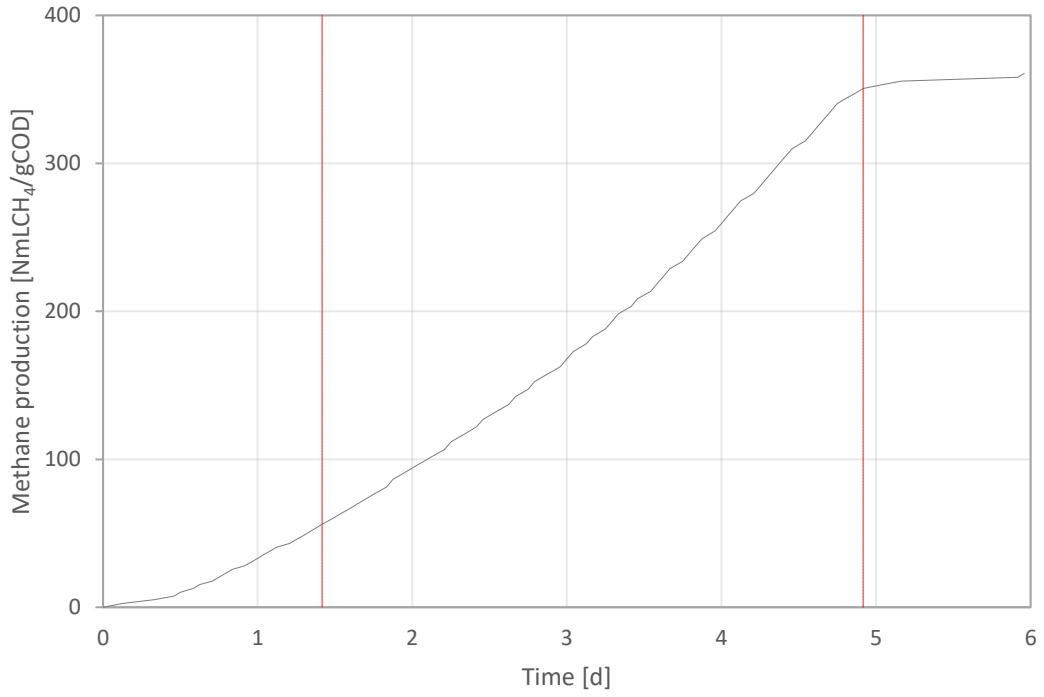
Figure E. 12 - Methane production of propionate activity test - 2 gCOD/L (29/06/2022).
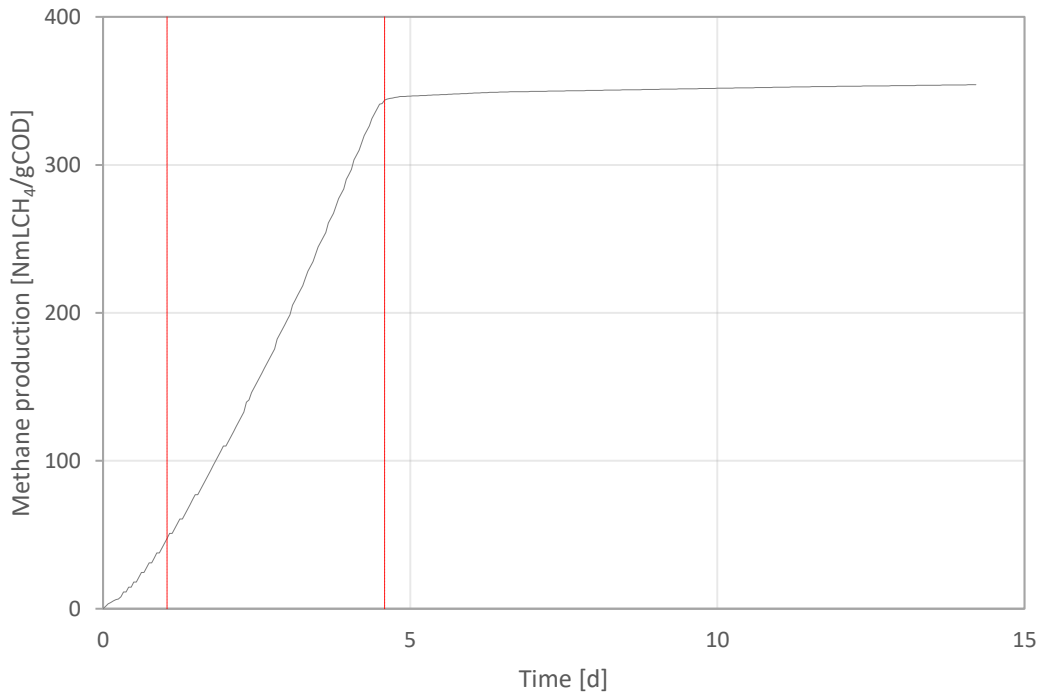
Figure E. 13 - Methane production of propionate activity test - 3 gCOD/L (07/07/2022).

Glucose activity tests
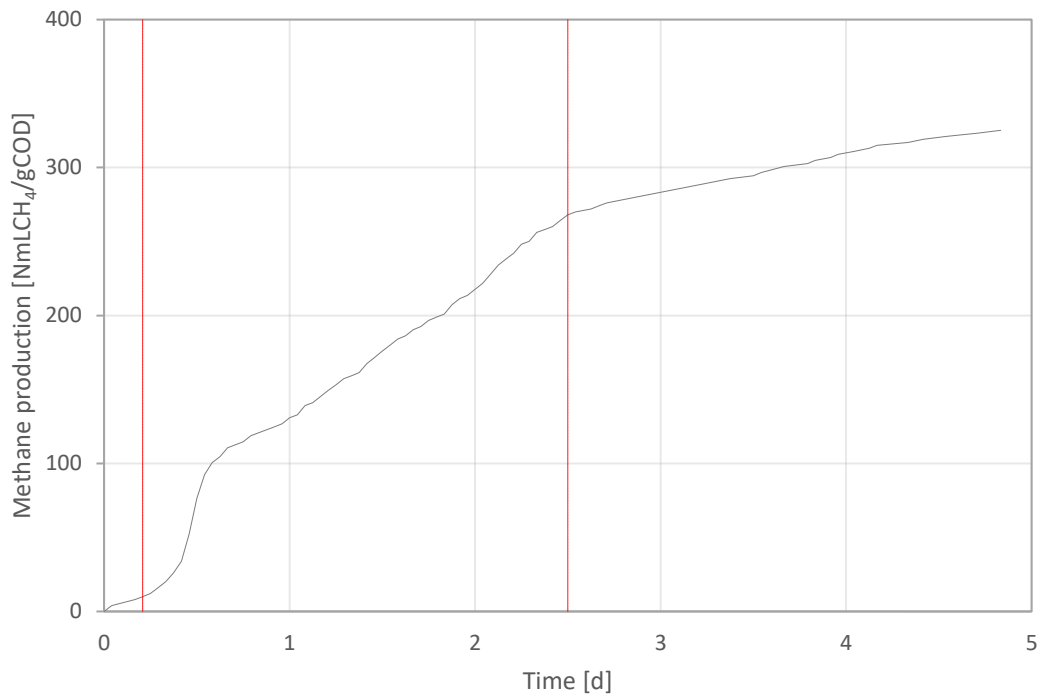
Figure E. 14 - Methane production of glucose activity test - 2.5 gCOD/L (01/04/2022).
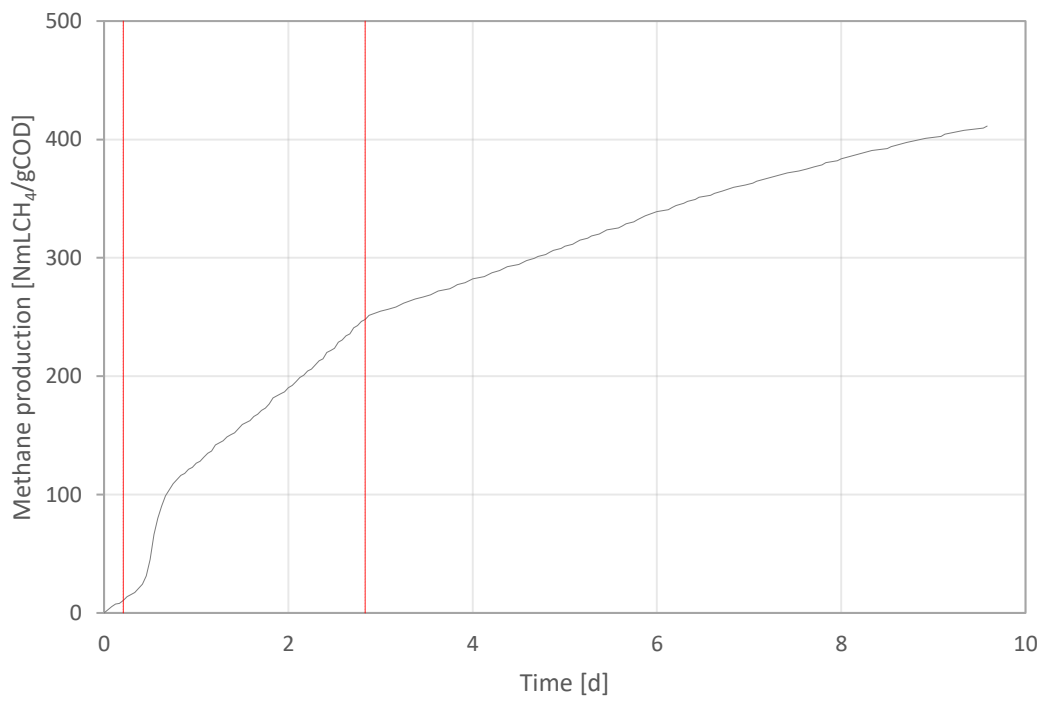
Figure E. 15 - Methane production of glucose activity test - 3 gCOD/L (06/05/2022).
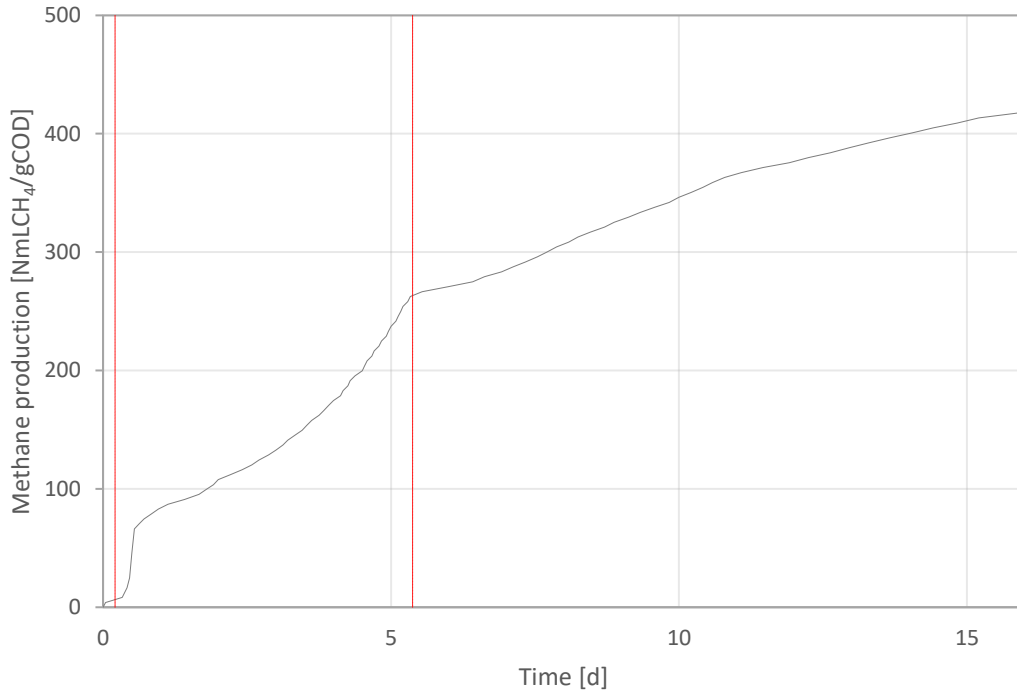
Figure E. 16 - Methane production of glucose activity test - 2.5 gCOD/L (20/06/2022).
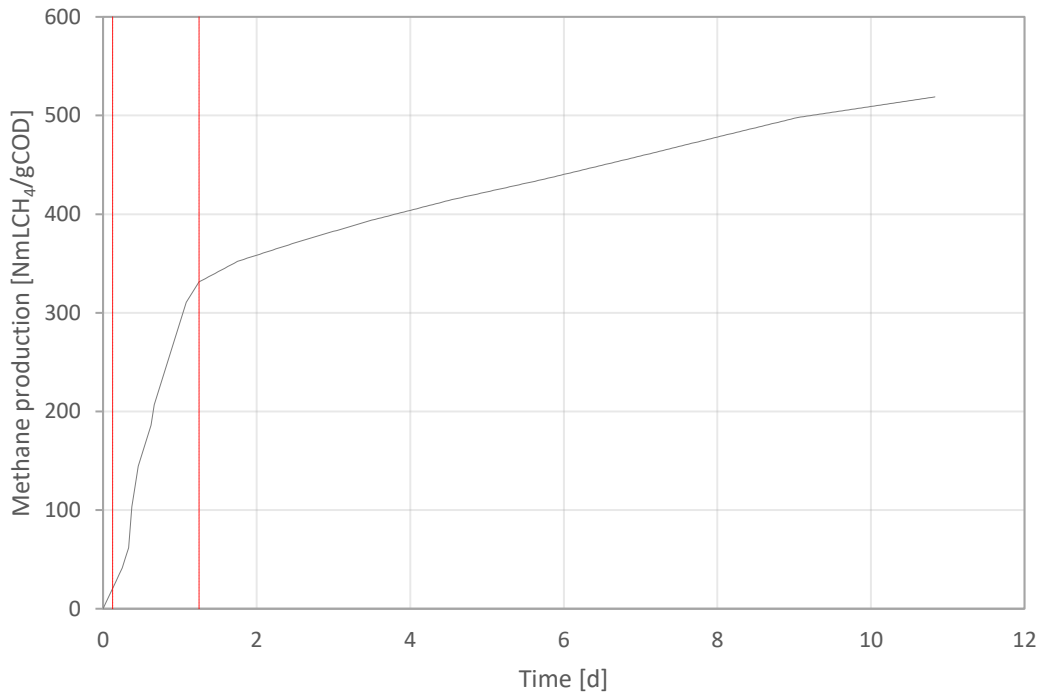
Figure E. 17 - Methane production of glucose activity test - 0.5 gCOD/L (06/07/2022).

Table E. 1 - Percentage of dosed COD converted into methane in biomass activity tests.

Substrate	Date	Concentration	%COD-CH$_4$	
		gCOD/L	End of the test	Curve's elbow
Acetate	01/04/2022	0.5	91.77%	74.95%
		2	93.21%	89.98%
	06/05/2022	2	98.58%	90.06%
	20/06/2022	0.5	94.35%	87.02%
	29/06/2022	1.5	95.62%	94.12%
	07/07/2022	3	75.47%	54.10%
Propionate	01/04/2022	0.5	88.33%	69.65%
		1	90.61%	76.57%
		2	89.06%	88.39%
	06/05/2022	1	94.94%	87.42%
	20/06/2022	0.5	79.56%	80.02%
	29/06/2022	2	94.06%	90.77%
	07/07/2022	3	95.99%	95.92%
Glucosio	01/04/2022	2.5	76.21%	68.31%
	06/05/2022	3	85.43%	66.85%
	29/06/2022	2.5	88.44%	61.42%
	06/07/2022	0.5	115.82%	88.75%

APPENDIX F

This appendix presents the graphs of all the simulations of the batch tests carried out during the experimentation.

Blank BMP tests
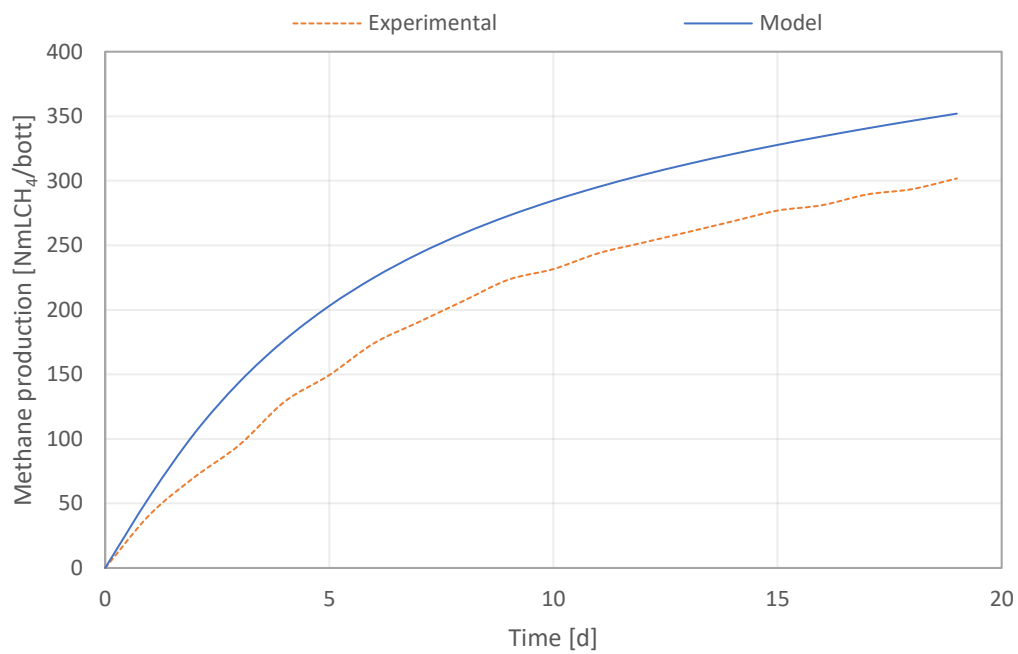
Figure F. 1 - Blank BMP test simulation (13/04/2022).
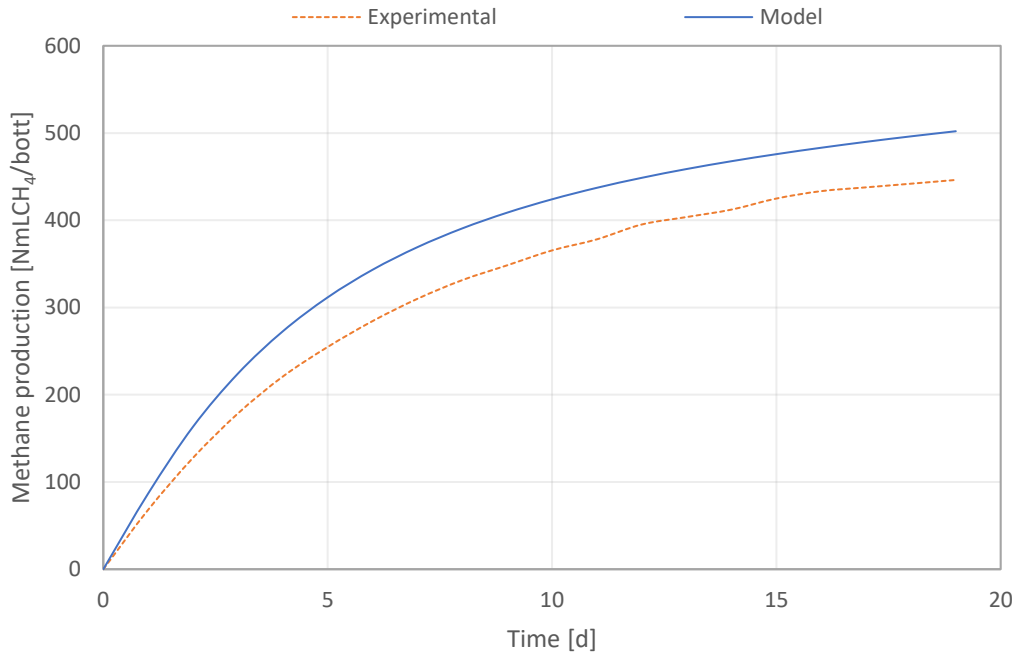
Figure F. 2 - Blank BMP test simulation (29/04/2022).
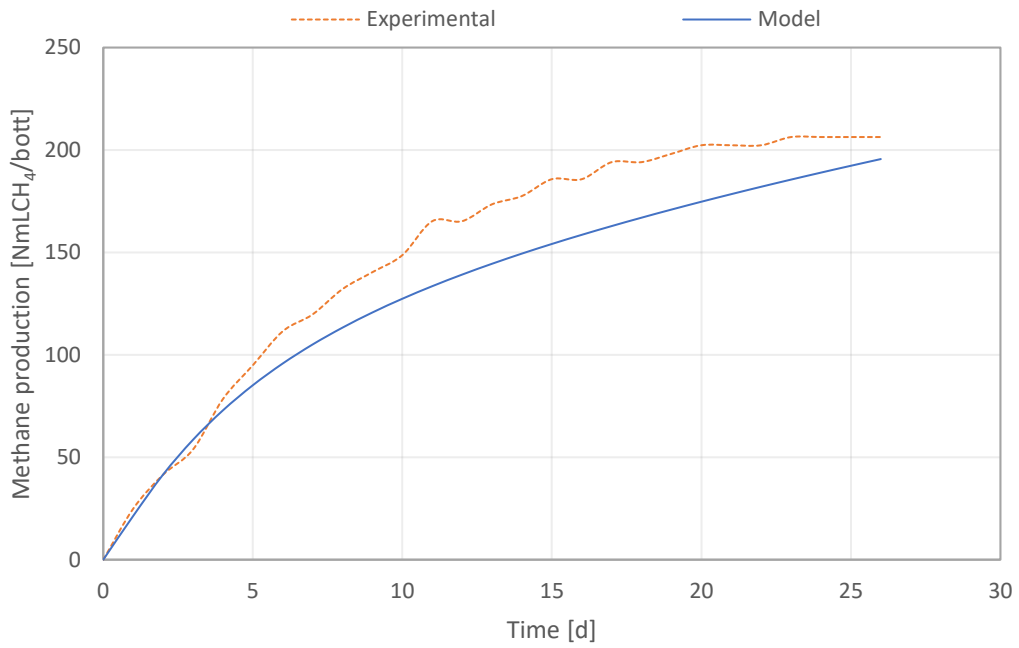
Figure F. 3 - Blank BMP test simulation (25/05/2022).
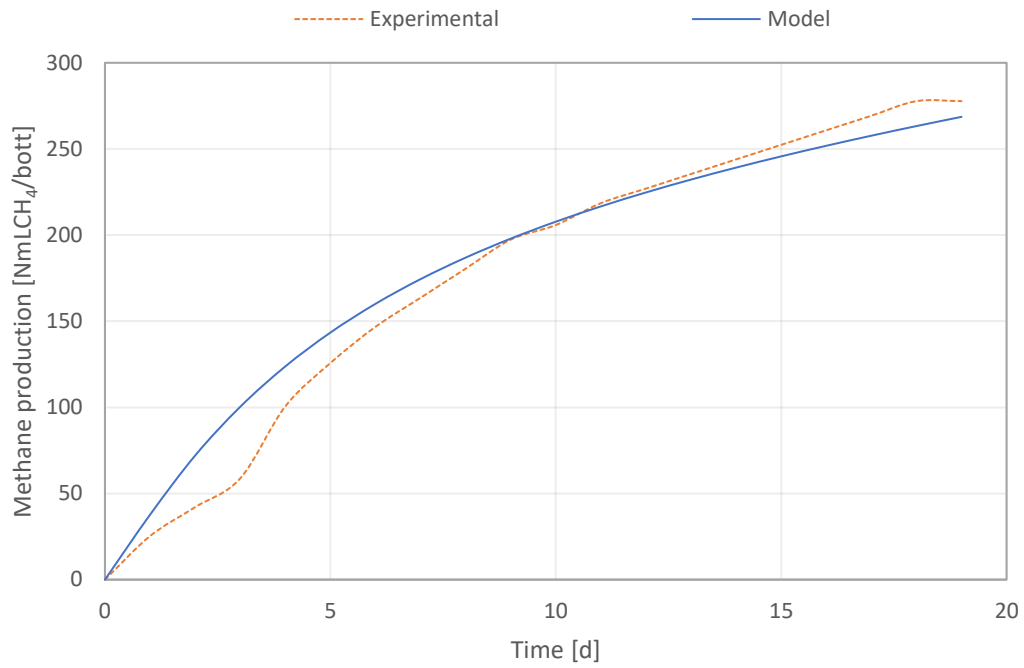
Figure F. 4 - Blank BMP test simulation (17/06/2022).

Sludge BMP tests
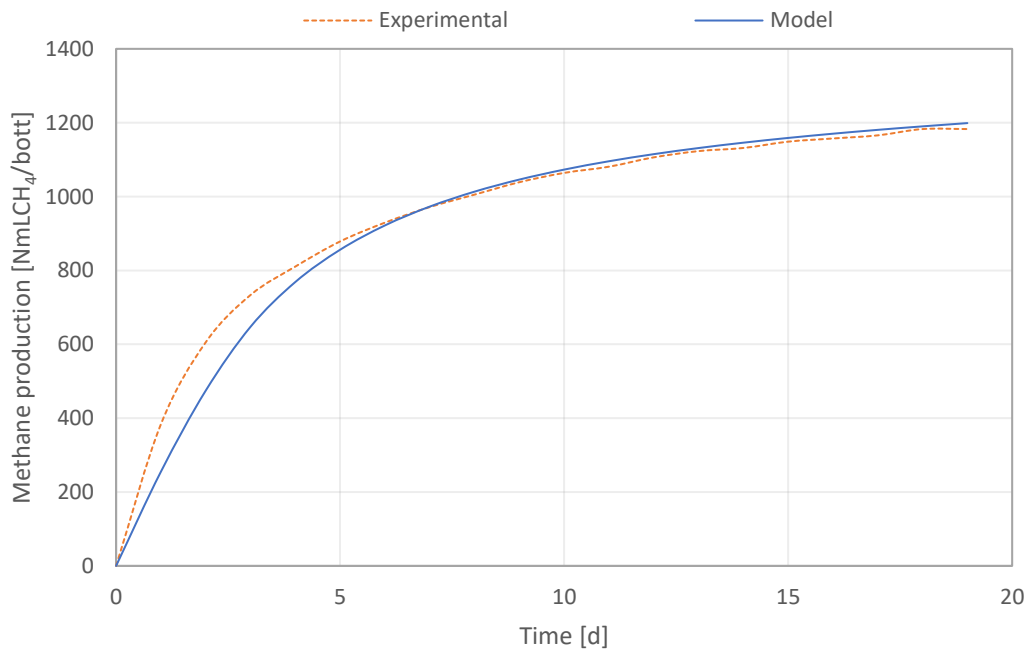
Figure F. 5 - Sludge BMP test simulation (13/04/2022).
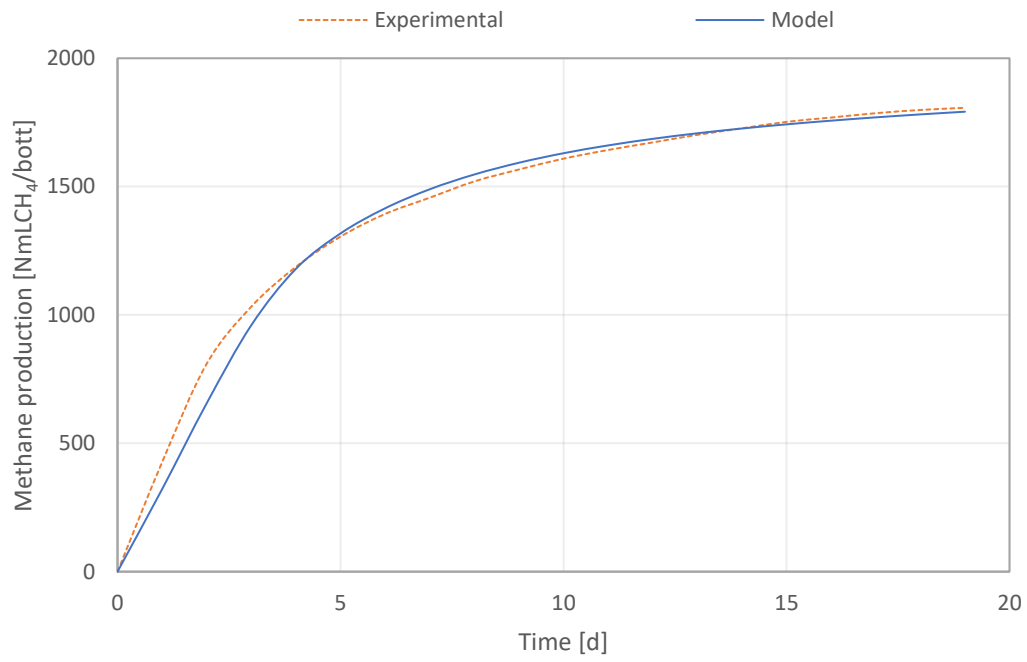
Figure F. 6 - Sludge BMP test simulation (29/04/2022).
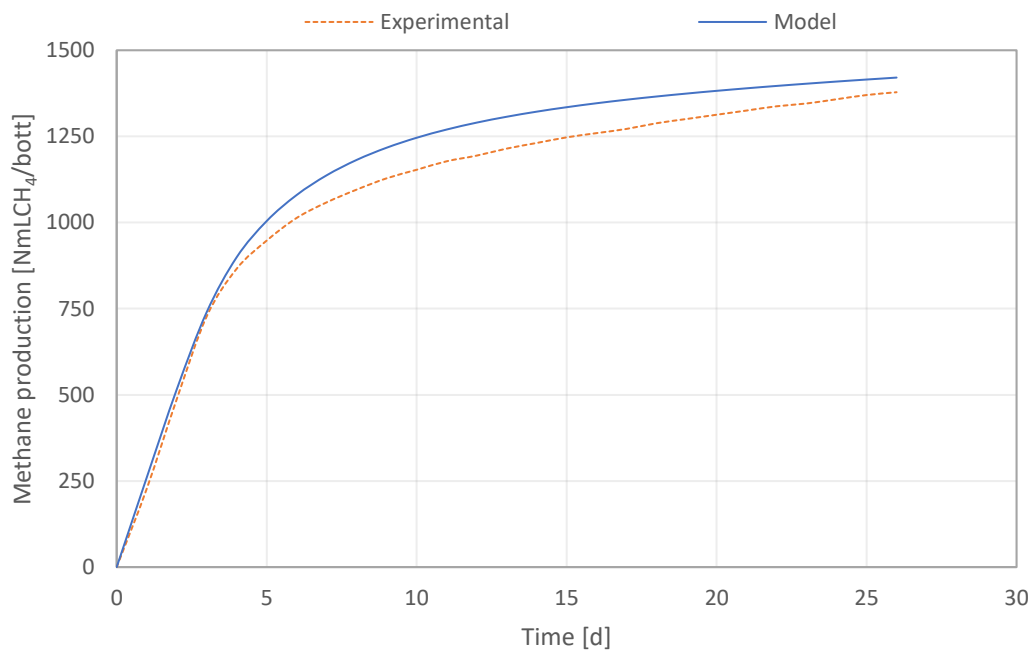
Figure F. 7 - Sludge BMP test simulation (25/05/2022).
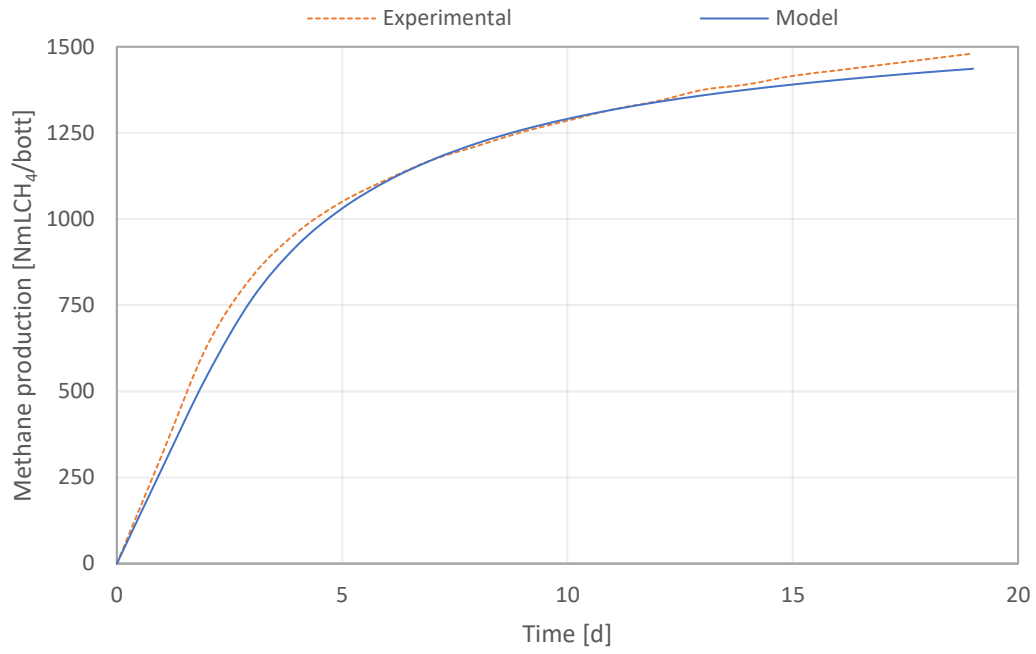
Figure F. 8 - Sludge BMP test simulation (17/06/2022).

Yogurt BMP tests
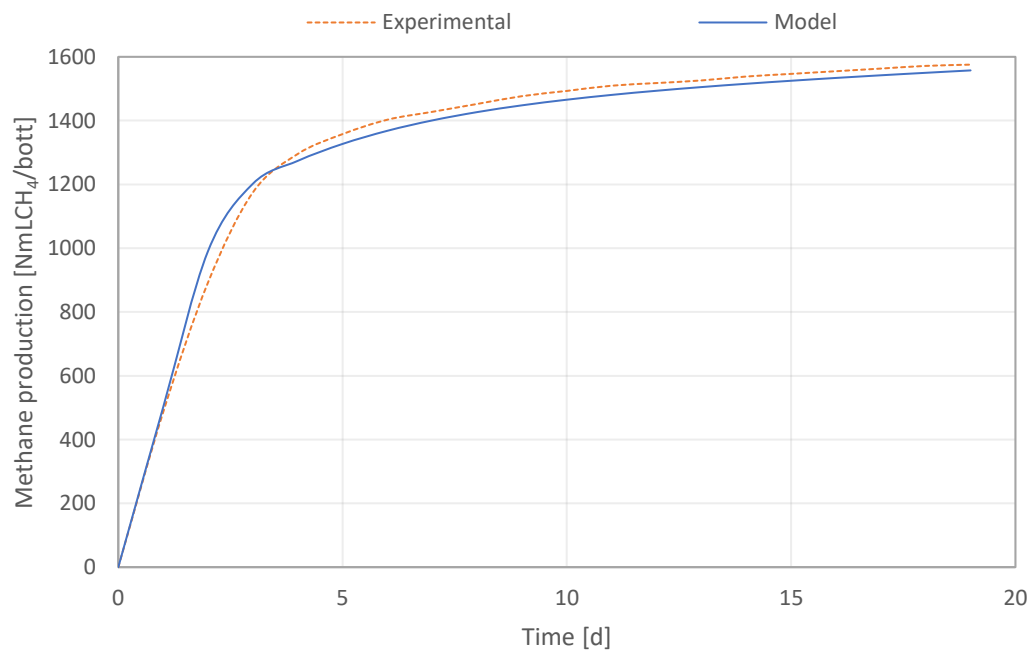
Figure F. 9 - Yogurt BMP test simulation (13/04/2022).

Co-digestion BMP tests
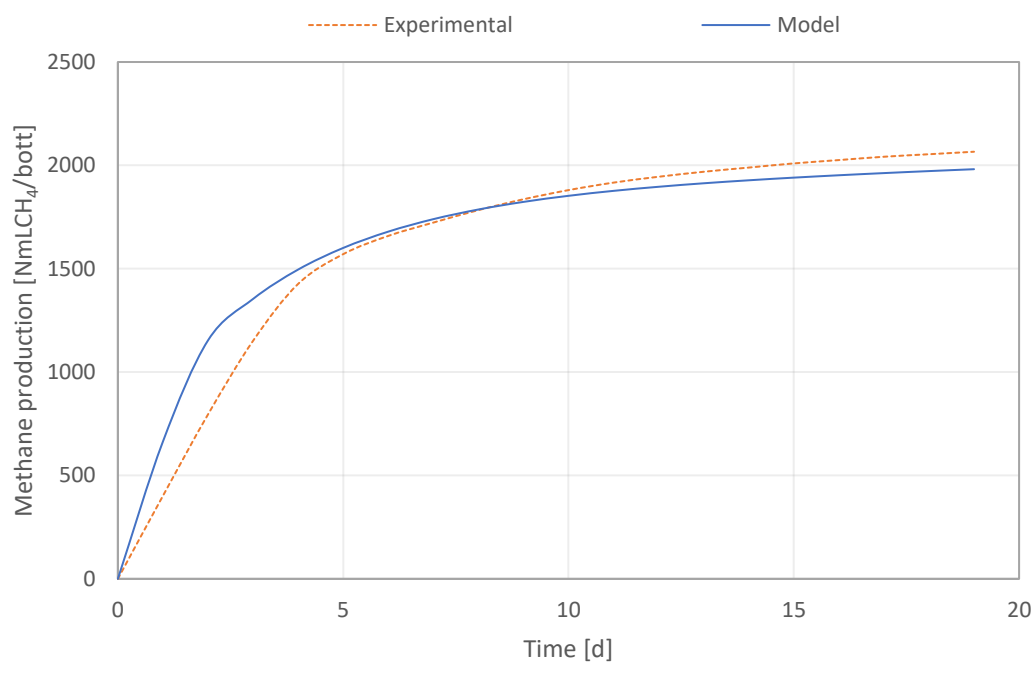
Figure F. 10 - Co-Digestion BMP test simulation (17/06/2022).

Residual BMP tests
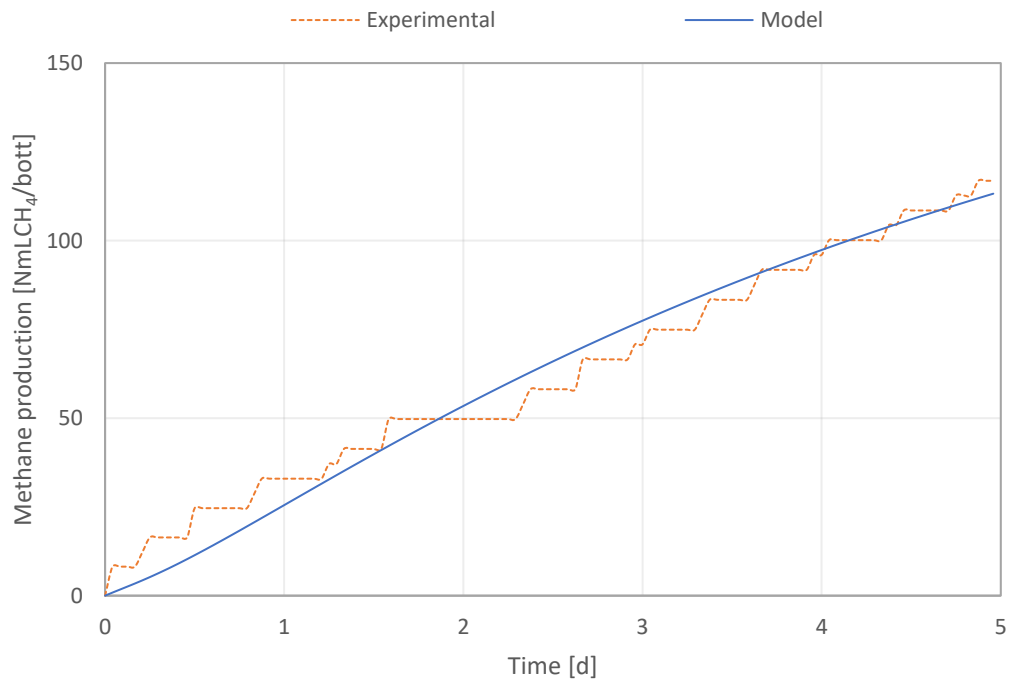
Figure F. 11 - Residual BMP test simulation (01/04/2022).
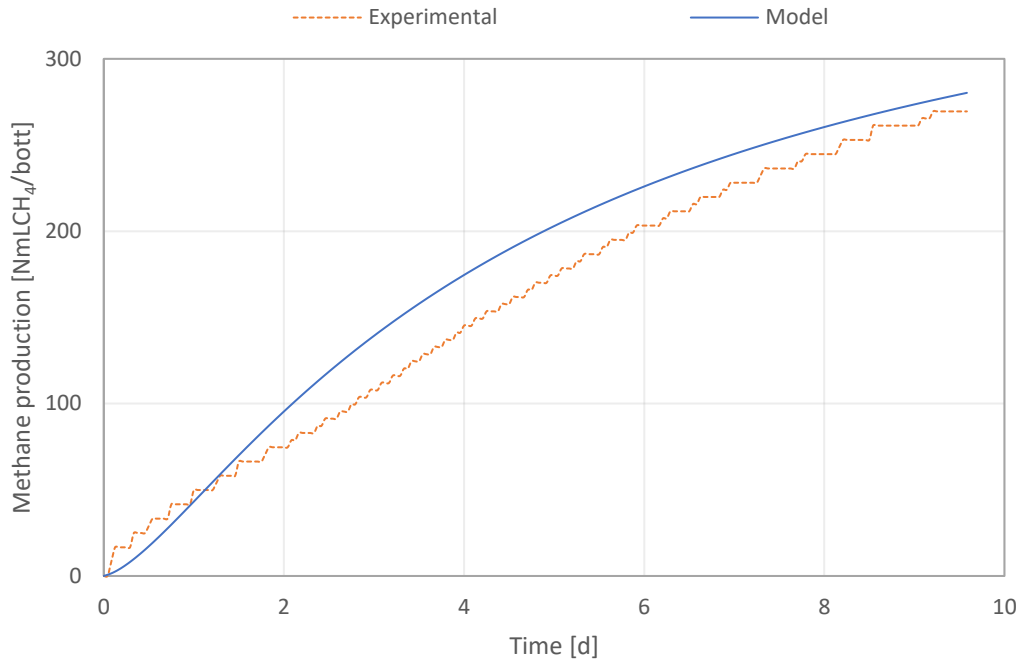
Figure F. 12 - Residual BMP test simulation (06/05/2022).
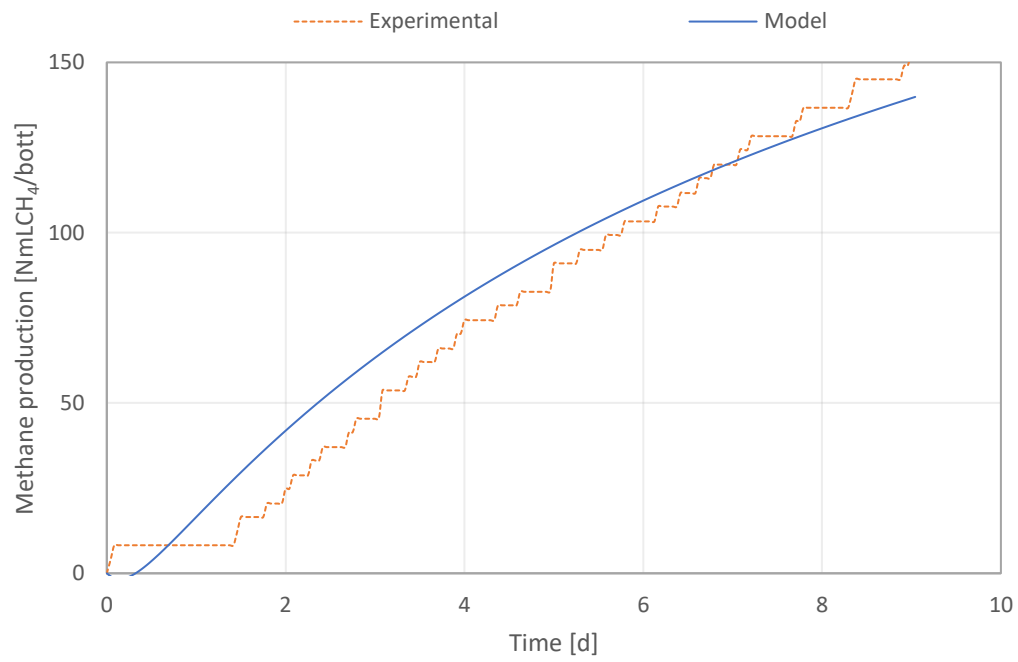
Figure F. 13 - Residual BMP test simulation (20/06/2022).

173
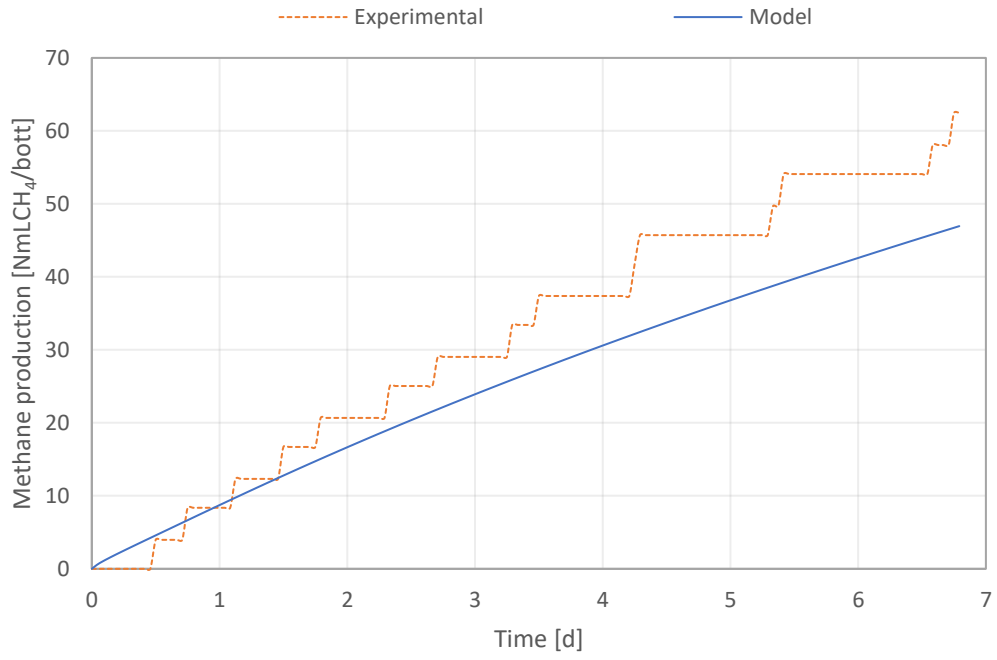
Figure F. 14 - Residual BMP test simulation (29/06/2022).

Acetate activity tests
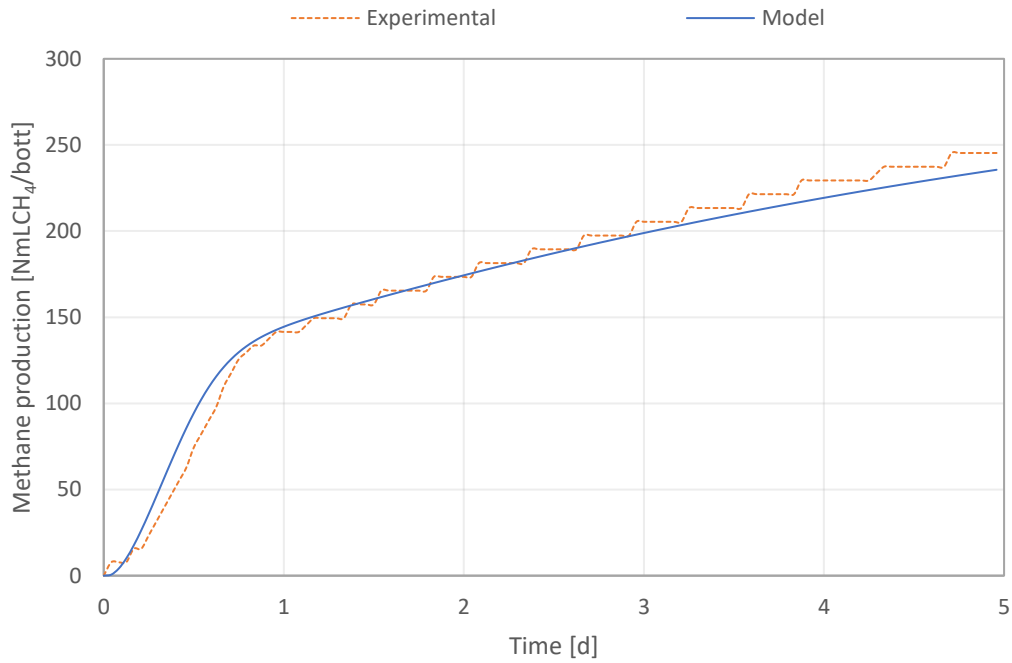
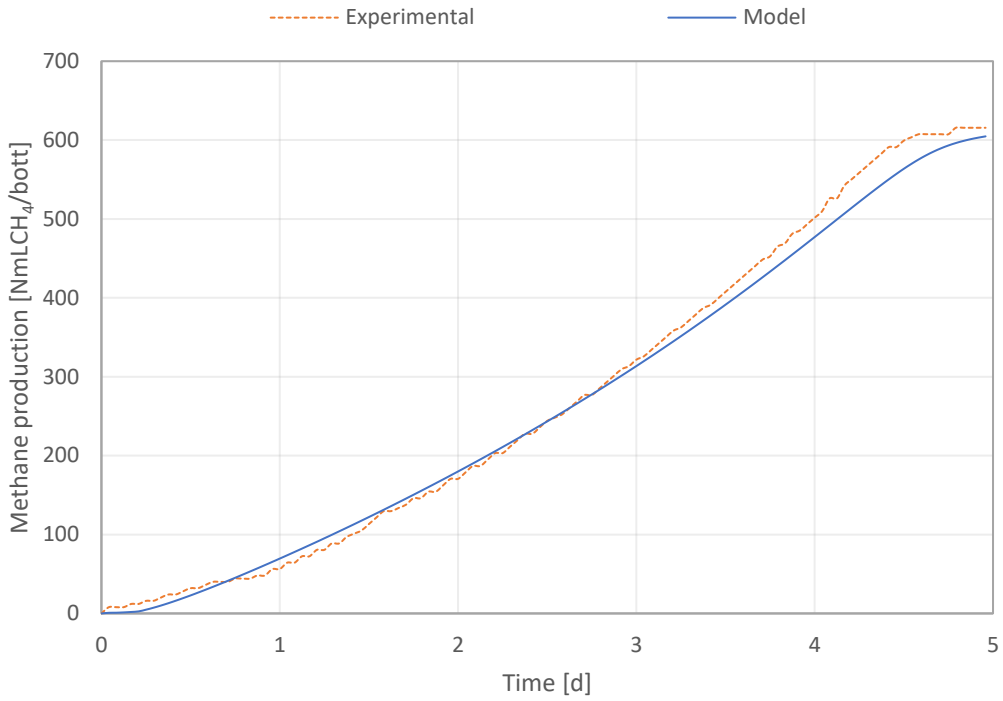Figure F. 15 - Acetate activity test simulation - 0.5 gCOD/L (01/04/2022).

174
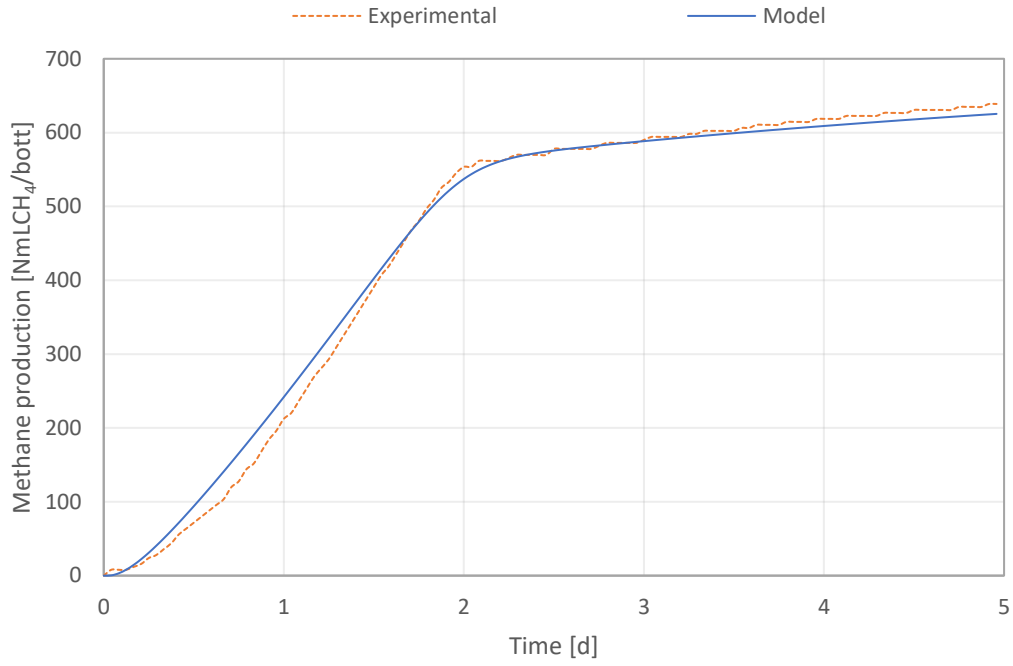
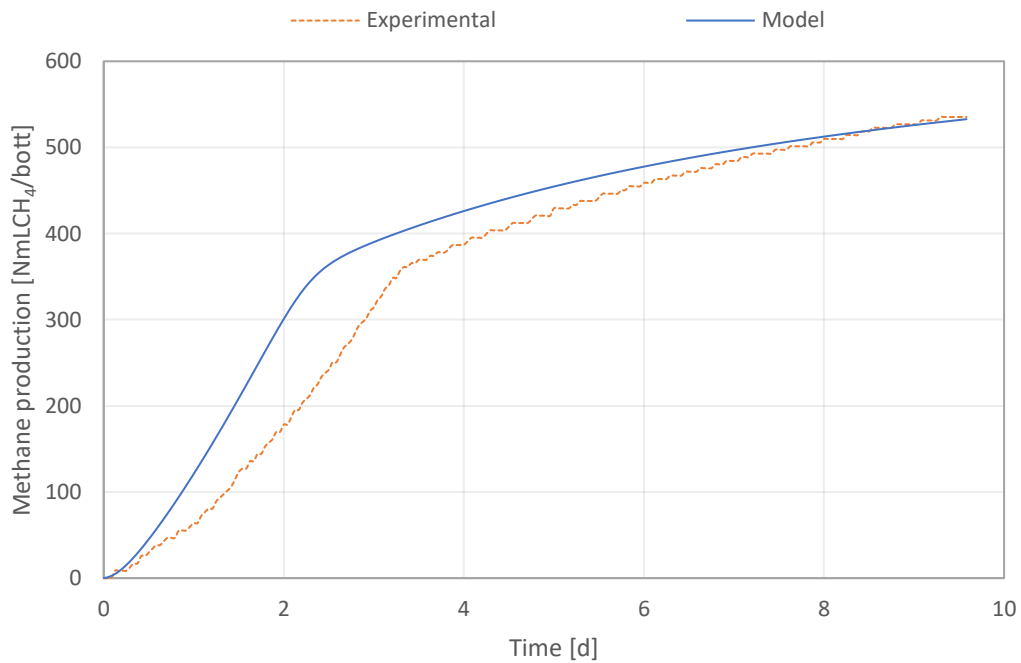Figure F. 16 - Acetate activity test simulation - 2 gCOD/L (01/04/2022).
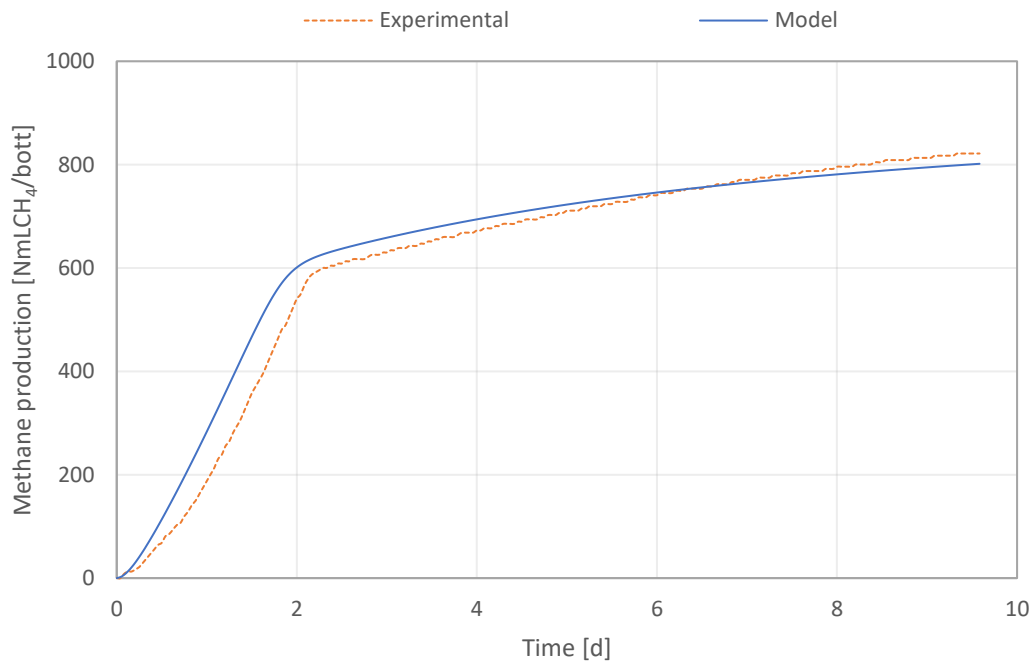
Figure F. 17 - Acetate activity test simulation - 2 gCOD/L (06/05/2022).
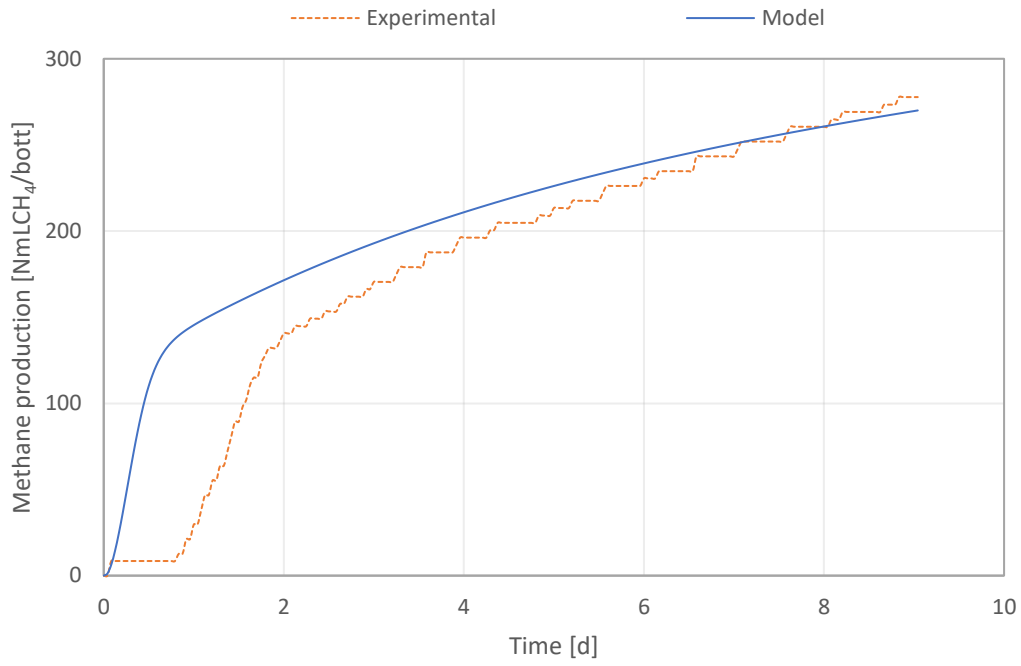
Figure F. 18 - Acetate activity test simulation - 0.5 gCOD/L (20/06/2022).
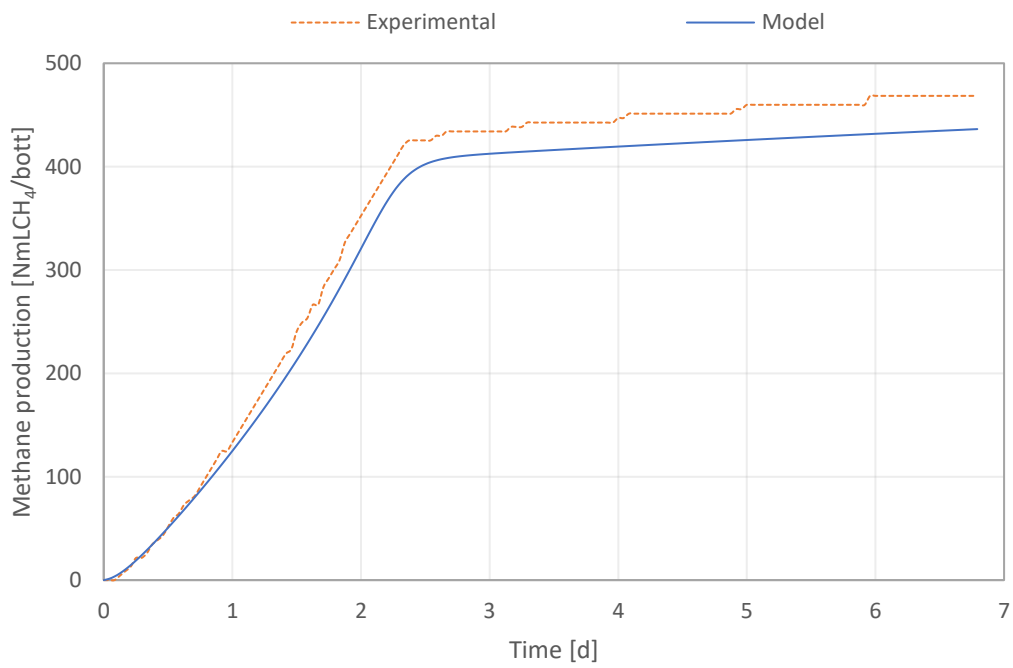
Figure F. 19 - Acetate activity test simulation - 1.5 gCOD/L (29/06/2022).

Propionate activity tests
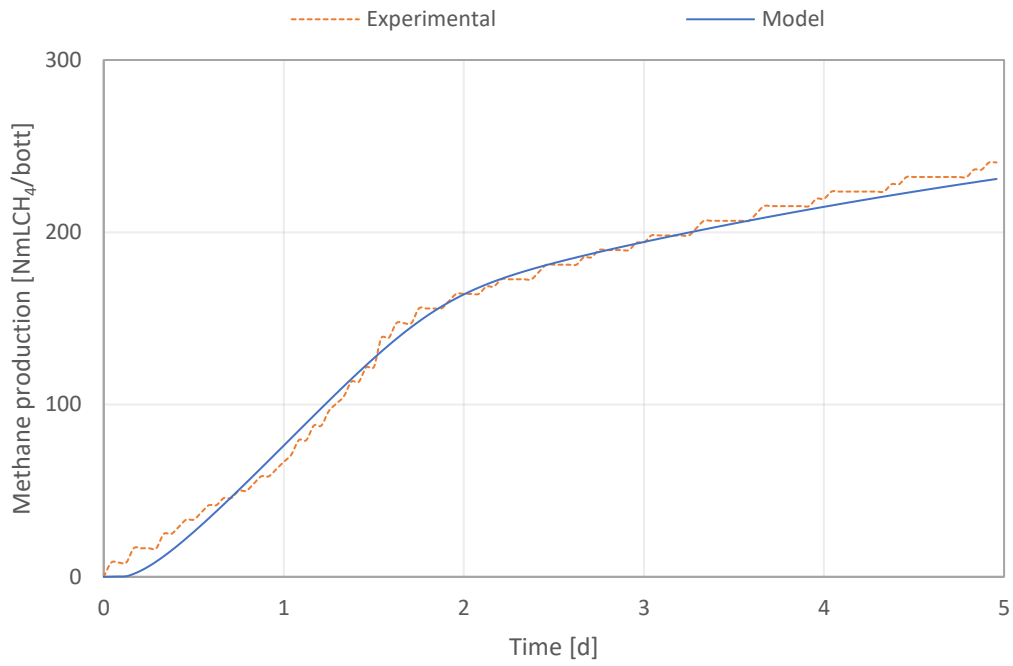
Figure F. 20 - Propionate activity test simulation - 0.5 gCOD/L (01/04/2022).
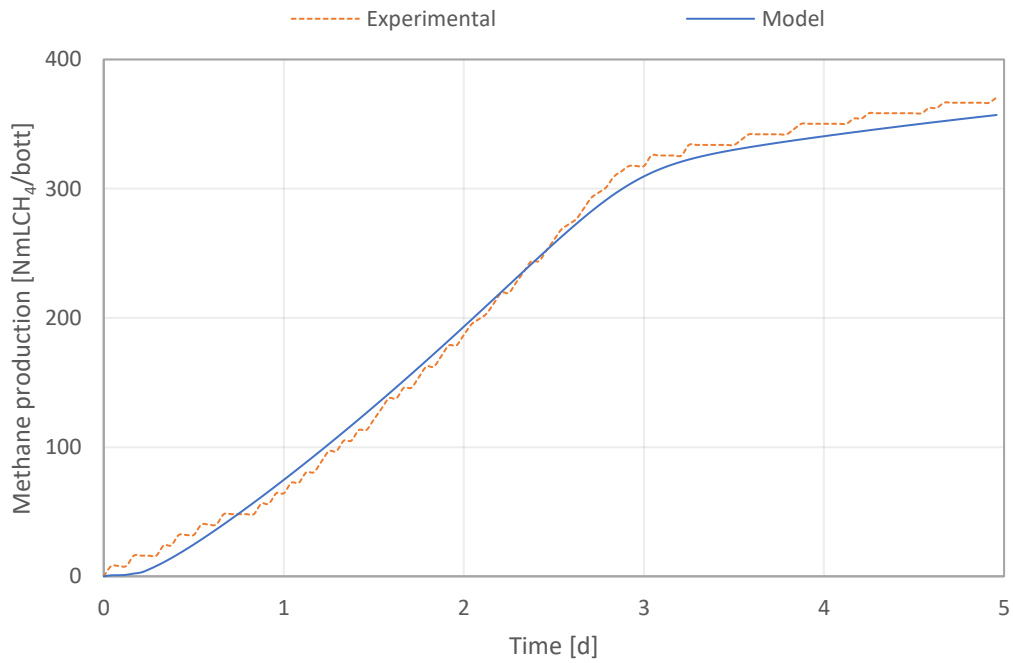
Figure F. 21 - Propionate activity test simulation - 1 gCOD/L (01/04/2022).

Figure F. 22 - Propionate activity test simulation - 2 gCOD/L (01/04/2022).
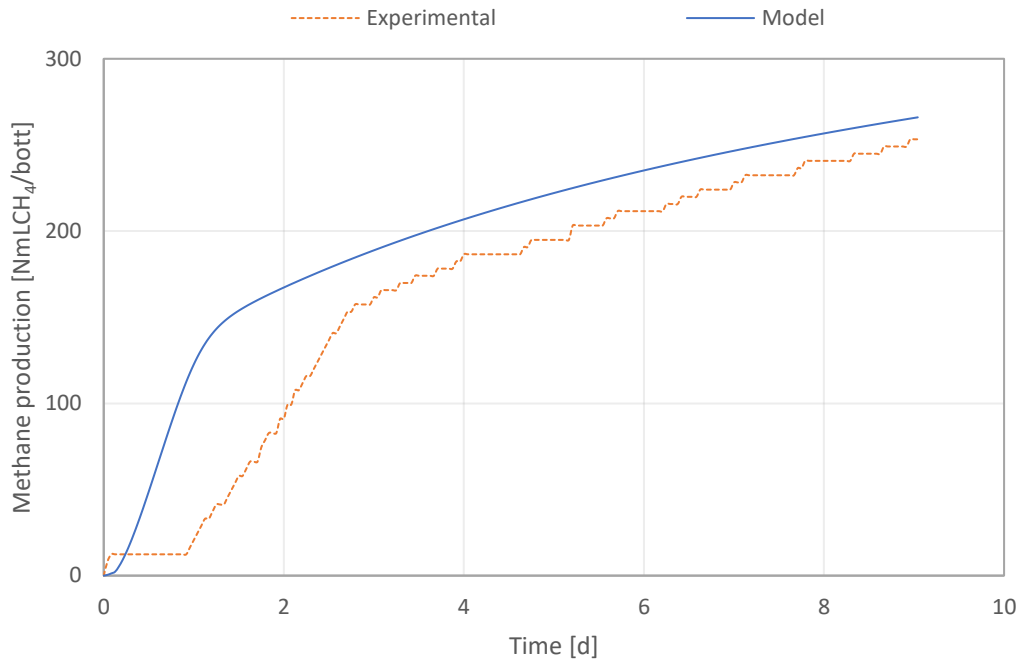

Figure F. 23 - Propionate activity test simulation - 1 gCOD/L (06/05/2022).

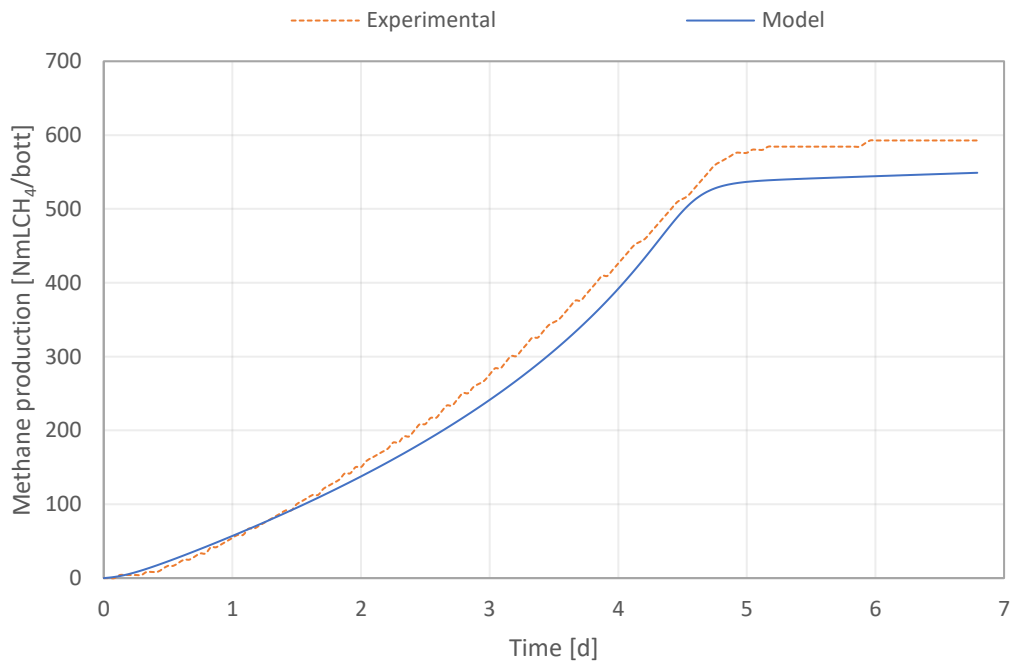Figure F. 24 - Propionate activity test simulation - 0.5 gCOD/L (20/06/2022).

Figure F. 25 - Propionate activity test simulation - 2 gCOD/L (29/06/2022).
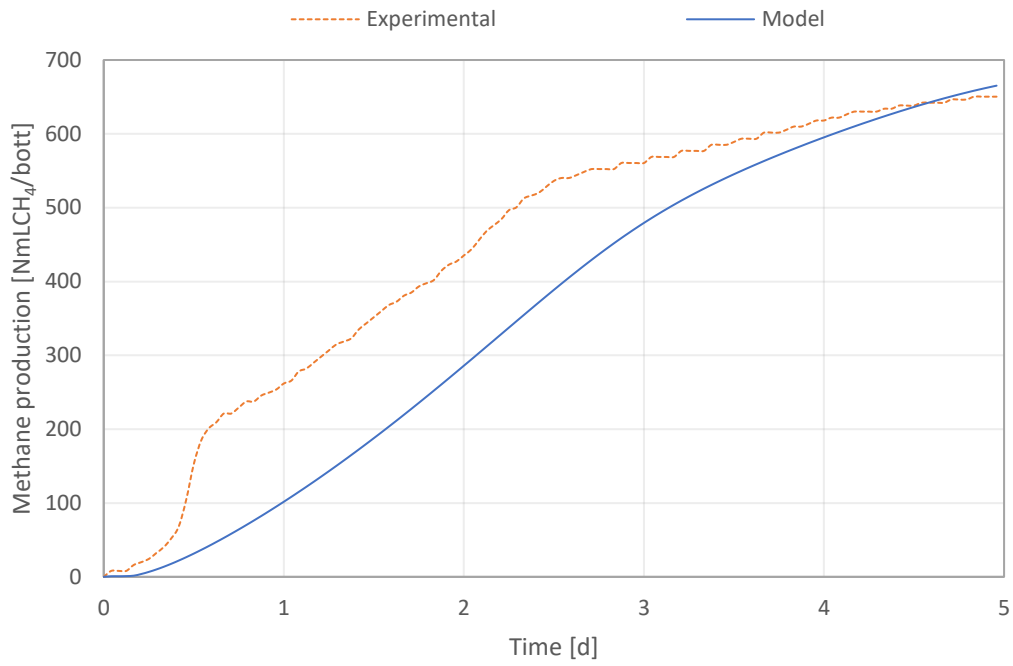
Glucose activity tests

Figure F. 26 - Glucose activity test simulation - 2.5 gCOD/L (01/04/2022).
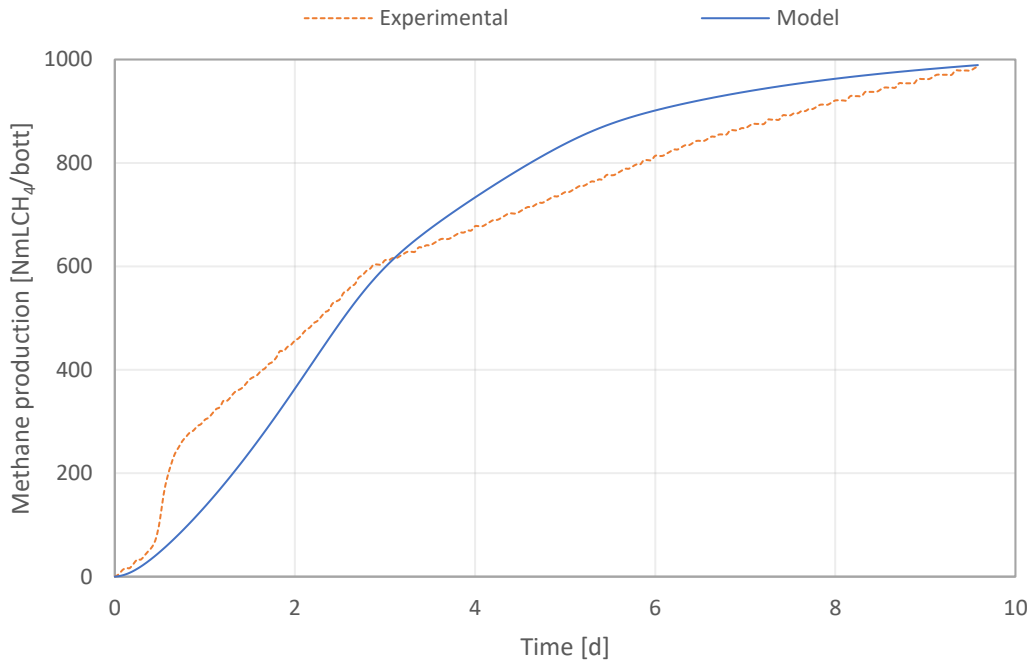

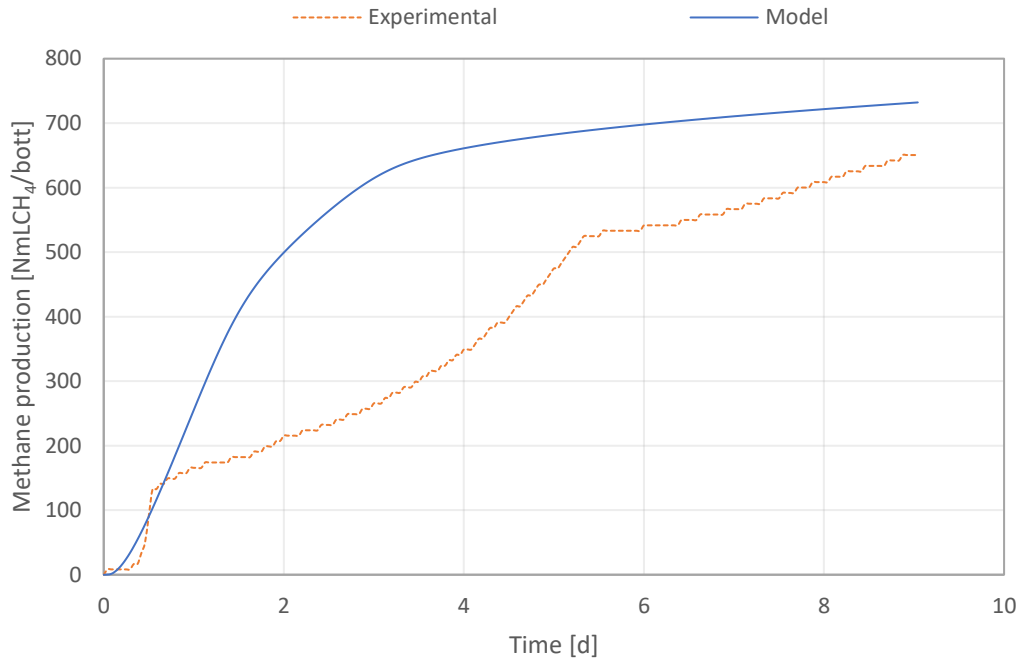Figure F. 27 - Glucose activity test simulation - 3 gCOD/L (06/05/2022).

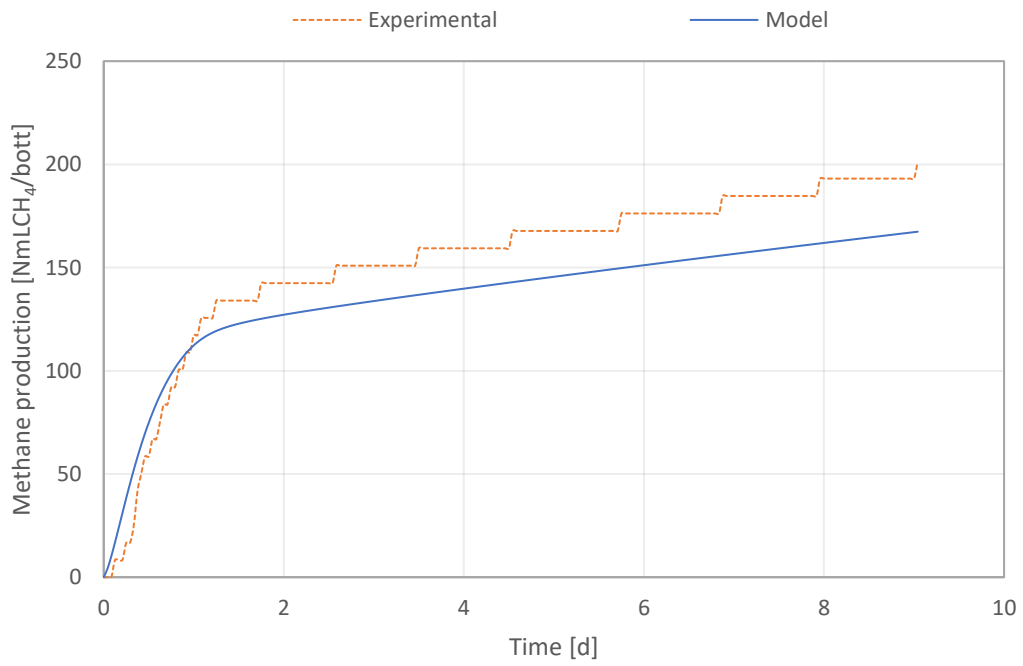Figure F. 28 - Glucose activity test simulation - 2.5 gCOD/L (20/06/2022).

Figure F. 29 - Glucose activity test simulation - 0.5 gCOD/L (06/07/2022).

APPENDIX G

The following tables show the ingredients used in the preparation of the nutrient solutions used for the BMP tests.

Table G. 1 - Ingredients of mother solution A.

Substance	Reagentary code	Mass (g)	Package number
KH_2PO_4	AR35	2.7	AR35
$Na_2HPO_4*12H_2O$	AR40	11.2	AR40
NH_4Cl	AR23	5.3	AR23

Table G. 2 - Ingredients of mother solution B.

Substance	Reagentary code	Mass (g)	Package number
$CaCl_2*2H_2O$	AR24	0.75	AR24
$MgCl_2*6H_2O$	AR28	1.0	AR28
$FeCl_2*4H_2O$	AR26	0.2	AR26

Table G. 3 - Ingredients of mother solution C.

Substance	Mass (g)
MnCl$_2$*4H$_2$O	0.05
H$_3$BO$_3$	0.005
ZnCl$_2$	0.005
CuCl$_2$	0.003
Na$_2$MoO$_4$*2H$_2$O	0.001
CoCl$_2$*6H$_2$O	0.1
NiCl$_2$*6H$_2$O	0.01
Na$_2$SeO$_3$	0.005

In a flask for each mixture, add distilled water to the mother solution A, B and C in order to obtain final volume of 0.5 L, 0.5 L and 1 L, respectively.

In the bottles with the samples for the test, solution A and B must be added due to 5% of the final test volume; solution C must be added due to 1% of the final test volume.